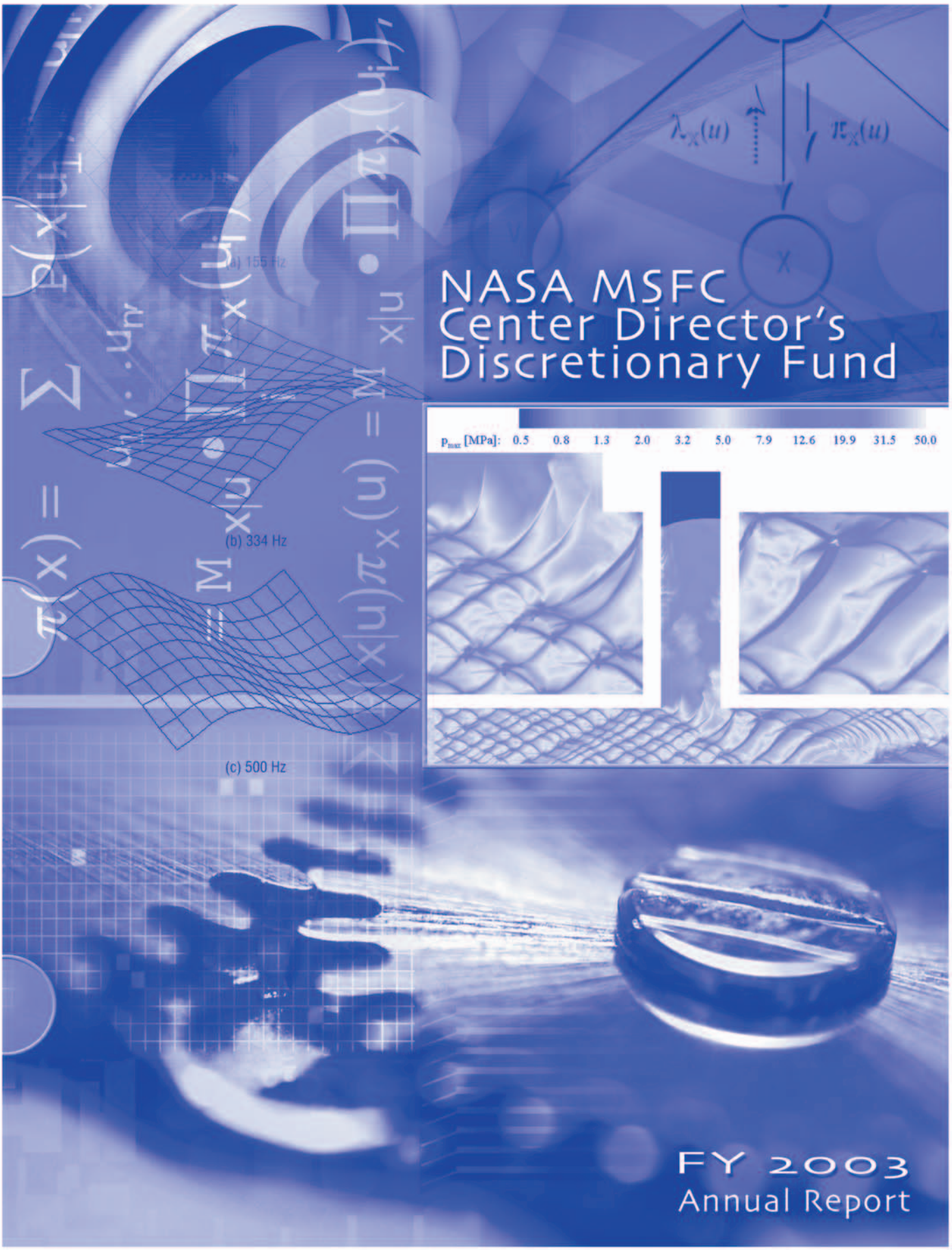

NASA MSFC Center Director's Discretionary Fund

FY 2003 Annual Report

Introduction

The purpose of the Center Director's Discretionary Fund (CDDF) at NASA's Marshall Space Flight Center (MSFC) is to allow the Center Director to encourage innovative ideas in research and technology not directly related to programs/projects in progress. Most CDDF research and technology development projects are conducted in-house, with the funding used primarily to purchase materials and equipment. Limited collaborative efforts with industry technologists or university researchers are encouraged if collaboration is in the best interest of MSFC.

The CDDF allows talented and innovative individuals the opportunity to investigate and bring to fruition high-risk/high-payoff research and development efforts central to NASA's mission and MSFC's products. These efforts provide advancements in the areas of transportation, microgravity, optics, space science, and crosscutting technology applicable to multiple research areas. This investment in the personnel at MSFC provides increased opportunities for MSFC scientists and engineers to conduct cutting-edge research and development activities.

The MSFC CDDF Selection Board (Technology Council (TC)) for fiscal year (FY) 2003 approved 26 new projects and 22 carry over projects. This is compared with the 22 new projects approved in FY 2003. The projects selected for FY 2004 are listed at the end of this 2003 Annual Report by title, with the amount of authorized funding specified for each new project. Progress reports for studies approved in FY 2003 are reported herein.

Making the results of CDDF projects readily available in a timely manner is an objective that helps ensure exposure to a larger audience and results in a broader application rate of this important NASA research. In addition to the CDDF Annual Report, the MSFC CDDF Program utilizes technical papers, technical memorandums, patents, and an Internet CDDF Home Page to help accomplish this important objective. The referenced Web site may be accessed at http://www.nasasolutions.com. It includes an electronic version of the guidelines and procedures for submitting a project investigator proposal, as well as many other technology transfer categories.

The program is aligned with the Center's products, and supports development of its core competencies. The Directorates involved (Engineering, Flight Projects, Science, and Space Transportation) solicited proposals separately from all MSFC personnel, received the proposals, and recommended those best suited to their priorities. The directorates are responsible for managing the technical aspect of the projects selected.

The newly formed TC acted as the forum for determining proposal adequacy and applicability, serving also as the committee to evaluate recommendations for project selections by the directorate. The MSFC Chief Technologist, Jim Bilbro, heads the TC.

In FY 2005, the CDDF is expected to undergo a transition to become an integral part of the MSFC Independent Research and Development (IRAD) Program. Although possibly no longer identified as the CDDF, it will still serve as the lowest technical readiness level (TRL) funding and will continue to meet the intent and maintain the spirit of the CDDF.

Fred Shramm prepared this report with primary assistance from Janine Roskowski, Stephen V. Fotovich, Jr., Jason Shoemate, and Maureen Euto of UNITeS. We gratefully acknowledge and extend our thanks to each Principle Investigator who submitted a paper for this report, to the technical departments and office coordinators who collected papers from the various authors and helped ensure a smooth editing process, to Sandy Brown/RS50, for assisting with the Financial Summary section of the report, and to Rebecca Caneer/AD01 and Bruce Weaver/ UNITeS for printing this document in a professional and timely manner.

MSFC's CDDF Program is currently managed by the Technology Transfer Department. Comments should be directed to Fred Schramm/CD30, at 256–544–0823 or fred.schramm@nasa.gov.

Table of Contents

Engineering

Flight Projects

Science

Transportation

Financial Summary


Engineering
Directorate
(a) 155 Hz
(b) 334 Hz
(c) 500 Hz
p_max [MPa]: 0.5 0.8 1.3 2.0 3.2 5.0 7.9 12.6 19.9 31.5 50.0
NASA MSFC
Center Director's
Discretionary Fund
FY 2003
Annual Report

Embedded Acoustic Emission Sensors Annual Report

Project Number: 02–01

Investigators: **W.T. Powers/ED12**
Sam Russell/ED32
James Walker/ED32
Dwight England/ED17

Purpose

The purpose of this Center Director's Discretionary Fund (CDDF) project is to develop technology to be used to produce small, inexpensive, lightweight acoustic emission sensors suitable for detecting microdamage accumulation in composite or metal structures resulting from proof test or in-service loading.

Background

Existing acoustic emission sensors and support instrumentation are restricted in their use to either localized areas of a flight structure or as ground support. Current off-the-shelf technology acoustic sensors are bulky and impractical for real-time flight analysis. Current technology embeddable electronic sensors do not have sufficient noise rejection and signal amplification to measure the microdamage accumulation in composite structures that lead to ultimate structural failure. Other embedded sensing schemes utilize transmit and receive functions where an amplitude signal component is detected and used to ascertain the direction and magnitude of the damage. These methods can be complex and may provide ambiguous results due to their susceptibility to electromagnetic noise pickup from the local environment. The sensors being developed at the Marshall Space Flight Center (MSFC) will combine the structural testing and monitoring capabilities proven by conventional acoustic emission nondestructive evaluation with the optimal structural coverage attainable with small, lightweight embeddable sensors. These sensors will have built-in amplification to give sufficient signal boost and minimize antenna noise pickup (fig. 1).

Approach

The following steps outline the investigating approach for this project:

- Research commercially available acoustic sensor elements suitable for embedding, or surface mounting on a very low profile.
- Perform signal strength/sensitivity testing on an assortment of qualified candidate sensors using basic breadboard electronics signal conditioning (fig. 2).
- Design and test comparable electronic signal conditioning to capture and elevate signal levels high enough for transmitting over long distances (several feet) (fig. 3).
- Manufacture sensor electronic prototype circuit boards and evaluate performance.
- Perform extensive in-system testing to verify design using the nondestructive evaluation (NDE) hardware currently in place. This will allow a comparison with other industry standard surface mount sensors mentioned above.

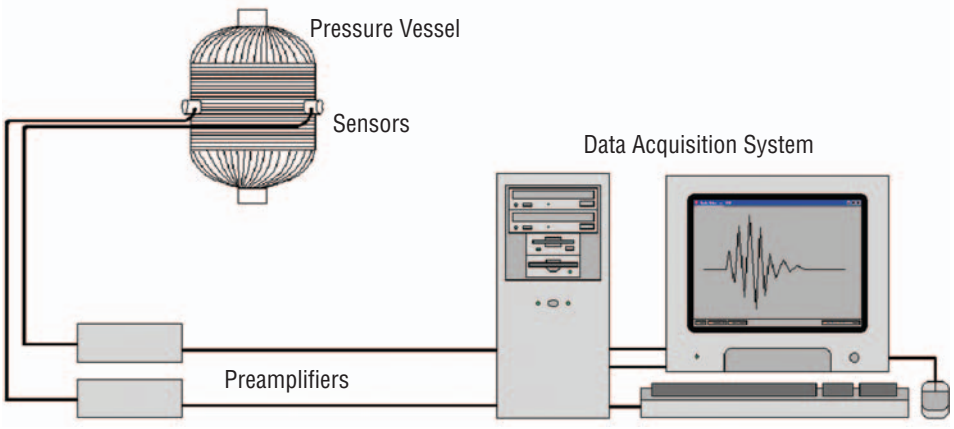

Figure 1. An acoustical emission sensor system.

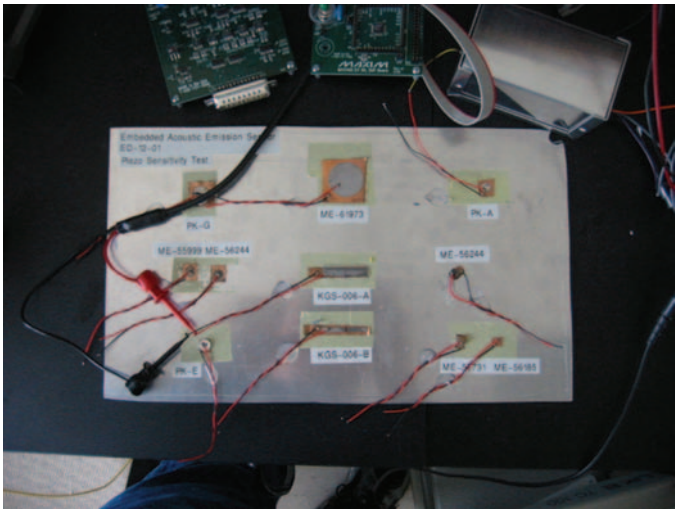

Figure 2. Sensor component evaluation.

Figure 3. Test setup with carbon fiber wrapped tank.

Accomplishments

We have studied the maturity levels of available technologies, acquired sensor materials, and collaborated with other experts in this field to determine the optimal approach based on parallel efforts that are similar in nature. Sensor sensitivity analysis was performed, sensors were selected, and demonstrations were given for the Engineering Directorate. Preliminary signal conditioning design is complete. Design is on going.

Planned Future Work

Complete signal-conditioning design, fabricate surface-mount electronics circuit board, and conduct extensive tests in the NDE facility.

Publications and Patent Applications

None presently. Patent applicability is being evaluated.

Funding Summary

Fiscal year (FY) 2002 expenditures were $15,500 and FY 2003 expenditures were $15,000.

Status of Investigation

This project was given an extension through July 30, 2004 due to the workload of other projects. Manufacturing and testing are the deliverables yet to be achieved. Much design, testing, and analysis work is still needed in the coming months, but, with an increased level of effort, the initial goals are still attainable.

Vision System Development for Miniature Robotics

Project Number: 02–02

Investigators: Jeri M. Briscoe/ED12
Eric L. Corder/ED12

Purpose

This Center Director's Discretionary Fund (CDDF) project has two objectives. The primary objective is to develop a test platform for the development, implementation, and evaluation of advanced vision systems to perform metrology and robotic vision. This test platform will support the development of innovations in robotic vision systems and miniaturization of such systems. The secondary objective is to investigate the unconventional use of traditional components to provide a simplified distance approximation device (DAD) that can be used for robotic vision.

The development of a DAD for use with miniature robots has applications for inspection and maintenance systems that do not require or cannot accommodate more complex systems. Inspection in areas inaccessible to tethered robots, such as Space Shuttle Main Engine (SSME) or hazardous environments, could be navigated using input from a DAD and a rudimentary processing system.

Background

The reliability of space related assets has been emphasized after the second loss of a Space Shuttle. The intricate nature of the hardware being inspected often requires a complete disassembly to perform a thorough inspection. Requalification of the hardware for space flight is sometimes prohibitively expensive and time consuming, which can be difficult as well as costly. In these cases, the use of machine vision can allow for inspection with greater frequency using less intrusive methods. A group of areas on launch vehicles that would benefit from such inspections was identified, and common barriers noted. Several measurement techniques were evaluated and compared against the environmental and performance requirements defined. A measurement technique using simple triangulation methods was adapted to accommodate these requirements. A miniature robot was developed as a platform to test the vision system. A test environment appropriately sized for the robot was constructed and the vision system was used to autonomously navigate the environment. The results were evaluated and further testing was conducted to define the miniaturization potential of the system.

Approach

Current plans for next generation spacecraft provide insight to possible environments requiring autonomous or semiautonomous inspections. An ideal inspection area was considered in a design for the X–34 program employing a skin raised off the spacecraft with a 10–12-in separation creating a cavity that could be used to flow coolant. Potential inspection areas identified during interviews with representatives of the SSME office included areas around turbine fan blades in the high-pressure turbo pump (HPTP), the injection forest where propellant and oxidizer enter the combustion chamber, and plumbing such as a cooling manifold around the nozzle.

The physical environment to be navigated was defined as follows: Constant lighting, curved walls, and confined spaces with 2–12-in length corridors. The width of the corridors would not be considered and for demonstration purposes would be defined by the platform developed to carry the vision system. Since miniaturization remains a goal, the prototype development would be required to show a path to miniaturization to be developed in a follow-on effort.

Performance requirements include avoidance of curved surfaces and corners while maintaining a measurement error less than one pixel within the specified range of 2–12 in. An additional performance requirement for the demonstration was to operate without a tether.

Investigation of other solutions to simplify navigation techniques produced useful results. Commercial range finders are widely available and relatively accurate. Unfortunately, most are designed for outdoor use and even those specifically for indoor use employ time-of-flight (TOF) techniques not effective for accurately measuring distances less than 2 ft.

Range finders using triangulation dominate simplified distance navigation devices. One notable effort[1] employs a laser line projected onto the target. This research used deformation in the laser line to identify and alert an automobile driver of his proximity to an object using the specific example of a curb. Alternative distance measurement techniques using a single camera also include pixel dithering techniques[2] and an optoelectronic technique[3] for target recognition. Of the techniques studied, the range finder was determined to be the simplest and easiest to modify for a given set of environmental parameters. The basic concept of triangulation is illustrated in figure 1.[4]

The distance from the camera to the target, point C to point T, may be calculated by using the Law of Sines:

$$B = A\frac{\sin b}{\sin a} = A\frac{\sin b}{\sin(b+c)} \ , \qquad (1)$$

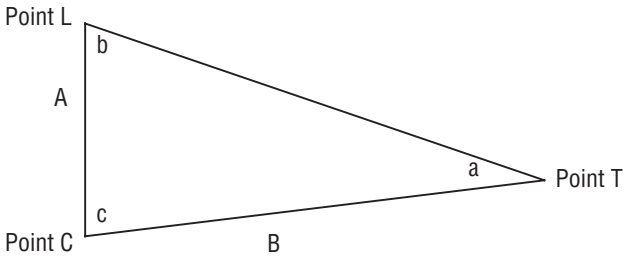

Figure 1. Illustration of the basic concept of triangulation.

where *A* represents the distance between the laser (point L) and the camera (point C).

Algorithm Development

Simple triangulation cannot account for curved surfaces, angles, or corners. The method using a laser line[1] is impractical for this application due the impact of increased computational requirements on size. Also, in an implementation, the distance *B* and angles *a* and *b* are very difficult to precisely define. A technique for obtaining range was demonstrated using a modular robotic test bed[5] and will be briefly discussed. The camera with the laser mounted directly above, was configured as shown in figure 2. The laser and the optical axis form a vertical plane with point P as the target.

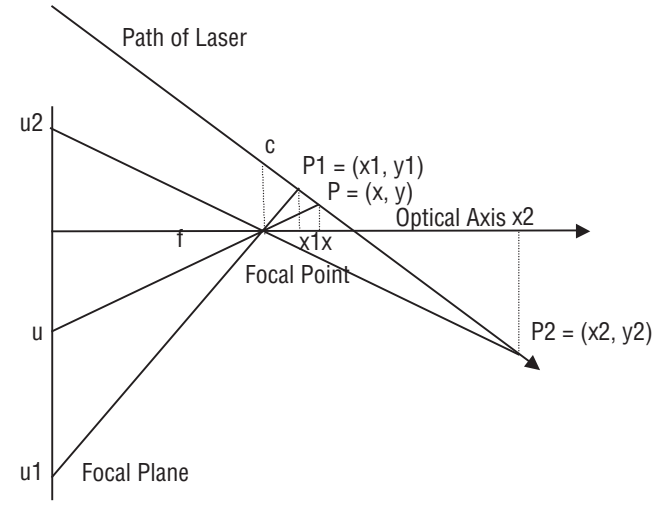

Figure 2. Application of triangulation with simplified calculation.

Using similar triangles and placing the origin of the coordinate system at the focal point we have,

$$C = \frac{u_2 x_2}{f} - \left(\frac{u_2 x_2 - u_1 x_1}{f(x_2 - x_1)} \right) x_2 \ . \qquad (2)$$

In order to find *x*, the projection of point *P* onto the optical axis, two calibration points, P_1 and P_2, are used. Given that points x_1, x_2, u_1, and u_2 are known, equation (3) may be derived.

$$x = \frac{N}{ud - k} \ , \qquad (3)$$

where $N = (u_1 - u_2)x_1x_2$, $d = x_2 - x_1$, and $k = u_2x_2 - u_1x_1k$, are known after calibration.

In this manner, Nguyen was able to calculate the range, *x*, without knowing the focal point of the camera or the distance *d*, angle a_1, or angle b_1 shown in figure 3. This calibration technique works well over a wide range with accuracy decreasing as distance increases.[5]

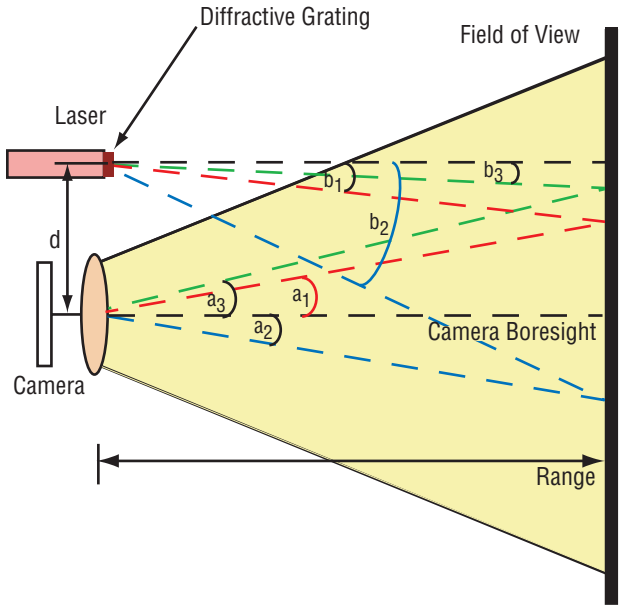

Figure 3. Application of triangulation with the addition of a simple diffractive grating.

While this technique achieves basic navigation, the confined space outlined in the environmental requirements requires a distance measurement error of less than one pixel. The miniature lens dictated by the environment allowed using the technique in reference 5 without modification. However, the well-defined environment for this effort allowed a modeling technique to be performed prior to navigation. A combination of the two techniques described above was used to obtain real-time range and environment information at the desired accuracy without the need to know *d* or angles a_1 and b_1.

In order to accommodate the environment defined above, the concept of a 3 × 3 grid of spots projected by a small laser onto the target was developed. Incorporating a simple prism or diffractive grating onto the laser allowed the design to remain compact while accounting for curved surfaces. Figure 3 is an illustration of the application of triangulation using a simple diffractive prism projecting multiple calibration points onto the target.

Using equation (1) the range for each point, p_1, may be calculated using,

$$range_i = \frac{d}{\tan(a_i) - \tan(b_i)} \ . \qquad (4)$$

Information from spots adjacent to the center point permits the calculation of a rough shape of the target surface. Only the center point range need be calculated. Curved surfaces and corners may be avoided by calculating distances relative to the center using spatial distortions of the grid.

Accomplishments

Evaluation of the feasibility of the concept was performed using the National Instruments software LabVIEW® in conjunction with the IMAQ® tool suite. This approach allowed rapid development of a concept into a working system and proved ideal for prototyping the vision system.

The assumption that lighting conditions are constant throughout the environment is reasonable as the inspection process is being performed in a controlled setting. This condition allows for the simplification of the image processing required to extract usable data from the image. This assumption is extended and the resulting requirements of the system, as implemented, include that the intensity of the laser exceed the intensity of the target in the image. With these conditions satisfied, an intensity threshold allows for the projected pattern to be easily discerned from objects in the environment. Each point to be measured in the image falls within a known region when the target is in the specified range. Performing edge detection in the regions of interest reveals the location of the projected pattern and allows the target position to be known. Should the edge detection fail to indicate a location within the region of interest, the measurement result is returned as off scale.

The relationship between target distance and point of interest in the image is inherently nonlinear. This nonlinearity is compounded by the spherical aberrations introduced by the lens of the camera. While it is possible to flatten the image, allowing coordinates in the frame to correspond to real world measurements, it is a costly endeavor in terms of processing time and power. A simplified approach would create a linear approximation for the sensor output allowing rudimentary calculations to correlate sensor output to approximate target distance. This approach, while giving a reasonable target distance, introduces further error into the system and is unacceptable for navigating a confined space.

The approach taken in implementing this system was to account for the nonlinear relationship with a reasonable model of the data that would provide an acceptable error across the range. A set of precision, linear stages was used to provide reference measurements, and the coordinates of the point of interest in the image were correlated to the actual measurements. A curve was fit to the data and the mean-squared error was evaluated to determine if the model was of appropriate accuracy. The sensor output allowed for single pixel measurements and resulted in the requirement that the model never vary from the actual measurement by half of a pixel in either direction. Through experimentation, it was found that a sixth-order polynomial could be consistently fitted to the data with the desired accuracy. The error between the model and the calibration data is shown in figure 4. The cyclical nature of the error was found to be consistent over many calibrations and can be attributed to the discrete nature of the imaging system. Figure 4 depicts this type of error well.

The angle b of the laser in relation to the camera, as defined in figure 1, was only slightly less than 90 degrees, limiting the vertical movement of the reference in the image to 6 pixels. As the target distance approaches a value accounted for by one of the discrete points associated with a pixel value in the image, the error approaches zero. As it moves away from this zero point, the error increases until the midpoint is reached between the two adjacent pixel values. At this point, the error begins to decrease and approach zero once again. It is not possible to account for

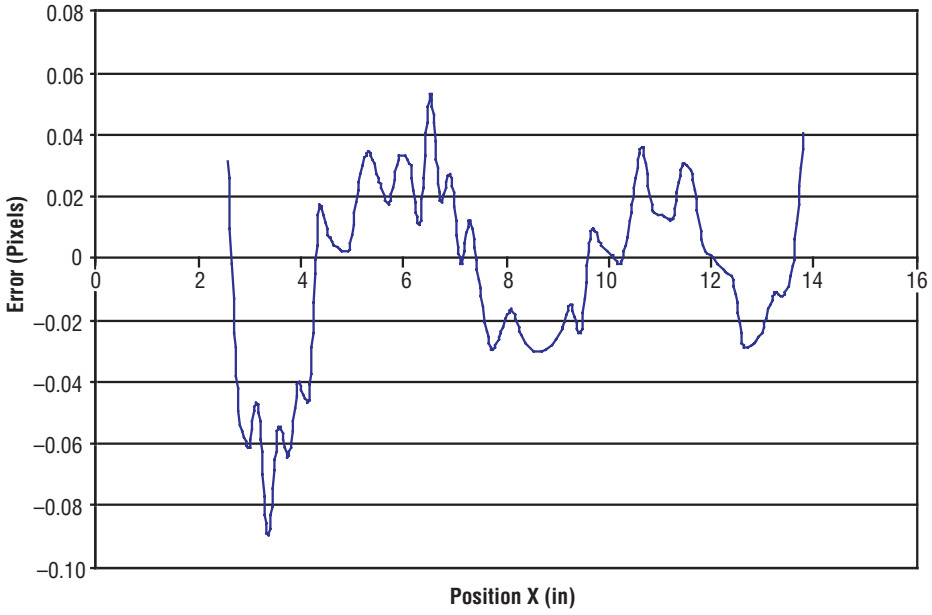

Figure 4. Vertical measurement error introduced by a mathematical model.

this error in the model as the relationship between the error and the target distance is not one-to-one. It is then necessary to limit the error introduced by this step so as not to further degrade the accuracy of the output. In practice, the reference in the image was made to traverse as much of the height of the image as possible. While this lessens the effect of the error on the outputted measurements, it is still present in the system.

Addressing Portability

LabVIEW® provided a platform for prototyping and experimentation; however, it did not lend itself to a portable implementation of the software. The code, originally implemented in the graphic-based language of LabVIEW®, was written using the same algorithm and in the more portable form of the C language. Compilers for C are common for a number of platforms including Texas Instrument's TMS3206416 digital signal processor (DSP). This processor was used to demonstrate the code in its new form.

The DSP used is found in an evaluation board purchased from Ateme, a Texas Instruments partner, and also provides a frame grabber. The output of the frame grabber is made available to the DSP in the UYVY 4:2:2 format. The first step in processing a frame of data is to strip the image of the chrominance planes. A black and white camera was used.

In the instances that good data is found in a region of interest, the fitted polynomial is employed to calculate the target distance in that region. The Newton-Raphson iterative method was implemented to determine the root of the polynomial offset by the location of the point of interest within the frame. This method was ideally suited for this case in that the polynomial was known to behave well in the neighborhood of the sensor range. Furthermore, Newton-Raphson provided the desired result with a minimum of computation making it ideal for implementation on a variety of low-end processors. As this was only a demonstration of the technique, the output of the system was overlaid on the image and displayed. All points obtained during measurement were also indicated on the image to provide feedback during development. Ultimately, the output of the system will take a form suitable to the target application.

Extension of the Algorithm to Three-Dimensional Orientation

Also addressed in this implementation was the orientation of the target in three-dimensional space. The projected pattern was extended to allow for multiple points to be measured in the vertical direction of the frame. This added ability allowed the system to distinguish objects that formed varying angles with the surface of travel as well as its horizontal orientation to the object.

Horizontal relation to the target was determined by measuring multiple points across the width of the image. Knowing the distance to these points and the horizontal separation in the image allows the angle of the camera in relation to the target to be determined on a single axis. The technique is extended to include the ability to measure relative angles on the vertical axis.

Additional points are introduced into the projected pattern to provide this extended reference. The calibration routine is required to account for this additional information, and ultimately the final system will put the new data to use. The cost of calculating the additional measurements can be prohibitive depending on the size requirements of the final device and the choice of processor chosen for implementation. In the case of the TMS3206416, the additional calculations had minimal impact on the performance of the system and structure of the implementation. As such, the ability to measure the relative roll as well as yaw with respect to the target proves a cost effective addition to the abilities of the system.

Demonstration of Navigation

A means of demonstrating the vision system's capability in a practical setting was developed. A robotic platform was controlled using data from the range sensor and made to navigate an environment that was confined in relation to the overall size of the device.

The platform, illustrated in figures 5 and 6, measured 5-in wide and 3-in long. The height of the device was not a concern given that the demonstration was two-dimensional. The test environment was created to allow 1 in on either side of the platform to allow for error and to provide the ability to turn in the same space. While turning in a corridor, the limiting size factor became the diagonal length of the robot. The routine the robot was designed to execute demonstrates its ability to determine not only distance to an object but the orientation of the system to the target. Using this data as feedback, it was possible to propel the system through an environment in a controlled fashion with consistency. The controllability and consistency of this technique, as demonstrated using the robotic platform, make it ideal for the purpose of inspection.

Results

Currently, the resolution of the camera is the limiting factor in determining the precision of the vision system. In tests with small format sensors, the resolution was not significantly reduced with sensor dimensions as small as 1 in. Each implementation thus far has depended on an analog camera and is therefore bound by the resolution of the NTSC standard, 720 × 480 pixels. The use of a higher resolution, low-frame-rate, digital camera that provides digital output would not only increase the precision of the system but also remove the need for a frame grabber, furthering the miniaturization of the overall system. This greater precision would directly result in improved accuracy.

With mission safety being scrutinized more closely than ever, steps must be taken to improve the processes with which we ensure reliable, safe operation. The design of this vision system addresses deficiencies in the ability to deliver diagnostic instrumentation into a confined area with precision and consistency.

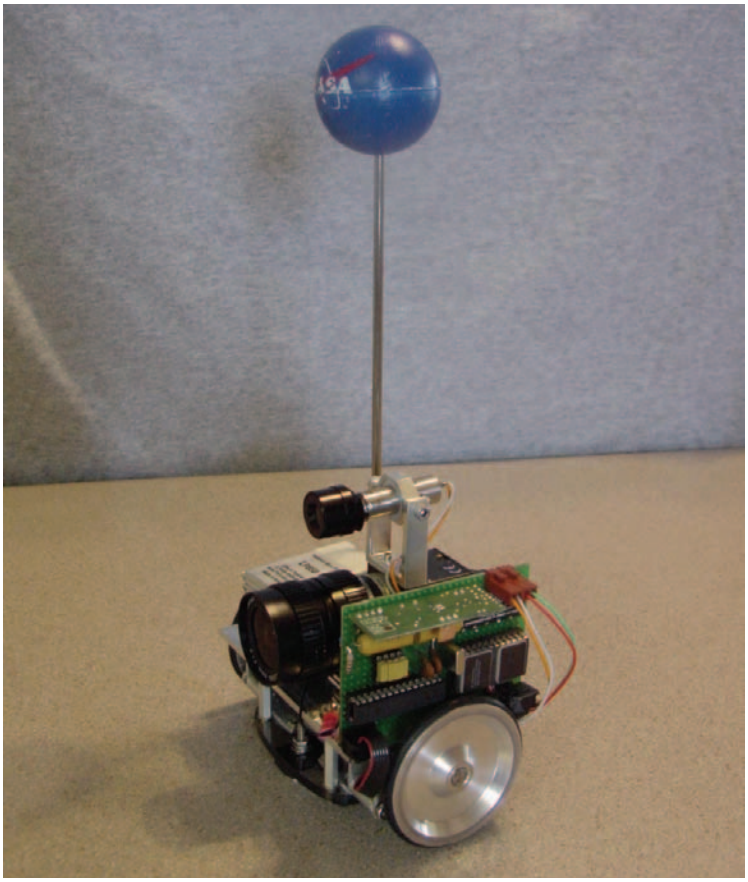

Figure 5. Miniature robotic platform.

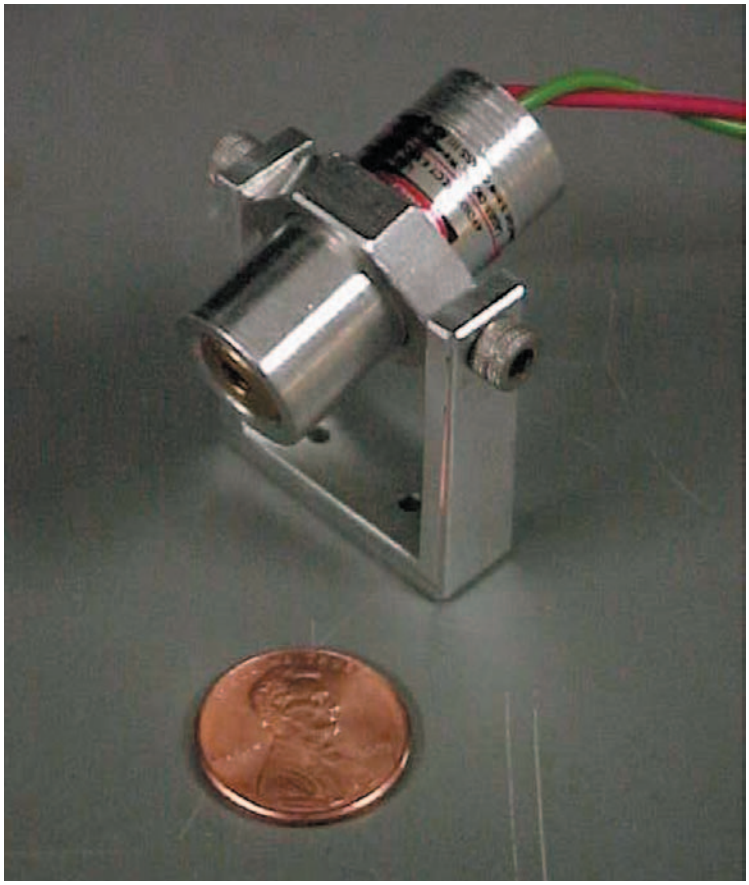

Figure 6. Scale image of laser used in the miniature robotic platform.

These abilities will allow for inspection with greater frequency and of a less destructive nature. The inclusion of an expanded pattern being projected onto the target allows for additional information to be extracted from each frame without a significant increase in processing requirements. It is these attributes, along with the ability to miniaturize the system, that make it ideal for the purpose of inspection.

Planned Future Work

Miniature Inspection Systems Technologies is currently underway. This is a follow-on CDDF that further develops the robotic platform. The areas under development include: Pattern recognition, miniature motion controller, and simulation software. The areas under development include: Pattern recognition, miniature motion controller, and simulation software.

Publications and Patent Applications

"Machine Vision Applied to Navigation of Confined Spaces," *SPIE*, Defense and Security Symposium, 2004.

A patent disclosure was filed but has not been processed to an application as of the date of this publication.

Funding Summary

All funding for this effort has been expended.

Status of Investigation

The investigation is closed.

Acknowledgements

The authors would like to thank David Broderick/Auburn University and Ricky Howard/Simulation Group-ED17 for their contributions to this effort.

References

[1] Mertz, C.; Kozar, J.; Miller, J.R.; and Thorpe, C.: "Eye-Safe Laser Line Striper for Outside Use, IV 2002," IEEE Intelligent Vehicle Symposium, December 2001 and June 2002.

[2] Ulichney, R.A.: "One-Dimensional Dithering," J. Bares (ed.), *Proc. SPIE*, Vol. 3,409, pp. 204–214,

[3] Padgett, C.; FangW.-C.; and Suddarth, S.: "Optoelectronic Sensor System for Recognizing Targets," *Suraphol Udomkesmalee*, NASA Tech Brief, Electronic Systems Category, NPO–20357,

[4] Everett, H.R.: "Sensors for Mobile Robots: Theory and Application," A.K. Peters (ed.), Wellesly, MA, 1995.

[5] Nguyen, H.G.; and Blackburn, M.R.: "A Simple Method for Range Finding via Laser Triangulation," *Technical Doc. 2734*, Naval Command, Control, and Ocean Surveillance Center, San Diego, CA, 1995.

Flight Critical Hardware Voting Development

Project Number: 02–03

Investigator: **Anthony R. Kelley/ED12**
Dwight England/ED17

Purpose

The objective of this Center Director's Discretionary Fund (CDDF) effort is to develop several techniques and harware to perform cross-link voting that supports the Scaleable, Fault-Tolerant Intelligent Network of X(trans)ducers (SFINX) architecture and fills an instrumentation and control industry gap. Methodologies and hardware implementations that provide patentable intellectual property building blocks are being developed that will meet NASA flight critical specifications for redundancy management for both data integrity and command validation. The capabilities of various voting schemes are being built and demonstrated in software and there are plans to implement the best performing methods as a hardware solution. Additionally, intelligent methods will be explored that ensure correct sensor or component placement and cabling integrity. Two or more potential patents have been identified for these components. One flowmeter disclosure that uses redundancy management has been submitted and is already under a license agreement. All of this hardware will directly support the SFINX architecture by providing one of the critical component building blocks, as shown in figure 1.

Background

Only one company is known to be developing a similar concept, and their approach does not provide the functionality of the devices in this research effort. A need was identified to produce a general purpose voting hardware component that is plug-and-play and to share these designs with multiple government vendors to drive down the cost of redundant electronic hardware. A summary of related efforts is as follows:

Past:

- SFINX: This Generation III activity was discontinued in 2000 due to budget reallocations. This $1.6 million program lasted 3 years and produced system and component specifications and hardware for a SFINX architecture, that is plug-and-play, intelligent, self-validating, expandable, single-to-quad redundant, etc. Experience, data, and hardware uncovered the need for the technology proposed in this project. Everything in this proposed effort will further the SFINX architecture.
- X–33 Avionics: The X–33 architecture did not conceive or implement low-level voting logic as is proposed here. This system used only high-level system voting that will not meet the objectives of SFINX.

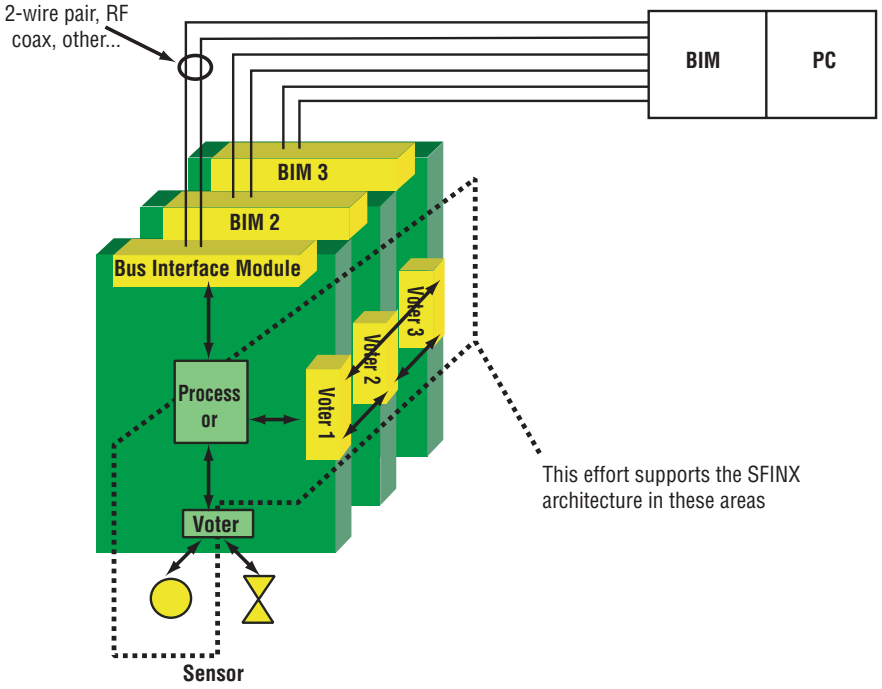

Figure 1. SFINX architecture critical component building blocks.

- Draper/Boeing logic voting patent: Draper Laboratories recently designed and patented a digital voting system for flight critical computers. This system works very well, has many good features, and demonstrates the ability to patent this type of technology. Their system applies to digital data streams and lacks many of the SFINX features that this CDDF plans to implement.

Current:

- Society of Automotive Engineers (SAE2001): This conference, held in Detroit, MI, provided an excellent overview of the automobile industry efforts in intelligent instrumentation and control systems. A clear need is seen in their safety-critical, drive-by-wire systems for the voting technology that will be developed here. Only a few of the systems discussed are coming close to the capabilities of a SFINX system, and none of them deal with redundancy management as the SFINX architecture does. Nothing similar to our voter was discussed.
- Military—U.S. Air Force (USAF) and U.S. Army: The USAF is managing a common event network test instrumentation system. This is an ongoing effort and project personnel support yearly reviews. This system is similar to a single-string, nonflight critical SFINX architecture. As such, it demonstrates a bussed system, but cannot do flight-critical applications or applications requiring low-level redundancy management. The Army is managing a similar effort with the same limitations. Neither has discussed technology similar to the voters planned as part of this project's development.

Proposed:

- Boeing Space Launch Initiative (SLI) in Avionics: Boeing has started an effort for modular avionics via SLI. However, it is believed that this project's planned voting components should be developed independently due to the potential patents involved. Once the ideas are protected, incorporation into the Boeing system architecture will be pursued.

Approach

An object-oriented hardware voter design is planned using the requirements developed in the SFINX program. In SFINX, several types of voting methods were identified as needed. Fortunately, these techniques, defined by the project's redundancy management expertise, are needed by NASA and the instrumentation and control industry. The plan is to catalog these methods and to define the common components and parts for single-to-quad redundant systems. These components will then be built and tested to prove their functionality and capabilities. Finally, patents and publications will be pursued on the relevant component technologies.

Accomplishments

To date, a list has been compiled of different voting schemes to handle redundant instrumentation. Various types of instrumentation signals have been categorized that must be voted, and work has started to prototype the algorithms in software code to verify performance. Due to this CDDF effort, two patent disclosures for a new type of low-intrusion flowmeter have been submitted for patents. One of these has been negotiated and has a significant patent license in work (MFS–31952).

Planned Future Work

Within several months, the top three sensor voting algorithms will be tested during a laboratory flowmeter test. Once they are fully characterized and analyzed, an effort will be started to perform their software functions in electronic hardware. This will make a basic voting building block and should generate at least one more patent.

Publications and Patent Applications

Applications have been made for the following patents:

- MFS–31952: Balanced flowmeter with no moving parts.
- MFS–31760: Minimally intrusive, highly accurate flowmeter with no moving parts.

Funding Summary

To date, no funds have been spent due to work in software. However, several purchase orders will be executed within 6 weeks that will consume all available funds. Table 1 presents the funding summary for fiscal year (FY) 2002 and FY 2003 for this project.

Table 1. Funding summary.

	FY 2002 ($)	FY 2003 ($)	Total ($)
Requested	35,000	10,000	45,000

Status of Investigation

This is the start of the second year of a 2-year effort. The investigation is proceeding with a 12-month delivery plan.

Soft Computing for Propulsion Control

Project Number: **02–04**

Investigators: **Luis C. Trevino/ED14**
Terry Brown/ED14
Bill Skipworth/Sverdrup

Purpose

The global objective of this Center Director's Discretionary Fund (CDDF) project was to explore how soft computing technologies could be employed to improve overall vehicle system safety, quality, reliability, and rocket engine performance. The aim was to address this by enhancing engine control using soft computing technologies and sound software engineering practices used in Marshall Space Flight Center's (MSFC's) Flight Software Group. Goals for addressing quality were to improve the following: Software management, development time, maintenance, processor execution, fault tolerance and mitigation, and nonlinear control in power level transitions. The intent was not to discover any shortcomings of existing engine control methodologies, but to provide alternative design choices for control, implementation, performance, and sustaining engineering, all relative to addressing reliability. This effort required knowledge in rocket engine propulsion, software engineering for embedded flight software systems, and soft computing technologies such as neural networks, fuzzy logic, data mining, and Bayesian Belief Networks (BBNs), of which BBNs were used and briefed in this report. For reasons of availability, a model of the demonstration engine test bed was the MC–1 engine initially used in this research. The MC–1 engine is simulated with hardware and software in the Marshall Avionics and Software Test-Bed (MAST) laboratory that currently resides at NASA's MSFC, building 4476, and is managed by the Avionics Department. The principle goal was to provide another avenue to address MSFC's Space Transportation Directorate's interest in improving overall engine control. Figure 1 is a presentation of the MAST.

An approach for investigating and demonstrating how the application of soft computing technologies can further address presented control issues in rocket engine control is presented. Because of the complexity of the algorithms and general control schemata, the SR–30 small turbojet engine at the University of Alabama (UA) was chosen as the final test-bed for researching the application of soft computing technologies and is another principal focus of this report. This test-bed engine is shown in figure 2.

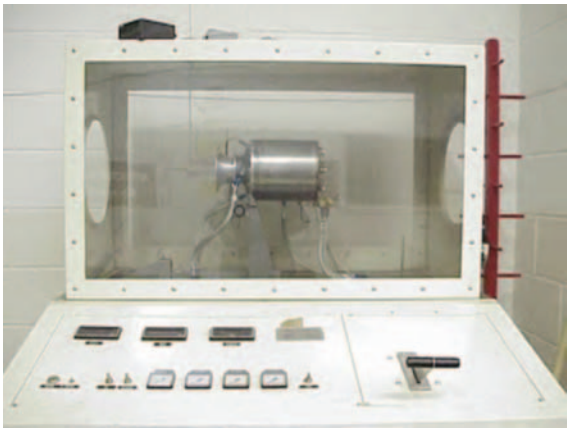

Figure 1. Marshall Avionics and Systems Test Bed.

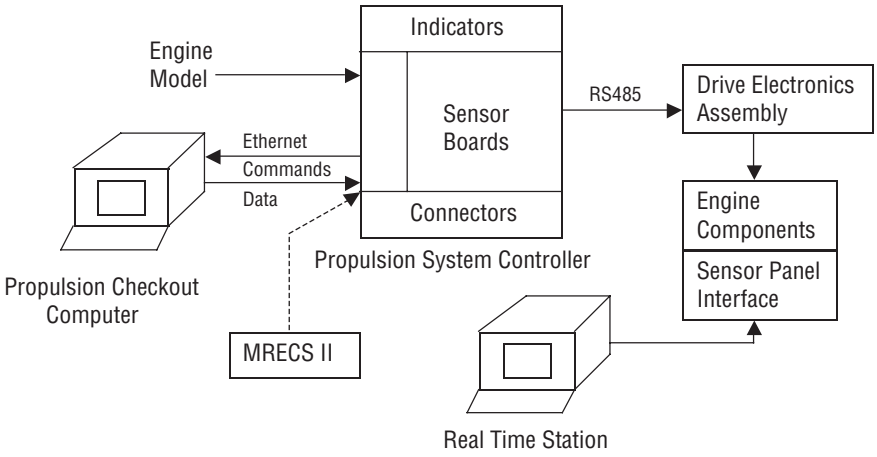

Figure 2. Turbine Technologies SR–30 turbojet engine.

Background

Many of the rocket engine programs initiated by NASA MSFC have been successful as evident by success of the Space Shuttle Main Engine, ground testing of the X–33 Aerospike engine, and the Fastrac X–34 engine. As a result, a database of test cases and lessons learned has been created from which improvements to engine control for future engine programs can be made. Such cases include premature engine shut downs (S/Ds), pump cavitation, propellant leaks, and numerous cases of anomalous sensors and data. Such cases are not only costly to the American taxpayer, but also present a risk in social acceptance of current and future space programs. The MSFC Space Transportation Directorate has continually expressed an interest in improving engine control, and many efforts in various areas for control and anomaly detection and mitigation have been undertaken. Some successful attempts have included nozzle plume analysis, engine vibration analysis, and turbine-blade detection algorithms. Other efforts, although successful in theory and simulation, have been partially successful in actual engine test firings. It is the harsh engine environment of cryogenics, vibrations, real-time control demands, and different engine configurations from test to test that continually encourage researchers to determine alternative solutions or improvements to approaches for engine control and anomaly detection and mitigation. Current control technologies depend on proven, sometimes archaic, hardware and logical programming techniques that are costly to implement and maintain and do not account for unforeseen conditions leading to the kinds of problems referenced earlier.

In this report, a description is further documented on the soft computing technology and its applicability and design approaches for both the BBN and details of its design. Automation and control of a small-scale turbojet engine is described in this particular work and UA has provided some preliminary data obtained by using a PID controller. Turbine Technologies' turbojet engine, as described further in the text, is equipped with instrumentation for monitoring the operating conditions of the engine. Some preliminary data are also obtained to demonstrate the safety of the engine under expected hazardous operating conditions, and, to demonstrate the applicability of one-dimension propulsion, equations to calculate the thrust induced by the engine are shown. Additional data obtained to determine the system transfer function to design a PID controller is also shown. The PID control algorithm design has been outlined.

The instrumentation includes several thermocouples and pressure transducers and a load-cell to measure the thrust generated by the engine. A valve controls the fuel-flow rate. In the present work, two separate control approaches were used. First, the difference between the desired thrust from the engine and the thrust measured using the load-cell was used as the feedback signal to control the fuel-flow rate to the engine. In the second approach, the temperature and pressure sensor data were used to calculate the thrust produced by the engine using the aerothermodynamic equations applying to turbojet engine operations, and the difference between the calculated thrust and the desired thrust was used as the feedback signal.

In the present approach, operation of a turbojet demonstration engine's operation will be automated and several control logics will be trimmed to show their capabilities. In this hardware-in-the-loop control demonstration effort, a simple PID control algorithm is demonstrated first. The test-bed development and some preliminary results obtained are presented using the experimental apparatus.

Approach

Bayesian Belief Networks

The primary soft computing technology to be utilized in this phase-1 effort is a BBN. BBNs have been proven to be good predictive and diagnostic mechanisms for reasoning about the state of events in environments where uncertainty is universal. BBN genealogy is strongly rooted in classic statistical Bayesian inference theory where a subjectivist viewpoint is taken. Bayesian inference uses a different interpretation of probability where one's degree of belief in some event is part of the reasoning. BBNs are computational architectures that permit declarative (prior conditional probabilistic values) and subjective (posterior probabilistic values) opinions about world (factual) knowledge to be part of the reasoning and assessment through a visual network representation and a unique syntactic message-passing feature. Furthermore, the visual network makes it easier to view the top-down cause and effect (or condition-to-consequence) relationships. For a more detailed account of this soft computing technology (SCT), the reader is referred to Pearl's treatment of the subject.[1] Figure 3 shows the specific BBN approach in this effort.

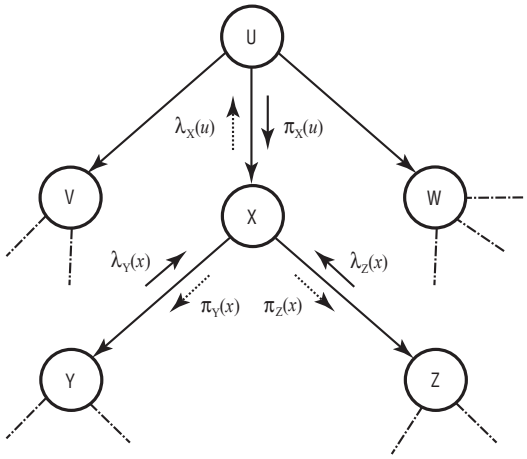

Figure 3. Bayesian Belief Network.

The procedure for the specific BBN in this effort is enumerated in the following equations.

The central equation for determining belief of $X = x$ is determined by,

$$\mathrm{BEL}(x) = \alpha\lambda(x)\pi(x) = \alpha(\boldsymbol{L}ikelihood)(\boldsymbol{P}rior), \qquad (1)$$

where α = Normalizing Constant. The diagnostic or retrospective support in equation 1 is,

$$\lambda(x) = \mathrm{P}\left(\mathrm{e}^{-}{}_{x}|x\right) = \mathrm{P}\left(\mathrm{e}^{-}{}_{y}|x\right)\mathrm{P}\left(\mathrm{e}^{-}{}_{z}|x\right), \quad (2)$$

and the causal or predictive support in equation 1 is represented by

$$\pi(x) = \mathrm{P}\left(x\middle|\mathrm{e}^{+}{}_{x}\right).$$

The overall basic propagation approach to updating is simply determined as follows, in any particular order:

- **Belief Updating:** When node X is activated to update its parameters for belief updating, it first inspects all messages transmitted to it by its parent (π) and its children nodes (λ). Then, using all inputs, it updates its belief by equation 1 where, specifically, the diagnostic support is,

$$\lambda(x) = \prod_{j} \lambda_{\mathrm{y}_j}(x), \quad (3)$$

  and the causal support is determined by,

$$\begin{aligned}\pi(x) &= \sum_{u_1,\ldots,u_n} \mathrm{P}\left(x|u_1,\ldots,u_n\right)\prod_{i}\pi_x\left(u_i\right)\\ &= \mathrm{M}_{x|u} \bullet \prod_{i}\pi_x\left(u_i\right),\end{aligned} \quad (4)$$

  where $\mathrm{M}_{x|u}$ is the probability link matrix.

- **Bottom-Up Propagation**: Using messages transmitted by Y and Z , compute the message to transmit to parent node U. This is accomplished as follows:

$$\lambda_x(u) = \sum_{x}\mathrm{P}\left(x|u\right)\pi_x(u) = \mathrm{M}_{x|u} \bullet \prod \pi_x\left(u_i\right), \quad (5)$$

  where $\mathrm{M}_{x|u}$ is the probability link matrix.

- **Top-Down Propagation:** Node X then computes new messages to be sent to its children nodes Y and Z. This is computed as follows:

$$\pi_{\mathrm{y}j}(x) = \alpha\pi(x)\prod_{k\neq j}\lambda_{\mathrm{y}k}\left(x_i\right), \quad (6)$$

  and,

$$\pi_{\mathrm{z}_j}(x) = \alpha\pi(x)\prod_{k\neq j}\lambda_{\mathrm{z}k}(x). \quad (7)$$

Software Engineering In Marshall Space Flight Center's Flight Software Group

In every software development organization, a set of processes and standards for their base product line are typically adhered too. Such processes and standards generally adhere to a type of software development life cycle. For the Flight Software Group, the popular Waterfall Model is used.[2] Furthermore, the Flight Software Group's process is ISO 9001 certified and, more importantly, has recently been certified as a Capability Maturity Model (CMM) level 3 organization; a first for any NASA organization. The CMM for software was developed by Carnegie Melon's Software Engineering Institute and has become an internationally recognized standard for evaluating software development processes where a level 5 is the highest certification a software development organization can achieve.[3] The principle function of the Flight Software Group is to develop flight critical software for embedded systems, requiring all software development processes to be stringent with software quality assurance functions underlying all activities of software development. The Flight Software Group traditionally views software engineering as the establishment and use of sound engineering processes to develop reliable software based on human processes and thinking that works on real machines. Furthermore, software engineering is also viewed as the design and implementation of a set of user requirements into software using sound engineering processes. The emphasis here is that the Flight Software Group uses sound software development processes based on empirically proven and sound practices. Reference 2 presents a more detailed account of software engineering.

Accomplishments

Status of Design, Development, Implementation, and Testing

During the initial phase of this CDDF project, control objectives were obtained by information gained from knowledge acquisition sessions from all accessible sources within the Avionics Department and the Space Transportation Directorate at MSFC. The objective was to acquire all relevant engine controller information, design variables, and data to generate the training databases to accommodate the chosen SCT of this effort. For the BNN modules, the network structures were developed in accordance with control objectives and design information gathered. Statistical/numerical techniques were performed to calculate the required parameters for the BBN (e.g., prior conditional probability values for the probability-conditional link matrices). Using software engineering guidelines based on the Flight Software Group processes, an object-oriented analysis and programming was performed for design and development of the overall BBN architecture, interfaces, and software executive. Reasoning for use of object-oriented programming is largely based on its main features of abstraction, encapsulation, modularity, and hierarchy. These not only allow for better overall design but also help address the key goals of this effort. Currently, the work has been fully developed and is hosted on an MRECS II processor. The engine start requirements are implemented as four BBNs and are as follows:

A. Initiate liquid oxygen (LOX) flow to thrust chamber assembly (TCA).
   1. Open main oxidizing valve (MOV) and check if MOV switches are disqualified.
      a. If yes, continue to wait 0.5 s then continue to open main fuel purge valve (MFPV).
      b. If no, start 0.5-s timer then continue until timer has expired.
         i. If yes, then continue to open MFPV.

ii. If no, then do switches indicate valve is open?
1. If yes, then continue to open MFPV.
2. If no, then return to timer step a.

B. Initiate spin start.
1. Open MFPV/open SV09 (facility shutoff valve) and begin 1-s timer.
2. Has timer expired?
a. If yes, then proceed to S/D.
b. If no, is fuel purge pressure (Pr), gas generator (GG) pressure chamber (PC), and fuel pump discharge (DS) Pr above minimum?
i. If yes, then continue to open ignition fuel valve (IFV).
ii. If no, then return to timer step 2.

C. Initiate triethenal aluminum and triethenal boron flow to TCA.
1. Open IFV and begin 0.5-s timer.
a. If timer expires, then proceed to S/D.
b. If timer does not expire, then is main combustion chamber (MCC) PC above minimum?
i. If yes, then continue to fire igniter.
ii. If no, then return to timer step a.

D. First initiate fuel flow to TCA.
1. Open the main fuel valve MFV and begin the 0.5-s timer.
a. If timer expires, proceed to S/D.
b. If Timer does not expire, proceed with MCC PC.
2. Are MCC and PC above minimum?
a. If yes, continue to close oxidizer bleed valve (OBV).
b. If no, go back to step 2 (0.5-s timer).

E. Terminate LOX bleed.
1. Close OBV and check if OBV switches are disqualified.
a. If yes, wait 0.1 s and continue to initiate fuel flow to GG.
b. If no, then begin 0.1-s timer.
i. Has timer expired?
1. If yes, then continue to initiate fuel flow to GG.
2. If no, do switches indicate valve is closed?
a. If yes, then continue to initiate fuel flow to GG
b. If no, return to step i (Has timer expired?).

F. Initiate Fuel Flow to GG.
1. Open GG fuel valve (GGFV) and begin 0.2-s timer.
a. If timer expires, then proceed to S/D.
b. If timer does not expire, then continue to open GGFV.
2. Is GGFV DS Pr above minimum?
a. If yes, then continue to open MOV valve.
b. If no, return to timer step 2.

G. Initiate LOX flow to GG/terminate spin-start flow.
1. Fire igniter/close GLPV, MFPV, and SV09.

H. Verify ramp to main stage (MS).
1. Wait 0.2 s and begin ramp up timer (1.1 s).
2. Has timer expired?
a. If yes, then initiate MS phase.
b. If no, then is GG Pc below minimum and is MCC PC below minimum?
i. If yes, then initiate S/D.
ii. If no, then return to timer step 2.

Step A comprises BBN one. Steps B through D comprise BBN two. Step E comprises BBN three. Steps F through H comprise BBN four. Offline testing has been performed on BBN one through three. All BBN's have been fully verified. A C^{++} compiler was procured and installed in the MRECS II development workstation in order to test the BBN in the environment. The MRECS II was executed in parallel with MRECS via virtual memory (fig. 1). However, the implementation was in building 4487. After the software was verified, all developed software was integrated with the MC–1 engine model supplied by the Transportation Directorate. MRECS II was a separate effort by Crook and other Avionics Department personnel.[4] Full testing included utilizing all capabilities in the simulated environment, verifying all communications, data recording, benchmarking as much as possible with similar MRECS functions, and verifying principle objectives.

Turbine Technologies SR–30 Engine

Soft computing technology hardware-in-the-loop experiments were conducted using Turbine Technologies' model SR–30 turbojet engine. The demonstration engine is located at UA's, Aerospace Engineering & Mechanics Department and consists of the turbojet engine manufactured by Turbine Technologies in its custom enclosure. The enclosure includes a control panel for engine operation and monitoring and a personal computer based data acquisition unit for measuring the engine operating conditions (fig. 2).

The SR–30 engine has a single-stage radial-flow compressor with a maximum pressure ratio of PR=3.4, single-stage axial-flow turbine, and reverse-flow annular combustion chamber and it operates obeying the Brayton thermodynamic cycle in the same fashion as the large turbojet engines. The engine as produced by Turbine Technologies includes many pressure and temperature sensors, a load-cell for thrust measurements, a custom motor winding for reading the engine RPM, and a fuel-flow-rate measurement system to monitor/measure the operating parameters of the engine. The engine generates 20 lbs of thrust at 90,000 RPM while ingesting m=1.1 lb/s of air. The engine has a length of 10.75 in, and the exit exhaust diameter of D_{exit}=2.25 in.

The engine available from the company is instrumented with pressure transducers in the compressor inlet and exit, in the combustor, in the turbine exit, and in the thrust nozzle exit. It also has K-type thermocouples in the compressor inlet and exit, in the turbine inlet and exit, and in the thrust nozzle exit. The engine available at UA was also equipped with a National Instruments (NI) PCI 4351, A/D board with 24 bit resolution for 16 analog inputs with a 60 samples/s capability, and an NI Virtual Bench Logger data acquisition program for monitoring the measured parameters on a personal computer.

Starting the engine requires an external source of high-pressure air at minimum 100 psi to spin up the engine to approximately 10,000 RPM. Subsequent fuel injection and ignition starts the engine. The fuel-flow rate is controlled by the person operating the engine by the use of a lever, which basically controls

a valve constricting the fuel flow to the engine. The engine idles at approximately 50,000 RPM and the generated thrust increases with the increased RPM. To obtain higher thrust values, the engine operator steadily increases the fuel-flow rate from the idle conditions. In order to stop the engine, the engine is brought to the idle conditions and is run until the exhaust temperature drops under 100 °C to minimize engine damage.

System Modifications

Turbine Technologies' data acquisition system, as purchased and used for classroom demonstrations, is not fast enough for use with the hardware-in-the-loop control algorithms. Since one of the main scopes of the present work is to implement and demonstrate different control algorithms in controlling a turbojet engine thrust, a new data acquisition system and software have been implemented into the existing system to increase the data acquisition speed and to increase the control capability. Additionally, the available system was designed and used to collect and present data and did not have provisions to send signals via computer for closed-loop control applications. Implemented changes include the replacement of the data acquisition board, connection panels for the sensors, addition of a low flow-rate fuel-flow-rate measurement unit, and a fast acting linear servocontroller.

Fuel-Flow-Rate Measurement System

The SR–30 engine as produced by Turbine Technologies uses a pressure transducer together with a calibration curve to determine the fuel-flow rate to the engine. The pressure values read on the fuel line are plotted against the fuel flow spent and also against the RPM of the engine to generate pressure versus the fuel rate and the pressure versus the RPM calibration curves for long-term operations. However, for the present purposes, since the fuel-flow rate is mainly the only control input to control the desired thrust of the engine, a more accurate and faster fuel-flow-rate measurement device has been implemented. The turbine flowmeter installed on the fuel line is an FTI-Flow Technology, Omniflo turbine flowmeter (FTO–2NINBULHA–5) together with an electronic output flow computer (LN–5–C–V1–9) capable of measuring fuel rates as low as 11.3–605 mm/min with a 0.25-percent accuracy, and a 3-ms response time. The output is 0–10 VDC.

Exit Conditions Monitoring

Turbojet propulsion equations used in calculation of the engine thrust requires the measurement of the exit conditions, namely the exhaust total pressure and the total temperature. Although the existing system available from Turbine Technologies incorporated a pressure transducer and a thermocouple for this purpose, the response time for the equipment was rather slow. In order to increase the time resolution of the data obtained at the exit conditions, a new pressure transducer (OMEGA, PX4201–015GV) with 0.2-ms and 0.1-s response times have been incorporated.

Preliminary Test Results

Preliminary tests were made to ensure the safety of the engine under expected operating conditions that could potentially damage the engine. Tests were also made to determine the range of applicability of the one-dimensional turbojet propulsion equations in comparison to the thrust values measured by the load cell.

Thrust calculations were made using the nozzle exit total temperature and total pressure measured data and with the knowledge that the nozzle exit flow is subsonic and exhausts into the ambient atmosphere. One-dimensional propulsion equations used are as follows:

$$Thrust = \dot{m} U_{exit} , \tag{8}$$

where the mass flow rate is calculated using,

$$\dot{m} = \rho_{exit} U_{exit} A_{exit} , \tag{9}$$

and the exit velocity is calculated using,

$$U_{exit} = M_{exit} \sqrt{\gamma R T_{exit}} . \tag{10}$$

Other relations to calculate the exit mach number, exit temperature and the exit pressure, are given with the following equations:

$$M_{exit} = \sqrt{\left[\left(\frac{P_{0exit}}{P_{atm}} \right)^{\frac{(\gamma-1)}{\gamma}} - 1 \right] \frac{2}{\gamma - 1}} \tag{11}$$

$$T_{exit} = \frac{T_{0exit}}{\left(1 + \frac{\gamma - 1}{2} M^2{}_{exit} \right)} \tag{12}$$

and

$$\rho_{exit} = \frac{P_{atm}}{R T_{exit}} \tag{13}$$

where the P_{0exit} and the T_{0exit} are the measured total pressure and the total temperature at the exit, respectively. In these equations, the specific heat ratio is λ=1.4, and the gas constant is R=287 kJ/(kg K).

Figures 4 and 5 show the variations of the total pressure and the total temperature values with time obtained at different locations along the flow path. Figure 5 also shows the RPM, fuel-flow rate and the thrust generated by the engine. Measurements were taken to show that shutting off the fuel-flow rate without cooling the engine at 70,000 RPM steady state operating conditions would not result in temperatures and pressures exceeding the values recommended by the manufacturer. Data show that the moment the fuel is cut off all the pressure and the temperature values steadily reduce without exceeding the values given by the manufacturer. Figure 4 also shows that the compressor inlet temperature measured within the inlet nozzle before the compressor increases to the ambient temperature, since the inlet total temperature is equal to the atmospheric temperature and the flow velocity is much larger than zero at this point.

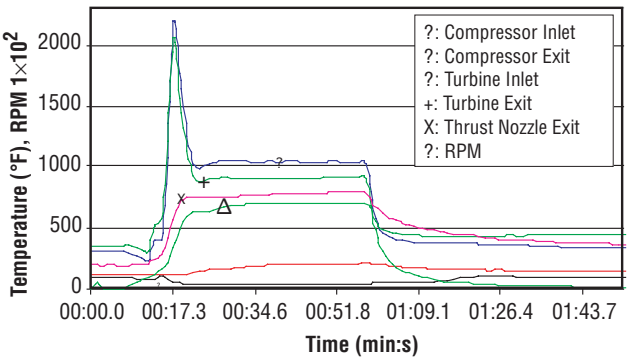

Figure 4. Temperature and RPM versus time.

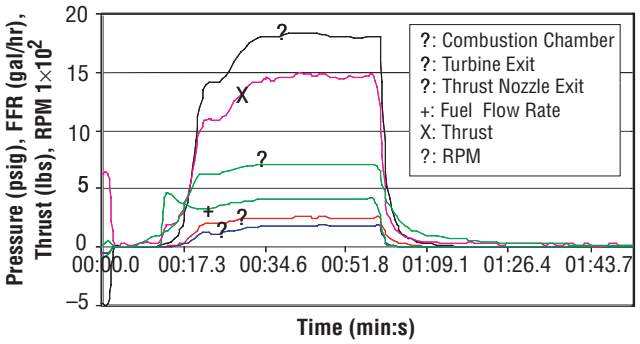

Figure 5. Pressure, fuel flow tate, thrust, and RPM versus time.

Figures 4 and 5 also show that during the start-up sequence, while the total pressure values steadily increase throughout the engine, the total temperature values obtained at the inlet and the exit of the turbine show large variations. This transient rapid increase and the decrease of the temperature is due to the delay of the rotating components of the engine due to their inertia in responding to the sudden introduction of the fuel in the combustion chamber. The starting sequence, which lasts approximately 5 s, is of interest for the operating region and application of the BBN soft control algorithm. Figure 6 shows the measured versus the calculated thrust values obtained during the engine run. The results show that the one-dimensional propulsion equations are adequate for the prediction of the thrust values.

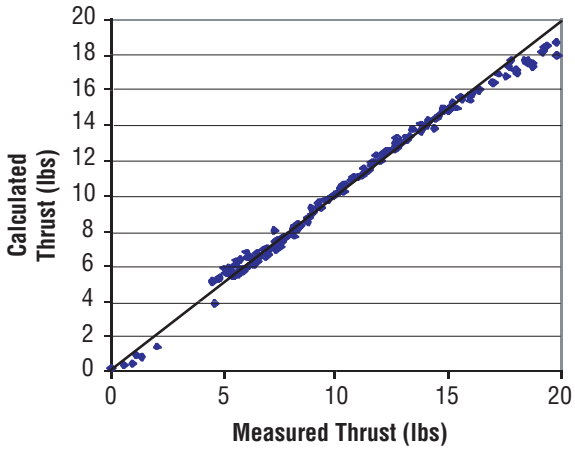

Figure 6. Calculated versus measured thrust.

Planned Future Work

As a result of this effort, new insight has been gained into the behavior and application of soft computing technologies in a rocket engine control environment. The methodology created here will provide a new approach to the area of employing SCT in rapid response engine control systems for future vision vehicles. It will yield better insight into incorporating SCT with proven and practical software engineering methods. It is expected that this effort will demonstrate that by employing SCT, issues in quality and reliability of the overall scheme of engine controller development can be further improved and safety can be further ensured. Furthermore, the use of these SCT is expected to supplement efforts in improving software management, software development time, software maintenance, processor execution, fault tolerance and mitigation, and nonlinear control in power-level transitions, all of which contribute to a better engine control system. It is projected that the final product that this effort will yield is a foundation for a path to further development of an alternative low-cost engine controller that would be capable of performing in unique vision spacecraft vehicles requiring low-cost and advanced avionics architectures for autonomous operations from engine prestart to engine S/D.

The specific planned future work is complete at MSFC. Opportunities for further research and collaboration type work will continue with the Space Transportation Directorate and UA. Aspects of this work may be applied to the Integrated Vehicle Health Monitoring research involving the Summer Faculty Fellowship Program.

Publications and Patent Applications

"Use of Soft Computing Technologies For A Qualitative and Reliable Engine Control System For Propulsion Systems," International Conference on Software and Applications, Anaheim, CA, August 2001.

"Soft Computing For Propulsion Control," 20th Digital Avionics Systems Conference, Daytona, FL, October 2001.

"Soft Computing Engine Controller," 22th Digital Avionics Systems Conference, Indianapolis, IN, October 2003.

"A Test bed for Evaluating Soft Computing Technologies for Rocket Engine Control," 42nd AIAA Aerospace Sciences Meeting and Exhibit, Reno, NV, January 5–8, 2004.

"Soft Computing Applications on SR–30 Turbojet Engine," 1st AIAA Intelligent Systems Technical Conference, Chicago, IL, September 20–22, 2004.

Awards

Best Paper of Session at 22th Digital Avionics Systems Conference.

Director's Commendation for excellence in the Investigation and Application of Methods for Soft Computing for Engine Control, July 2003.

Patents

Submitted for patentability to Office of Chief Patent Council: MFS–32174–1: "Soft Computing Rocket Engine Control Software."

Funding Summary

Table 1 identifies the fiscal year (FY) 2002 funding summary for this project.

Table 1. Project funding summary.

Funding Element	FY 2002 ($)
Fuzzy tech software	3,000
Statistical software	2,000
Hugin Bayesian software	6,000
Misc: C++ software, cables, etc.	2,000
UA	17,000
Total	**30,000**

Status of Investigation

The work at MSFC is complete but the work is still ongoing at UA. A full demonstration of the engine with the MSFC developed algorithms is expected to take place during the summer of calendar year 2004.

References

[1] Pearl, J.: "Probabilistic Reasoning in Intelligent Systems: Networks of Plausible Inference," Morgan Kaufmann Publishers, San Mateo, CA, Inc., 1988.

[2] Humphrey, W.: "A Discipline for Software Engineering," Addison-Wesley, Reading, MA, 1995.

[3] Paulk, M.; Weber, C.; Curtis, B.; and Chrissis, M.B.: "The Capability Maturity Model: Guidelines for Improving the Software Process," Addison-Wesley, Reading, MA, 1994.

[4] Tarrant, C.; and Crook, J.: "Modular Rocket Engine Control Software (MRECS) an Overview of the Architecture and Design," *Internal Report,* Lockheed Martin, August 2001.

Architecture for a Fault-Tolerant Smart Servomotor Controller

Project Number: 02–05

Investigators: David A. Gwaltney/ED17

Purpose

The objective of this Center Director's Discretionary Fund (CDDF) project is to design the architecture for a smart servomotor controller suitable for inclusion in a network of fault-tolerant transducers as a part of a spacecraft avionics system. This effort will provide the design of electronics for the controller of a servomotor-driven actuator that can provide enhanced reliability through redundant capability, voting, and fault-tolerant control approaches. This task will improve the state of the art by leveraging recent advances in smart transducer concepts due to IEEE 1451.3 (draft) and 1451.4 (draft) standards. The controller will have the flexibility to support any type of motor with standard or redundant windings. In addition, fault detection in the motor driver and motor electrical subsystem will be developed for inclusion in fault-tolerant control approaches. Such a controller will be able to support power by wire actuation systems in aerospace vehicles. This project will focus on the design and demonstration of unique components to support the controller.

Background

The requirements for the controller electronics are drawn from sources concerned with the deployment of distributed real-time control systems for safety critical applications. In 1999, the Scalable Fault-Tolerant Intelligent Network of X(trans)ducers (SFINX) project was sponsored by NASA Marshall Space Flight Center (MSFC) to demonstrate an advanced avionics architecture employing a serial communications network between a network capable application processor (NCAP) and transducers. The SFINX concept included triplex redundancy for fault tolerance and intelligence embedded with the transducers. The concept architecture utilized modified specifications from the IEEE 1451.2 and 1451.3 standards to define smart transducer modules that are communication network independent and provide a Transducer Electronic Data Sheet (TEDS) for automated transducer identification and configuration by the NCAP. All communications between transducers and the NCAP is digital, requiring all analog signal conditioning to be done by the smart transducer. NASA MSFC teamed with Oak Ridge National Laboratory and Draper Laboratory on the SFINX project to create specifications and designs for several components to be included in the concept demonstration. A review of reference 1 will provide a further understanding of the SFINX concept. The project was cancelled prior to integration and demonstration of the modules for the SFINX concept. Earlier, Draper Laboratories developed a laboratory demonstration of a network of smart transducer and smart actuator nodes using the controller area network (CAN) bus.[2] This research was motivated by the desire to create affordable hardware redundancy for wider application of ultrareliable systems by creating electronics for transducer interfaces with reduced weight, size, and cost. Additionally, the research included the development of integral voting electronics for the interface electronics to allow distributed voting between input values and output commands. These concepts served as the basis for the SFINX concept.

Research in the development of distributed fault-tolerant systems has been ongoing for several decades, in the United States and abroad. Work in fault-tolerant computing for high-reliability applications has been conducted for more than 30 years at the Jet Propulsion Laboratory (JPL), Draper Laboratories, Carnegie-Mellon University, the University of Vienna, and SRI International, among others.[3] At the University of Vienna, a time-triggered architecture (TTA) was developed and demonstrated in a laboratory by 1997 in a prototype brake-by-wire car. This architecture is based on a time-triggered communication protocol (TTP/C) that was first published in 1993. Reference 4 provides an overview of the TTA and related research by other parties. The TTA leverages decades of research in fault-tolerant systems and is designed with the goal of providing affordable safety critical systems for wider deployment.

Fault-tolerant approaches and redundancy are being used in the design of electromechanical actuators for fly-by-wire aircraft.[5] Redundant systems are an integral part of the Boeing 777 fly-by-wire system.[6] This system makes use of hydraulics as its power source for actuation. The Control Electronics Group at MSFC has been involved in the development of drive electronics for a triple-redundant brushless DC (BLDC) motor for valve actuation in spacecraft propulsion systems. This activity included triple duplication of three drive-electronics assemblies and dual-redundant resolver feedback.

In industry applications, there is interest in using fault-tolerant control in reducing manufacturing downtime or providing a wider margin of safety in products. Recent work has been presented concerning fault-tolerant control of induction motors in a production line.[7] This work applied to systems without redundancy and with the primary goal of saving equipment from damage in the event of control system component failures. Other work has included the addition of a fourth inverter leg that can be switched into a standard three-phase motor drive or always be connected to the neutral in a star winding configuration. After fault detection, this allows a failed inverter leg to be isolated and the fourth to be used to continue drive operation.[8] Additional efforts involve the fast diagnosis of faults using analytical models of the drive and motor in the drive-control software.[9]

The automobile industry is actively pursuing fault-tolerant distributed real-time control systems for applications such as throttle-by-wire, brake-by-wire, and steer-by-wire. These systems will make extensive use of motor-driven actuators and redundant sensor networks. The TTA development was supported by the automobile industry in Europe as a cost-effective means of implementing safety critical drive-by-wire systems. The cost of such systems in the past has been so high as to limit the application of fault-tolerant systems in motor vehicles or light aircraft (not airliners) for civilian use. The TTA is now being aggressively targeted for application to aviation and aerospace systems.

The notion of cost effective fault-tolerant systems can also be applied to existing aerospace systems to provide affordable fault tolerance at all levels. The goal of this effort is to provide a controller that can be a common module in distributed control systems throughout a space vehicle. This controller will have the flexibility to provide fault tolerance and early fault identification in less critical single-string applications, as well as fault detection, isolation, and recovery (FDIR) and support of redundant operation in more critical vehicle systems. This effort will provide a design for electronics to be the controller of a servomotor-driven actuator that can provide fault tolerance through scalable redundancy, voting, and fault-tolerant control approaches.

Approach

The focus of this effort is the development of an advanced embedded controller module for a distributed real-time control system that provides enhanced reliability through fail-silent control modules, scalable redundancy, fault detection and isolation (FDI), and supports fault-tolerant control for recovery in the face of fault conditions. The controller module will provide actuator intelligence for improved command and control capabilities and the flexibility to support any type of electric motor with standard and redundant windings. This will support power-by-wire actuation systems in aerospace vehicles

The benefits of this controller include the capability to tolerate or recover from faults. Current dual-redundant electromechanical actuator controllers detect faults and rollover to the nonfaulty controller without attempting fault isolation and remediation. The developed controller can tolerate sensor faults if redundant measurements are available. Additionally, the controller will provide a fail-silence indication during transient failures and then continue normal operation after a transient passes. The module will have the processing capacity to support early detection of incipient faults through failure identification using parameter estimation techniques. Parameter estimation can detect small changes over time (i.e., overheating, coil failure, and bearing failure). In a redundant configuration, the processing capability for local voting of feedback and measurement signals reduces the burden on higher level system control processors. The control module will provide the flexibility for module replications, fault detection, and failure modes as required by the application.

This effort first developed an overall architecture design to provide all the functionality and benefits mentioned in the paragraphs above. There is an extensive body of work concerning the design of fault tolerance via redundancy. Reference 10 is an excellent reference on the topic. Many of the concepts used in the design of the architecture came from this source. Because the design of such systems is well developed, the implementation of the hardware to demonstrate redundant operation is given a secondary focus in this work. The effort will leverage the recent developments in smart transducer technology through use of the IEEE 1451.2, 1451.3, and 1451.4 standards with respect to communication network independence, digital data transmission, digital control commands, and Transducer Electronics Data Sheets for plug-and-play operation. The architecture is described in the next section. However, the implementation of this architecture in redundant operations is deferred to development and demonstration under the Propulsion High Impact Avionics Technology (PHIAT) Project currently supported by the Next Generation Launch Technology Program at MSFC.

The primary focus of this effort is the investigation fault detection techniques suitable for use in fault-tolerant control approaches. Fault-tolerant control combines identification of faults with reconfiguration or adaptive strategies to maintain stable control. Many fault detection approaches utilize a system model, estimator, or observer to identify off-nominal operating conditions. This effort utilizes parameter estimation to detect both incipient and abrupt system faults that affect the operation of a controlled BLDC servomotor.[11] Parameter estimation was chosen as the method for fault identification because indirect adaptive control also requires estimation of the parameters of the controlled system.[12] Common use of estimation techniques makes it possible to implement a more compact fault-tolerant and adaptive controller design.

Hardware implementation is primarily concerned with demonstration of the controller module characteristics and capabilities in a lab environment. Therefore, the design of the architecture extensively utilizes commercial electronic and electromechanical components, but the architecture is designed with the capability to be targeted for a future flight demonstration.

Accomplishments

The core of the proposed controller module is a dual-processor design illustrated in figure 1. This represents the basic elements of a fail-silent controller in that the module will not produce a command output in the event of a failure, but will only provide a fail signal indicating that one or both processors has failed. One processor is responsible for producing the required commands for the actuator while the other is responsible for executing the same control algorithm to provide a second command for comparison. In this configuration, the two calculated control outputs must agree or the module will be failed and a fail-safe condition must be reached. Each processor has the capability to invoke the fail-silent condition. The switches will be configured to be normally open to prevent

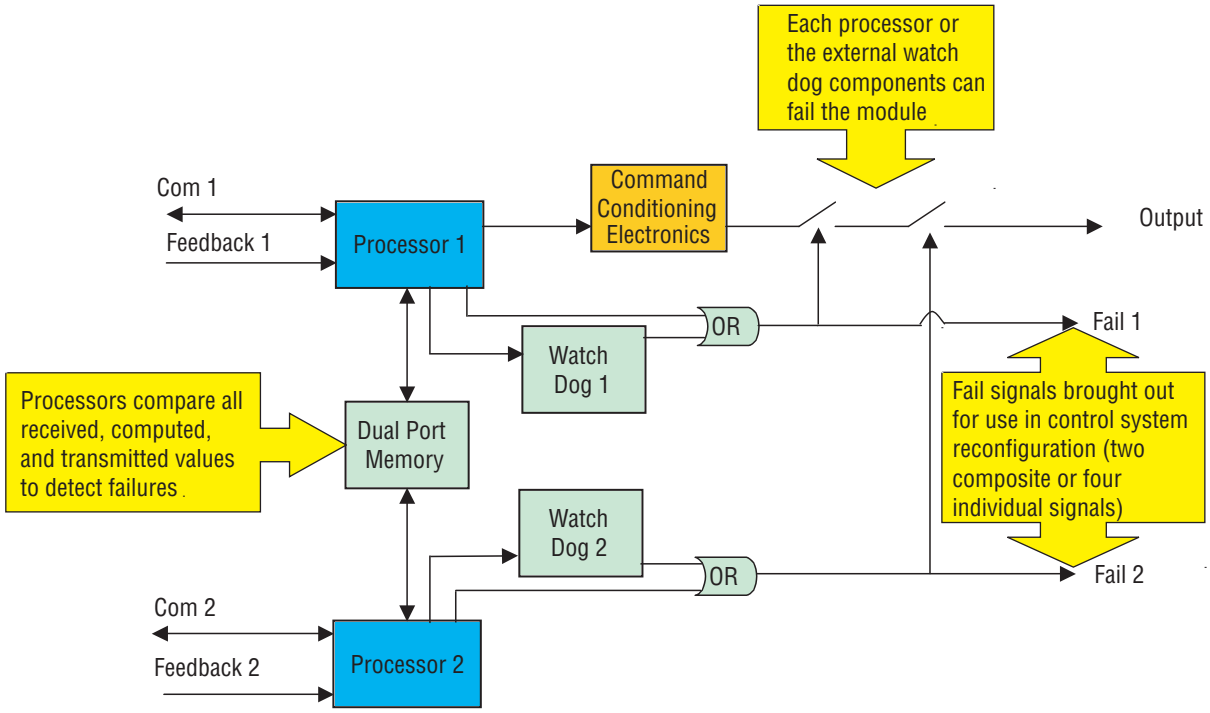

Figure 1. Core fail-silent controller structure.

any control output signal from being generated by the board until both processors are functioning properly. Each processor will receive redundant commands and feedback from redundant sensors and these values will also be compared for agreement. In a fully redundant configuration, each processor will receive data from all the sensors available. Both processors will compare sensor and command values and the results of the comparisons will be compared. The dual-port memory facilitates the exchange of data for comparison and for synchronization of the processors. Each processor will have its own clock in a fully redundant configuration. Therefore, synchronization of control system updates will need to be made. Further, each process will have a watchdog timer to monitor the processor for lock-up conditions or other malfunctions that prevent it from updating the control command at the required interval. The watchdog timers can also fail the module. The processors will operate from the same power supply, since a power supply failure for either processor means the module must be failed. If required, this module can implement design diversity through the use of different processors or different software designs that provide the same results given the same input data, or both methods of introducing diversity can be employed.

The controller module description and figure are a representative overview of the core controller module. The processor may be a digital signal processor (DSP) or some other suitable processor. Peripherals such as data converters or digital input/output may be integral or external. In deployment, there are many practical issues that must be addressed. The module will likely not be failed immediately upon detecting disagreement, but only after a series of disagreements are detected up to a threshold imposed by the particular control application. Reachable fail-safe conditions will need to be part of the overall system design. The module must be designed so that it will not produce unsafe conditions in an unpowered state or at startup. Due to cost, hardware and software design diversity may not be required or desired. Initially, the controller module will be implemented without design diversity to keep cost low.

The full configuration of a single module in a configuration without controlled system redundancy is shown in figure 2. In this case, a single module is shown controlling a single motor. The redundancy of the fail-silent controller module provides many advantages over a controller without redundancy in a similar application. The fail-silent controller module can utilize redundant sensors if available, or provide redundant measurement of signals from singular sensors. In the event of sensor failure, one processor can still receive sensor values from the other. If redundant measurements of singular sensors are utilized, the controller can once again obtain measurements made by the other controller if a sensor measurement channel fails. A broken connection is a likely failure in this scenario. If the criticality of the application requires it, both processors can make measurements from redundant sensors and first locally vote the values before comparing them with the voted values.

The configuration in figure 2 allows the implementation of fault detection techniques via parameter estimation by providing motor-state feedback in the form of motor-phase voltage and current, as well as, motor shaft speed. Such fault detection techniques can be executed using a single processor, as will be shown later, but the redundant architecture provides a means of verifying the existence of a fault through comparison of fault detection results.

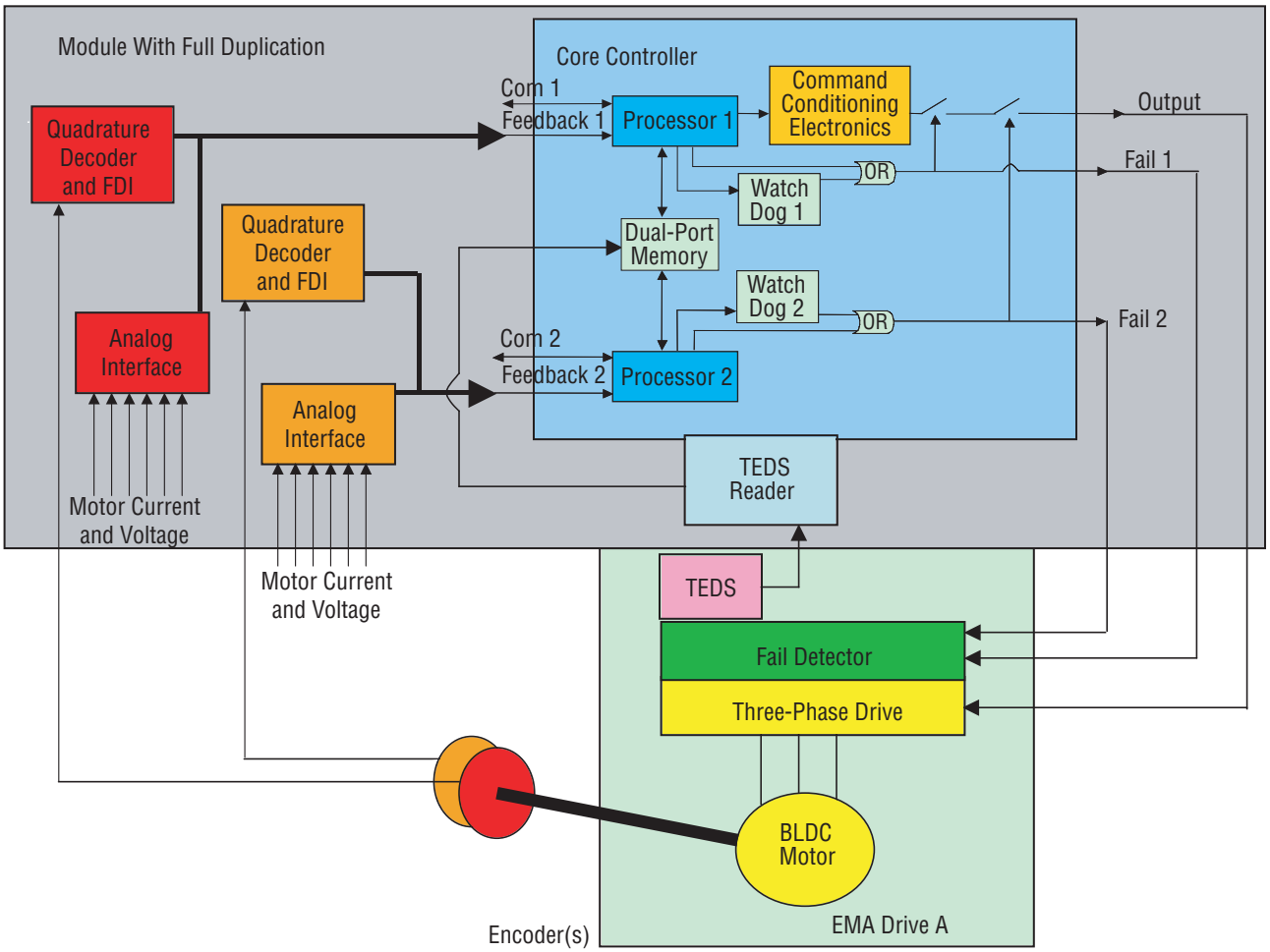

Figure 2. The controller module architecture in a configuration without redundancy in the controlled system.

The controller architecture leverages the concepts in the IEEE 1451 standards by providing local conversion of analog data, digital communication, and support for TEDS. Most processors come equipped with serial communication interfaces adhering to a variety of electrical standards. Many now come standard with a CAN controller. Such a serial interface can provide digital communications with other smart transducers or a higher level controller. Communication bus independence is achieved by using a processor with onboard timers, an external memory interface, and external interrupt pins that can be integrated with a communication controller of choice. For instance, the TTP/C communication chip developed for use in the TTA has a host processor interface designed to accommodate a device with a 16-bit (or greater) external memory interface, one external interrupt, and one 16-bit internal timer. The same basic controller module design can easily be used with the appropriate communication controller for a given system or application. The controller module will have a TEDS reader interface to support the use of a common control module for a variety of actuators within a given system. The TEDS memory that is part of the actuator interface to the controller will contain information designating the actuator specifications and controller gains required. This way, one common controller module can configure itself to control a variety of actuators without the need for different versions of controller software. Since the actuator TEDS include the gains (configuration parameters) for the control algorithm required for that actuator, no software modification on the controller is required when actuators are swapped out.

The controller module is capable of supporting any level of redundancy desired. Figure 3 illustrates the application of the controller module to a dual-redundant configuration common in control of actuators in space vehicles. Since the controller module itself is a dual-redundant configuration, this is called a dual-dual redundant controller. A triple-redundant configuration is depicted in figure 4. In figure 4, commands are received from the triple-redundant bus and voted onboard the controller. This voting may be done in hardware or by the processors in the controller module. Another possible configuration provides each controller with commands from two of the busses or from a single bus. The level of reliability required by the application will dictate the level of redundancy. This configuration depicts hybrid redundancy in which triple voting is used to mask faults, but the capability exists to reconfigure the system to continue operation in the event of module failure. The voter can switch spares when modules fail or the voter can shift to agreement mode for comparison of two modules or pass-through mode when only one good module remains. These modes represent degraded operation in this case, but provide a means of limping

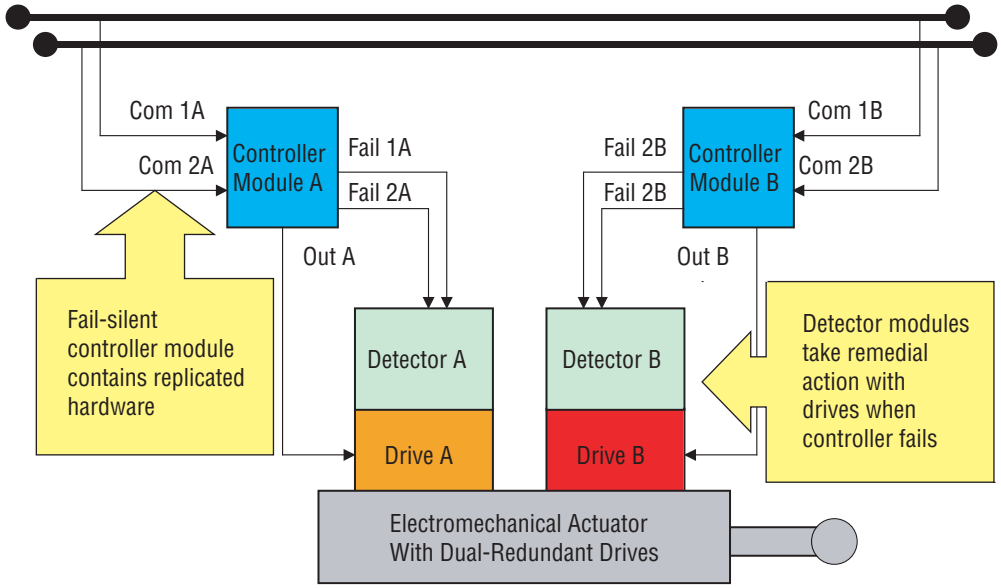

Figure 3. Dual-dual redundant EMA controller with dual-redundant communication bus.

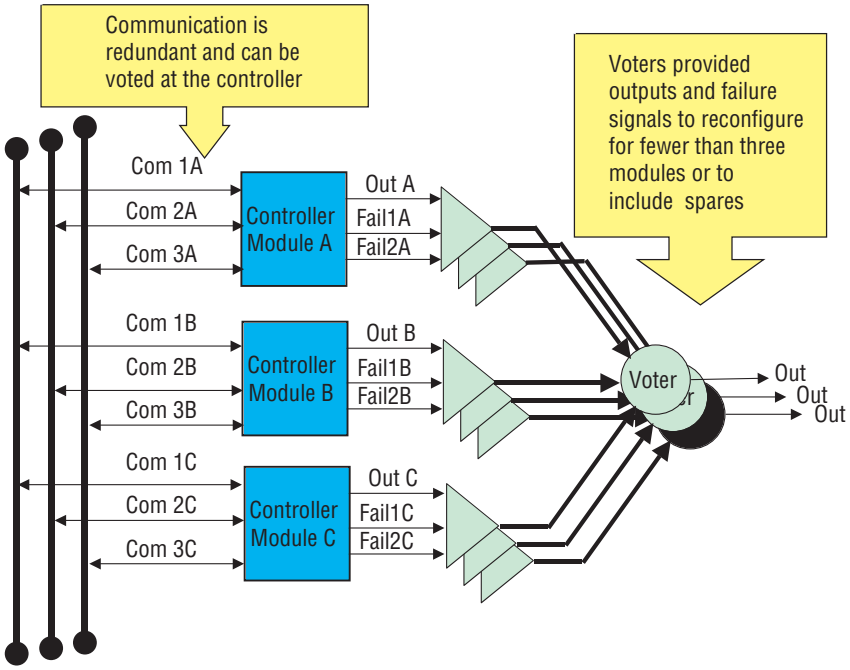

Figure 4. Hybrid redundancy using fail-silent modules and triple voting with triple-redundant communications bus.

home in the event of multiple failures. These schemes and others are fully described in reference 10.

As described previously, the method of FDI investigated in this effort uses parameter estimation. For the lab experiments in FDI for a BLDC motor, no redundancy was implemented in the controller. The experimental configuration is illustrated in figure 5. A DSP is used as the processor for implementation of control algorithms and FDI algorithms. A field programmable gate array (FPGA) is used to implement a pulse-width modulated (PWM) digital command to the motor driver and a quadrature signal decoder for motor-shaft velocity feedback. An encoder on the motor shaft provides relative shaft position. This data can be used to derive the shaft velocity. An external analog-to-digital converter is used to make motor voltage and current feedback available for use in control and FDI. The motor controller consists of an inner current control loop and an outer speed control loop. Both control loops are implemented on the DSP and the controller update rate is 2,000 Hz. The average phase voltage and current are used in the FDI algorithm along with the motor speed feedback. The motor shaft is connected to a dynamometer to provide a controllable load for the motor.

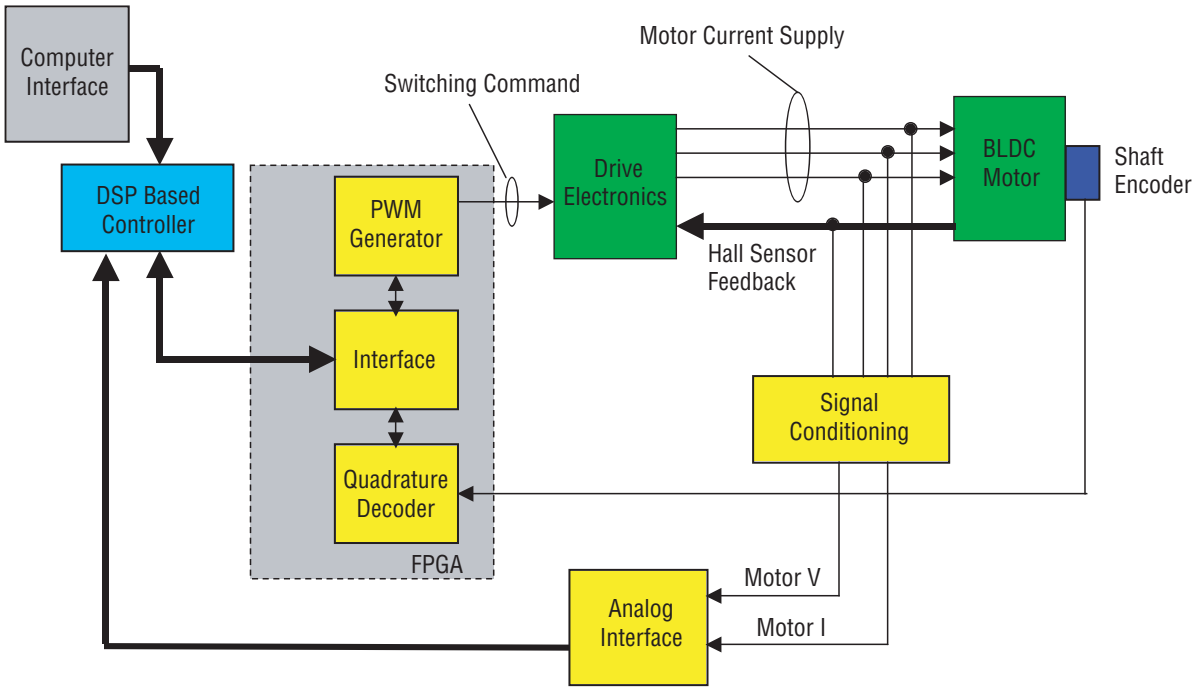

Figure 5. Fault detection and isolation experimental configuration.

Pictures of the experimental configuration are provided in figures 6 and 7. A printed circuit board that replaces the prototype controller in figure 6 has been designed and fabricated. It was not available in time to be used in the experimental trials for FDI. This board is a flexible platform that will be used in future fault-tolerant control experiments and is shown in figure 8.

The FDI approach follows the approach described in reference 11. In this paper, FDI using parameter estimation is applied to a simulated motor operated in open-loop mode and an actual motor operated under closed-loop position control. In this effort, the parameter estimation technique is applied to the motor under closed-loop current and velocity control, as described above. The FDI algorithm uses the measured motor voltage, current, and speed, along with an analytical model of the motor electrical and mechanical subsystems to estimate unmeasured parameters in the motor and driver. The measured data represent the standard measured values used in motor speed control. The motor electrical system parameters estimated are the combined phase resistance and back-emf constant (Ke). The motor mechanical subsystem parameters estimated are the load torque (Tl), load intertia (J), viscous friction (Bv), and coulomb (static) friction (Bc).

One fault identification experiment performed to detect incipient faults used a variable resistance placed in one phase of the BLDC motor. This resistance was varied between 0 and 2 ohms and the estimated parameters clearly indicated the change in phase resistance. Because the estimated resistance is an average for the three phases, the value does not increase by the change induced in one phase, but by a fraction of that change. The results of this experiment are shown in the estimated parameters in figure 9, and the associated measured data is shown in figure 10. Measured data in these plots are noisy due to the wire-wrapped connections between the DSP and the peripheral devices in the controller. The printed circuit board implementation of the controller should have considerably less noisy measurements when used in the experimental system. In figure 9, the no fault condition is depicted by the dotted line, with the 1- and 2-ohm conditions depicted by dashed and solid lines respectively. In each case, the fault is introduced at time equal to 20 s in the plots. In figure 9, note that the estimated resistance shows a clear divergence after 20 s, while the other estimated parameters remain relatively steady over the 50 s displayed in the plots. There is a constant offset visible in the estimated mechanical parameters between the nominal case and the cases where faults are induced. However, these offsets are established earlier in the experiment than 20 s, and remain constant during the remainder of the experiment. Note that there is no significant change in the measured values plotted in figure 10. A small change in phase resistance like this could be an early indication of the motor overheating, or an impending failure in a phase. The FDI approach can therefore be used to detect faults that are slow in developing, but would not be detectable in the measured data.

Another fault experiment performed induced a broken motor phase fault; inserting a circuit breaker in one phase connection between the motor and the driver can accomplish this. The measured and estimated parameters are plotted in figure 11. The fault is induced at time equal to 20 s by opening the breaker. Note that the control system continues to maintain speed

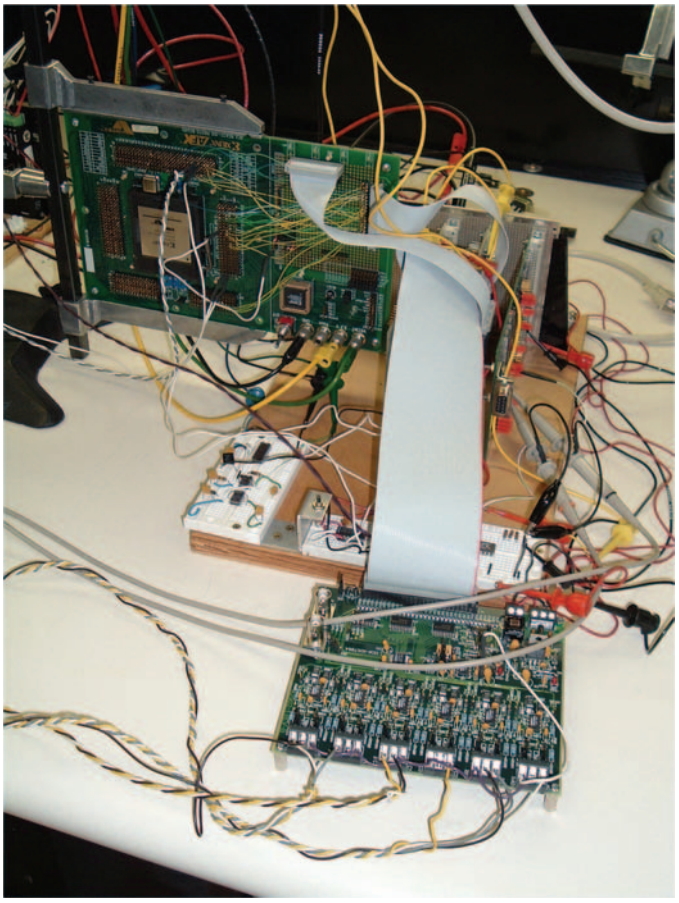

Figure 6. Protoype controller for fault detection and isolation experiments.

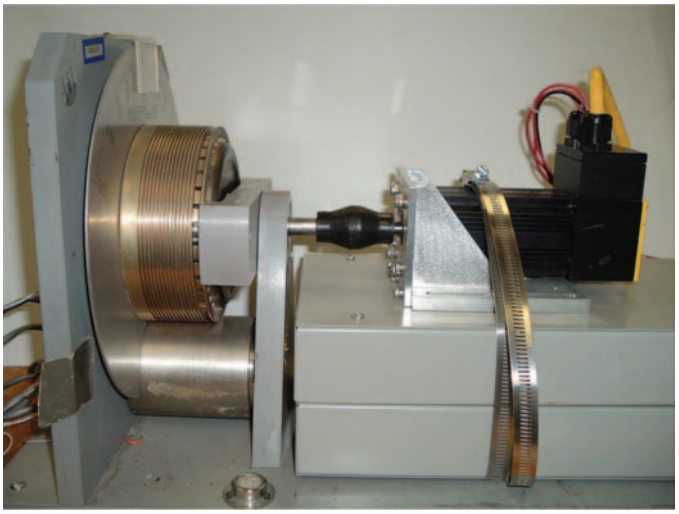

Figure 7. Brushless DC motor and dynamometer.

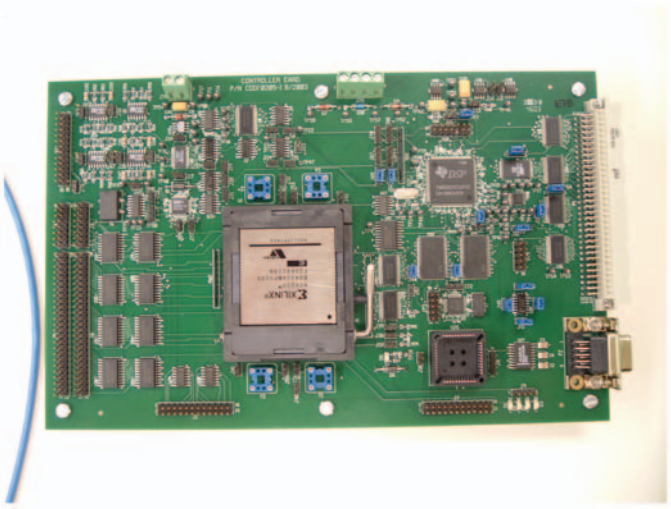

Figure 8. Flexible controller printed circuit board.

control. When such a fault occurs while the motor is spinning, the load inertia allows the controller to keep the motor spinning with only a little degradation in speed performance. If the motor were halted, it would probably not start moving again. In a deployed system, such a fault may not be noticed until the motor is halted and no longer spins, despite being commanded to turn. The estimated parameters show a rapid and distinct divergence of the estimated motor resistance and a notable change in the estimated Ke. Even though the motor voltage and current clearly change, they are not out of the valid range. Additionally, they have values that are considered part of the normal range during operation over a variety of motor speeds at a given load. This makes it difficult to use these measured parameters to detect faults early. However, the estimated parameters should remain nearly constant unless there is a fault. The increases in resistance and Ke provide an early warning before the motor fails. This allows a fault recovery strategy to be used, while acceptable control of the motor is still maintained.

Other experiments were performed in which the characteristics of the mechanical system were changed. In these experiments, the load is changed by 30 and 60 percent at time equal to 20 s by changing the control voltage on the dynamometer. In figure 12, the no fault condition is depicted by the dotted line, with the 30- and 60-percent increased load conditions depicted by dashed and solid lines respectively. Note that the estimated electrical parameters (R and Ke) in figure 12 stay constant, while the estimated mechanical parameters are affected. The measured values are shown in figure 13. These show an increase in current after 20 s, while the other parameters stay the same. The increase in current indicates an increase in the torque produced by the motor in response to the change in load, but does not indicate which load components have changed. The estimated parameters show that the increase is in the load and friction components, not in the inertia. This is consistent with the use of the dynamometer as a load for the motor. The dynamometer uses eddy current effects to increase the load on the motor.

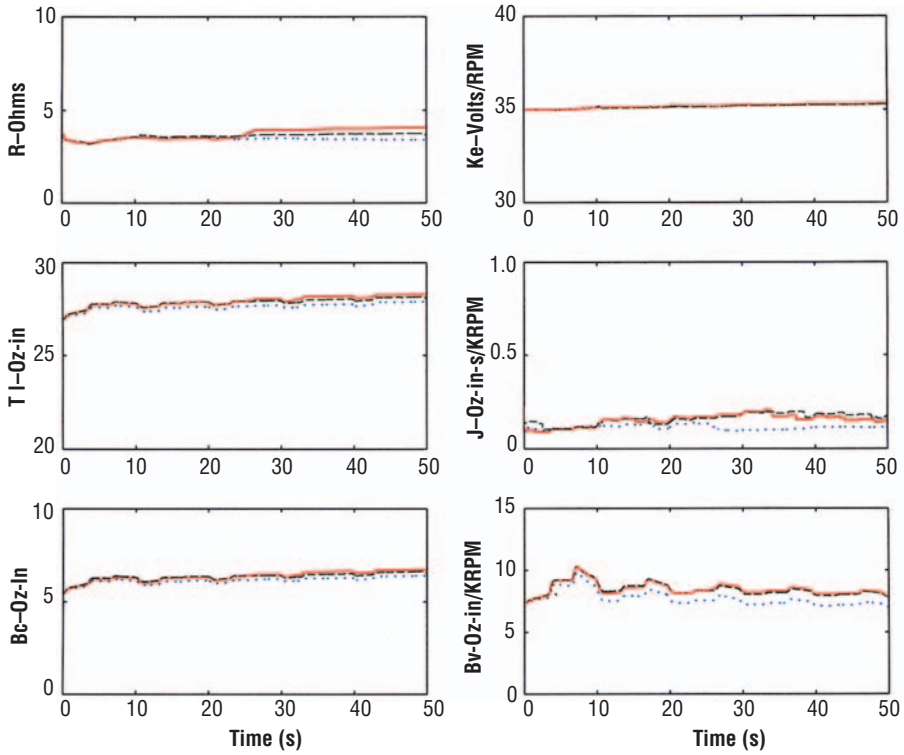

Figure 9. Estimated parameters for the induced increased phase resistance fault in the controlled motor. The no-fault case is depicted by the dotted (...), the induced 1-ohm fault case is depicted by the dashed (--) line, and the 2-ohm fault case is depicted by the solid line.

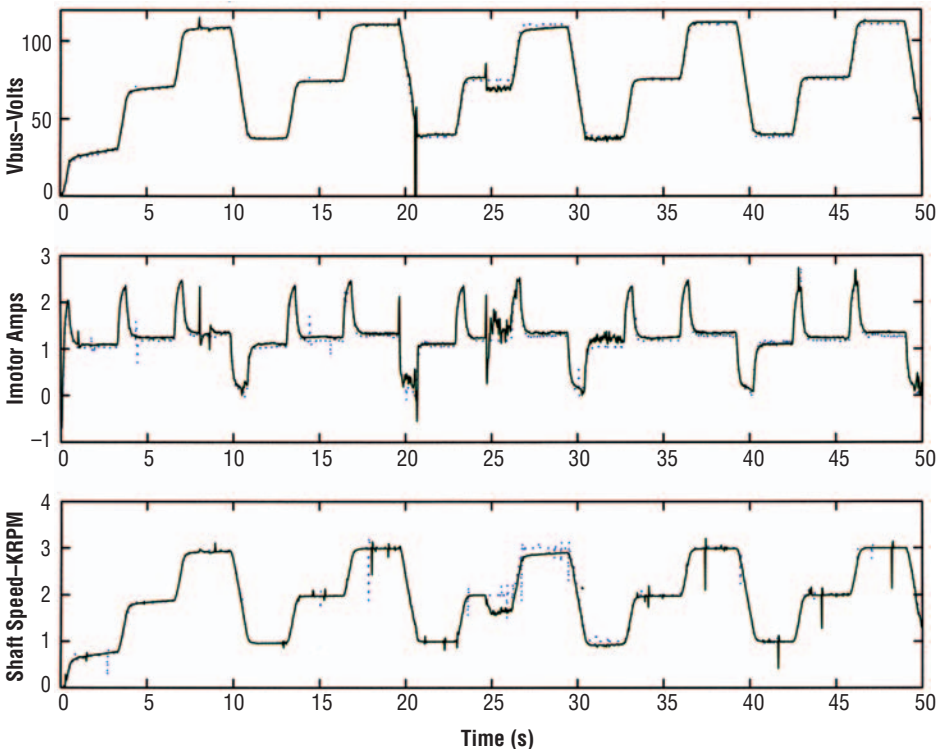

Figure 10. Measured parameters for the induced increased phase resistance fault in the controlled motor. The no-fault case is depicted by the dotted (…) line and the 2-ohm fault case is depicted by the solid line.

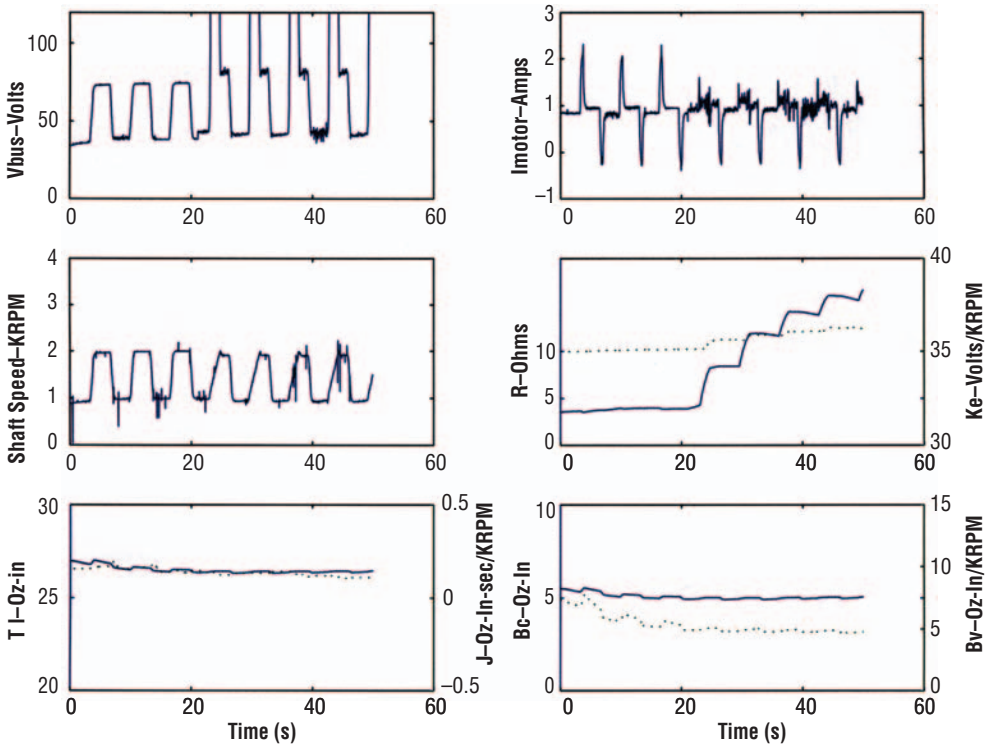

Figure 11. Measured and estimated parameters for the broken-phase fault case during motor closed-loop control.

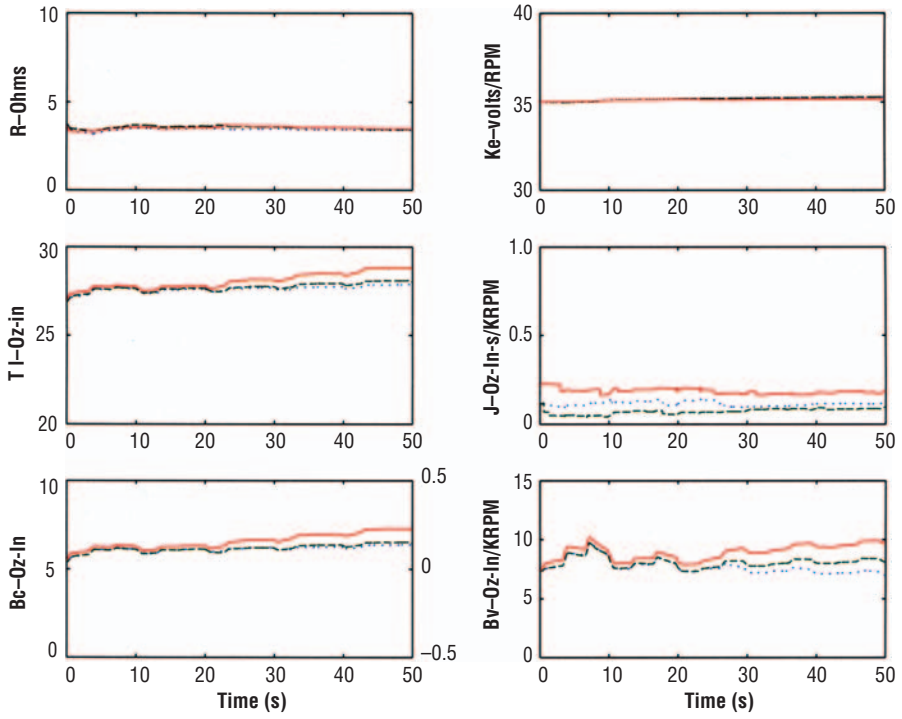

Figure 12. Estimated parameters for the induced increased load fault in the controlled motor. The no-fault case is depicted by the dotted (…) line, the induced 30-percent increased load case is indicated by the dashed (--) line, and the 60-percent increased load case is depicted by the solid line.

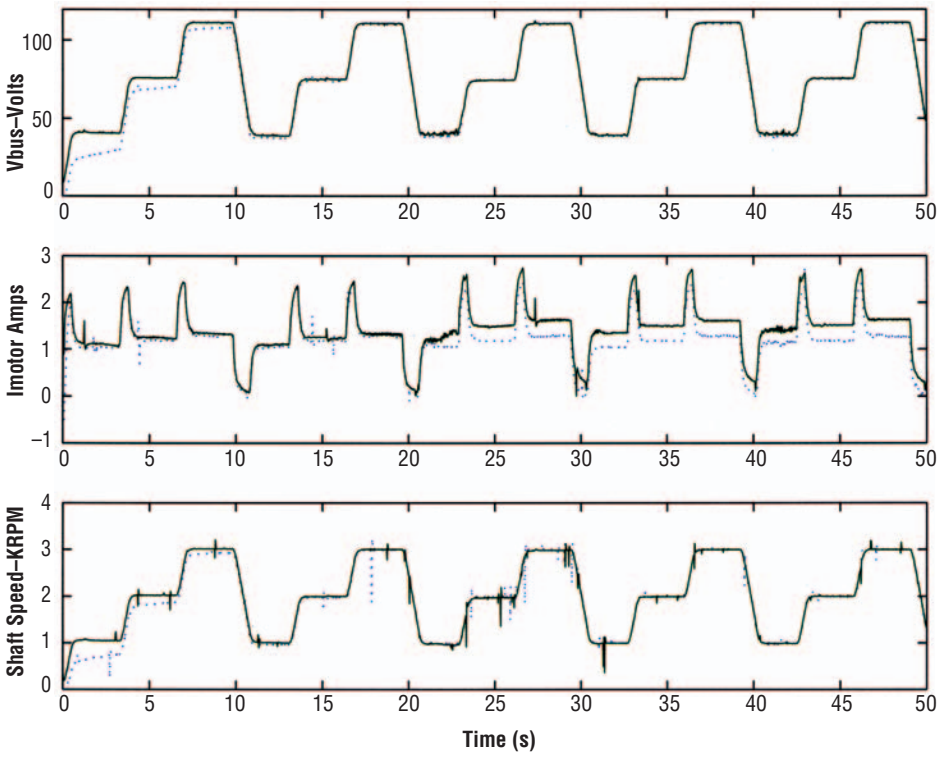

Figure 13. Measured parameters for the induced increased load fault in the controlled motor. The no fault case is depicted by the dotted (…) line and the 60-percent increased load case is depicted by the solid line.

Changes in the control voltage primarily affect Bv and total Tl applied to the motor. Bc shows changes, but is not affected as much as the viscous friction. This data shows that changes in the mechanical subsystem can be separated from changes in the electrical subsystem using parameter estimation.

While the use of parameter estimation for FDI is clearly successful, the implementation of parameter estimation is still an art. The estimation algorithm parameters must be tuned similar to the way a control system must be tuned. Also, parameter estimation is sensitive to initial conditions, so there must be knowledge of reasonable initial values for the parameters of the system to be controlled. There is a clear opportunity for development of procedures to streamline the process of deploying an FDI algorithm based on parameter estimation.

Planned Future Work

The results of this effort will be leveraged in the deployment of a fault-tolerant smart servomotor controller as part of a fault-tolerant distributed real-time control system. Currently, it is expected that such a controller will be developed and implemented as part of the Propulsion High Impact Avionics Project funded by the Next Generation Launch Technology Program at MSFC.

Publications and Patent Applications

The work concerning fault detection using parameter estimation will be published as a NASA Technical Memorandum.

Funding Summary

This effort was originally authorized $25,000 in fiscal year (FY) 2002 funds and $20,000 in funds for FY 2003. All funding was expended during the execution of this task.

Status of Investigation

The investigation is complete.

Acknowledgments

The investigator would like to thank Keary Smith for his help with VHDL coding and the design and configuration of experimental hardware. Additionally, the investigator would like to thank Randy McNichol and David Howard for their circuit designs that were incorporated in the experimental hardware.

References

[1] Hammett, R.C.: "Networking Intelligent Components to Create Intelligent Space Craft," IEEE Aerospace Conference, Big Sky, MT, March 2001.

[2] Hammett, R.C.: "Ultra-Reliable Real-Time Control Systems-Future Trends," *IEEE AES Systems Magazine*, pp. 31–36. August 1999.

[3] "The Evolution of Fault-Tolerant Computing: In the Honor of William C. Carter," A. Avizienis, H. Kopetz, and J.C. Laprie (eds,), *Dependable Computing and Fault-Tolerant Systems*, Vol 1, Springer, Vienna, New York, 1987.

[4] Kopetz, H.; and Bauer, G.: "The Time-Triggered Architecture," *Proceedings of the IEEE***,** Vol. 91, Issue 1, pp. 112–126, January 2003.

[5] Raimondi, G.M.; et al.: "Large Electromechanical Actuation Systems for Flight Control Surfaces," IEE Colloquium on all Electronic Aircraft, 1998.

[6] Yeh, Y.C.: "Triple-Triple Redundant 777 Primary Flight Computer," Proceedings IEEE Aerospace Applications Conference, 1996.

[7] Thybo, C.: "Fault-Tolerant Control of Inverter Controlled Induction Motors," Ph.D. Thesis, Aalborg University, January 2000.

[8] Bolognani; et al.: "Experimental Fault-Tolerant Control of a PMSM Drive," *IEEE Transactions on Industrial Electronics*, Vol. 47, No. 5, October 2000.

[9] Ribeiro, R.L.A.; et al.: "Fault Detection in Voltage-Fed PWM Motor Drive Systems," IEEE 31st Annual Power Electronics Specialists Conference, Vol 1, 2000.

[10] Johnson; and Barry, W.: "Design and Analysis of Fault-Tolerant Digital Systems," Addison-Wesley, 1989.

[11] Moseler, O.; and Isermann, R.: "Application of Model-Based Fault Detection to a Brushless DC Motor," *IEEE Transactions on Industrial Electronics,* Vol. 47, No. 5, pp. 1,015–1,020, October 2000.

[12] Gwaltney, D.A.: "Test Platform for Advanced Digital Control of Brushless DC Motors," *NASA TM–2002–211917*, MSFC CDDF Final Report, Project Number 00–04, MSFC, Huntsville, AL, August 2002.

Adaptive Structures Applications in Microgravity Vibration Control and Isolation

Project Number: **02–08**

Investigators: **Christy Gattis/ED21**
Greg Frady/ED21
John Jennings (Part of Year 1 only)/ED21
Steve Shepard/The University of Alabama
J. Wang/The University of Alabama

Purpose

A main function of the *International Space Station* (*ISS*) is to serve as a microgravity platform for performing laboratory experiments. Some of these experiments have the additional requirement of a calm, vibration free environment. Due to a variety of disturbances on the experiment shelves, from both steady state and transient sources, the acceleration levels on a particular shelf may exceed the requirements of some of these experiments. To address this issue, methods are needed to prevent these vibrations from impacting experiments on the *ISS*. Therefore, the purpose of this work is to examine new methods of using adaptive structures to apply vibration isolation and control in a microgravity environment. To that end, both active vibration control methods that implement piezoelectric actuators and new passive vibration control methods are being studied. These methods are being applied to a shelf that simulates one used for experiments on the *ISS* as well as to simulated components that might be located on these shelves. The studies conducted under this effort involve analytical modeling and experimental evaluations. Results for the second year of this effort, which include the development of a control system and experimental results demonstrating a 20-dB reduction in vibration levels, are described along with plans for future research.

Background

As noted in the first year report, there are two vibratory transmission paths that must be considered in controlling the vibrations that can impact experiments on the *ISS*, as illustrated in figure 1. One path is between the rack and the *ISS* structure. To mitigate vibrations along this path, some racks use the Active Rack Isolation System (ARIS). The other path is at the shelf level and occurs within the rack. These vibrations are transmitted across the same shelf or into the rack and subsequently onto another shelf. For example, a motor automating an experiment can produce vibrations that enter other shelf components requiring a calm environment. The vibrations generated by this motor can also enter the rack and disturb vibration sensitive experiments located on other shelves. For example, the Materials Science Research Rack (MSRR–1) includes two experiment modules that can be operated simultaneously. There is the potential for operations associated with one of these experiments to impact the other experiment. This same issue may arise on other *ISS* racks.

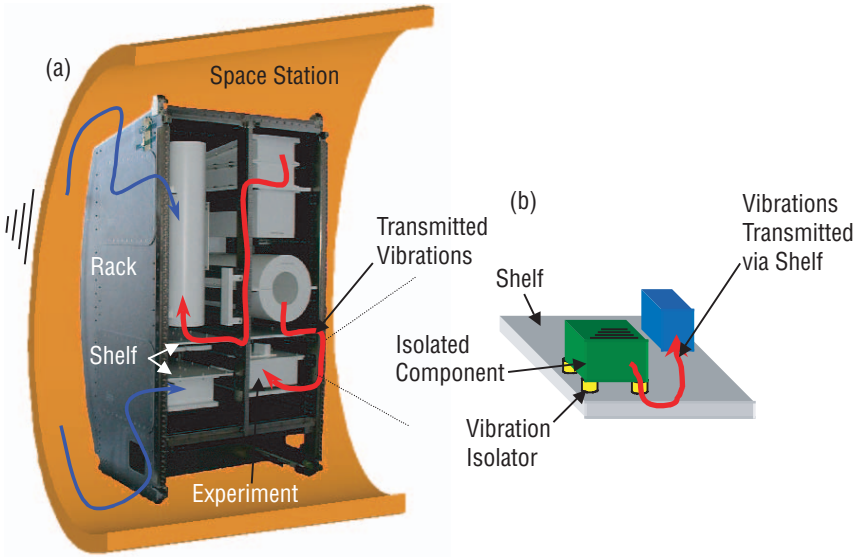

Figure 1. (a) Vibration transmission paths in *ISS* experiment rack. (b) Vibrations transmitted into and through the shelf.

To reduce the vibration level within the shelf, two control techniques are considered in this project. One technique is to control vibrations before they enter the shelf by using improved semiactive isolators. The resulting shelf vibration environment can therefore be improved. The second technique addresses the control of vibrations once they enter the shelf. By controlling shelf vibrations via active methods, a full range of vibration control can be achieved. Detailed accomplishments during the first year were described in the last annual report[1] and a short summary of those accomplishments is listed as follows:

- Extensive research and background study on passive, active, and semiactive control (including meetings with experts at the Langley Research Center (LaRC)).
- Data acquisition system acquired.
- Adaptive structure demonstrator beam constructed.
- Performance of demonstrator beam measured.
- NASA faculty fellow appointed in summer 2002.
- Report from NASA faculty fellow completed.
- Designed, analyzed, and fabricated a BOSS isolator prototype and conducted initial testing.
- Other methods for applying semiactive isolators examined.
- Shelf simulator structure designed.
- Finite element analysis (FEA) model of shelf simulator completed.
- Shelf and actuators modeled to predict expected control levels.
- Shelf simulator and test-fixture adapters constructed.
- Piezoelectric patches and piezoceramic disks obtained.
- Modal testing of shelf simulator conducted.
- Initial shelf actuation tests with QP40W actuators performed.

As a continuation of the research summarized above, the fiscal year (FY) 2003 efforts were mainly focused on the following:

- Analytical modeling of the adaptive structure including the shelf simulator and the bonded actuators.
- Improving the controller design.
- Conducting real-time control experiments.

To date, a combined analytical and experimental system model has been developed. Additionally, two control strategies have been studied and real-time experiments have been implemented and evaluated. Experimental results have demonstrated a 20-dB reduction in vibration levels for the first two vibration modes.

Approaches

The approach taken in this shelf vibration-reduction effort is active vibration control utilizing a feedback control technique. The principle of feedback control is represented in figure 2. The output y, which represents the vibration response of the shelf, is compared to the reference input r, and the difference in these two signals is the error e. Since the object of vibration control is to cancel the vibration amplitudes, the reference input here is zero. The error signal is then passed into a compensator $H(s)$. The resulting signal is that which drives the actuator(s) in the system. This signal is therefore applied to the system, which is modeled using the function $G(s)$. The primary problem consists of finding the appropriate compensator H(s) such that the closed-loop system is stable and be able to reject any disturbance d, which in this case would represent vibrations generated by components on the shelf.

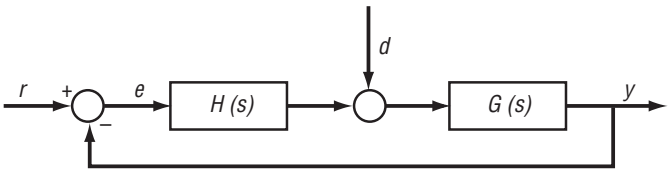

Figure 2. Principle of feedback control.

A validated system model is critical for structural control. As a result, one of the primary focuses is to obtain such a model. The two-dimensional asymmetric actuator patch bonded on the uniform shelf simulator is first modeled. Then, a two-dimensional Ritz expansion is used to develop the equations of motion for the adaptive structure, which includes the shelf simulator and the patches bonded to that shelf. The basis functions in the Ritz expansion are based on an interpolation of the measured mode shapes. This approach leads to a modal transformation from physical coordinates to modal coordinates. As will be seen in the next section, an experimental modal analysis and a modal controller are combined to create active vibration control.

To verify the system model, the frequency response function (FRF) predicted using the system model is compared with an actual measured FRF. Since the two FRFs match very well within the frequency range of interest, the analytical model of the system (i.e., $G(s)$) is considered validated. Based on the validated model, two control strategies, modal control and collocated control, are studied in this research. The state feedback gains are obtained by using a Linear Quadratic Gaussian (LQG) compensator.[2] A prototype digital controller developed using dSPACE is used to implement real-time experiments to analyze the effectiveness of the designed controller.

Accomplishments

As stated above, the three major accomplishments this year include system modeling, controller design, and experimental evaluations of the control system. The following section describes the modeling efforts. In addition to providing more insight into the system behavior, this modeling was essential to the development of a suitable controller, which is also described below. After the system modeling and control system development are described, some of the experimental results are presented.

Two-dimensional Asymmetric Piezoelectric Actuator Modeling

The analytical relationship between the dynamic voltage applied to the actuator and the resultant structural excitation was developed first. Figure 3 shows a piezoelectric patch element located

on the uniform plate. Although Fuller provided a development for a two-dimensional antisymmetric actuator (two actuator patches sandwiching the plate),[3] there are some significant differences for the one asymmetric actuator case that is used in this project. Although detailed derivations of the actuator and plate modeling results are provided in reference 4, some of the important results for this development are provided here.

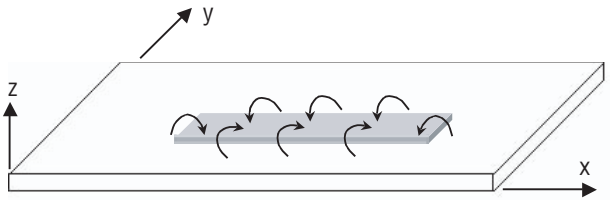

Figure 3. Two-dimensional piezoelectric actuator and structure (uniform shelf).

When a voltage is applied across the bonded piezoelectric patch, which is bonded to a uniform plate as shown in figure 3, that patch will attempt to expand. However, this expansion will be somewhat constrained by the stiffness of the plate. Due to the asymmetric nature of the actuator load, the plate will both bend and stretch, leading to an asymmetric strain distribution in both the *x* and *y* directions, as illustrated in figure 4.

Strain in the unconstrained piezoelectric patch with an applied voltage *V* is,[3]

$$\varepsilon_{pe} = \frac{d_{31} \cdot V}{h_{pe}} \tag{1}$$

where d_{31} is the piezoelectric strain constant, and h_{pe} is the thickness of the piezoelectric patch.

Using the moment equilibrium and force equilibrium about the center of the plate, the bending moment distribution in the *x* direction under the actuator patch can be calculated as,

$$m_y = c_0 \varepsilon_{pe} \left[H(x - x_1) - H(x - x_2) \right] \bullet \left[H(y - y_1) - H(y - y_2) \right]. \tag{2}$$

where c_0 is a function of the material properties and thickness of the piezoelectric patch and the plate (See equation (A.8) in reference 4.), and $H(s)$ is the unit Heaviside step function defined as,

$$H(x) = \begin{cases} 1, & x > 0 \\ 0, & x \le 0 \end{cases}, \tag{3}$$

The coordinates x_1, x_2, y_1 and y_2 are the corner coordinates of the actuator patch. Similarly, it can be shown that the bending moment distribution in the *y*-direction under the actuator patch is,

$$m_y = c_0 \varepsilon_{pe} \left[H(x - x_1) - H(x - x_2) \right] \bullet \left[H(y - y_1) - H(y - y_2) \right]. \tag{4}$$

The distributed moments m_x and m_y, induced on the plate by the actuator, will be used in the next section for calculating modal generalized forces resulting from the actuators. These applied forces are used to reduce vibration levels within the plate. Now that the relationship between the voltages applied to the actuator and the resulting dynamic excitations are known, the equations of motion for the actively controlled structure can be obtained.

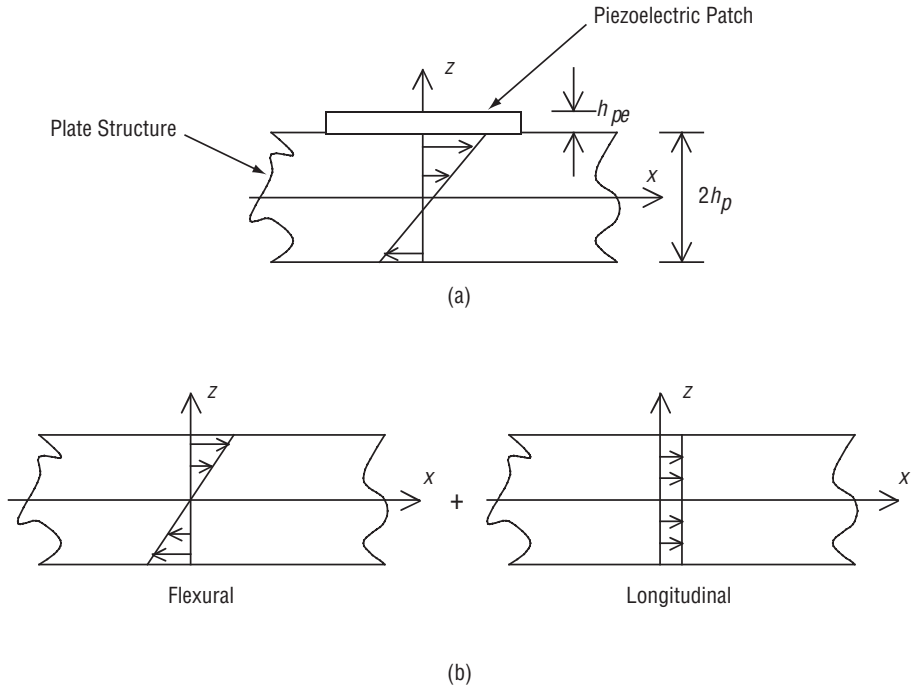

Figure 4. (a) Asymmetric strain distribution in *x* direction. (b) Decomposed into bending and axial strain.[3]

Equations of Motion Formulation for the Active Structure

A Ritz expansion technique[5] is used to represent the transverse displacement of the plate. Again, while some of the important results are provided here, a detailed derivation can be found in reference 4.

The plate's vibratory displacement $w(x,y,t)$ is described by,

$$w(x,y,t) = \sum_{j=1}^{N} \psi_j(x,y) q_j(t) \ , \qquad (5)$$

where the $\Psi_j(x, y)$ are linearly independent basis functions that satisfy the specific geometric boundary conditions of the plate. The generalized coordinates $q_j(t)$ are assumed to have a harmonic time dependence such that,

$$q_j(t) = \mathrm{Re}(W_j e^{-i\omega t}) \ . \qquad (6)$$

Here, W_j are the unknown modal displacement coefficients.

The equations of motion of the active structure are derived using Lagrange's equations. First, the kinetic energy T and strain energy V of the structure are determined. The kinetic energy is described as,

$$T = \frac{1}{2} \sum_{j=1}^{N} \sum_{l=1}^{N} M_{jl} \dot{q}_j \dot{q}_l \ , \qquad (7)$$

and the potential energy is described as,

$$V = \frac{1}{2} \sum_{j=1}^{N} \sum_{l=1}^{N} K_{jl} q_j q_l \ , \qquad (8)$$

where M_{jl} and K_{jl} are defined by equations (A.15) and (A.19) in reference 4. The generalized forces are derived by forming the virtual work δW_e due to the action of the actuators,

$$\delta W_e = M_x \delta\theta_x + M_y \delta\theta_y \ , \qquad (9)$$

where M_x and M_y are the total moment excitations in the x and y directions, and $\delta\theta_x$ and $\delta\theta_y$ are the slope variations in the x and y directions, respectively. Note that the total moments are directly related to the moment distributions given in equations (2) and (4).

After applying Lagrange's equations to the kinetic energy, strain energy, and generalized force expressions, the resulting equations for structural vibration are,

$$\sum_{l=1}^{N} M_{jl} \ddot{q}_l + \sum_{l=1}^{N} K_{jl} q_l = Q_j^e \ . \qquad (10)$$

To simplify notation, equation (10) can be written in matrix form as,

$$[M]\{\ddot{q}\} + [K]\{q\} = \{Q^e\} \ . \qquad (11)$$

Now that an analytical model of the system including the actuators has been described, the development of the control approach will be presented.

Modal Control Development

Modal control is an approach in which the generalized modal coordinates and their derivatives are chosen as the state variables. State-space form is used here for the controller design.

The active structure can be represented by second-order differential equations in modal coordinates by using modal truncation. In equation (11), if we choose the mode shape functions as the basis functions, the equations of motion will be decoupled into N independent modal equations,

$$\ddot{q}_j + 2\zeta_j \omega_j \dot{q}_j + \omega_j^2 q_j = f_j \ , \quad j = 1,2,...,N \ , \qquad (12)$$

where q_j is the modal generalized coordinate, ζ_j is the modal damping ratio, ω_j is the modal natural frequency, and f_j is the modal excitation. The values for ζ_j and ω_j can be obtained from the experimental modal analysis. The normalized modal excitation can be obtained using the relationship,

$$f_j = \frac{\iint_A Q_j \psi_j dxdy}{\iint_A 2\rho h_p \psi_j^2 dxdy} \ . \qquad (13)$$

Equation (13) can be calculated by using an interpolation of measured mode shapes. In the present work, the mode shapes were measured using a laser vibrometer (See reference 4 for a description of the measurement process.). The measured mode shapes are shown in figure 5.

Equation (12) can be written into state-space form,[6]

$$\begin{Bmatrix} \dot{q}_j \\ \ddot{q}_j \end{Bmatrix} = \begin{bmatrix} 0 & 1 \\ -\omega_j^2 & -2\zeta_j\omega_j \end{bmatrix} \begin{Bmatrix} q_j \\ \dot{q}_j \end{Bmatrix} + \begin{bmatrix} 0 & 0 & 0 \\ b_{j1} & b_{j2} & b_{j3} \end{bmatrix} \begin{Bmatrix} u_j \\ u_2 \\ u_3 \end{Bmatrix} . \qquad (14)$$

The modal excitation f_j is replaced by the control input b_{ji} and driving actuator voltage u_j, where b_{ji} is the modal control input coefficient from the ith actuator to the jth mode. The u_j are the applied voltages for the ith actuator.

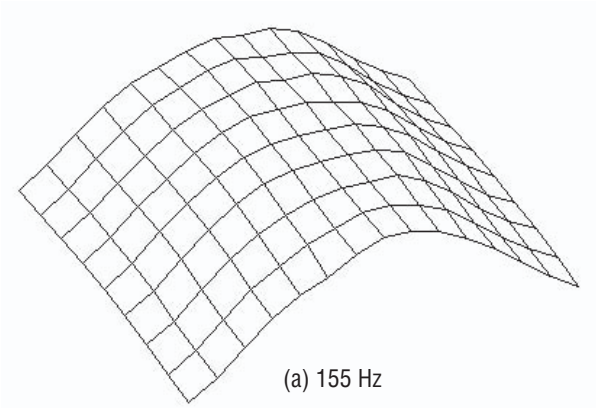

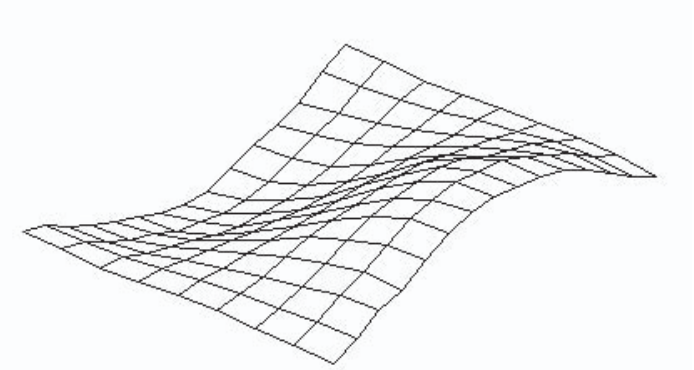

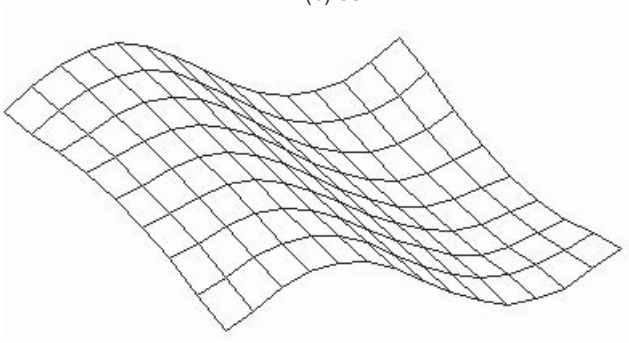

Figure 5. Measured vibration mode shapes of shelf: (a) Mode 1, (b) mode 2, and (c) mode 3.

In order to control the first three vibration modes using three piezoelectric patch actuators and three accelerometers as sensors, the state-space form is,[7]

$$\begin{aligned} \dot{x} &= Ax + Bu \\ y &= Cx + Du \end{aligned} \tag{15}$$

where x, y, u, A, B, C, and D are defined in reference 4.

Linear Quadratic Gaussian Compensator Formulation

The LQG method is used to obtain the state estimation and regulation.[2] The LQG compensator includes the LQR and a Kalman filter as the state observer. The LQG control diagram is shown in figure 6.

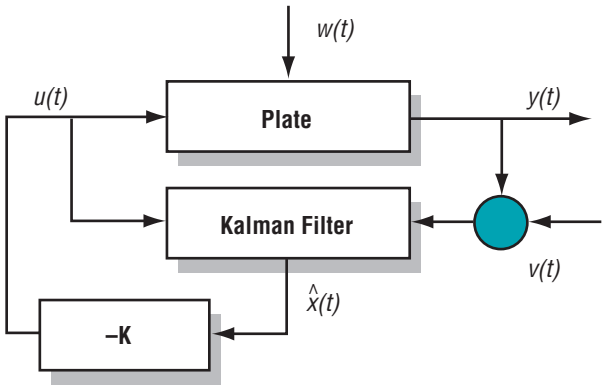

Figure 6. LQG control system.

For a completely controllable and observable linear system,

$$\begin{aligned} \dot{x} &= Ax + Bu + w \\ y &= Cx + Du + v \end{aligned} \tag{16}$$

where $w(t)$ and $v(t)$ are uncorrelated gaussian white noise. The goal is to find a control u that minimizes the cost functional,

$$J = E\left[x^T Q_c x + u^T R_c u\right], \quad Q_c \geq 0\,, \quad R_c > 0\,, \tag{17}$$

where Q_c and R_c are weighting matrices. The cost function J has two contributions, one is from the states and the other is from the control efforts. The solution of the this problem is a linear, constant-gain feedback,

$$u = -G\hat{x}\,, \tag{18}$$

where G is the solution of the LQR problem and $\hat{x}$ is the reconstructed state obtained from the Kalman filter.[8]

Determination of the weighting matrix in the cost functional is of particular importance. In the modal controller designed in this research, Q_c is chosen in such a way that $x^T Q_c x$ represents the total energy (kinetic plus strain) in the system,[8]

$$Q_c = diag\left\{K_{11}, M_{11}, K_{22}, M_{22}, K_{33}, M_{33}\right\}, \tag{19}$$

and

$$R_c = \gamma\ I\,, \tag{20}$$

where I is identity matrix and γ is an adjustable positive scalar.

Output Feedback Control with Collocated Actuators and Sensors Development

Another control strategy that is considered in this project is collocated control, as illustrated in figure 7. In this approach, an accelerometer is used as feedback to the control system, which

in turn drives a nearly collocated actuator. The concept in this configuration is simple since no coordinate transformation to decouple modes is necessary.[9] Figure 7 shows three independent control channels. Figure 8 presents the corresponding test setup showing the piezoelectric patches bonded to the plate as well as the accelerometers. The harmonic excitation used to excite the plate, referred to elsewhere as the disturbance, is introduced via the electromagnetic shaker.

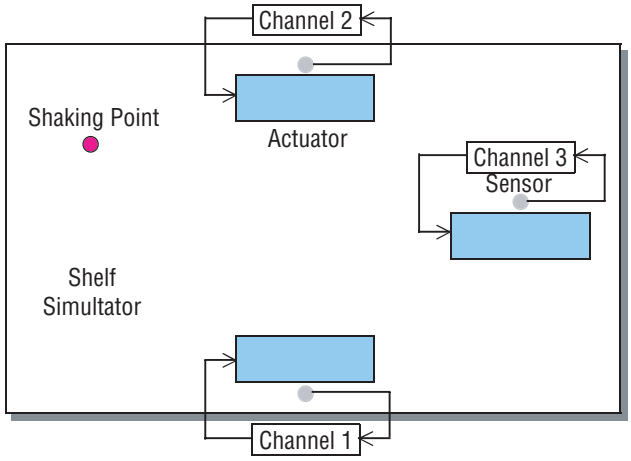

Figure 7. Collocated control strategy on shelf structure.

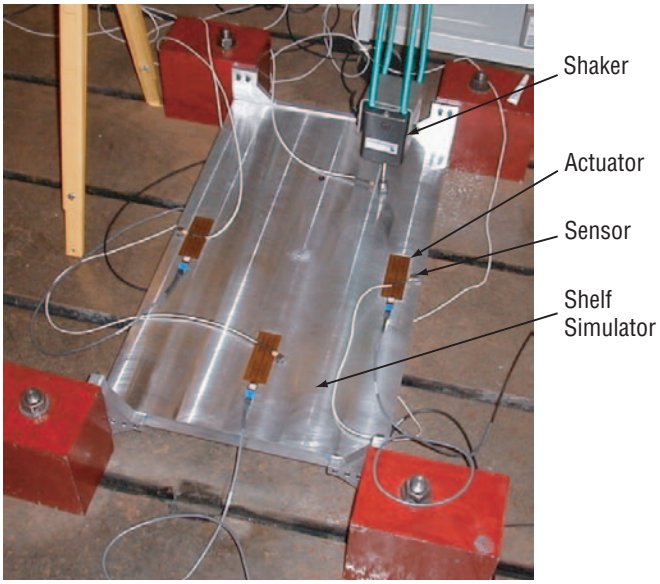

Figure 8. Collocated control test actuators and sensors.

Figure 9 shows two FRFs. One of these FRFs is from the model prediction as described above, and the other FRF was obtained using experimental measurements. As shown in the figure, these FRFs match very well in the frequency range below 400 Hz. As a result, the analytical model developed above is reliable for use in a control system designed to reduce the vibration levels of the first two modes. The LQG compensator is also used for each channel.

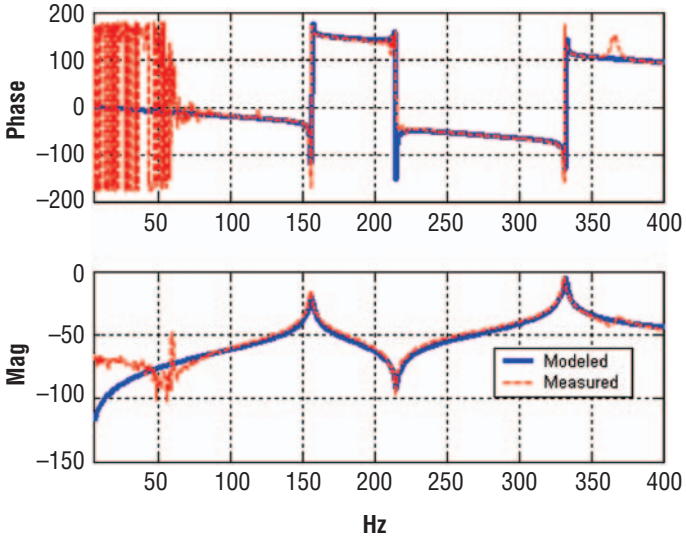

Figure 9. Comparison of FRF between measurement and model prediction.

Figure 10 shows the root locus for the channel 1 collocated control using the LQG method. Figure 10(a) is for an uncompensated system. The structure poles are very close to the imaginary axis because of light damping. From the root locus, one can determine that the system is stable but the stability margin is very small. Figure 10(b) is for a compensated system. From this plot, one can see that the stability robustness has significantly increased.

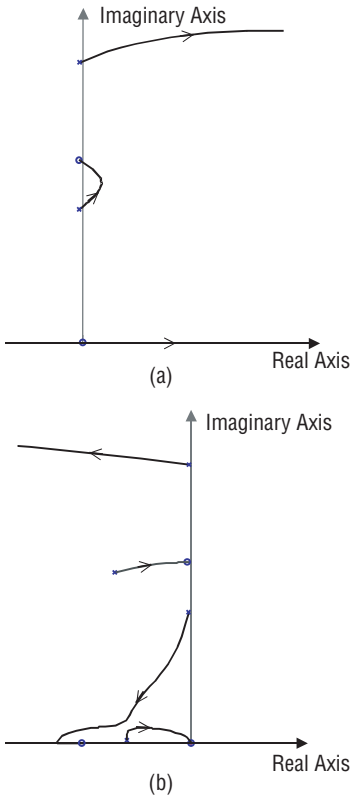

Figure 10. Root locus for LQG control:
(a) Uncompensated system.
(b) Compensated sysftem (x: system pole, o: system zero)

Real-Time Experiment Using dSPACE Control Prototype

A digital control system that consists of MATLAB/SIMULINK modeling software and a dSPACE DS 1104 controller board in a personal computer was constructed. SIMULINK was used to build the control block diagrams that are shown in figure 11. Then, the dSPACE real-time workshop was used to generate a C-code model from the SIMULINK model. The C-code model was then connected by the dSPACE real-time interface to the dSPACE real-time hardware system. The experiment software control desk can operate the hardware. The interface designed in the control desk is shown in figure 12.

An accelerometer is used to detect the signal. After passing through a second order analog Butterworth low-pass filter, the filtered signal then goes into the dSPACE system. In the dSPACE system, the signal first passes through an analog-to-digital (A/D) converter. The software then uses the programmed control algorithm to determine the necessary control output based on the input and integrated system model. Then, the resulting drive signal passes through a digital-to-analog (D/A) converter. The sampling time is 0.1 ms. The signal finally passes to the power amplifier before arriving at the collocated actuator. A picture of the actual experiment

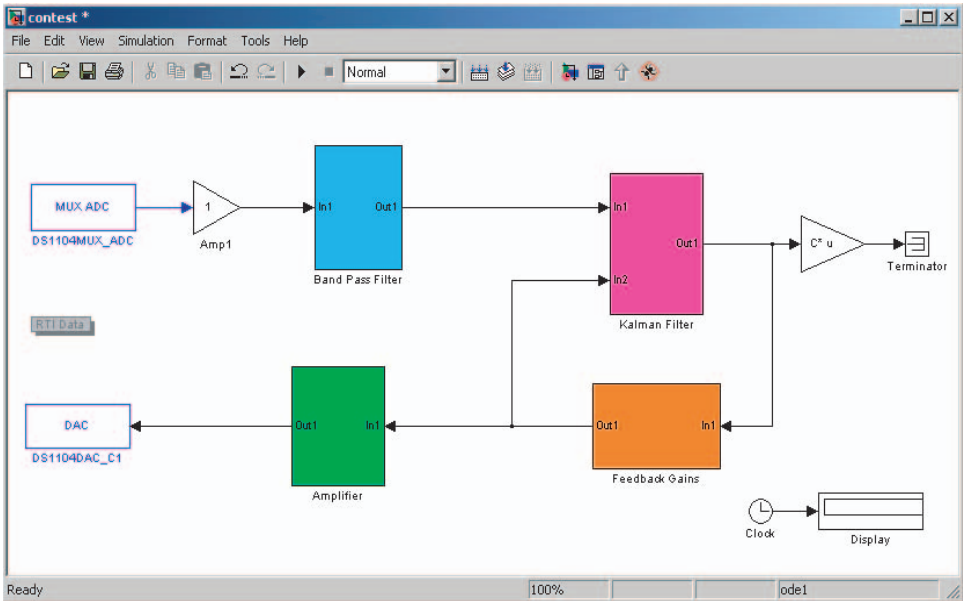

Figure 11. Control block diagram in Simulink.

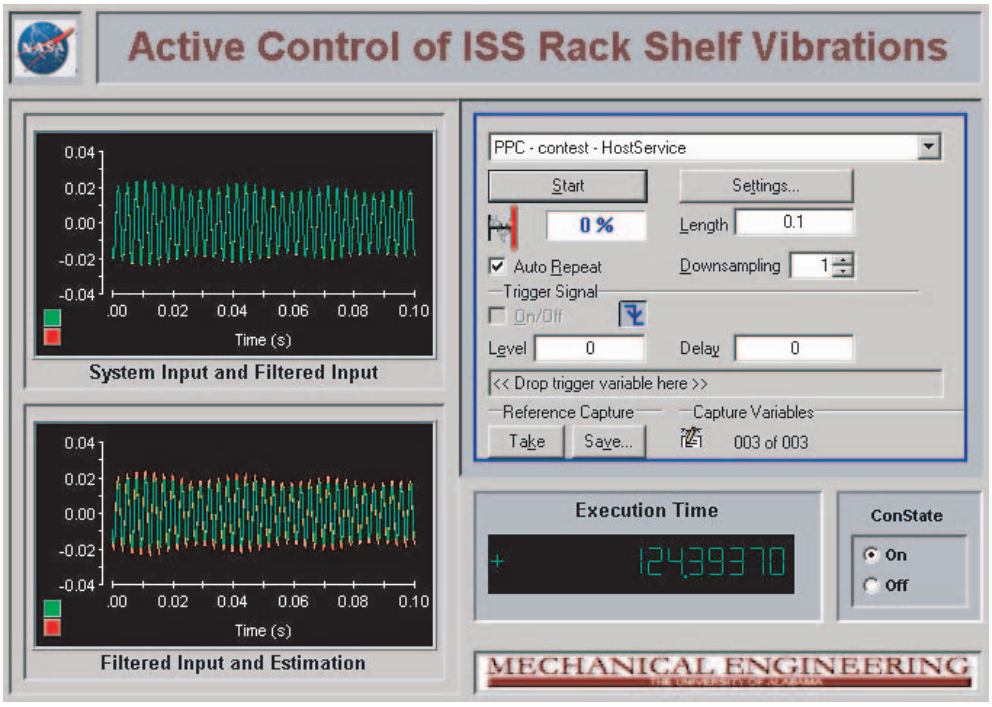

Figure 12. Control desk interface.

setup is shown in figure 13. There are two systems used in this setup. The dSPACE system is for control, whereas the signal analyzer system is used for monitoring the resulting vibration levels. In the experiments, swept sinusoidal noise and Gaussian white noise were used as the disturbance to excite the shelf simulator. To avoid requiring a high-power amplifier for the control actuators, the excitation signal was designed to be relatively small. However, since the shelf simulator is a relatively large structure, a larger disturbance was required to generate a sufficiently high signal-to-noise ratio. Here, the signal source voltage used was 150 mV. As a result, the requirement for the applied actuation voltage into the patch actuator was less than 15 V. Figure 14 shows the experiment results on the channel 1 control. As shown in the figure, the peaks at the resonances (155 and 334 Hz) of the controlled modes are reduced by 20 dB for a swept sinusoidal noise disturbance. Consequently, the control system has been shown to be effective at reducing the vibration levels within the shelf for this particular disturbance and frequency range.

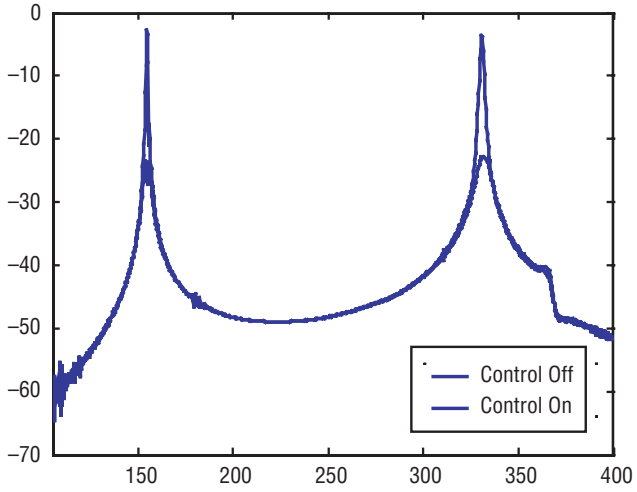

Figure 14. Control results on channel 1.

Planned Future Work

The next phase of the research will be to develop an analytical model for the rectangular shelf simulator with discontinuous boundary conditions. Since the manner in which the shelf is mounted in a rack is not a form commonly found in analytical approaches, a superposition approach will be used to analytically describe the mode shapes. This research is currently in progress. Once this model is complete, the influence of the controller on the residual modes (spillover) will be studied and a real-time experiment for collocated control on channel 2 and channel 3 will be implemented. The goal of this approach is to obtain further reduction for the first two vibration modes as well as the third mode.

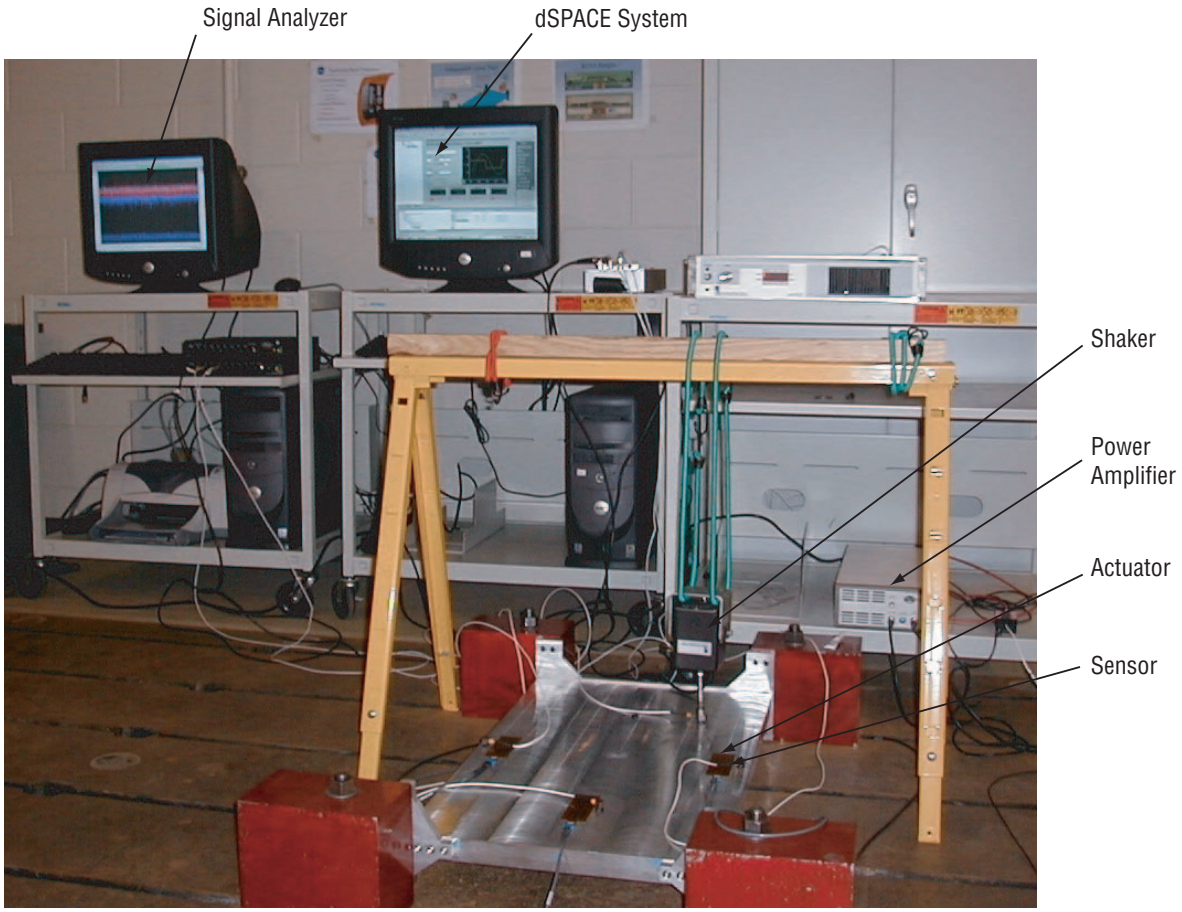

Figure 13. Control test layout.

In the tests conducted thus far, swept sine excitations and random excitations have been used. In future experiments, the frequency spectra and excitation levels will be more representative of actual on-orbit excitations. In using this approach, a more accurate assessment of the control system requirements and control levels can be made. Furthermore, the geometric nature of the excitation will be modified to determine the impact of an excitation that better mimics a component placed on the shelf. This approach will provide a means for assessing controllability when the excitation is like that due to actual hardware mounted on the shelf. Additionally, the differences between the actual control test boundary conditions and the *ISS* rack mounted boundary conditions, which are illustrated in figures 15 and 16 respectively, will be noted.

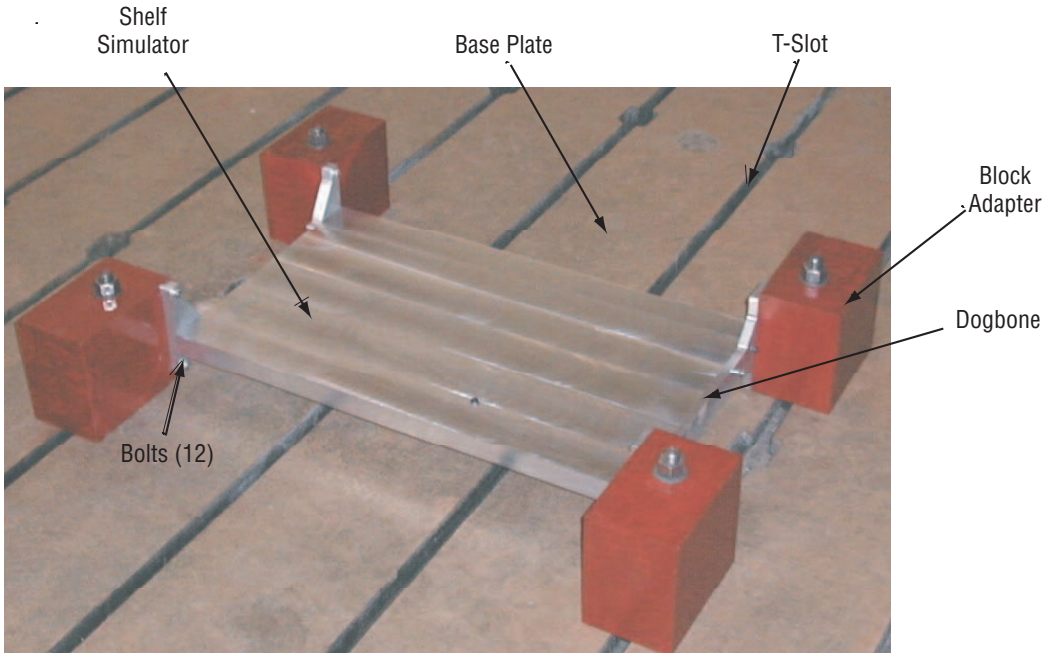

Figure 15. Shelf simulator and its boundary conditions.

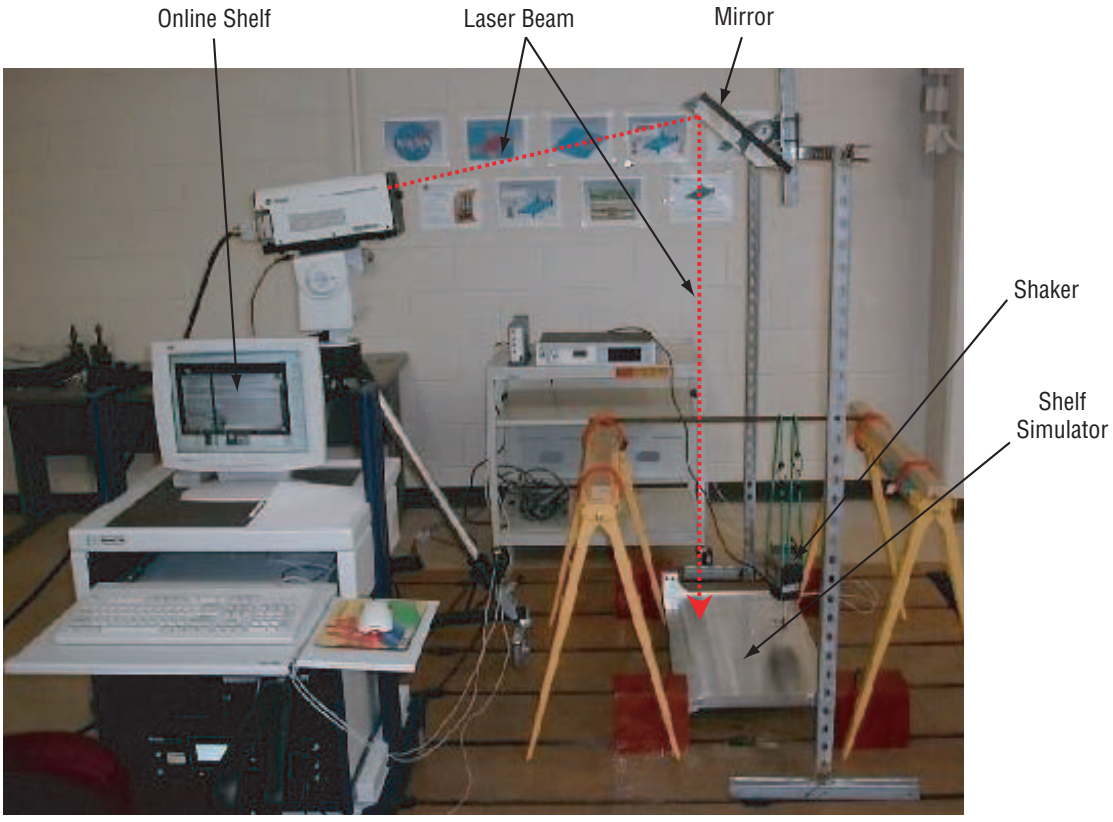

Figure 16. *ISS* rack and its boundary conditions.

Since a modal controller can be used for selective independent mode control, and the simulation results showed good control effects, a real-time experiment will be implemented in future research to attempt a demonstration for modal control.

Publications and Patent Applications

Shepard, Jr., W.S.; and C. B. Gattis, C.B.: "Active and Passive Control of *ISS* Rack Shelf Vibrations," *NASA Faculty Fellowship Program Report*, MSFC, 2002.

Gattis, C.B.; and Shepard, Jr., W.S.: "Adaptive Structures for Microgravity Vibration C\control and Isolation," P*aper 1700 AIAA–2003–1872*, Presented at the 11th AIAA/ASME/AHS Adaptive Structures Conference, Norfolk, VA, April 7–10, 2003.

No patent applications have been made as a result of this project. A follow-on AIAA paper is planned for the 2005 AIAA/ASME/AHS Adaptive Structures Conference.

Funding Summary

Table 1. Fiscal year (FY) 2002 funding summary.

Funding Element	FY 2002 ($)
Initial budget amount	36,000.00
The University of Alabama	22,803.80
Remaining funding	**13,197.20**

Status of Investigation

Most of the second-year objectives of this 2-year CDDF project were achieved. The specific accomplishments are described and listed above. Note that the University of Alabama utilized the funding in such a way that research is still continuing. First-year delays in shelf construction resulted in a delay of initial characterization testing of the shelf simulator. This situation caused a waterfall effect to the overall schedule. However, once this testing was accomplished, the following tasks moved along well. An effective control system was designed, and optimization for power consumption and size is still in work. Control of the system against realistic hardware excitation conditions (i.e., measured random spectra) is underway. Integration of an actual vibrating component with the system will take place soon thereafter. The only remaining objective for the second year is integration of the shelf and control system with a rack. Depending on rack availability, this objective still may be achieved. Overall, this investigation has been very successful in meeting the objectives outlined at the start.

Reference

[1] Gattis, C.B.; Shepard, Jr., W.S.; and Wang, J.: 44th AIAA Structures, Structural Dynamics, and Materials Conference, April 2003.

[2] Stein, G.; and Athans, M.: "The LQG/LTR Procedure for Multivariable Feedback Control Design," *IEEE Transactions on Automatic Control*, Vol. 32(2), pp. 105–114, 1987.

[3] Fuller, C.R.; Elliott, S.J.; and Nelson, P.A.: *Active Control of Vibration*, Academic Press, 1966.

[4] Gattis, C.B.: "Modal Tests."

[5] Craig, Jr., R.R.: *Structural Dynamics: An Introduction to Computer Methods*, John Wiley & Sons, New York, NY, 1981.

[6] Stogbener, U.; and Gaul, L.: "Active Vibration Control of a Car Body Based on Experimentally Evaluated Modal Parameters," *Mechanical Systems and Signal Processing*, Vol. 15(1), pp. 173–188, 2001.

[7] Gawronski, W.K.: *Dynamics and Control of Structures: A Modal Approach*, Springer-Verlag, 1998.

[8] Preumont, A.: *Vibration Control of Active Structures: An Introduction*, Kluwer Academic Publishers, 2002.

[9] Shen, Y.; and Homaifar, A.: "Vibration Control of Flexible Structures With PZT Sensors and Actuators," *Journal of Vibration and Control*, Vol. 7, pp. 417–451, 2001.

[10] Timoshenko, S.: *Theory of Plates and Shells*, McGraw-Hill. 1940.

Evolutionary Structures Analysis and Testing

Project Number: 02–09

Investigators: Russel Parks/ED27
Jim Steincamp/ED10

Purpose

The purpose of this Center Director's Discretionary Fund (CDDF) project is to develop the capability to design, analyze, build, and verify the dynamic characteristics of an evolutionary structure called a tensegrity. To accomplish this, a tensegrity analysis package (TAP) will be developed in MATLAB, which provides the ability to design, visualize, and analyze a tensegrity structure. A microgenetic algorithm will also be developed that will interface with the analysis package and provide a means to design a frequency-enhanced cylindrical tensegrity structure starting with a baseline structure

In conjunction with these efforts, a baseline tensegrity will be designed and constructed. Once the dynamic characteristics of the baseline structure have been predicted by the analysis package, a frequency-enhanced structure will then be designed through the interaction of the analysis package and the microgenetic algorithm. The optimized structure will be constructed once it is defined. The baseline and optimized structure will be modal tested to validate the computational design tools.

Background

Tensegrity structures are built of compressive members (bars), and tensile members (strings). In pure tensegrity structures, the bars are joined only to strings; in general tensegrities, bars may be joined by torque-free joints. A tensegrity structure is said to be regular if the lengths of its members are uniform or vary according to a simple formula. For most materials, the tensile strength of a longitudinal member is larger than its buckling strength; therefore, a large stiffness-to-mass ratio can be achieved by increasing the use of tensile members.[1] Tensegrities are the epitome of lightweight structures because they take advantage of the larger tensile strength of materials. Furthermore, an astoundingly wide variety of natural systems, including carbon atoms, water molecules, proteins, viruses, cells, tissues, and even human and other living creatures are tensegrity structures.[2] Through the process of evolution, nature continually improves the design of living creatures for the environment they live in. Since tensegrities are nature's structure of choice, it is conceivable that they have other benefits we are unaware of.

Currently, a notable amount of work has gone into the academics of developing analytical models of tensegrity structures. Most of this work has been focused on determining stability and structural characteristics. Also, there has been some work done in building and testing two dimensional tensegrity structures. This project is an attempt to bridge the gap between analysis and testing activities in the form of structural analysis verification.

With respect to structural optimization, there have been studies in applying genetic algorithms in truss structure optimization. In particular, A. Keane and S. Brown designed a satellite boom-truss system with enhanced vibration performance. They started with a standard truss system (fig. 1) and then used a genetic algorithm to alter the design (fig. 2) while optimizing the vibration performance. An improvement of over 20,000 percent in frequency-averaged energy levels was obtained using this approach.[3] The goal of this project is to fuse tensegrity analysis and genetic algorithm optimization to minimize or even eliminate the need for active control.

Figure 1. Baseline truss structure.

Figure 2. Performance enhanced structure.

Approach

A TAP written in MATLAB will be developed. The TAP will consist of a tensegrity visualization tool (TVT), a tensegrity stability analysis tool (TSAT), and a tensegrity dynamic analysis tool (TDAT). The TVT generates a visual display of a tensegrity structure defined by a tensegrity definition file (TDF). The TVT will also provide animation capabilities for display of modes of vibration. The TSAT will also accept a TDF as input and determine the degree of stability of the tensegrity. The TDAT will accept a TDF and determine the modes of vibration for a stable tensegrity structure. A microgenetic algorithm written in MATLAB will be developed and will interact with the TSAT and TDAT to evolve a frequency-enhanced tensegrity structure starting with the baseline structure.

To investigate the effectiveness and accuracy of the TAP and microgenetic algorithm, a baseline and frequency-enhanced cylindrical tensegrity structure will be designed and built. A modal test will then be conducted on both structures to verify the analytical predictions.

Accomplishments

Tensegrity Definition File Completed

A MATLAB m-file for constructing a TDF was completed. The TDF describes the compression and tension members of a pure or general tensegrity structure or conventional truss together with the physical geometry, material properties, and other relevant parameters including those useful for the visualization of the structure.

Tensegrity Visualization Tool Completed

A TVT has been written that accepts input from a TDF describing regular and irregular tensegrity structures and generates a computerized display of the tensegrity described by the TDF. The TVT allows the user to manipulate the various views of the structure; this can be done on any computer platform currently supported by MATLAB (Windows, Macintosh, Linux, Unix, Solaris, etc). The TVT does not allow structures described by separate TDFs to be linked at this time.

Tensegrity Stability Analysis Tool Progress

A TSAT has been developed that accepts input of a baseline cylindrical tensegrity structure in the form of a TDF. The original goal was for the TSAT to determine the degree of stability of the proposed baseline tensegrity. However, the new TSAT is able to determine a stable tensegrity from virtually any TDF input. This was accomplished by minimizing the potential energy of the system.

To do this, some assumptions were made. It was assumed that the bars would maintain a fixed length and hence contribute nothing to the total potential energy P. The wires were assumed to have unstretched lengths L and to obey a simple Hooke's law in terms of the difference between the length $|w|$ of the wire and L so that the potential energy of one wire was given by $k(|w|-L)2/2$ where k is the Hooke's law constant. Using a sum of such expressions and the connection matrix A allows w to be represented as $A(x)$ where x is the vector of nodal coordinates. The equilibrium position of x will be found if P is minimized while keeping the bar lengths constant.

To minimize P, the gradient of P, dP, is calculated and minimized. This is done by finding a local trough in the dP function. Since the minimized dP is a local minimum, it is possible that a given tensegrity could have several stable configurations. However, it has not yet been attempted to find every stable configuration.

The forces acting on the rigid bars (wire tensions) had to be calculated in order to determine the gradient of P. These forces can be plotted in the TSAT giving a wire tension profile. It was determined that there can be many different wire tension combinations for one shape solution. The stiffness of the tensegrity in essence is determined by the wire tensions.

Tensegrity Dynamic Analysis Tool Progress

A TDAT is still in the early stages of development; however, it is functional at this point. In order to avoid a second order theory, it was assumed that the bars have very high Hooke's law constants and the corresponding energy terms were added to P. This allowed a straightforward derivation of the traditional truss equations for the linearized small disturbance motion. The eigenvalues of the resulting matrix were then computed giving the frequencies as the square roots of the eigenvalues. This method avoids the complications of fixed bar length. The first frequencies computed are essentially zero, which corresponds to the rigid-body frequencies. But the nonzero eigenvalues give the square of the structural frequencies, which is all that is needed for genetic algorithm optimization.

Baseline Tensegrity Built and Modal Tested

A baseline six-stage cylindrical tensegrity structure has been constructed and is shown in figure 3. A modal test has been conducted and the first few structural modes of the baseline tensegrity have been determined.

Figure 3. Six-stage baseline cylindrical tensegrity structure.

Planned Future Work

Expand Tensegrity Stability Analysis Tool

The TSAT needs to be able to map the space of possible shapes the baseline tensegrity can take. A microgenetic algorithm can help and may also be helped in determining a dynamically optimized structure.

Upgrade and Verify Tensegrity Dynamic Analysis Tool

The TDAT needs to be expanded to utilize second order theory. A second order theory is essential for the following reasons:

- First: The modified gradient technique is sensitive to the scaling factor and requires manual intervention.
- Second: The accuracy of the frequencies is very dependent on choosing the bar stiffness (too small and the results are inaccurate; too large and several convergence difficulties occur).
- Third: Computation of the full dynamic motion of the tensegrity requires the second order corrections.

The TDAT also needs to be put to the test. To do this, the current baseline structure needs to be dynamically analyzed utilizing the TDAT. The analysis should be verified using the modal test results previously acquired.

Develop Microgenetic Algorithm

A microgenetic algorithm needs to be developed that works in conjunction with the TSAT and the TDAT to analytically determine a dynamically optimized tensegrity structure. To do this, the best parameters to be altered (bar length, bar diameter, etc.) need to be determined.

Build Frequency-Enhanced Tensegrity

The previously built and tested baseline tensegrity needs to be dynamically optimized using the microgenetic algorithm. The optimized tensegrity can then be built using the same methods used to build the baseline tensegrity. Modal testing will be used to verify optimization.

Publications and Patent Applications

None at this time.

Funding Summary

Table 1 identifies the funding summary for fiscal years (FYs) 2002 and 2003.

Table 1. Funding summary.

	FT 2002 ($)	FY 2003 ($)
Received	23,000	10,000
Spent	23,000	10,000

Status of Investigation

In FY 2003, a TAP written in MATLAB had almost been fully developed. The TAP consisting of a TVT, TSAT, and TDAT needs only minor upgrades and additions to be able to accomplish the original objectives of this CDDF. With the previously mentioned upgrades and additions to the TAP and future development of a microgenetic algorithm designed to work with the TAP, it will be possible to at least design a dynamically optimized cylindrical tensegrity structure from a baseline. Using the baseline tensegrity structure already built, the optimized design can be verified by building the optimized tensegrity and determining its modal characteristics through modal testing

Optimization of a Time-Domain Parameter Estimation Procedure Using a Genetic Algorithm

Project Number: 02–10

Investigators: **Kathy O. Kappus/ ED27**
Alan F. Patterson/ED27
Russel A. Parks/ED27

Purpose

The primary purpose of this Center Director's Discretionary Fund (CDDF) research project is to implement a genetic algorithm (GA) to optimize the estimation of modal parameters using a time-domain technique.

Background

The purpose of parameter estimation is to extract modal parameters (frequency, damping, and mode shapes) from experimental data. In many cases, these extracted modal parameters are used to update a finite element model. Most traditional parameter estimation methods are based on frequency-domain methods (Fourier transforms and frequency response functions) that have limitations. The proposed methodology would provide an additional parameter estimation tool beyond those typically used in the industry. Time-domain modal-parameter estimation has the added advantage that it may be applied to nonlinear data. Current frequency-domain techniques are based on the assumption that the data are linear. The application of a genetic algorithm to optimize the modal parameters provides an evolutionary approach to analysis of dynamic time histories.

This research is an extension of previous research conducted by Alan F. Patterson through a prior CDDF project. Mr. Patterson successfully developed extensive MATLAB code to implement a time-domain modal-parameter estimation algorithm. Figure 1 illustrates the time-domain based system identification algorithm implemented by Mr. Patterson. Due to changes in his assignments at Marshall Space Flight Center (MSFC), Mr. Patterson did not have time to complete the implementation of the genetic algorithm intended to optimize the estimation of the modal parameters.

Approach

This research effort includes four primary tasks:

1. Develop proficiency with current algorithms and software.
2. GA trade studies.
3. Implementation of selected GAs.
4. Documentation of project.

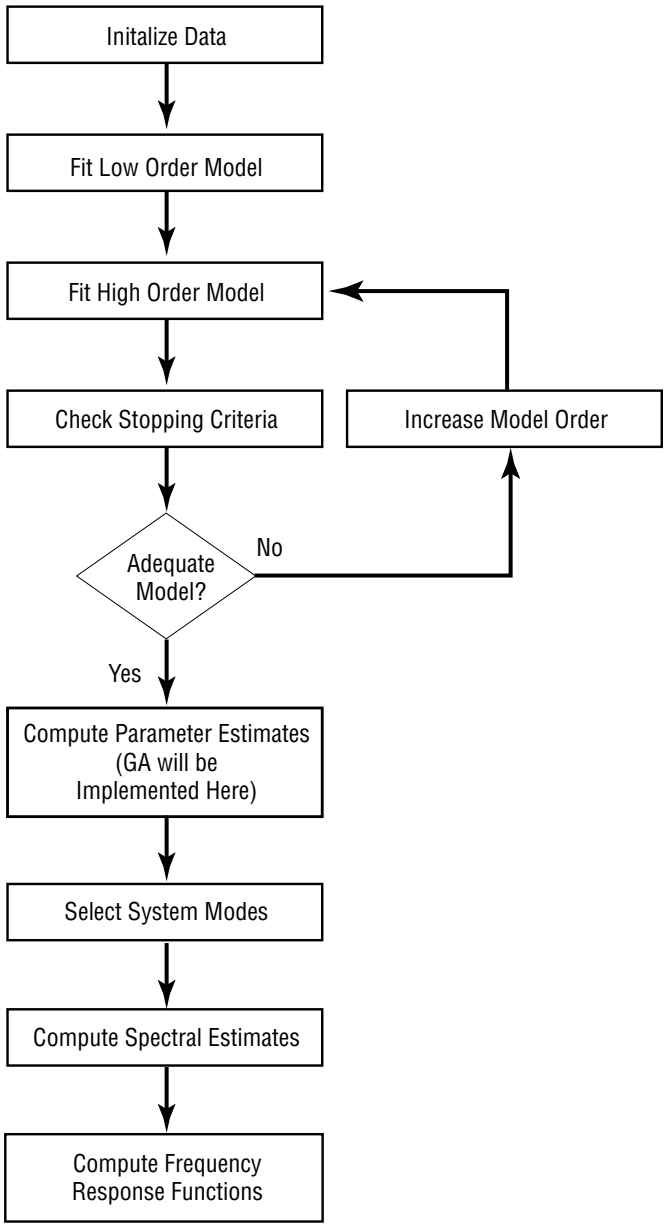

Figure 1. The time-domain based system identification algorithm implemented by Mr. Patterson.

In the first phase, the principal investigator (PI), Mrs. Kappus, is reviewing the previous work conducted by Mr. Patterson. This includes reading reference papers and books related to the research, as well as reviewing documentation developed by Mr. Patterson. A literature search is being conducted to determine

if related research has been conducted in the industry since the time of Mr. Patterson's research. The MATLAB code developed in the previous CDDF has been provided to the PI and has been implemented on her desktop computer. Some enhancements to the code may be undertaken, taking advantage of recent improvements in MATLAB. Analytical and experimental data will be used to learn the algorithms, as well as to test and improve the robustness of the code.

In the second task, trade studies will be conducted to determine the optimal GA to determine the modal parameters. Some specific studies to be conducted include determination of the encoding scheme for the modal parameters and a comparison of traditional mutation versus a hybrid technique using a local search via simulated annealing. Using theoretically generated data, the different GA techniques will be compared based on accuracy and efficiency.

The selected GA will be integrated with the existing time-domain parameter estimation code during the third phase of the project. The new code, including the GA, will be exercised using experimental data and will be compared with results from traditional frequency-domain methods. The algorithm will also be used to analyze nonlinear data, both analytical and experimental.

In the final phase, the results of the research project will be documented and recommendations will be made for further study.

Accomplishments

Minimal progress has been accomplished due to a number of unplanned, high-priority return-to-flight tests requiring the attention of the PI. The PI has extensively reviewed statistical methods, regression analysis, and the prior work of Mr. Patterson. In addition, the PI has been becoming more proficient with MATLAB and a matrix toolbox that will be used in the research. A GA toolbox was also acquired and used by a summer student to investigate the potential for implementing the toolbox into the algorithm.

Planned Future Work

As test schedules allow, the familiarization with the previous research will continue, as will the use of the previously developed MATLAB codes. Work will focus more on the implementation of the GA for optimization of the parameter estimation.

Publications and Patent Applications

None

Funding Summary

The funding received for fiscal year (FY) 2002 was $20,000 of which $18,050 was spent. No Funds were requested for FY 2003.

Status of Investigation

As previously discussed, the PI has made only minimal progress in the research. The project is still in the first phase due to other obligations by the PI.

Fiber Placement Module for Processing of Thin Films and Adhesives Into Composite Structures

Project Number: 02–12

Investigator: Bruce Hulcher/ED34

Purpose

Automated fiber placement of polymer matrix composites is a technology that allows for the automated layup of preimpregnated carbon fiber tow and unitape. However, such technology does not currently allow for the incorporation of barrier films, liner materials, or film adhesives (e.g., honeycomb core adhesive) into the composite structure by automated means. Automated fiber placement for the layup of thermosetting composite materials is a proven technology that allows for very high accuracy, resulting in improved component/structural performance and lower fabrication costs over traditional hand layup techniques. The innovation described herein will be designed to function on an existing fiber placement machine in the National Center for Advanced Manufacturing (NCAM) facility at Marshall Space Flight Center (MSFC), but may also be custom designed to fit to any fiber placement machine. The combination of a film/adhesive laydown module and fiber placement technology will enable the placement processing of both the composite structure and the film or film adhesives on the same placement machine without having to interrupt either process. It is also envisioned that this technology can be modified such that both film materials and composite prepreg tow/tape can be processed simultaneously on one machine, resulting in a further decrease in processing costs and part fabrication time.

Background

The fabrication and successful implementation of very large composite structures, such as for launch-vehicle propellant cryogenic tanks and airframe, requires the development of out-of-autoclave processing methods. One such method is automated fiber placement, a relatively mature technology that allows for increased part layup accuracy and lower part fabrication costs as well as shorter part build cycles. Automated fiber placement is currently, and is expected to remain, a leading candidate for the fabrication of very large launch vehicle propellant tanks and airframe structures.

Much investigation in recent years has centered on the performance of composite materials at cryogenic temperatures. Thermal cycling to very low temperatures results in microcracking of the polymer matrix resin, leading to permeability of the tank, and the potential for decreased mechanical performance. One possible solution is to incorporate thin polymeric or metallic films within the wall of the tank that are resistant to thermal cycling-induced microcracking. Figure 1 shows a photomicrograph of a cross section of four-ply PEEK/IM7 thermoplastic composite specimen having a 3-mil thick PEEK barrier film located at the midplane. This specimen was fabricated by the principal investigator at the NASA Langley Research Center and was funded under the High-Speed Research Program.

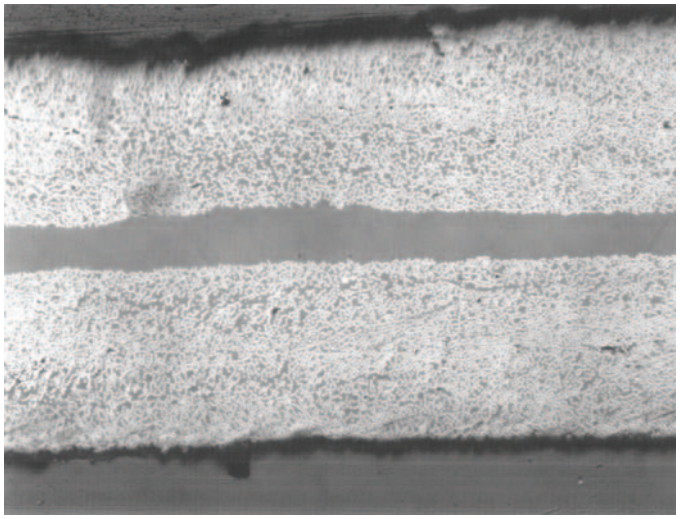

Figure 1. Photomicrograph of a PEEK/IM7 composite having a 3-mil PEEK barrier film fabricated by fiber placement.

Recently, an effort was initiated to develop test hardware and procedures so that MSFC would have an in-house capability to test various composite materials for cryogenic thermal cycling performance. Barrier film and foil materials were some of the materials that exhibited promise. As these investigations continue, methods to fabricate large structures incorporating such films should be addressed. The development of a film-processing module as herein described is an attempt to respond to this challenge.

Another area of large potential benefit in the successful development of the film module technology is in the application of honeycomb core adhesive to composite structures. Such adhesives are now currently applied using hand layup techniques. Increases in part size and complexity greatly complicate the application of these adhesives. For very large (e.g., 30-ft diameter by 80-ft length) composite propellant tanks, the application of core adhesives by manual means would be unacceptable. The development and proof-of-concept of the film module technology will enable and greatly enhance the fabrication of very large honeycomb core composite structures. A carbon fiber composite tank having an adhesively bonded honeycomb core is shown in figure 2.

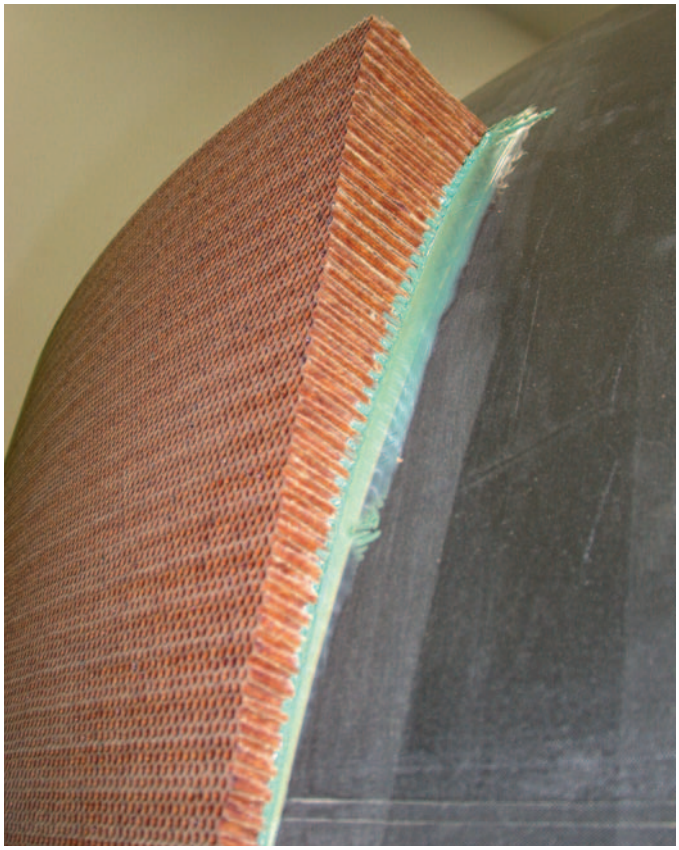

Figure 2. Honeycomb core bonded to composite tank. The core is adhesively bonded to the tank outer wall.

Approach

The basic approach is to design, construct, and demonstrate a film/adhesive laydown module that is to be fitted to an existing in-house fiber placement machine. The NCAM facility houses two fiber placement processing machines: One of these, the CMI 7-Axis Fiber Placement Machine, is a machine that represents near state-of-the-art in fiber placement processing of composites. This machine has a placement head that is readily adaptable to accept the addition of the film module hardware. This machine is shown in figure 3.

Film Application

The application of thin films onto flat open-section parts is a trivial task and can be accomplished manually using film in sheet form, enabling the coverage of a large area in a cost-effective manner. However, for complex curved part geometries, the application of film sheets is not possible due to the excessive wrinkling of the film that would occur. One way to avoid such difficulties is to make use of narrow filmstrips. The fiber placement machine, as currently configured, deposits 2.54-cm wide composite towpreg to the tool surface. The width of the film/foil strips to be processed by the film module will therefore be 2.54-cm wide. Materials that may be supplied to the film module include thermoplastic and thermosetting polymeric films, film adhesives, and metallic films and foils.

Integration Considerations

The film module is designed to be a fully automated feed and delivery system for the supply of film, foil, and core adhesives

Figure 3. Fiber placement machine in the NCAM facility at NASA MSFC.

materials to the automated fiber placement machine. Although it is possible that such a device may function as stand-alone processing equipment, great benefit lies in the coupling of such a device to the fiber placement machine. The film module thus conceived will consist of a supply, feed and delivery system, a film cut-off system, and a material preheating system. The module can have more than one embodiment: It may be designed to utilize the compaction device of the host placement machine or it may be designed having it's own such device. The width range of the film or foil used is not specifically limited, however when the compaction device of an existing fiber placement machine is used to deposit the film, the film width will be constrained by this dimension.

System Control

The film module is designed to be digitally controlled and programmable via a Direct-Logic™ 205 programmable logic controller (PLC). All motion devices are pneumatically actuated. The device is fitted with an infrared (IR) radiant energy source that will allow the film and/or composite substrate to become soft or tacky so that adhesion of the incoming film/adhesive to the substrate material is accomplished. The IR source is fully controllable via the PLC such that energy ramp ups and ramp downs can be made to correlate with placement head accelerations and decelerations. IR radiant energy is ideally suited for this purpose as it is a noncontact (nonconductive) thermal energy source.

Device Checkout and Panel Fabrication

Subsequent to mating the film module to the fiber placement machine, a series of bench-level checkouts were conducted. All module functions were actuated, sequenced, and timed to correspond with several existing placement processing files from the CMI placement machine library of programs. Upon completion of this checkout phase, the module will then be installed onto the fiber placement machine. Further checkout activities, which will primarily include timing sequence adjustments, will be conducted prior to actual material deposition. Upon final checkout of the film module, several demonstration panels will be processed and tested. Testing will consist of both mechanical property evaluations and micrographic inspection of the composite/film interface to assess void content and film edge-to-edge placement accuracy. This project will be considered successful upon the demonstration of the film module to accurately and consistently process film materials into composite materials. It should be noted that is it outside the scope of this effort to assess the cryogen barrier properties of any of the materials produced with the film module.

Accomplishments

Module Controls Integration

The module control system was shipped to MSFC and installed during the reporting period. The controls engineer who developed the system provided 2 days of technical support with controls integration and device troubleshooting. Complete and thorough documentation and operation training were also provided.

System Laboratory Checkout

A series of preliminary system bench tests were performed upon completion of the control system integration. The checkouts included independent actuation of the module film feed, film cut, and IR lamp functions prior to full-scale laboratory simulation testing of the device. Upon successful completion of these preliminary checkouts, full-scale simulation testing was performed using 3-mil thick polyester film. Several design problems were found during testing that lead to various minor modifications to the device.

Integration With Fiber Placement Machine

Several modifications to the device were found to be necessary upon fit checking of the device to the fiber placement machine. These modifications were primarily concerned with creating appropriate clearances between the film module and the fiber placement machine head. The most significant task associated with the module integration was the routing and bundling of the pneumatic hoses and electrical wiring. Care was taken during the routing of the hoses and wires to ensure that sufficient free length was used to accommodate the range of motion of the fiber placement machine. The fully integrated film module is shown attached to the fiber placement machine in figure 4. Figure 5 shows how film is fed into the film module device and how it exits the device.

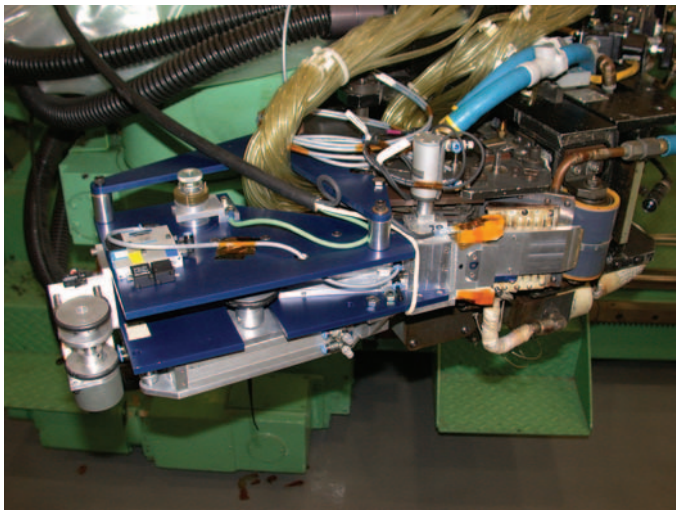

Figure 4. The fully integrated film module (left) attached to the fiber placement machine head.

Planned Future Work

Due to technical difficulties with the NASA MSFC fiber placement machine, full-scale operational demonstrations and panel fabrication were not possible during the reporting period. This project has been granted an extension of time to allow these demonstrations to be undertaken. Once the placement machine has been brought back to operational status, several test panels will be fabricated.

A preliminary search by Research Triangle Institute resulted in the identification of two aerospace companies (Boeing and Raytheon) who are interested in the further development of this

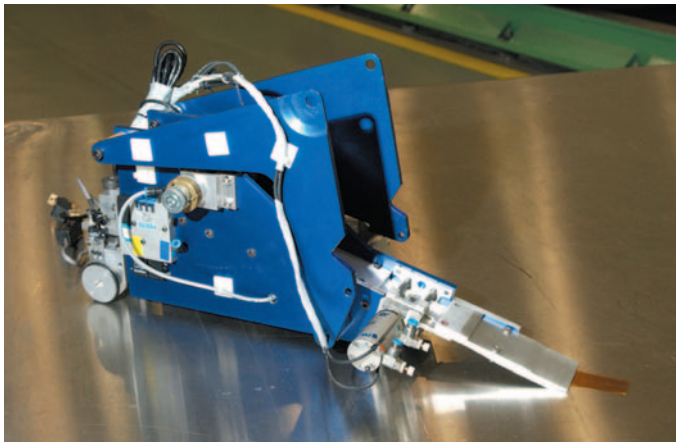

Figure 5. Film module device. Film is fed from a spool at the upper left side of the device and can be seen exiting the film delivery guide at lower right.

technology. The MSFC Technology Transfer Office is planning to showcase the prototype film module developed under this program at the NASA Technology Transfer exhibit at the May 2004 Society for the Advancement of Materials and Process Engineering (SAMPE) Symposium and Exhibition. Additionally, the principal investigator will present this technology during the NASA Technology Briefings Session at this conference. The MSFC Commercial Technology Lead, Mr. Sammy Nabors, will invite various company representatives to this presentation to discuss potential licensing opportunities.

It is anticipated that funding will be sought to allow for processing research studies to be performed using the film module technology. These studies will allow for further identification of processing/machine related effects, processing quality studies, and the fabrication of large-scale demonstration components. Such funding may be provided through a TIPS award or through IR&D sources.

Publications and Patent Applications

An invention disclosure has recently been filed on this innovation with the Technology Transfer Office.

Funding Summary

Table 1 presents a summary of the funding for this project. Accudyne Systems Incorporated performed the controls system contract. The fiber placement contract funds have been committed to an ATK contract and will be utilized pending repair of the placement machine.

Table 1. Funding summary for this project.

Description	Fiscal Year 2003 ($)
Total Funding:	24,000
Expenses:	
Machining services	5,000
Controls contract (ASI)	11,000
Fiber placement contract (ATK)	8,000
Total	**24,000**

Status of Investigation

The film module has been fully assembled and is considered to be 100 percent operational. Laboratory-scale control system checkouts have been performed on the device and debugging operations and minor modifications have been performed. A full-scale physical integration of the film module to the fiber placement machine head has been completed.

Prior to final demonstrations of the film module on the fiber placement machine, maintenance of this machine must be performed to return it to operational status. Project funds have been committed to a fiber placement support contract to allow for demonstration and panel fabrication once the machine has been repaired.

Advanced Sensor Concepts for General Avionics Applications

Project Number: 03–11

Investigators: **Dean Alhorn/ED17**
David Howard/ED17
Dennis Smith/ED17

Purpose

The purpose of this Center Director's Discretionary Fund (CDDF) project is to develop several novel sensor concepts into patents and commercial prototypes.

Background

The original effort that started this CDDF project is the development of a position sensor technology for the GLovebox Integrated Microgravity Isolation Technology (g-LIMIT) project. The dual-axis position sensor developed for the g-LIMIT project was patented under patent number 6,246,228. The concepts developed in this CDDF stem from that original patent. Another patent being studied under this CDDF project is the Rotary Position Sensor (RPS), patent number 6,313,624. These technologies have been demonstrated at several sensor trade shows during the past few years and are currently seeking partners for commercialization.

Approach

Due to the patent process, the technologies developed with this CDDF cannot be fully explained in detail. Therefore, until the concepts have been developed and patents applied for, only general concepts and results that are not specific to the design will be presented. The basic premise of the approach to testing the sensor concepts was to design an engineering prototype and then determine the capabilities of the design. Then, either refine the design and retest or develop the design into a commercially viable design and develop a demonstration unit to display the concept's functions and capabilities.

A sensor board with multiple design options was developed and fabricated. This procurement provided several options and concepts to be tested. The components for the linear-test fixture were designed, fabricated, and the entire test fixture was assembled. A control program was developed and integrated with the test fixture and associated measuring equipment. Figure 1 illustrates the linear test setup. A precision linear table with drive capabilities has been used as the reference for determining the accuracy and resolution of the sensor concepts. The prototype sensors are placed into the test fixture and multiple test runs are performed to generate statistically significant data. These data are then analyzed to determine the accuracy and resolution of the sensor concepts.

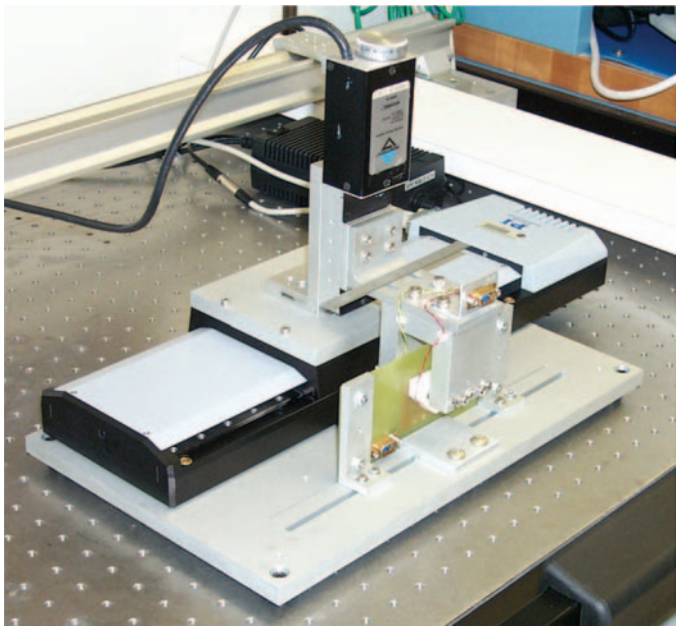

Figure 1. Linear test setup.

Similarly a rotary text fixture has been designed and is currently being fabricated. This rotary fixture will be used to determine the accuracy and resolution of the rotary sensor concepts.

To produce a commercially viable product, several signal conditioning electronics designs have been developed to aid in the testing of the sensor concepts and for demonstrating the technology to commercial interests. Figure 2 shows a signal conditioning electronics printed wiring board developed for one of the sensor concepts. Figure 3 presents the components for a rotational transformer. This rotary transformer is needed to produce a product that is brushless and more reliable. The rotary transformer will be designed into the commercial prototype.

Accomplishments

Several engineering prototypes for sensor concepts have been developed. A linear test fixture has been fabricated and some of the sensor concepts have been either fully tested or are still in process. A set of signal conditioning electronics has been developed and more electronic designs are in development. Two rotary transformer designs have been fabricated and are being tested.

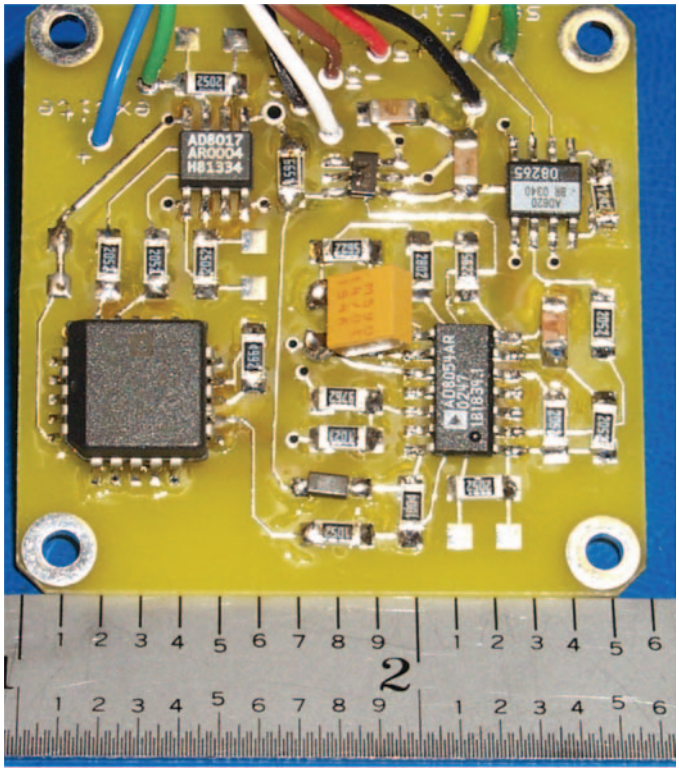

Figure 2. A signal conditioning electronics printed wiring board developed for one of the sensor concepts.

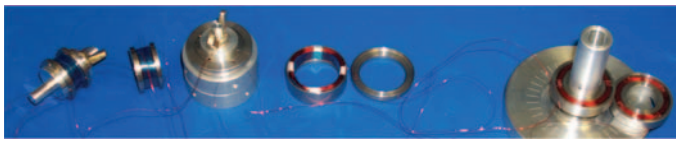

Figure 3. Components for a rotational transformer.

One of the significant accomplishments in this project has been the increase of the signal-to-noise ratio. The signal levels that the sensor produces are in the millivolt range. An increase of this magnitude has aided in the ability to analyze the sensor capabilities and has improved the basic sensor concept. In addition, this finding will significantly enhance the design of the RPS. This development will be incorporated, tested, and submitted as an improvement to the existing RPS technology.

Another significant accomplishment has been the testing and subsequent analysis of one of the sensor concepts. Figure 4 illustrates the linearity of one of the sensor prototypes. Several test runs are illustrated and it is apparent that the sensor is highly repeatable from run to run. One measure of the repeatability is the correlation of the data sets. Another measurement and analysis of the data is the overall accuracy of this sensor concept. Table 1 presents the data for this sensor concept. The analysis indicates that the overall resolution for this sensor concept is 10–12 bits over the full-scale range of 5 mm.

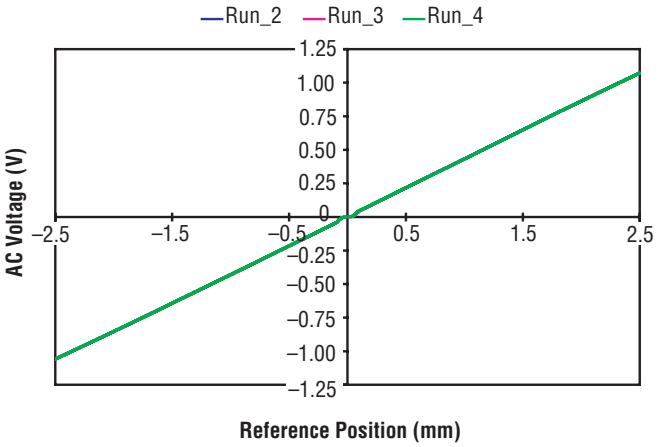

Figure 4. The linearity of one of the sensor prototypes.

Table 1. Sensor capabilities.

	Run/Run	Accuracy
Correlation	0.9999999	N/A
Maximum Error	1.72 µm	3.7 µm
Average Error	0.59 µm	0.86 µm
Standard Deviation	0.41 µm	0.67 µm

It is important to note that in figure 4, near zero, there is a nonlinearity in the data. Figure 5 presents a magnification of the data about zero. Analysis of the data and further testing revealed that this nonlinearity is actually caused by the test equipment used to measure the signal. The sensor capabilities presented in table 1 included this nonlinearity in the analysis and it is expected that the overall accuracy of the sensor is better than what is presented herein.

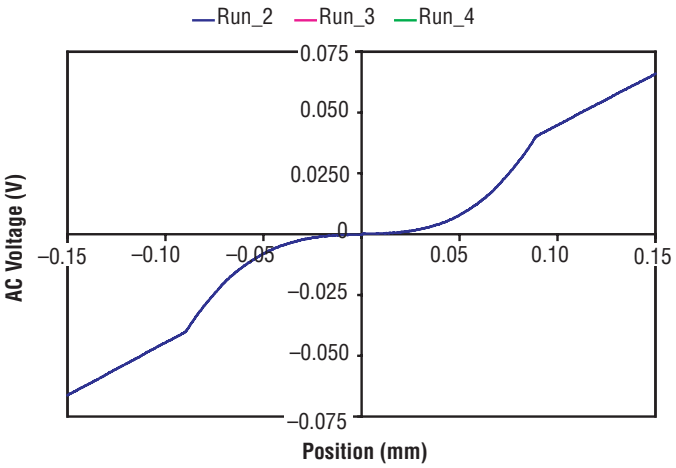

Figure 5. Magnification of the data about zero.

Planned Future Work

During the second year of the project, the investigators plan to continue sensor design, testing, and analyses. The rotary sensor designs will be tested using the rotary test fixture, which is in fabrication. The rotary transformer will be analyzed and modifications will be made as warranted and will undergo further testing. Demonstration units will be designed and fabricated to illustrate the functions and capabilities of the sensor concepts. This effort will be coordinated with the Technology Transfer group.

The technological advancement from the design of these sensor concepts will be used to enhance the technology of the RPS sensor.

An invention disclosure will be submitted for this first sensor concept in March 2004. Other disclosures will be submitted as designs reach maturity and preliminary testing has been performed on the sensor engineering prototypes.

Publications and Patent Applictions

An Invention Disclosure was submitted for the first sensor concept in March 2004. Other disclosures will be submitted as designs reach maturity and are tested.

Funding Summary

The Advanced Sensor Concepts for General Avionics Applications project has committed approximately $25,000 of the planned $50,000 for this effort. The remaining funds will be used to design and fabricate the commercial prototypes of the sensor technologies and to design and fabricate demonstration units for the sensor concepts.

Status Investigation

The Advanced Sensor Concepts for General Avionics Applications CDDF project is continuing in its second year of effort.

Torque Limits in Composites

Project Number: 03–13

Investigators: **Frank Thomas/ED23**
Brett Smith/ED34
Doug Fox / ED22

Purpose

The objective of this Center Director's Discretionary Fund (CDDF) effort is to experimentally determine recommended torque values for mechanically fastening composite materials and to develop an analytical approach, based on material properties, to be used as a tool for determining torque values as parameters are varied.

Background

Composite materials are typically joined together via bonding, mechanically fastening, or a combination of both methodologies. Joining of composite materials via mechanical fasteners is the focus of this effort. Because of the anisotropic nature of composite materials, the same methodology used for joining isotropic materials is not compatible with joining composite materials. Specifically, through exhaustive testing and statistical analysis, the torque recommended for joining isotropic materials is documented and available for inclusion on design drawings and for analytical verification. However, there is not a similar recommendation for torquing anisotropic materials.

Approach

To ascertain a reliable value for assigning torque limits to mechanical fasteners when joining composite components, a statistically valid set of torque versus tension tests are justifiable. The approach is to build a significant quantity of composite test specimens and perform sufficient tests to quantitatively determine appropriate torque limits to use when joining composite components with mechanical fasteners.

Accomplishments

An initial representative set of aerospace composite components has been fabricated, tested, and the results summarized. The goal of these initial tests was to determine a reliable test procedure and failure detection methodology. Torque versus tension tests were performed at Marshall Space Flight Center's (MSFC's) torque-tension testing facility in building 4612 using an ultrahigh-strength aerospace quality composite, IM7/8552. An acoustic emission transducer was placed on the samples during testing for later analysis. Testing was manually stopped when the following conditions occurred: An auditable sound was heard and the tension, as displayed by the data acquisition system, suddenly decreased. Results from these preliminary tests (see table 1) indicate that, for the small diameter fasteners used, the bolt would exceed its maximum recommended torque value before failing the composite. However, the opposite was observed for the larger fasteners tested.

Planned Future Work

Additional tasks include analyzing the AE data and the torque versus tension data to develop margins of safety. Also, because there is a multitude of composite materials available, additional materials are being fabricated and are to be tested.

Publications and Patent Applications

None

Funding Summary

Fiscal year 2003: $40,000 ($38,000 Obligated)
Fiscal year 2004: $40,000

Status of Investigation

A reliable test plan has been developed along with a verification technique. Additional tests are required to determine trends and relationships between the various composite materials and the bolted joint interaction. Four composite material systems have been purchased and are being fabricated with testing and data analysis to follow.

Table 1. Comparison of torque/tension limit for IM7/8552 (0°, 45°, $\alpha\nu\delta$, 90°)

Fastener Size	Specimen Thickness	Torque Limit (in*lb)		
		Test	Test/1.5	MSFC–STD–486
1/4 in	0.132	271	181	70–85
	0.176	224	149	
	0.220	235	157	
1/2 in	0.132	638	425	620–730
	0.176	596	397	
	0.220	500	333	
3/4 in	0.132	1,155	770	1,930–2,270
	0.176	2,236	1,491	
	0.220	2,215	1,477	

MSFC-STD–486 torque values correspond to fastener failure.

- Test torque values correspond to composite failure during torquing.
- Test data greater than MSFC–STD–486 values, (with a factor of safety) corresponds to a SAFE utilization of the torque values specified in MSFC–STD–486.
- Test data less than MSFC–STD–486 values corresponds to a an UNSAFE utilization of the torque values specified in MSFC–STD–486.
- Observations:
  - These results are preliminary since they are based on limited tests.
  - Test methodology provides a conservative approach for developing torque-tension relationships for mechanically joining composite components

High-Strength and Compatible Aluminum Alloy for Hydrogen Peroxide Fuel Tanks

Project Number: 03–14

Investigators: Jonathan A. Lee/ED33
Po Shou Chen/Morgan Research Corp

Purpose

The purpose of this Center Director's Discretionary Fund (CDDF) project was to develop a high-strength and chemically inert aluminum alloy as fuel tanks for long-term storage of liquid hydrogen peroxide (H_2O_2). If successful, it could be an enabling material technology for the development of NASA's next generations of Hypersonic-X vehicles, where flight weight reduction from fuel tanks is a critical requirement.

Background

This proposal supports the advancement of lightweight and high-strength aluminum alloys for H_2O_2 fuel tanks and airframe technology. As shown in figure 1, the proposal supports the development for NASA's series of Hypersonic-X flight test air-breathing vehicles such as the X–43B flight demonstrator, using a Rocket-Based Combine-Cycle system, which could revolutionize access to space and air transportation in the next quarter century. One of the tests has demonstrated the first successful hot fire of a thruster using a mix of decomposed H_2O_2 and JP–7 jet fuel to generate combustion. This 90-percent peroxide trifluid approach will allow the thrusters to fit within the engine's extremely tight packaging restraints, yet deliver high performance.

Approach

The goal is to develop a new aluminum alloy that has the same compatibility rating (class 1) with H_2O_2, similar to the conventional AL5254 alloy, but with a dramatic improvement in tensile strength by a factor of two to three times more than AL5254. The development strategy is to modify the composition of AL5254, by scientifically selecting certain rare-earth or transition elements with unique chemical properties, to enhance its tensile strength. An exploratory effort will be conducted for welding of the new alloy using friction stir welding (FSW). All planned activities will be conducted in-house using Marshall Space Flight Center (MSFC) existing facilities.

Accomplishment

Several aluminum-scandium based alloy compositions have been successfully formulated, cast, and rolled into thin metal sheets for mechanical testing and chemical inert compatibility testing. From the preliminary test data, all these experimental alloys reportedly are completely chemically inert when exposed to H_2O_2. One of these alloys was also identified to have more than two times the tensile strength of the state-of-the-art 5254 alloy, while maintaining excellent H_2O_2 compatibility (class 1 category) similar to 5254 alloy. Figure 2.a (left) shows a vial

Figure 1. Development for NASA's series of Hypersonic-X flight test air-breathing vehicles.

that contains liquid H_2O_2 and an alloy test coupon. Figure 2.b (right) shows the isothermal microcalorimeter instrument used to determine the H_2O_2 decomposition rate when exposed to the alloys. Moreover, test data also show that these experimental alloys can be welded successfully using FSW.

Planned Future Work

This is a 1-year program plan for fiscal year (FY) 2003, and the principal investigators have successfully completed all technical objectives. There is no planned future work on this task.

Publications and Patent Applications

The writing and submission for the comprehensive final report is in progress. There is no patent application filed for this technology.

Funding Summary

This was a 1-year program plan with a total funding request of $35,000. The estimate total full time equivalent value is 0.25 for FY 2003. The total program funding and expenditure plan is summarized in table 1.

Table 1. Funding summary.

	FY 2003	FY 2004
Authorized by letter:	$35,000	$35,000
Obligated to date:	$35,000	$35,000

Status of Investigation

Project approval: March 2003

Figure 2. (a) A vial contains liquid H_2O_2 and an alloy test coupon, (b) The isothermal microcalorimeter instrument.

Rotational Vacuum-Assisted Resin Transfer Molding

Project Number: 03–15

Investigator: Bruce Hulcher/ED34

Purpose

Carbon-fiber reinforced composite materials have inherent advantages for use in many aerospace applications. Some of these applications include launch vehicle propellant tanks, and launch vehicle and commercial aircraft airframe structures. The high specific strength (strength per unit weight) of these materials makes them highly desirable for use in such applications. Most high-performance aerospace composites specified for fabrication are autoclave-processed materials. In both the second and third generation Reusable Launch Vehicle (RLV) programs, the dimensions of propellant tanks and airframe structures are significantly too large to be accommodated by the largest autoclaves that currently exist in the United States (U.S.). Accordingly, the capital expense associated with the procurement of such a facility would be very high and would likely not be supported by either program. Out-of-autoclave processes are therefore being investigated to produce such large components as are needed for the next generation of RLVs.

One such out-of-autoclave process is the vacuum-assisted resin transfer molding (VARTM) process. This process has been used extensively for many years to manufacture a wide variety of composite articles. Although this process is a relatively low-cost fabrication method, it has some limitations that have precluded its use in the processing of high-performance components. It is the intent of this Center Director's Discretionary Fund (CDDF) project to investigate the rotational vacuum-assisted resin transfer molding (RVARTM) process as a technique for increasing the properties of VARTM-processed composite materials.

Background

VARTM processing has a long and successful history as a low-cost, low-tech composite materials fabrication method. Due to limitations in attainable fiber volume content inherent with the VARTM process, materials thus fabricated are of lower performance capability than their autoclaved counterparts. In a fiber reinforced composite material, the tensile strength of the material is dominated by the tensile strength of the fiber and the compression properties are dominated by the modulus of the polymer matrix component. It is therefore advantageous to maximize the fiber content of the composite. In VARTM-processed composites, the fiber volume tends to be less than optimal due to two factors. The first factor is related to the structure of the fabric preform materials that are used in the VARTM process. The second factor that compromises fiber volume is the inherently lower compaction force that is attainable when using this method. The primary purpose of this CDDF project is to address the issue of compaction force through the development of the novel processing technique of RVARTM.

A new carbon-fiber preform material, spread-tow fabric, has been developed. This fabric significantly reduces the out-of-plane waviness, or crimp, of the carbon fiber tow. This reduction in crimp increases the in-plane fiber-dominated properties and decreases the resin-rich void spaces that result upon infusion of the material with resin. These benefits lead to an increase in the composite fiber volume fraction and therefore an increase in performance. Furthermore, it has been shown that a reduction in composite ply thickness results in a substantial reduction in the amount of microcracking seen in cryogenic thermal cycling tests. Since the spread-tow fabric has a significantly reduced thickness as compared to standard fabric preforms (0.0015-in versus 0.024-in. thickness for 8 Harness Satin) materials made with these new preforms will have increased microcracking resistance. These new fabric material forms will be excellent candidates for trials with the RVARTM process.

Approach

In the VARTM process, the only compaction force applied is that attained by evacuating the preform of air. This results in a compaction pressure of 14.7 psi (atmospheric pressure) on the composite. One possible approach to increase the compaction force on the composite is to place the preform on the inside surface of a rotating cylindrical shell either during the resin infiltration process or immediately after the preform has been infiltrated. Rotation produces an outward-acting radial component of acceleration that, together with an additional mass overlying the composite, can serve to provide additional compaction forces. Such a mass can take the form of thick rubber sheeting, sand, or a large number of small steel spheres. The following graph of figure 1 illustrates the combined effect that part diameter and compaction mass have on the rotation speed needed to produce a compaction pressure of 80 psi, which is typical of pressures commonly used in autoclave processing of composites.

Several comments should be made with reference to this figure. For a constant part diameter, as the mass of the compaction material increases, the required rotational velocity of the tool necessary to achieve 80 psi decreases. Similarly, as the part diameter is increased, tool rotational speed again decreases for constant compaction pressure. Based upon this and similar data, a decision was made to use steel spheres as the compaction mass for this project.

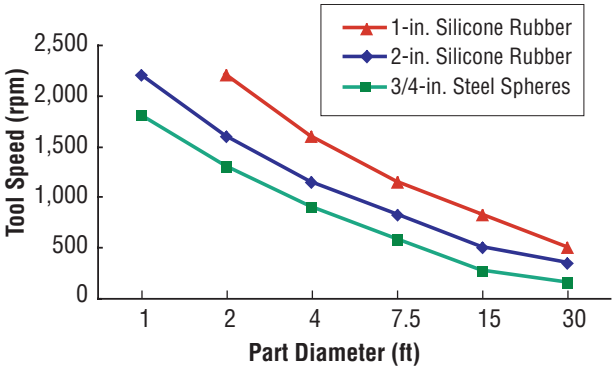

Figure 1. Tool rotational speed as functions of both part diameter and compaction mass necessary to produce 80 psi of pressure on the composite. Note that tool speed is lowest when using steel spheres.

In order to investigate the RVARTM process, a machine test-bed is needed to rotate the tooling and composite setup during processing. A standard metal working engine lathe was selected for this purpose. An engine lathe is ideal for this purpose as it allows for a wide range of rotational speeds and provides both the rigidity needed for high-speed rotation of the tooling and the flexibility to accommodate design changes and process modifications. Initially, a series of processing trials will be run to verify the machine setup and to uncover any unforeseen problem areas. This set of tests will not include compacting mass. As confidence in the overall test setup is gained, compaction mass, in the form of 0.125-in diameter steel spheres, will be added. A series of tests using various compaction masses and rotation speeds will then be undertaken to assess the efficacy of the process in increasing part fiber volume fractions.

Accomplishments

Calculations were made during the period to understand the magnitudes of the compaction forces as functions of the processing parameters (tool radius, the compaction mass, and rotation speed). Knowledge of these parameters was necessary in designing the tool, specifying an appropriate engine lathe, and choosing the material that would serve as the compacting mass. Additionally, these calculations made it possible to define the range of compaction mass that would provide the range of pressures desired. This range extends from just above atmospheric pressure to 80 psi.

Processing trials were performed to determine the feasibility of using the VARTM process to produce a cylindrical component. These trials were also helpful in identifying process setup difficulties that might be unique to VARTM processing of cylindrical articles; this experience was invaluable in designing the tool to be used in the actual RVARTM process trials. The resin infusion setup and the resulting test article are presented in figures 2 and 3, respectively.

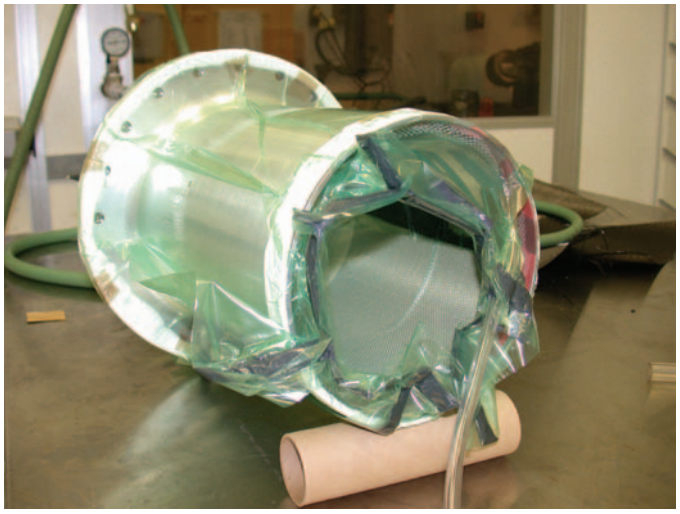

Figure 2. VARTM test setup for processing of cylindrical articles. Tool inside diameter is 7.5 in.

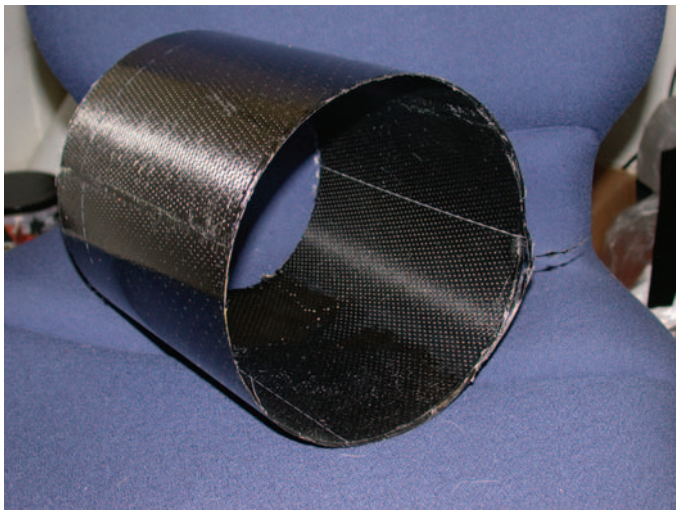

Figure 3. Composite cylinder successfully fabricated by VARTM.

The specification, acquisition, and installation of the engine-lathe processing test-bed were also accomplished during the period. The lathe acquired for this project had a speed range upper limit of 2,000 rpm, and can accept tool diameters of 13 in having lengths up to 36 in, and diameters up to 19.5 in having lengths up to 6 in.

The design and fabrication of the RVARTM tooling was completed during the reporting period. Aluminum was chosen as the material for the tool due to weight and cost considerations. The tool is essentially a hollow tube having an attachment plate on one end for attachment of the tool to the lathe and a cover plate at the opposite end that holds the tool spindle. This spindle allows for the tool to be supported on the end opposite to where it is attached to the lathe. A steady-rest device, which was provided as an accessory to the engine lathe, is mounted to the lathe and allows for support of the tool as well as tool rotation. The disassembled tool is shown in figure 4 and the tool/lathe processing setup is shown in figure 5.

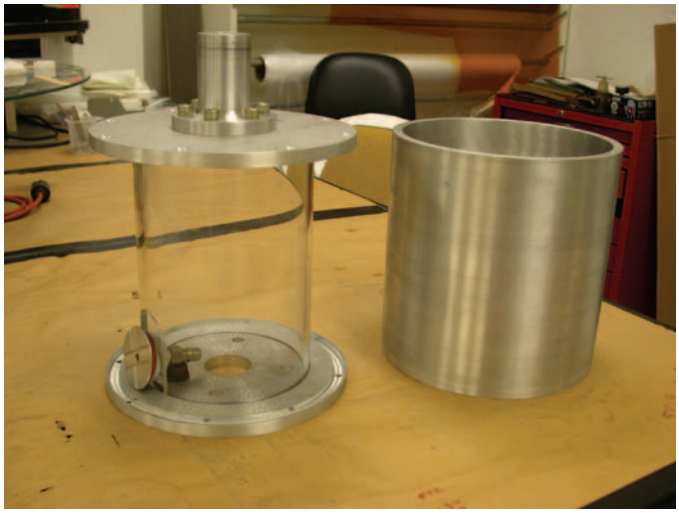

Figure 4. Disassembled RVARTM tool showing plexiglass compaction mass barrier and vacuum port.

Figure 5. Assembled tooling mounted in the engine lathe. The steady-rest support for the tool is at center right. Note the hole in the spindle for resin infusion and the heat lamp at upper right.

The connection of a vacuum hose to the rotating VARTM tool requires the use of special rotary fittings. Hardware has been designed and fitted to the headstock of the lathe that permits the mounting of the rotary flow joint to the machine.

Planned Future Work

Due to the potential of fabric preform springback, it is desired that the composite be brought to some level of cure prior to discontinuing rotation of the tool. Curing of the resin system will require that the temperature of the resin be elevated for several hours. In order to maximize the heat transfer from the radiant heat source into the composite, the tool will be anodized and dyed black. The heat lamp shown in figure 5 will provide the radiant energy heat source.

The tool must be modified prior to the initiation of test trials. A small window will be cut into the wall of the tool to allow for a visual check to determine when the resin flow front has moved across the composite preform, indicating that rotation of the part can be initiated.

A series of tests with various compaction masses and rotation speeds will then be undertaken to assess the efficacy of the process in increasing part fiber volume fractions. Optical analysis of photomicrographs taken of the cross section of the composite wall will be performed to quantify the increases in fiber content. Another way to assess the quality of the composite is to submit the article to destructive testing. A meaningful assessment would be to submit the cylindrical test articles to uniaxial compression testing. A series of test articles, fabricated with two or more preform types, will be processed and tested. A one-to-one comparison of failure strengths between cylinders processed by standard VARTM and by RVARTM will then possible.

Publications and Patent Applications

An invention disclosure was filed on this innovation with the Technology Transfer Office and a patent search was conducted, resulting in the decision to submit a patent application for this technology. A presentation of this technology will be given at the SAMPE Conference in May 2004 in the NASA Technology Briefings Session to explore possible licensing and partnering opportunities with the private sector.

Funding Summary

The total funding for fiscal year (FY) 2003 was $40,000 and is identified in table 1. Funding for composite article processing and testing support, although obligated and committed, has not been used, as the project has not yet moved into this phase.

Table 1. FY 2003 funding summary.

Expense Description	FY 2003 ($)
Machining services	14,000
Engine lathe	11,000
Testing and processing support contract (ATK)	10,000
Miscellaneous supplies, materials, and hardware	5,000
Funding total	**40,000**

Status of Investigation

All equipment and materials needed to run a full schedule of processing trials are in hand. The modifications to the tool will be completed by May 31, 2004. The initial full-scale processing checkout trials will then be performed. Fabrication of test articles will be started in June 2004. A plan of parallel part processing and testing will then be followed to maximize the amount of data returned.

Low-Power High-Voltage Power Supply With Fast Rise Time

Project Number: 03–16

Investigator: Douglas B. Bearden/ED11

Purpose

The purpose of this Center Director's Discretionary Fund (CDDF) project was to develop a closed-loop low-power high-voltage power supply with a fast-rise/fast-fall time of less than 100 us. The supply shall be programmable from 0–1,250 V and capable of delivering up to 300 uA at full output voltage.

Background

An open-loop high-voltage power supply with a fast-rise/fast-fall time was initially designed for Solar X-Ray Imager (SXI) and Solar Extreme Ultraviolet Research Telescope Spectrograph (SERTS). This supply was used to electronically shutter a microchannel plate (MCP) intensified charged-couple devices (CCD) by controlling the accelerating voltage across the MCP. These techniques have functioned successfully for the SXI telescope and in four different SERTS flights. A closed-loop high-voltage power supply, requiring a fast-rise/fast-fall time, is needed for future projects. By using a closed-loop design, the supply can be operated from no load to full load without using a preload. Not only will this make the supply more universal, it will also be more efficient.

Approach

This CDDF developed a closed-loop high-voltage power supply, based on the open-loop design, with a fast-rise/fast-fall time by using multiple feedback loops. The open-loop design used a preregulator, voltage doublers, and a preload to generate a high-voltage output with a fast-rise/fast-fall time. The closed-loop design used a second feedback loop that eliminated the need for a preload. A block diagram of the closed-loop design is shown in figure 1.

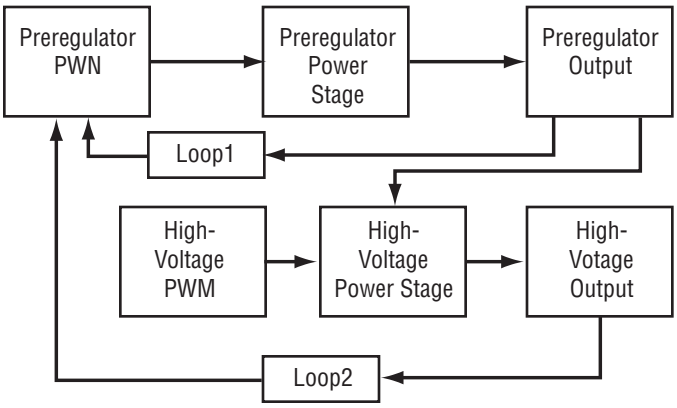

Figure 1. Block diagram of the closed-loop high-voltage power supply.

Accomplishments

To verify the closed-loop design, a breadboard was fabricated and tested. The closed-loop design consists of two feedback loops to control the output voltage. The first feedback loop controls the output of a preregulator that can be programmed to the desired voltage while the output stage of the power supply is inactive. The second feedback loop controls the output stage of the high-voltage power supply after the output has been activated, which eliminates the need for a preload. Figure 2 illustrates how the rise time of the output met the 100-us requirement when the output was turned on. Figure 3 illustrates how the fall time of the output met the 100-us requirement when the output was turned off. Figure 4 shows how the output could be used to generate a 0–1,250-V 500-Hz square wave by using a 0–5-V 500-Hz square wave to drive the on/off circuit of the power supply.

Planned Future Work

A fully packaged prototype of this proposal, including printed wiring board and chassis, will be used to verify the test data taken from the breadboard unit. Electric field analysis software will be used to verify the magnitude of the field strengths are within the design criteria in the critical high-voltage areas.

Publications and Patent Applications

A Disclosure of Invention and New Technology was filed for the closed-loop design on November 3, 2003.

Funding Summary

A total of $25,000 was used to fund this CDDF project for the following procurements: High-voltage potting supplies, miscellaneous high-voltage parts, prototype printed wiring board, chassis, and electric-field analysis software.

Status of Investigation

The fully packaged prototype has been fabricated and tested. Contact Douglas B. Bearden at 256–544–3340 for additional information regarding the prototype unit.

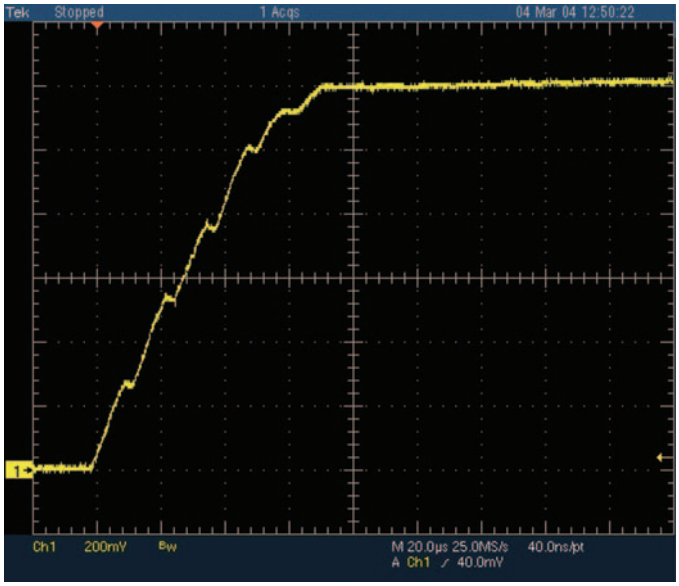

Figure 2. Rise time of high-voltage output when power supply is programmed to 1,250 V and output is turned on.

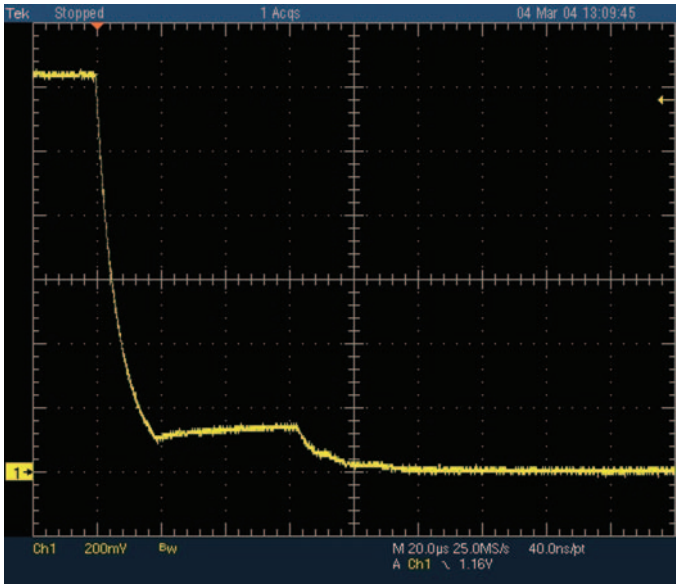

Figure 3. Fall time of high-voltage output when power supply is operating at 1,250 V and the output is turned off.

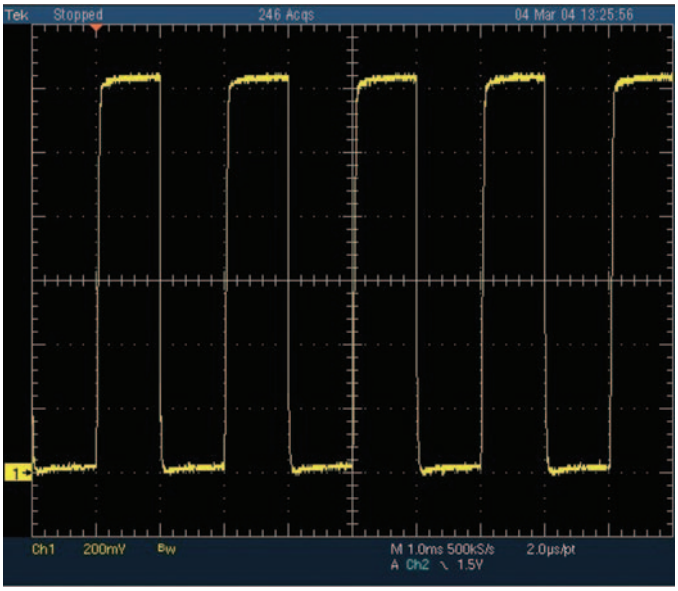

Figure 4. High-voltage output when power supply is programmed to 1,250 V and the on/off circuitry is driven by a 0–5-V 500-Hz square wave.

Coupled-Resonator-Enhanced Sensor Technologies

Project Number: 03–17

Investigators: **Dr. David D. Smith/SD46**
William K. Witherow/SD46
Dr. Kirk A. Fuller/UAH

Purpose

The objectives of this Center Director's Discretionary Fund (CDDF) investigation were the development of ultrasensitive advanced sensing technologies based on coherence phenomena in coupled optical resonators, with applications to vehicle health monitoring of propulsion and space transportation systems, as well as for biological and chemical sensors for the monitoring of astronaut and planetary atmospheres.

Background

Multiplicative Sensitivity Enhancement in Coupled Microresonators

We discovered that when multiple resonators are coupled together, either concentrically, or in side-by-side chain-like fashion, a splitting of the spherical modes is possible, provided that the optical thicknesses of each of the individual subresonators are identical (i.e., they are phase matched); and further, that these split modes are of a higher Q than the single-sphere modes. Interestingly, enormous intensity magnification factors, M, are possible for odd numbers of coupled rings provided the reflection coefficient of the numbered couplers r_{even} is made small, while that of the odd numbered couplers r_{odd} is kept large. Figure 1 shows the intensity magnification factor M in the central mode as a function of the number of rings N, for various values of r_{even} and r_{odd}. M is found to increase exponentially with N, subject to absorption limitations (dashed curves). This multiplicative sensitivity enhancement has an application to the development of advanced sensors.

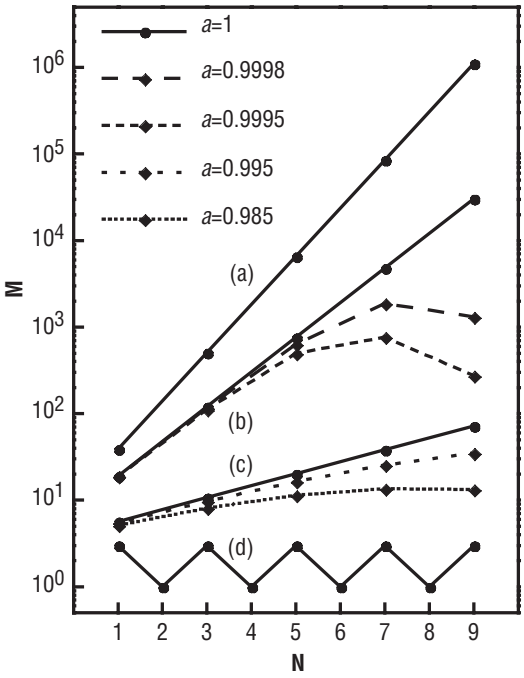

Figure 1. Intensity magnification factor *M* for odd numbers *N* of coupled ring resonators where $r_{even} = 0.5$ and (a) $r_{odd} = 0.95$, (b) $r_{odd} = 0.9$, (c) $r_{odd} = 0.7$, and (d) $r_{odd} = r_{even} = 0.5$. Case (d) includes even numbers of resonators. The dashed curves demonstrate the effect of loss for cases (b) and (c), where the attenuation factor *a* is 0.9998, 0.9995, 0.995, and 0.985, from top to bottom. Loss is neglected for the solid curves.

Cavity-Amplified Spectroscopic Analysis

Surface-enhanced Raman scattering (SERS) produced by molecules residing on metal nanoparticles has proven to be of great value in analytical chemistry and biomolecular research, pushing detection levels to the single-molecule limit. The metal nanoparticle essentially acts as a (surface plasmon) dipole antenna, efficiently coupling the light to the Raman active molecules. Our preliminary theoretical treatments of the optics of a gold (Au) nanoparticle on a microcavity resonator indicate that the SERS effect can itself be boosted by several orders of magnitude by strong evanescent fields arising near the cavity surface. We refer to this predicted gain in Raman signal as cavity-amplified SERS (CASERS) and are developing photonic microprobes to demonstrate the CASERS effect. In the same manner as CASERS, whispering-gallery modes (WGMs), interacting with metal nanoparticles, produce local fields that are enhanced in comparison with direct excitation as a result of the enormous circulating intensities in the microsphere, and these enhanced local fields in turn produce intensified fluorescence. We refer to this process as cavity-amplified fluorescence (CAF). Together, these processes may be referred to as cavity-amplified spectroscopic analysis (CASA). These effects can be exploited in miniature, fully spectroscopic biosensors that can actually identify agents rather than merely indicate their presence.

Approach

The project was proposed in August 2002, approved for funding in January 2003, and estimated for completion at the end of fiscal year (FY) 2004. First year tasks involved procurement of the external cavity diode laser (ECDL) and development of methods for fabricating fiber tapers and microspheres, as well as methods for manipulating and viewing the components. The experimental configuration is shown in figure 2.

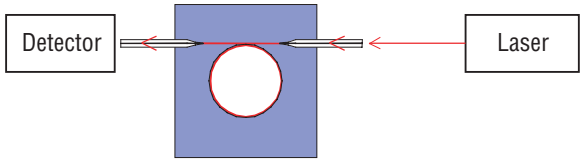

Figure 2. WGMs in a fused-silica microsphere are excited through a tapered fiber by a tunable ECDL and detected with a photodiode after interacting with an analyte.

In addition, a method for attaching Au and silver nanoparticles to the microspheres was developed. The metal nanoparticles are used to produce the desired enhanced Raman and fluorescence effects. Sol-gel coatings were also applied to the microspheres to enable incorporation of active species such as fluorescent probes and quantum dots. A Sensor Development Laboratory was established at the Marshall Space Flight Center (MSFC) and outfitted with new and reutilized equipment. Approximately $18,000 in equipment was obtained from the NASA reutilization program. In addition to the experimental work, analytical work was performed for the development of the formalism describing coupled optical resonators, and a variety of novel phenomena were predicted. Additionally, the project supported an on-site University of Alabama in Huntsville (UAH) graduate student (Hongrok Chang), as well as the involvement of Dr. Fuller through the NASA Faculty Fellowship Program. An undergraduate UAH student (Amanda Duffell) was also involved during the summer through the Undergraduate Student Research Program. Two technical exchange meetings were held at the Oklahoma State University (OKSU) with Professor Albert T. Rosenberger. One meeting with Dr. Rosenberger was also held at MSFC. Additional technical exchange meetings took place with the Quantum Computing Technologies Group at the Jet Propulsion Laboratory (JPL), and the Nonlinear Optics Group at the University of Rochester. A presentation was also given at the weekly meeting of the Science Directorate. The findings from the first year's activities are summarized in the discussion below.

Initial CASA experiments involved functionalizing microspheres with Au nanoparticles as shown in figure 3. Functionalized microspheres were then probed by the ECDL. In preliminary experiments at OKSU, we detected WGMs from microspheres functionalized with Au nanoparticles, and found that the cavity Q is sufficiently maintained at high values ($>10^6$) to retain technological relevance. These initial experiments have also revealed that the excitation wavelength can be extremely important for the success of CASERS experiments. Importantly, the optimum Raman gain for SERS occurs when the excitation wavelength lies midway between the surface plasmon resonance (SPR) and the Raman emission. Therefore, further studies will be conducted using a Sacher Lasertechnik ECDL available at MSFC. The advantage of the MSFC laser is that it is currently configured for 670 nm, which is closer to the SPR wavelength than the laser available at OKSU.

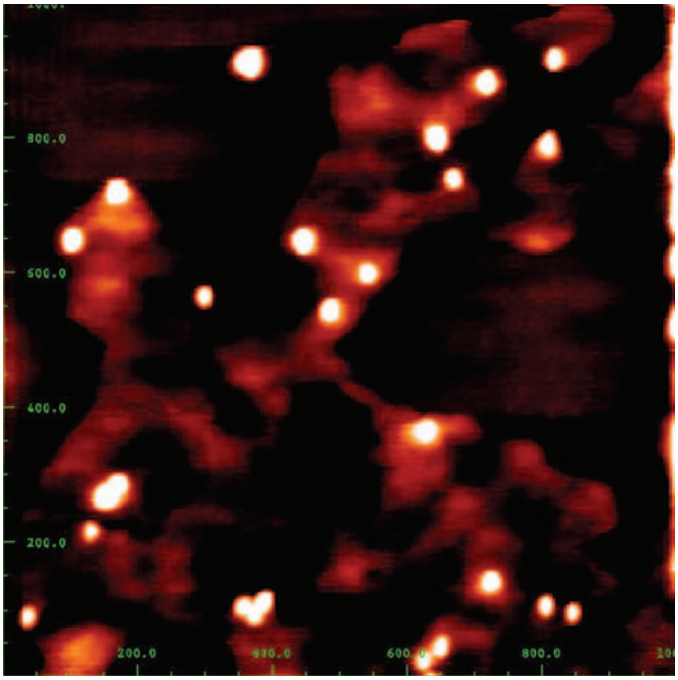

Figure 3. AFM of 20-nm Au nanoparticles attached to the surface of a 300-μm silica microsphere.

Accomplishments

The following accomplishments have been achieved for this project:

- Five technical reports.
- Four peer-reviewed journal articles.
- Ten conference presentations.
- Two new-technology reports.
- Procurement and setup of ECDL.
- Development of procedures for fused-silica microsphere fabrication, manipulation, and excitation, as well as for adiabatic tapered fiber fabrication.
- Establishment of the Sensor Development Laboratory and observation of WGMs in microspheres at MSFC.
- Establishment of collaborations with OKSU, University of Rochester, and JPL.
- Discovery of new phenomena including coupled-resonator-induced transparency (CRIT), coupled-resonator-induced absorption (CRIA), lasing without gain (LWG), cooperative cavity emission, coherent photon trapping, and adiabatic photon transfer. Several of these effects are summarized below.
- A proposal was submitted to the Office of Aerospace Technologies (OAT) NASA Research Announcement.

Coherence Phenomena in Passive Systems: Coupled-Resonator-Induced Transparency and Coupled-Resonator-Induced Absorbtion

Passive coupled resonators can be characterized according to their absorptive response. Two distinct phenomena can occur, distinguished by their spectral character. CRIT is characterized by an absorption minimum on resonance, whereas CRIA

is characterized by an enhanced absorption maximum. These spectra are shown in figure 4. Most interestingly, the transparency in CRIT is accompanied by slow light. Hence slow light can be achieved without absorption. Thus, one application of CRIT is to provide enhanced gyroscopic response of fiber gyros for inertial navigation. In preliminary experiments at OKSU, CRIT was observed in systems of two and three resonators.

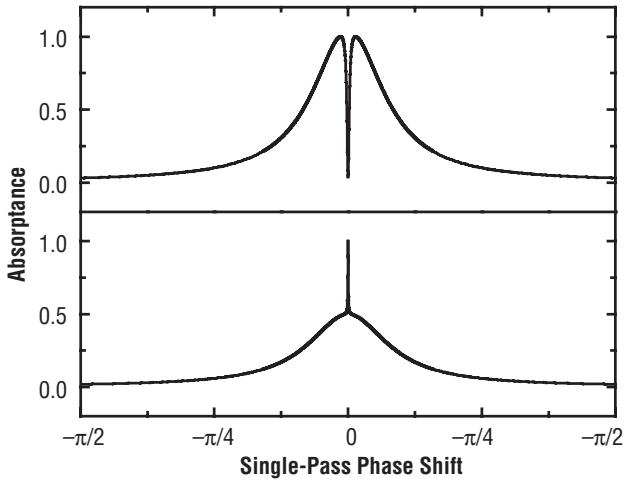

Figure 4. CRIT (top) and CRIA (bottom).

Coherence Phenomena in Active Systems: Lasing Without Gain and Cooperative Cavity Emission

The coherent coupling between optical resonators can lead to an effect analogous to lasing without inversion (LWI). In LWI, lasing occurs even though a net population inversion is not apparent in the bare-state basis. Examination of the steady-state and dynamic response of coupled resonators reveals that lasing can occur even though the gain per-unit-length does not exceed the loss per-unit-length (i.e., The product of the gains for the two resonators is less than unity (G_1G_2<1).). This result, referred to as LWG is shown in figure. 5 (a). The product G_1G_2 is the gain for the system in the absence of the coherent interaction between the resonators. Hence, it is clear that lasing would not occur without this coherence. The reason that lasing is possible is that, through constructive and destructive interference, paths through the resonator containing gain become more favorable. Thus, to achieve lasing, the gain must only exceed the loss for these paths, i.e., it is required that either G_1>1 or G_2>1 but not both.

Another consequence of the coherent coupling between resonators is that a significant reduction in the laser threshold can be obtained when the resonators are properly phased. Specifically, the threshold is reduced when the resonator furthest from the excitation waveguide is resonant, while that closest to the excitation waveguide is antiresonant. This arrangement compensates for the π phase shift that occurs due to the coupling between the resonators, and thus rephases the resonators. Consequently, the laser threshold can be reduced by orders of magnitude, as shown in figure 5 (b). This effect is analogous to the atomic phenomena of coherent spontaneous emission or superradiance, and applies to microcavities as well as larger laser cavities, provided proper stabilization techniques can be employed.

Planned Future Work

Future work will involve investigations of CRIT and CASA phenemona using the Sacher ECDL at MSFC. The advantage of the MSFC laser is that it is currently configured for 670 nm, which is closer to the SPR wavelength than the laser available at OKSU. This should facilitate the observation of CASERS and CAF. Because of the small excitation wavelength, very small (~2 micron) fiber tapers must be fabricated, which will require fine control over the fabrication process. To accomplish this, a computer-controlled fiber taper fabrication system must be built, including a translation stage and a minitorch. Achieving coherence effects such as CRIT in macroscopic resonators will require the application of frequency stabilization techniques. However, we are studying single polarization-coupled resonant

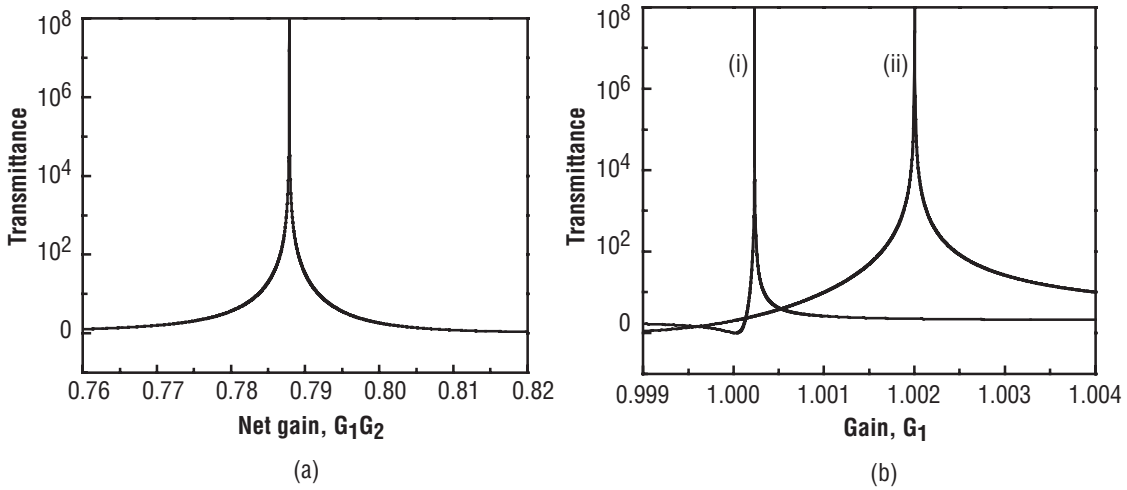

Figure 5. (a) LWG in two identical coupled resonators. The product of the gain factors at threshold is less than unity. (b) Reduced lasing threshold in two coupled resonators. The gain, G_1 required for lasing is lower for two coupled resonators (i) than for a single resonator (ii).

cavities as an alternative approach because of their inherent stability. Incorporation of active and nonlinear optical species via sol-gel coatings will also proceed in the second year. This will allow experimental investigation of coherence effects in active systems.

Publications

Technical Reports

Fuller, K.: "Compounded Microspheres in Photonics: Potential Biosensing and Bandgap Applications," *NASA SFFP Final Report*, Department of Atmospheric Sciences, UAH, 2001.

Fuller, K.: "Partial Wave Analysis of Coupled Photonic Structures," *NASA SFFP Final Report*, Department of Atmospheric Sciences, UAH, 2002.

Fuller, K.: "The Matrix Reloaded: Characteristic Matrices for Spherical Shell Photonic Systems," *NASA SFFP Final Report*, Department of Atmospheric Sciences, UAH, 2003.

Gates, A.L.: "Whispering-Gallery-Mode Resonances in Silica Microspheres," *MSFC USRP Final Report*, UAH, 2002.

Gates, A.L.: "Coupling Enhanced Lasing in Resonators," *MSFC USRP Final Report*, UAH, 2003.

Peer-Reviewed Journal Articles

Smith, D.D.; and Fuller, K.A.: "Photonic Bandgaps in Mie Scattering From Concentrically Stratified Spheres," *J. Opt. Soc. Am. B: Special Issue on Nonlinear Optics of Photonic Crystals*, Vol. 19, p. 2,449, 2002.

Smith, D.D.; and Fuller, K.A.: "Photonic Bandgaps in Mie Scattering From Concentrically Stratified Spheres," *Virt. J. of Nanoscale Sci. and Tech.*, Vol. 6, p. 16, 2002.

Smith, D.D.; Chang, H.; and Fuller, K.A.: "Whispering-Gallery Mode Splitting in Coupled Micro-Resonators," *Journal of Optical Society of America B*, Vol.10, p. 1,967, 2003

Smith, D.D.; Chang, H.; and Fuller, K.A.: "Whispering-Gallery Mode Splitting in Coupled Micro-Resonators," *Virt. J. of Nanoscale Sci. and Tech*, Vol. 8, p. 11, 2003.

Smith, D.D.; Chang, H.; and Fuller, K.A; et al.: "Coupled-Resonator-Induced Transparency," *Physical Review A,* in press, 2004.

Smith, D.D.; and Chang, H.: "Coherence Phenomena in Coupled Optical Resonators," *Journal of Modern Optics*, in press, 2004.

Conference Proceedings and Presentations

Chang, H.; Smith, D.D.; and Fuller, K.A.: "Enhancement of Optical Nonlinearities via Whispering Gallery Mode Splitting," *Proceedings of the SPIE 4813*, Vol. 103, Seattle, WA, July 2002.

Smith, D.D.; and Fuller, K.A.: "Mie Scattering in Concentric Microparticles," *CLEO/QELS*, Longbeach, CA, May, 2002.

Fuller, K.A.; and Smith, D.D.: "Photonic Bandgaps in Lorenz-Mie Scattering by Concentrically Stratified Spheres," Joint Spring Meeting. of the Texas Sections of the APS and AAPT, and Zone 13 of the SPS, Nacogdoches, TX, March 7–9, 2002.

Chang, H.; Gates, A.L.; Fuller, K.A.; et al.: "Slow Light in Coupled Resonator Optical Waveguides," Optics in the Southeast, Huntsville, AL, October 24–25, 2002.

Smith, D.D.; Chang, H.; Gates, A.L.; et al.: "Photonic Bandgaps in Photonic Molecules," Optics in the Southeast, Huntsville, AL, October 24–25, 2002.

Fuller, K.A.; and Smith, D.D.: "Partial Wave Analysis of Coupled Photonic Structures," Optics in the Southeast, Huntsville, AL, October 24–25, 2002.

Smith, D.D.: "Enhanced Nonlinear Optics in Composite Media: Local Fields and Electromagnetic Coupling Effects,"Physics of Quantum Electronics XXXIII, Snowbird, Utah, January 2003.

Smith, D.D.: "Coherence Effects in Coupled Resonators," Physics of Quantum Electronics XXXIV, Snowbird, UT, January 2004.

Fuller, K.A.; and Smith, D.D.: "Matrix Representation for Coupled Photonic Structures," Southeast Ultrafast and High-Resolution Spectroscopy Conference, Huntsville, AL, January 2004.

Chang, H.; Smith, D.D.; Fuller, K.A.; et al.: "Coherence Phenomena in Coupled Optical Resonators," Southeast Ultrafast and High-Resolution Spectroscopy Conference, Huntsville, AL, January 2004.

Funding Summary

Table 1 provides the funding summary for this project for fiscal year (FY) 2003.

Table 1. Funding summary.

	FY 2003 ($)
Authorized	37,500
Processed	37,500
Balance	0

Status of Investigation

The investigation is currently in its second year, and is scheduled to continue until the end of FY 2004.

Space Environmental Effects on Ablative Laser Propulsion Using Multilayer Material Systems

Project Number: 03–18

Investigators: Mary Nehls/ED31
David Edwards/ED31

Purpose

The purpose of this Center Director's Discretionary Fund (CDDF) research project is to characterize various multilayered materials through the measurement of their coupling efficiency both before and after exposure to space environmental effects (SEE), and thereby determine and evaluate SEE on ablative laser propulsion efficiency of multilayer materials.

Background

When a laser pulse of sufficient energy density impacts a single layer material, a small amount of the material is ablated, and the material experiences a force in the direction opposite to that of the incident beam. The efficiency of converting light energy to kinetic energy is measured by the coupling coefficient, where the coupling coefficient, $C_{m,}$ is the ratio of the momentum transferred, p, to the power density of the laser, P.[1]

$$C_m = p/P\,. \qquad (1)$$

During the investigation to determine coupling coefficients for single-layer materials, a multilayered material, silver Teflon®, was examined. The coupling coefficients were measured to be significantly higher than those for single-layered materials. Further examination on aluminized Teflon® led to coupling coefficients up to an order of magnitude higher than those for single-layer materials.[2]

The multilayer material system consists of three layers: A thin transparent polymeric material, an adhesive between the layers, and a thin metallic ablative layer. The material is oriented such that the incident laser energy passes through the transparent polymeric layer first, and then interacts with the metallic layer. The laser pulse is transmitted through the outer transparent polymeric layer and is partially reflected and partially absorbed by the metallic under layer (i.e., reaction mass). The reaction mass is vaporized and rapidly expands, causing the transparent polymeric outer layer to plastically yield. This yielding process leads to the formation of a cone in the polymeric material. The cone finally ruptures as a result of the high pressure of the vaporized reaction mass. When the cone ruptures, the vaporized reaction mass is allowed to vent, producing a force and thus a coupling coefficient that is several times higher than those recorded for single-layer materials.

The increased force produced by multilayer material systems is dependent on the plastic deformation of the polymeric layer, which allows both the buildup of contained vaporized reaction mass as well as the formation of a crude nozzle to give a directed release of the vapor. Exposure to space environment radiation will potentially cause embrittlement of the polymeric material. As the material becomes more brittle, the plastic yielding of the transparent polymeric layer will be reduced or eliminated. This reduction in plasticity is predicted to lead to premature tearing of the polymer and reduced propulsion performance.

In addition, with exposure to the space environment, materials tend to darken as a result of environmental degradation.[4] Transmissivity in the outer layer will be reduced as the material darkens. When utilized as a beamed energy propulsion system, a reduction of transmissivity in the outer layer will change the coupling coefficient of the material and will therefore change the propulsive efficiency of the material system. This research will examine the effects of the space environment on these materials and quantify their functional lifetime as a propulsion system.

Approach

The work is divided into four tasks.

Task 1: Baseline Characterization of Multilayer Material Systems for Propulsion

Several multilayer materials are commercially available and will be used for this task in the investigation. Candidate materials that will be characterized are aluminized Teflon®, chromium coated Teflon®, silver Teflon®, and metallized CP1. These materials will be mounted on a torsion balance. A 5-J, 25-ns pulsed ruby laser will impact and ablate the material, and the response of the torsion balance will be observed. The transferred momentum will be measured by the angular deflection of the torsion pendulum. Energy density will be measured using an existing laser beam profiling system. The propulsion efficiency of each multilayered system will be quantitatively determined by calculating an optimized coupling coefficient.

Task 2: Exposure of Polymeric Materials to Space Environmental Effects

The ability of a multilayered system to function as a beamed energy propulsion system is dependent upon the plasticity of the polymeric layer. Previous SEE testing on polymers indicates

these materials will become brittle with prolonged exposure in space.[5] The candidate materials will be subjected to ultraviolet radiation combined with a uniform dose of 50-keV electrons. The electron exposure dose levels will be 10, 100, and 1,000 Mrads.

Task 3: Determination of Space Environmental Effects on Propulsion Efficiency

Subsequent to each level of SEE exposure, the candidate materials will again be characterized following the steps outlined in task 1. The materials will then be evaluated to determine any resultant loss of propulsion efficiency due to space environmental effects.

Task 4: Presentation of Results

A written report will be generated and results will be presented.

Accomplishments

The materials for characterization were procured and included the following: Aluminum/Teflon®, Black Chromium/ Teflon®, and Silver/ Teflon®. Aluminized CP1 was also requested for investigation.

The baseline characterization of the materials was initiated. The characterization of unexposed aluminized Teflon® was completed. The results of the baseline characterization of aluminized Teflon®, in comparison to those of several single-layer materials, are shown in figure 1.

The exposure of the materials to SEE was also initiated. Aluminized Teflon® was exposed to electron radiation at two different radiation dose levels.

Planned Future Work

The baseline characterization of the other materials will be completed. The selected materials will then be exposed to electron radiation, and post SEE-exposure characterization will be performed.

Publications and Patent Applications

A final report documenting the results of this task will be published and made available. No patents are foreseen at this time.

Funding Summary

The fiscal year (FY) 2003 request of $7,000 has been obligated.

Status of Investigation

Baseline characterization of the selected materials has been initiated. The SEE exposure of the materials has also been initiated. Work during FY 2004 will include continuation of the baseline characterization and SEE exposure. The exposed materials will then be recharacterized to determine the effect of the space environment on the ablative laser propulsion efficiency of the materials.

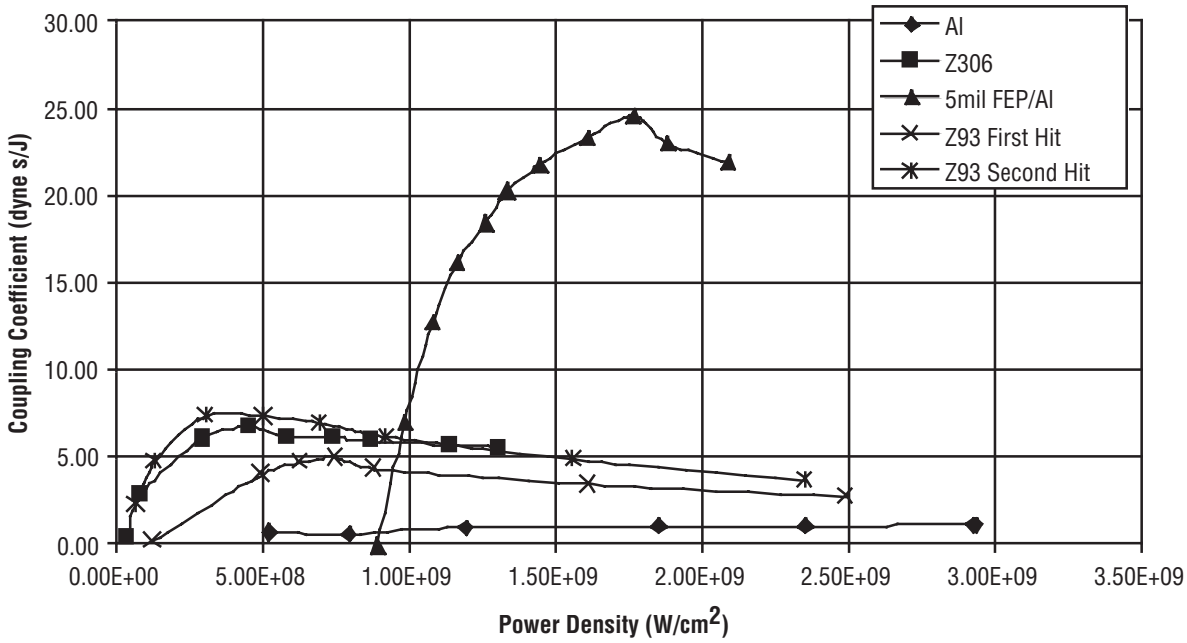

Figure 1. Coupling coefficients for aluminized Teflon® and several single-layer materials.

References

[1] Campbell, J.W.: "Project ORION: Orbital Debris Removal Using Ground-Based Sensors and Lasers," *NASA Technical Memorandum—108522*, October 1996.

[2] Nehls, M.K.; Edwards, D.L.; and Gray, P.A.: "Ablative Laser Propulsion Using Multi-Layered Material Systems," *AIAA–2002–2154*, Plasmadynamics and Lasers Conference, May 2002.

[3] Gray, P.A.; et al.: "Laser Ablative Force Measurements on Manmade Space Debris," *AIAA–2001–0605*, Aerospace Sciences Meeting and Exhibit, January 2001.

[4] Edwards, D.L.; et al.: "Optical Analysis of Transparent Polymeric Material Exposed to Simulated Space Environment," *SPIE, Photonics for Space Environments VII*, Vol. 4,137, pp. 56–64, July 2000.

[5] Edwards, D.L.; et al.: "Characterization of Space Environmental Effects on Candidate Solar Sail Materials," *SPIE, Photonics for Space Environments VIII*, Vol. 4,823, No. 4823–04, July 2002.

Hardware Evolution of Configurable Closed-Loop Controllers

Project Number: 03–19

Investigators: **David A. Gwaltney/ED17**
Ken King/ED17
Eric Corder/ED12

Purpose

The objective of this Center Director's Discretionary Fund (CDDF) project is the application of hardware evolution to a configurable closed-loop controller design. Specifically, experiments will be designed and executed in which control structures are evolved using an evolutionary algorithm to provide hardware configurations that meet a defined control performance specification. Ultimately, the goal is to provide a framework for the on-line evolution of closed-loop control structures that can be used in the automatic configuration of an embedded control system.

Background

Adrian Thompson is credited with pioneering intrinsic hardware evolution with the presentation of his doctoral thesis in 1996. His thesis has since been published under the Springer Distinguished Dissertation Series with the title "Hardware Evolution."[1] Thompson's work is called intrinsic hardware evolution because the electronic circuit is implemented in hardware to determine fitness during evolution. It is also possible to implement extrinsic hardware evolution in which the electronic hardware design is evaluated in a software simulation such as SPICE. The design may then be implemented in hardware after the evolution is complete. Since that time, many researchers have studied the evolution of electronic circuits both in software and in hardware. For example, Lohn and Columbano at NASA Ames Research Center (ARC) have developed a circuit representation technique that can be used to evolve analog circuitry in software.[2] This technique was used to conduct experiments in evolving filter circuits and amplifiers. Researchers at the Jet Propulsion Laboratory (JPL) have done extensive work on the evolution of electronic circuits using both intrinsic and extrinsic approaches. They are actively involved in developing new approaches to enable the evolution of more complex circuitry.[3]

Work done in Japan on the control applications of evolvable hardware includes an evolvable hardware chip applied to a prosthetic hand controller and a robot navigation control system. The prosthetic hand controller provides a mapping between the electromyography signals produced by the human user and the signals required to move the prosthetic hand.[4,5] This has been done internally using training data collected from a user with an operational hand and not in an on-line adaptive fashion with a disabled user. The robot navigation controller builds a model of its environment in order to evaluate a population of evolved controllers during evolution.[4] This is a computationally demanding technique, and the paper appears to indicate that the robot has to spend some time crashing into obstacles to create its internal model of the outside world before evolving a population of useful controllers.

Other researchers have explored the use of evolutionary techniques in the design of control systems. Koza, et al. presented automatic synthesis of control laws and tuning for a plant with time delay using genetic programming.[6] This was done in simulation. Keane, Koza, and Streeter recently presented results on the evolution of a general-purpose industrial controller that improves on the response of the widely deployed Proportional-Integral-Derivative (PID) controller.[7] The controller evolution was also conducted in a simulated environment. Another example of a controller evolved to control a simulated bioreactor is given in the work of Conradie et al.[8] In this paper, the use of a technique called Adaptive Neural Swarming is presented, in which an adaptive controller and an evolutionary operation are combined.

Approach

This effort will utilize a reconfigurable programmable circuit device as the hardware medium for implementation of evolved designs. Initially, the JPL developed Stand-Alone Board Level Evolvable System (SABLES) [8,9] will be utilized for implementing analog or mixed-signal control electronics. This system employs the JPL designed second generation, field programmable transistor array (FPTA2). A digital signal processor (DSP) device is used to execute the code that implements the evolutionary algorithm and to configure the FPTA2. For purely digital control structures, a Xilinx field programmable gate array (FPGA) will be used in conjunction with software that implements the evolutionary algorithm. This software will be executed on a DSP or a personal computer (PC) platform. Originally, the intent was to use a printed circuit board called the RC1000 as the medium for implementation. Produced by Celoxica for exploration of reconfigurable computing, the RC1000 is the carrier for a Xilinx FPGA and supporting circuitry. The RC1000 is installed in a desktop PC on which the code for the evolutionary algorithm is also installed. Recent efforts, by Jason Lohn and his coworkers at NASA ARC, have produced software that can be used with the RC1000 to evolve fault tolerant digital circuitry.[11] Evaluation of this code and the RC1000 determined that the RC1000 was not a suitable platform for evolving embedded controllers that must interact with an external environment. SABLES and the RC1000

were not designed with control system implementation in mind. Therefore, this effort will include the design of a new printed circuit card and components to support the use of the FPTA2 in embedded control system applications. The development of a similar printed circuit card to support the use of a Xilinx FPGA will also be explored.

For the experiments, a controller performance goal will be established and the evolutionary algorithm will start with a population of seed hardware configurations that are loaded on the programmable device being utilized. The designs will be exercised using a test rig in which the dynamic system to be controlled is implemented, and the results will be stored. The evolutionary algorithm will then evaluate the fitness of the hardware designs and modify them in a prescribed manner. Genetic algorithms are generally employed to evolve the design population. The process will then be repeated using the new evolved designs. This continues until the fitness of the population plateaus and the design converges.

Accomplishments

Much of the first year was spent investigating paths to achieving research objectives. The use of a Java software package called JBits for evolution on a Xilinx Virtex FPGA was evaluated. The JBits software was developed by Xilinx to allow the direct manipulation of Virtex FPGA configuration bit streams. As mentioned above, JBits was used by researchers at NASA ARC to develop an evolutionary algorithm approach to fault tolerance for digital circuitry. This capability was demonstrated by Lohn et al. using a state machine application for decoding quadrature encoded signals.[11] An optical encoder is used in practice to detect the direction of rotation and relative position of a motor shaft or other rotary device. While their approach is successful in tolerating induced faults in the circuit design, the investigators here at Marshall Space Flight Center (MSFC) have decided to pursue another approach to support evolution on an FPGA.

FPGAs were originally developed to support prototyping of digital circuitry prior to implementation of the circuit in an application specific integrated circuit (ASIC). They are still widely used in this capacity, but are also now used to provide in-circuit reconfiguration capabilities via static random access memory (SRAM) based FPGAs. The FPGA configuration is held in SRAM and must be reloaded every time the FPGA is initially powered up. FPGAs are widely used in systems that are not going to be manufactured in high enough volume to warrant design of an ASIC, and may be antifused based (configure once) or SRAM based (reconfigurable) depending on the requirements of the application. In any case, a hardware description language (HDL) that is used by circuit synthesis and place-and-route tools to create a configuration for an FPGA specifies the FPGA configuration. The investigators plan to develop an HDL representation of an evolvable machine and implement it on an SRAM based FPGA. This way, the investigators have complete control over the configuration method and the capabilities of the evolvable machine. The representation of the configuration bit stream can be tailored to be evolution oriented and thereby allow greater capability when an evolutionary algorithm generates the configuration. Further, the configurable blocks can be tailored to suit the application at hand. Ultimately, this evolvable machine can be implemented in a custom ASIC, or remain in an FPGA for deployment.

A custom HDL representation of an evolvable machine has several advantages over direct evolution of FPGA via manipulation of the bit stream. Nearly all commercial FPGA vendors are protective of their configuration bit stream representation, and are reluctant to make it easily available to the public. Further, the bit stream representation can change as new FPGA devices are introduced. Therefore, all the time and effort expended for one FPGA will not necessarily support new products introduced by the same manufacturer. Such products are guaranteed not to support the products produced by other manufacturers. JBits only supports the Xilinx Virtex FPGAs. It does not support the Virtex-E. While there is a prerelease of JBits to support the Virtex II family of chips, it currently has less capability than JBits for the Virtex Family. Further, JBits based evolutionary approaches do not support other vendor's FPGAs. An HDL representation of an evolvable machine can be targeted to any FPGA made by any vendor, with minor modification to account for differences in pin assignments. Further, an HDL evolvable machine is not dependent on software provided by a third party, such as JBits. Therefore, it will not become obsolete as new devices are introduced. The evolutionary algorithm to support such an evolvable machine can be written in a standard language such as C. The manufacturer's bit stream representation is designed to suit the manufacturer's requirements for configurable block layout and the organization of configuration memory on their chips. This results in a bit stream format that is almost undecipherable by a human and does not lend itself well to evolution. The investigators can design an easily understandable and evolution friendly bit stream for an HDL based evolvable machine.

The initial development platform for evolution of digital controller structures on a Xlinx FPGA is shown in figure 1. This platform consists of a custom DSP processor card mated with an FPGA evaluation board manufactured by Xilinx. The firmware implementing the evolutionary algorithm and controlling the configuration of the FPGA will be run on the DSP device. A host PC will be used to develop the firmware and download it to the DSP device. A graphical user interface to the evolvable digital controller will be executed on the host PC.

Investigators spent some time evaluating commercially available reconfigurable analog array products. The most widely used product of this type is manufactured by Lattice. But these products are limited in their capability and are primarily useful for implementing analog filters. These devices have configurable routing between input amplifiers with variable gains and output amplifiers with variable capacitors to set bandwidth. This limited reconfigurability makes the Lattice devices not capable enough for complex control applications. Another configurable

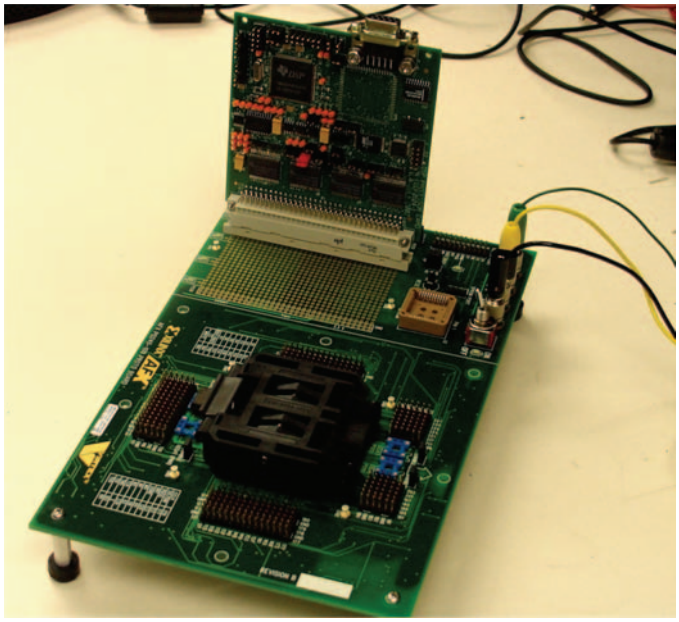

Figure 1. Development platform for evolution of digital controllers.

analog device was created by Zetex and has been used by other researchers in evolvable hardware. But Zetex recently discontinued this product. The most capable devices available are the field programmable analog arrays (FPAA) produced by Anadigm and configurable analog blocks that include amplifiers, routing resources, variable capacitors, an eight-bit analog-to-digital converter (ADC), and a look-up table. The ADC and look-up-table can be used to implement nonlinear analog functions. While Lattice is known for providing details of its configuration bit stream, Anadigm is not. While this situation may change, at this time the investigators are not planning to use a commercial FPAA in this effort, but may consider this for future efforts.

Previous research in the development of an evolvable analog controller was conducted at MSFC using the FPTA2 and SABLES.[12,13] Figure 2 depicts the SABLES configured for experiments in the evolution of motor speed controllers. The principal investigator is continuing the collaboration with researchers at NASA's JPL using SABLES for analog control applications. To this end, a portion of the funding was used to purchase FPTA2 devices for use at MSFC. The investigators have a concept for a controller board employing the FPTA2, and PC board design is underway. The principal investigator has conducted system identification experiments using FPTA2 as part of JPL SABLES. Open loop models approximating a DC motor and driver combination have been successfully evolved.

Additionally, the principal investigator and Ian Ferguson, at JPL, have submitted joint step 1 and step 2 proposals to the ARC Intelligent Systems NASA Research Announcement (NRA) concerning the development of enabling technologies for a deployable evolvable analog controller. At the time of writing, the NRA selection process was not complete.

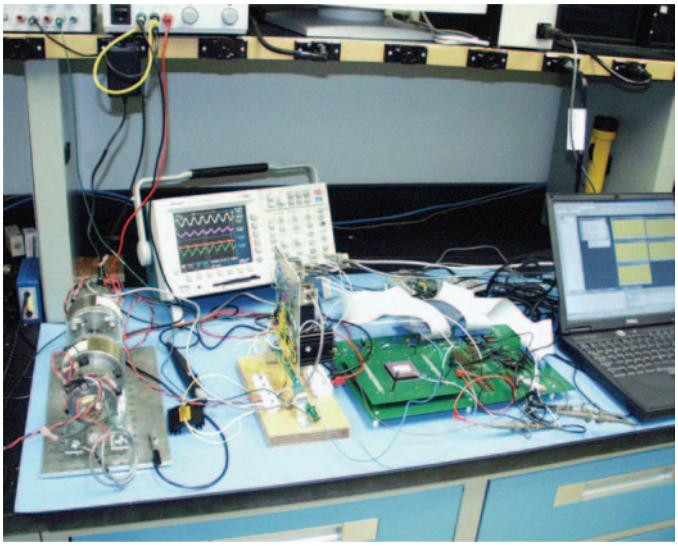

Figure 2. Experimental hardware for evolution of motor speed controllers.

The principal investigator is collaborating with Dr. James Hereford, at Murray State University, and is coauthor on a conference paper submitted to the 2004 NASA/DoD Conference on Evolvable Hardware. Dr. Hereford and the principal investigator are currently working on proposals for hardware evolution of neural networks in reconfigurable electronic devices.

Planned Future Work

The following tasks will be completed in the second year of this effort:

- Fabrication/testing of the first cut FPTA2-based evolvable controller (EC).
- Firmware development for an FPTA2–based EC.
- Configuration/testing of an FPGA-based EC.
- Firmware development for an FPGA-based EC.
- Experimental testing of both EC types.

Publications and Patent Applications

Hereford, J.; and Gwaltney, D.: "Design Space Issues for Intrinsic Evolvable Hardware," submitted to the 2004 NASA/DoD Conference on Evolvable Hardware, Seattle, WA, 2004.

Funding Summary

This effort received $26,000 in fiscal year (FY) 2003 funding. At the time of writing, $24,000 has been expended. The balance of the FY 2003 funding will be expended in FY 2004.

It is expected that this effort will receive $23,000 in FY 2004 funds.

Status of Investigation

This investigation is proceeding as planned after the authority to proceed was received in April 2003. There are currently no concerns.

Acknowledgments

The principal investigator would like to thank researchers at JPL for making their FPTA2 and SABLES available for use. The analog controller evolution experiments would not have been possible without the support provided by Ian Ferguson, at JPL, in configuration and documentation of the SABLES and valuable insights during the design and execution of the control experiments. The principal investigator thanks Jason Lohn and Greg Larchev, both at NASA ARC, for providing their software designed for use with the RC1000. Additionally, the principal investigator is grateful for the support received from NASA ARC that was used to supplement this work by providing software development resources.

References

[1] Thompson, A.: "Hardware Evolution," *Springer Distinguished Dissertation Series*, 1998.

[2] Lohn, J.D.; and Columbano, S.P.: "A Circuit Representation Technique for Automated Circuit Design," *IEEE Transactions on Evolutionary Computation*, Vol. 3, No. 3, September 1999.

[3] Stoica, A.; Zebulum, R.; Keymeulen, D.; et al.: "Scalability Issues in Evolutionary Synthesis of Electronic Circuits: Lessons Learned and Challenges Ahead," AAAI Spring Symposium on Computational Synthesis, Stanford University, CA, March 24–26, 2003.

[4] Higuchi, T.; et al.: "Real World Applications of Analog and Digital Evolvable Hardware," *IEEE Transactions on Evolutionary Computation*, Vol. 3, No. 3, September 1999.

[5] Kajitani, I.; Murakawa, M.; Nishikawa, D.; et al.: "An Evolvable Hardware Chip for Prosthetic Hand Control," *MicroNeuro '99*, Proceedings of the Seventh International Conference on Microelectronics for Neural, Fuzzy and Bio-Inspired Systems, 1999.

[6] Koza, J.R.; et al.: "Automatic Synthesis of Both the Control Law and Parameters for a Controller for a Three-Lag Plant With Five-Second Delay Using Genetic Programming and Simulation Techniques," American Control Conference, June 2000.

[7] Keane, M.A.; Koza, J.R.; and Streeter, M.J.: "Automatic Synthesis Using Genetic Programming of an Improved General-Purpose Controller for Industrially Representative Plants," *Proceedings of the NASA/DoD Conference on Evolvable Hardware, pp. 60–67,* July 2002.

[8] Conradie, A.E.; Miikkulainen, R.; and Aldrich C.: "Adaptive Control Utilizing Neural Swarming," *Proceedings of the Genetic and Evolutionary Computation Conference (GECCO–2002)*, pp. 60–67, July 2002.

[9] Ferguson, M.I.; Zebulum, R.; Keymeulen, D.; and Stoica, A.: "An Evolvable Hardware Platform Based on DSP and FPTA," Late Breaking Papers at the Genetic and Evolutionary Computation Conference (GECCO-2002), pp. 145–152, July 2002.

[10] Stoica, A.; Zebulum, R.; Ferguson, M.I.; et al.: "Evolving Circuits in Seconds: Experiments With a Stand-Alone Board Level Evolvable System," *Proceedings of the NASA/DoD Conference on Evolvable Hardware*, pp. 67–74, July 2002.

[11] Lohn, J.; Larchev, G.; and DeMara, R.: "Evolutionary Fault Recovery in a Virtex FPGA Using a Representation That Incorporates Routing," International Parallel and Distributed Processing Symposium (IPDPS'03), Nice, France, April 22–26, 2003.

[12] Gwaltney, D.A.; and Ferguson, M.I.: "Intrinsic Hardware Evolution for the Design and Reconfiguration of Analog Speed Controllers for a DC Motor," NASA/DoD Conference On Evolvable Hardware, Chicago, IL, July 2003.

[13] Gwaltney, D.A.; and Ferguson, M.I.: "Hardware Evolution of Analog Speed Controllers for a DC Motor," E. Cantu-Paz, et al., (eds.), *GECCO 2003*, LNCS 2723, pp. 442–453, July 2003.

Orbital Global Positioning System Health Management

Project Number: 03–20

Investigators: **Ken Schrock/ED18**
Todd Freestone/ED18
Greg Franks/ED18
Dr. Russell Carpenter of Goddard Space Flight Center

Purpose

The objective of this Center Director's Discretionary Fund (CDDF) effort is to examine the increase in navigational reliability and accuracy for a launch vehicle or satellite that incorporates a Global Positioning System (GPS) receiver using the Wide-Area Augmentation System (WAAS) corrections and health alerts. The effort will investigate the orbital GPS reliability and accuracy synergistically by combining two GPS technologies: The Federal Aviation Administration's (FAA's) WAAS and Receiver Autonomous Integrity Monitoring (RAIM). The endeavor will investigate what can be done in real time, in orbit, using a system originally designed for aircraft.

Background

For an en-route aircraft navigating with the GPS, the FAA developed WAAS to generate navigation correction and integrity warnings. Since WAAS was certified as operational, an aircraft can now legally navigate using only GPS. In an open question time at the end of the spacecraft application session of the Institute of Navigation (ION) Global Navigation Systems Conference in 2002, the principal investigator (PI) queried the assembled audience as to whether any one had investigated using WAAS for a spacecraft. Dr. Russell Carpenter of NASA's Goddard Space Flight Center said he had done some software only simulations, but no one had used a real receiver.

Approach

The investigation plan is to use existing laboratory GPS simulators with WAAS capabilities to test receivers capable of both WAAS and orbital operations (i.e., without International Traffic in Arms Regulations (ITAR) altitude or speed-limit restrictions). The initial testing of the receiver will investigate the increase in static accuracy using WAAS signals with a live sky antenna to validate the simulator. Next will be a simulation for using WAAS position corrections for an orbital vehicle, followed by the performance of a static integrity test. To close out the experiment, an orbital integrity simulation will be performed, analyzed, and written in the final deliverable, an integrity report.

Accomplishments

The PI began by reviewing the Radio Technical Committee for Aeronautics (RTCA) standard DO–229C, Minimum Operational Performance Standards For Global Positioning System/Wide Area Augmentation System Airborne Equipment. He also conducted a literature search and review. The generation of requirements and the subsequent search and procurement of the test receiver that utilizes both GPS and WAAS signals was the result of this work.

Since then, the GPS simulator has been set up to output Satellite-Based Augmentation System (SBAS) signals compatible with those generated by the FAA's WAAS, the European Geosynchronous Navigation Overlay System (EGNOS), and Japan's Multi-Functional Transport Satellite (MTSAT–1R) Satellite-Based Augmentation System (MSAS) (with assumed Australian/United States (U.S.) monitor site collaboration). A validation of the simulation has been performed by comparing 5 hours of data from a WAAS capable GPS receiver connected to a surveyed antenna to that same position and time put in to the simulator. Analysis of this static survey is ongoing.

Also, an orbital simulation has been set up with the test vehicle in a Space Station orbit, receiving signals from WAAS, EGNOS, and MSAS, the U.S., European, and Japanese GPS SBASs, respectively.

Planned Future Work

The static navigation validation and then analysis of the test data will be completed, and then the orbital navigation test data will be analyzed. To summarize the effects on navigation, the first deliverable will be a navigation accuracy report.

Phase two of the experiment is to look at the health management type benefits of integrity warnings for failing satellites. Static and orbital navigation tests will be performed with an ensuing integrity report as the final deliverable.

Publications and Patent Applications

Since others have not published this type of work, a conference paper is being considered. Also, a NASA Tech Briefs article is being contemplated. If a unique method of analyzing integrity is utilized, it may warrant patent application.

Funding Summary

With the initial proposal, $13,000 was requested mainly for purchase of the test GPS receiver in fiscal year (FY) 2003. An additional $3,000 was requested for FY 2004 for cables and connectors.

Status of Investigation

For the test receiver, a reputable, accurate receiver was selected, procured, and integrated. The static and orbital navigation scenarios for the simulator have been designed and validated. Subsequently, the static and orbital navigation scenario tests have been completed and their analysis is on going.

Structural Testing of a Silicone-Carbon Fiber/Silicon-Carbon Matrix Membrane

Project Number: 03–21

Investigators: Eric Poole/ED22
Diep Trinh/ED34

Purpose

The primary objective of this Center Director's Discretionary Fund (CDDF) proposed task is to characterize the structural stiffness and strength properties of silicon-carbide (SiC) fiber/SiC matrix (SiC/SiC) ceramic composite membranes. A secondary objective is to develop manufacturing, handling, and testing experience with ceramic membrane structures.

Background

This research will have direct application to the Microwave Lightcraft (MWLC) effort since the current design uses SiC as the principal structural material. The thickness of the proposed test specimens is exactly the same as the proposed thickness of the MWLC hull face sheets. This material could also have applications in other high-performance aerospace structures. SiC composites have the potential to increase specific stiffness by a factor of five and to increase specific strength by a factor of four over steel. However, little experience exists with using SiC/SiC composites as a structural element, and there has been no research conducted with SiC/SiC structural membranes.

Approach

Thin circular disks, roughly 60 cm in diameter and 0.25-mm thick, are fabricated from SiC/SiC material. The specimens are tested in the Marshall Space Flight Center (MSFC) Hydrogen Test Facility. Test set up and procedures are similar to those used in the recent permeability study for composite tank materials. The same test fixtures and test equipment are used. The specimen is sealed and then pressurized on one side to create maximum membrane stress at the center of the specimen. Center deflection of the membrane specimen is measured by a laser device provided by ED27. This measurement is used to calculate the structural stiffness of the specimens. Failure data is used to determine strength.

Accomplishments

Starfire Systems Inc. of Malta, New York fabricated SiC/SiC panels. The panels were 64 cm in diameter and 1- to 2-mm thick. The panels were very fragile and many were damaged during the manufacturing, transportation, and machining. Of the 12 panels that were initiated, only 2 specimens were generated.

While there was a heavy attrition rate through the fabrication procedure, much was learned about processing this type of material into thin sheets. Starfire Systems has submitted a Process Evaluation Report that provides details of their processing trials and corrective action for future attempts to reproduce the work. Also, once the panels were received at MSFC, specimens were machined and tested without further damage. These techniques can be used for future testing of similar materials.

A single test was completed. The specimen was drilled with the required holes, and then bolted to the test fixture at the Hydrogen Test Facility. A neoprene bladder was used to seal the pressurizing fluid. ED27 provided a laser vibrometer to measure center deflection of the panel during testing. The data show that the stiffness of the specimen was 149 GPa, which is less than anticipated but still greater than titanium. The calculated specific stiffness of the SiC/SiC panel is 1.75 times greater than titanium. Strength of the panel was very weak, and would have to be greatly improved before the material could be considered for structural applications.

Planned Future Work

Future work is currently under consideration. Funds are insufficient to purchase new material. However, resources remain in the planning that could be used for testing. Other avenues of obtaining material to test are being pursued.

Publications and Patent Applications

The final results of research will be written in a formal paper and published, but no paper is in work at this time. A patent application is not expected to arise from this research.

Funding Summary

As of December 31, 2003, $39,754 of the $40,000 were obligated.

Status of Investigation

Research is still considered to be ongoing, since other materials are being sought for testing. If no other material can be found, the work done to date will be considered sufficient to complete the research.

Deployable Structures Utilizing Spiral-Wrapped Engineered Fibers

Project Number: 03–22

Investigators: Mark Vaccaro/ED24
Ken Welzyn/TD54

Purpose

The purpose of this Center Director Director's Discretionary Fund (CDDF) research is to develop the technology to produce extremely high length (L) to diameter (D) ratio (10–1,000 m/0.25–5 cm), on-orbit deployable booms, struts, and tethers. Specifically, this research deals with the stiffening effect that occurs when braided engineered rope is spirally wrapped with additional fibers (fig. 1).

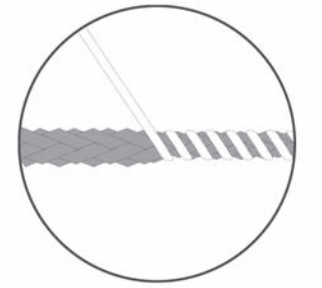

Figure 1. Stiffening effect that occurs when braided engineered rope is spirally wrapped with additional fibers.

Background

While supporting the Propulsive Small Expendable Deployer System (ProSEDS) project, a bench-top process was developed for applying spiral-wrapped copper wire cross straps to the tethers for risk mitigation. This same process has now been adapted to produce a stiffened, dynamically stable tether leader section for attachment to the end mass. While performing this work for ProSEDS, the coinvestigators observed the surprising level of stiffness that can be imparted to a simple braided fiber by spirally wrapping it with a single fiber under tension. It was then realized that a flight system could be developed in which a high length-to-diameter (L/D) structure with excellent stiffness properties could be manufactured in space by a compact device. This technology could have many uses in space where deployable structures are needed. The advantages to the technology would be its compactness, simplicity, and ability to manufacture structures of very long lengths. Spools wound with flexible engineered fiber would feed into a wrapper/nib roller system producing a stiff structural member on-orbit (fig. 2). Since the parent materials are lightweight and flexible, such a design could reduce/eliminate the need for heavy, complex deployment systems. Based on initial samples, it is believed this same technology can be applied to produce lightweight, rigidized deployable booms and struts. Single line elements could be used to deploy lightweight probes many kilometers away from the parent spacecraft; or multiple, nested lines could be produced to deploy solar sails, antennas, and sunshades.

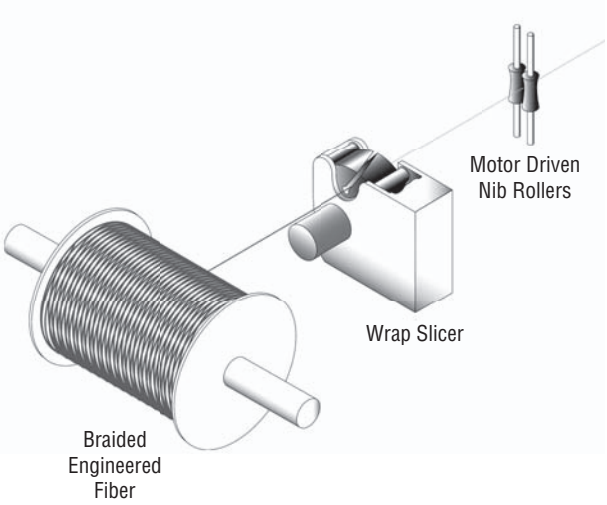

Figure 2. Spools wound with flexible engineered fiber would feed into a wrapper/nib roller system producing a stiff structural member in space.

Approach

This research focused on producing and characterizing various fiber configurations and their associated stiffness and load carrying capabilities. The approach to answering these questions was largely experimental in nature. Utilizing experience gained and prior investments made in the Tether Winding and Spark Testing (TWST) Facility (fig. 3), the following five tasks were proposed:

1. Procure sample lengths of braided engineered fibers and overwrap material. These samples consisted of various braid configurations (number of strands, lay pattern, denier, etc.).
2. Utilize current TWST Facility and wrap-splicing hardware setup (figs. 4 and 5) to produce smaller diameter test samples.
3. Modify/upgrade existing TWST Facility and wrap-splicing hardware to produce larger diameter test samples.
4. Load and stiffness characterization testing of samples.
5. Develop prototype design of flight-like manufacturing mechanisms.

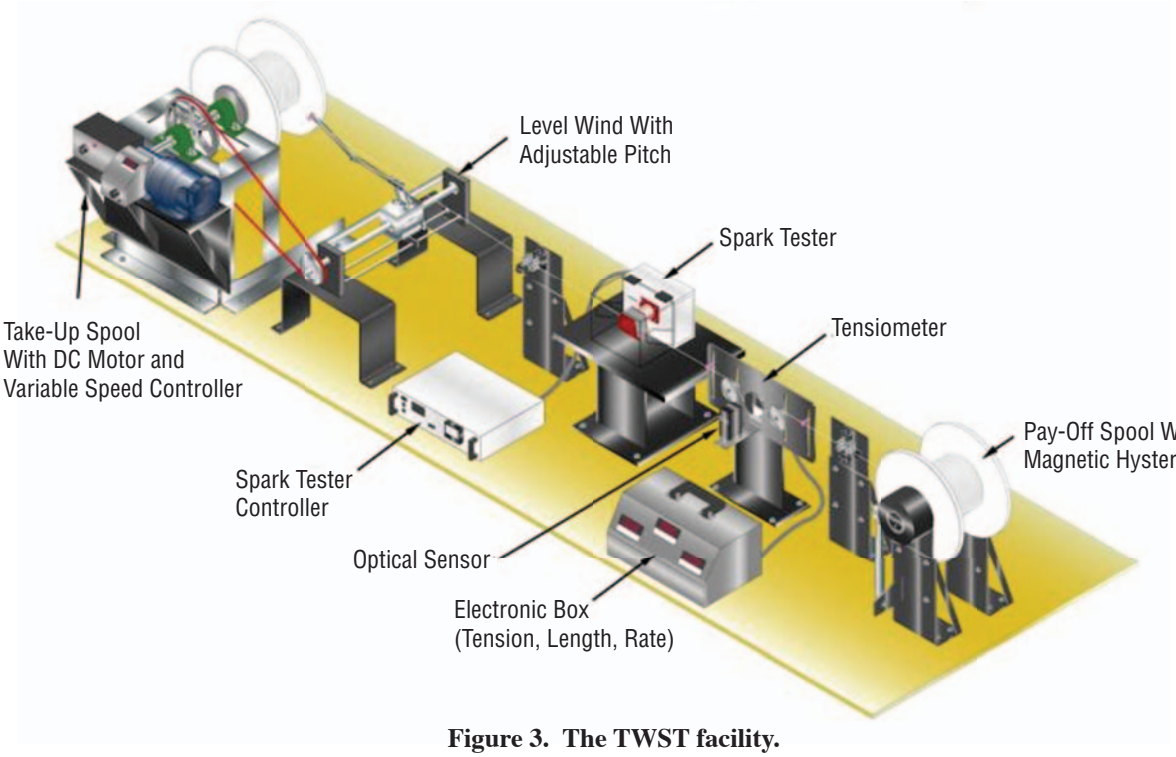

Figure 3. The TWST facility.

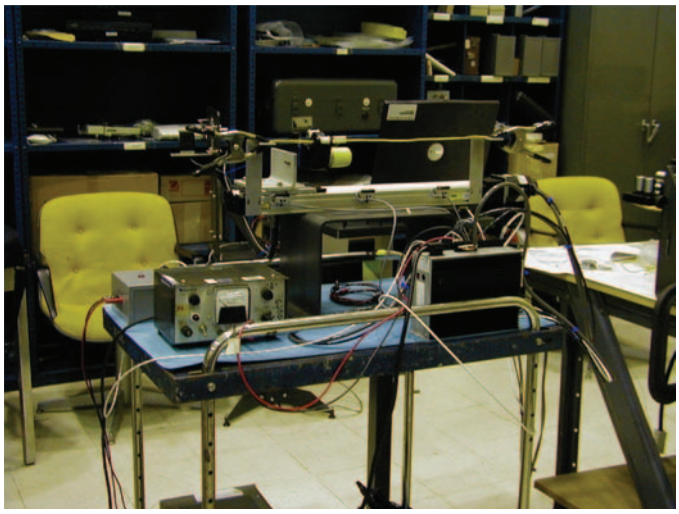

Figure 4. Using current TWST facility and wrap-splicing hardware setup to produce smaller diameter test samples.

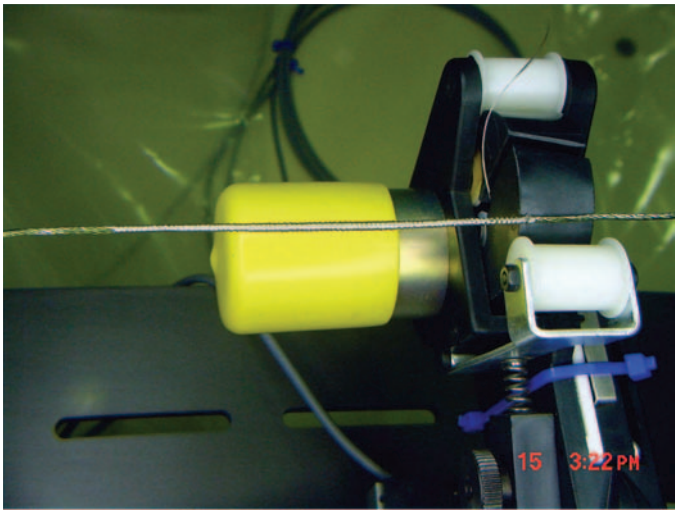

Figure 5. Using current TWST facility and wrap-splicing hardware setup to produce smaller diameter test samples.

Accomplishments

Approximately 24 small-diameter (less than 0.25 in), 18-in length samples were produced to address tasks 1, 2, and 4. These single and multiple nested samples were fabricated using combinations of materials including: Kevlar, Spectra, and Aracon (figs. 6 and 7). It was quickly realized that a certain minimum amount of friction needed to exist between the braid and overwrap materials. Spectra, being an inherently slippery material, was discarded due to poor results upon initial testing. In addition, the single-line element samples revealed no appreciable increases in stiffness when any of the variables, such as tension, lay pattern, or number of overwraps, were changed. Although the multiple, nested samples did show some minor increases in stiffness, it was felt that substantial increases would have to be made in order for the concept to prove viable as an on-orbit, deployable system, as proposed. Typically, the best samples could only support 10–14 in-oz in bending and 1–11.5 in-lb, in buckling. Additionally, all of the samples demonstrated a flaw that could never be overcome. Once a sample had buckled, or had been bent over a small radius, it developed a weak spot. The overwrap material would separate, forming a hinge point with almost zero stiffness.

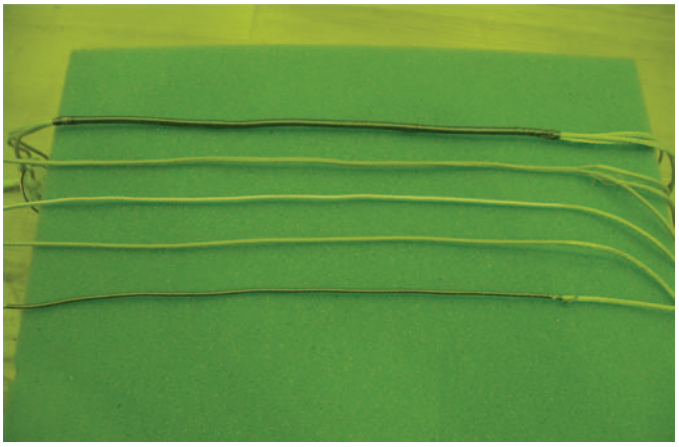

Figure 6. Wrap winding test samples.

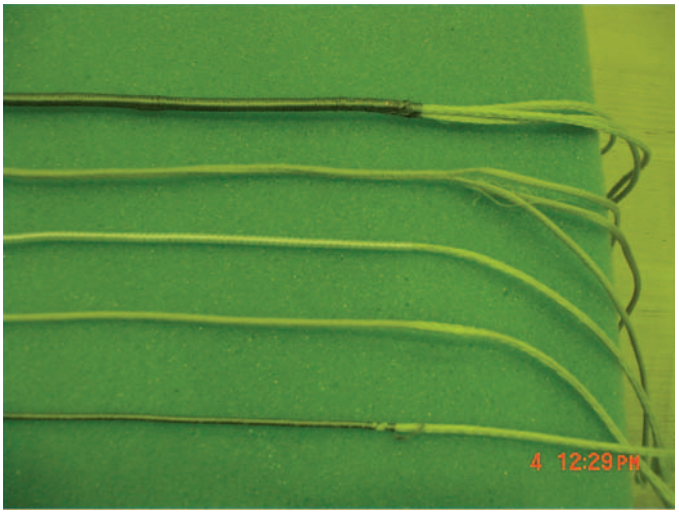

Figure 7. Wrap winding test samples.

Planned Future Work

None planned for at this time.

Publications and Patent Applications

None planned for at this time.

Funding Summary

Due to the availability of ProSEDS and TWST Facility hardware and materials, approximately $1,000 of $25,000 has been committed and spent.

Status of Investigation

It should be noted that from the start of this effort, very little manpower was available to expend upfront. Both investigators were heavily involved with the ProSEDS project and its impending launch. After ProSEDS was cancelled, the coinvestigator moved on to other tasks and stopped supporting the CDDF. With that being said, the effort that was put forth did not yield very promising results. At the beginning of the proposal, it was felt that if substantial gains in stiffness of the wrapped structure could be made, then the concept of an on-orbit deployable system would be viable. We were able to utilize a substantial amount of hardware and material from the ProSEDS project, without having to draw funds from the CDDF. Although conceptual designs were developed and samples were fabricated, testing showed no signs of significant increases in stiffness. At this point, it is believed that additional expenditures of time and money would not change these results. Therefore, no resources have been expended to address task 3, large-diameter samples; or task 5, development of a prototype flight mechanism.

Cryogenic Fracture Toughness Evaluation of Cast Aluminum-Berylium Alloys for Structural Applications

Project Number: 03–23

Investigators: **Wayne R. Gamwell/ED33**
Preston McGill/ED33

Purpose

The object of this Center Director's Discretionay Fund (CDDF) program is to evaluate the cryogenic temperature fracture properties (Kc, Jc, and da/dN) for promising new aluminum-beryllium (AlBe) alloys produced using the investment casting process. The data will provide baseline fracture properties at cryogenic temperatures (–320 °F and –423 °F) for users of these materials.

Background

AlBe metal matrix composite materials have been around for some time now, beginning with the material developed in the 1960s by Lockheed called Lockalloy. However, interest in their use waned in the 1970s and the materials became unavailable. In the past decade, due to the desirable performance characteristics of this family of composite materials for aerospace applications, new alloys have been developed with improved mechanical properties, along with improved processing techniques and process controls for their production. AlBe materials are available in the form of extrusions, rolled plate, forgings, and, most recently, near net shape investment castings. The recent new family of AlBe alloys in the form of investment castings shows desirable properties available in near net form. The fracture toughness characteristics of these investment cast materials have not been evaluated at cryogenic temperatures (–423 °F).

Desirable characteristics of AlBe composite materials include lightweight, dimensional stability, stiffness, good vibration damping characteristics, low coefficient of thermal expansion, and workability. These materials are 3.5 times stiffer and 22 percent lighter than conventional Al alloys. Their use is attractive for weight critical structural applications such as advanced electro-optical systems, advanced sensor and guidance components for flight and satellite systems, components for lightweight high-performance aircraft engines, and structural components for helicopters. As these materials become more highly used in aerospace and space programs, fracture properties down to liquid hydrogen temperatures will be needed for structural analyses. These properties are currently not available for these families of alloys.

Approach

Beralcast 363 alloy in the form of investment cast plates will be purchased from the Starmet Corporation, Concord Massachusetts. Test specimens for basic mechanical properties (UTS, YS, %e, and E) and fracture properties will be machined from the investment cast plates. Machining will be contracted out since Be is a hazardous material and Marshall Space Flight Center (MSFC) does not have the facilities to machine Be in-house. Basic mechanical properties at room temperature will be obtained as a screen to verify the material meets advertised mechanical properties. Fracture toughness testing on Al 2219 material at room temperature will be conducted as shakedown tests in preparation for cryogenic fracture testing. Basic mechanical properties for the Beralcast 363 alloy will be obtained at cryogenic properties in preparation for fracture toughness testing. Fracture toughness testing at cryogenic temperatures will be obtained for the Beralcast 363 alloy.

Accomplishments

In fiscal year (FY) 2003, 11 investment cast plates of the alloy Beralcast 363 were obtained from the Starmet Corporation. The plates were approximately 0.5 × 3 × 11 in. Each plate was received with a radiograph showing its internal discontinuity condition. Each plate was reradiographed in-house to verify its internal condition. All the plates were relatively clean with respect to internal defects. One plate was used to verify the basic mechanical properties of the material at room temperature. Flat and round tensile specimens were extracted from the plate to determine which type of specimen would be used for the remainder of the program. Both types of specimens provided similar ultimate and yield strengths, but the flat specimens provided more uniform elongation and reduction in area information. Flat tensile specimens were chosen for cryogenic properties testing because of their larger cross-sectional areas. Basic mechanical properties were typical of those expected (e.g., UTS=40 ksi, YS=30 ksi).

Planned Future Work

Tensile and fracture test specimens will be procured. Delivery of specimens is expected in June 2004; approximately 12 weeks after initiation of a purchase order for machining of specimens. Basic mechanical properties and fracture properties (K_Ic, Jc, and

da/dn) at cryogenic temperatures will be determined in the L, L–T, and 45° directions. Testing is expected to take approximately 8–12 weeks. Crack growth rate curve fitting parameters for NASGRO will be determined. All the mechanical testing is expected to be completed by the end of fiscal year (FY) 2004.

Publications and Patent Applications

A NASA Technical Manual will be written at the conclusion of the work. A paper will be submitted to a peer review materials journal for potential publication.

Funding Summary

Table 1 identifies FY 2003 and FY 2004 funding requirements and table 2 identifies project costs to date and expected costs.

Status of Investigation

We are making acceptable progress. We are procuring tensile and fracture specimens. We expect to begin cryogenic tensile and fracture testing in June 2004. The program is taking longer than expected due to the late receipt of initial funding in FY 2003, and working higher priority efforts (principally the Columbia investigation). Table 3 identifies the manpower requirements for completion as well as the schedule of activities to achieve completion of this project.

Table 1. FYs 2003 and 2004 funding requirements.

Item	FY 2003 ($)	FY 2004 ($)	Total ($)
Yearly Funding	40,000	20,000	60,000

Table 2. Project costs to date and expected costs.

Item	Costs to Date ($)	Expected Remaining Costs ($)	Total ($)
Material Cost (11 investment cast plates)	8,000	N/A	8,000
Machining tensile specimens (nine specimens from one plate)	3,000	N/A	3,000
Room temperature tensile testing (nine specimens from one plate)	0	N/A	N/A
Machine tensile and fracture specimens from 10 plates	N/A	25,000	25,000
Tensile and fracture testing	N/A	30,000	30,000
Totals	11,000	55,000	66,000

It appears that we may be short on funding by $5,000–$10,000, but that depends upon the actuals for the remaining costs.

Table 3. Manpower and schedule requirements for project completion.

		FY 2003 (quarter)				FY 2004 (quarter)			
Manpower	Mmos	1 st	2 nd	3 rd	4 th	1 st	2 nd	3 rd	4 th
	CS	0	0.2	0.1	0.1	0.1	0.1	0.1	0.1
	Contractor				$20,000				
Schedule	SOW		X						
	Obtain Matl. (20,000)		X		X				
	Specimens Machined (20,000)								
	Mechanical Testing (20,000)						X	X	X
	Reporting								X

Modular Avionics Redundancy and Testability Architecture

Project Number: 03–24

Investigators: Kosta Varnavas/ED13
David Hyde/ED13

Purpose

ED13 is researching the state of the art in serial back-plane technology in order to provide scalable, fault tolerant, advanced computing systems, more applicable to today's connected computing environment, and to better meet the needs of future requirements for advanced space instruments and vehicles. After choosing an appropriate technology for NASA's needs, ED13 will design/build and demonstrate a high-speed serial back-plane system.

Background

Current back-plane technology such as Virtual Matrix Encryption (VME) and current personal computer back planes such as Peripheral Component Interconnect (PCI) are shared bus systems that can exhibit nondeterministic latencies. This means a card can take control of the bus and use resources indefinitely, affecting the ability of other cards in the back plane to acquire the bus. This provides a real hit on the reliability of the system. Additionally, these parallel busses only have bandwidths in the 100s of MHz range and electromagnetic interference (EMI) and noise effects get worse the higher in bandwidth you get. The shared bus nature of these busses can cause a complete system failure from even one signal not working right. Signal integrity of so many shared signals also poses a reliability challenge.

Approach

The approach followed for this Center Director's Discretionary Fund (CDDF) project is to investigate the state-of-the-art in industry and choose a serial back-plane protocol. After a protocol is chosen, the CDDF team will implement the chosen protocol using a commercial development board and a custom designed board that will be designed and built by the CDDF team. Testing of the two boards will determine how well this approach works compared to current technology.

Accomplishments

Accomplishments as of April 2004 consist of significant amount of research into the state-of-the-art in industry. An Aurora protocol was chosen due to its well-developed and available status. Plus, it could be a platform to upgrade from. A development board has been ordered and a custom design, implementing the protocol, has been completed and simulated.

Planned Future Work

Future work will be to take the custom board schematics and have the board built, and write software to run tests in the lab to indicate performance improvements compared to established technology.

Publications and Patent Applications

None yet

Funding Summary

Figure 1 on the following page is a presentation of the fiscal year (FY) 2004 funding for this project.

Status of Investigation

This investigation is currently on schedule (see fig. 1) and on budget.

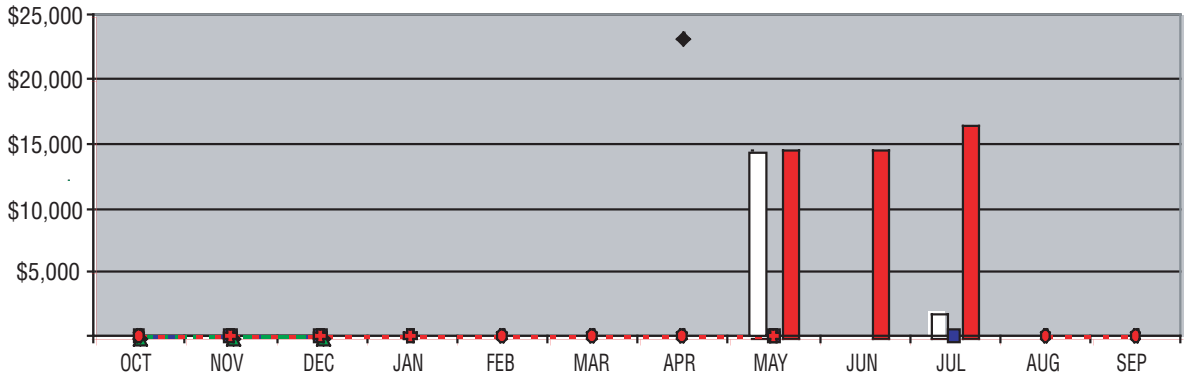

	Authority Received	0.0	0.0	0.0	0.0	0.0	0.0	$23,200	0.0	0.0	0.0	0.0	0.0
	Cum Plan (ODC)	0.0	0.0	0.0	0.0	0.0	0.0	0.0	0.0	0.0	1,790	0.0	0.0
	Cum Actual (ODC)	0.0	0.0	0.0	0.0	0.0	0.0	0.0	$14,700	0.0	1,790	0.0	0.0
	Cum Plan (Contractor)	0.0	0.0	0.0	0.0	0.0	0.0	0.0	0.0	0.0	0.0	0.0	0.0
	Cum Actual (Contractor)	0.0	0.0	0.0	0.0	0.0	0.0	0.0	0.0	0.0	0.0	0.0	0.0
	Cum Plan (Total)	0.0	0.0	0.0	0.0	0.0	0.0	0.0	0.0	0.0	$1,790	0.0	0.0
	Cum Actual (Total)	0.0	0.0	0.0	0.0	0.0	0.0	0.0	$14,700	$14,700	$16,490	0.0	0.0

APPROVED
Note:

Figure 1. Project funding summary and investigation status for FY 2004.

Characterization and Selection of Carbon Fibers Fabricated in Ceramic Matrix Composites for Propulsion and Third Generation Thrust Applications

Project Number: 03–25

Investigator: Diep Vo Trinh/ED34

Purpose

Purposes of this proposed Center Director's Discretionary Fund (CDDF) project are as follows:

- To select commercially available carbon fibers based on carbon-fiber property-selection metrics.
- Selected carbon fibers will undergo heat treatment to modify the carbon fiber purposes at different elevated temperature and duration time conditions.
- Heat treated carbon fibers will be characterized for various physical and chemical properties such as strength, strain, surface roughness, geometric surface area (BET), active surface area (ASA), carbon essay, axial thermal expansion (CTE), radial thermal expansion, and environmental durability.

Background

Because of their low weight, superior strength, high-thermal conductivity, and stiffness, carbon fibers are finding increasing use in a wide variety of applications ranging from sporting goods to spacecraft structures and missile nose cones. Ceramic matrix composites (CMCs) fabricated out of carbon fibers in a silicon carbide matrix offer improvements in durability at a large elevated temperature range with a corresponding reduction in weight for propulsion components such as blisk, heat-duct exchangers/cooled panels, combustor, nozzles, and leading edges. The two main sources for manufacturing the fibers are polyacrylonitrile (PAN) and petroleum pitch (Mesophase pitch). The physical and chemical properties of these carbon fibers depend on the carbonization process of the fiber precursor. In spite of all the wonderful properties of CMCs for aerospace applications, there is a significant drawback of these materials due to oxidation of the carbon fiber when the matrix microcracks under a hostile environment.

One of the possible means of protecting carbon fiber from oxidation is heat treatment. A heat treatment process will improve stability and oxidation resistance of the carbon fiber due to improved carbon structure (improved ordering, and increased density) and change in other material properties such as reduced pore volume, increased thermal conductivity, decreased strength, increased modulus, etc. The heat treatment method for modified carbon fiber has not been investigated elsewhere. There is very limited information concerning the heat treatment of carbon fibers. Understanding the physical and chemical properties of heat-treated carbon fibers will greatly benefit NASA and the space program. Improving carbon fiber properties will lead to reduced matrix microracking and improved environmental durability for CMCs in propulsion applications.

Approach

The proposed project consists of three major tasks:

(1) Select about 30 different carbon fibers based on carbon fiber property selection metrics from different vendors, different fiber precursors, different processes, and different types of carbon fiber.
(2) Establish the heat treatment conditions and parameters. The selected fibers will be heat treated at different temperatures ranging from 1,700–3,000 °C and at dwell times of 1–3,600 s.
(3) Characterize and compare various physical and chemical properties before and after heat treatment. These properties include strength, strain, surface roughness, interlayer spacing, BET, ASA, carbon essay, CTE, radial thermal expansion, and environmental durability. The modified carbon fibers that meet the oxidation-reduction criteria will be fabricated into a panel CMC to study the properties of the composite for material thrust applications.

Accomplishments

Nineteen different types of fibers from six different manufacturers for both PAN and pitch fibers had been selected for heat treatment as listed in table 1.

The selected fibers in table 1 were heat treated at three different temperatures: 1,700 °C, 1,850 °C, and 2,450 °C. Pitch and PAN fibers were heat treated separately in an argon environment. The heating rate was 2,000 °C/h. The dwell time was 4 h at 4,000 °C to remove sizing and the hold time was 2 h for heat-treated fibers. Figures 1, 2, and 3 show the images of three different types of fibers under scan electron microscopy (SEM) at different heat treatment temperatures. These fibers are NGF–CN 60–30S, Toray M60JB–6K, and HEXCEL ASU–W–12K respectively. At 1,700 °C, all sizing on the fibers was completely removed. However, they were only slightly affected on the fiber surface at different heat treatment temperatures for all three different types of fibers.

Table 1. Fibers selected for heat treatment.

Fiber No.	Mfr.	Fiber	Type	Tow: Size, K	Sizing	Nominal Diameter (mm)
1	NFG	CN–60–30S	Pitch	3	3 %m	10
2	NFG	YSH–60A-30S	Pitch	3	1.7 %m	7
3	NFG	YSH–70A–60S	Pitch	6	1.6 %m	7
4	NFG	XN–05–30S	Pitch	3	2.6 %m	10
5	Hexcel	HMU–X55	PAN	12	0	10
6	Hexcel	AS4	PAN	12	TBD	7
10	Hexcel	IM9–3000	PAN	12	No	4.4
15	Hexcel	IM7–5000	PAN	6	1 %	5
7	MRC	TR40	PAN	1	1.3 %m	7
8	MRC	TR30S	PAN	3	1.4 %m	7
9	MRC	TR30S	PAN	3	No	7
11	Toho	Besfight G30–400:HTA–7W*	PAN	1	TBD	7
12	Toho	Besfight G40–800: (IM600)*	PAN	6	TBD	5
13	Toray	M40JB	PAN	6	1	10
14	Toray	T1000GB	PAN	12	0.7	10
19	Toray	M60JB	PAN	6	1	10
16	Thornel (Cytec)*	T900	PAN	12		10
17	Cytec	T300	PAN	1	1.01 %	7
18	Cytec	T300	PAN	3	0.98 %	7

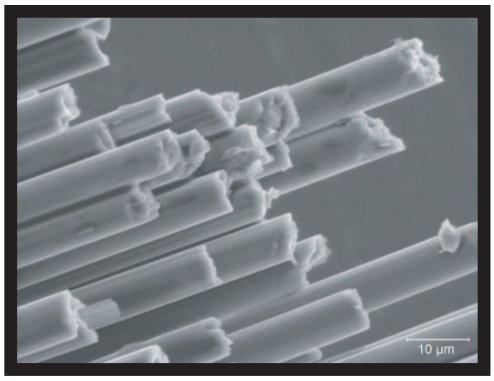

NGF–CN 60 30S–Virgin

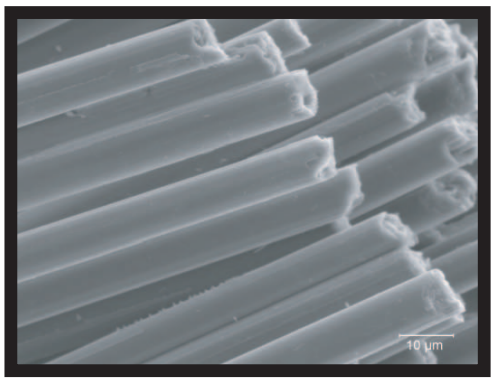

NGF–CN 60 30S–1,700 °C

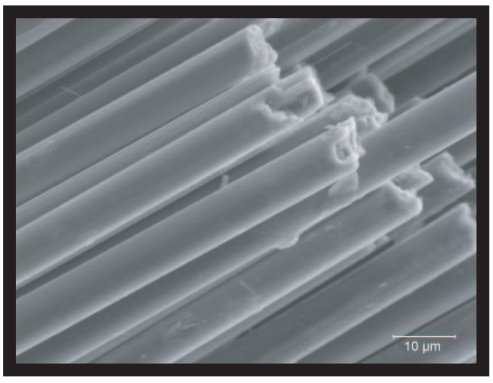

NGF–CN 60 30S–1,850 °C

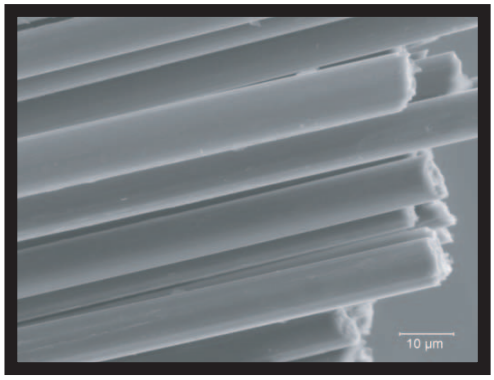

NGF–CN 60 30S–2,450 °C

Figure 1. SEM image of NGF CN60–30S at different heat treatment temperatures.

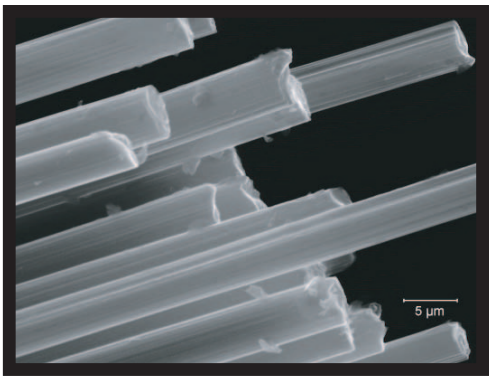

Toray: M60JB–6K—Virgin

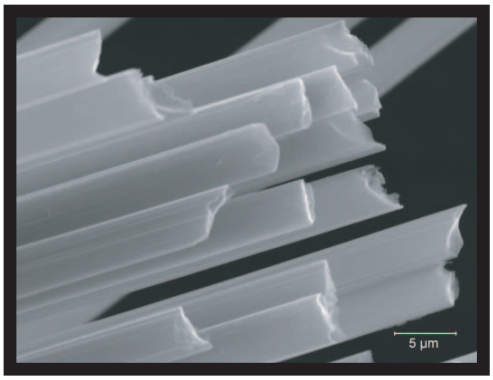

Toray: M60JB–6K—1,700 °C

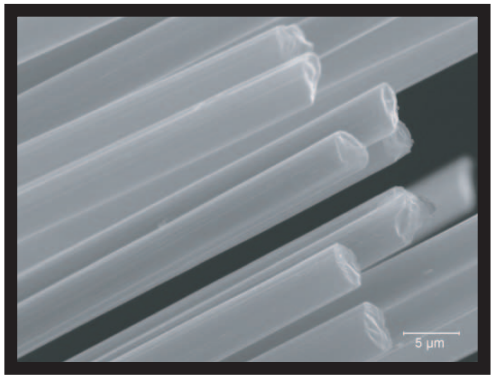

Toray: M60JB–6K—1,850 °C

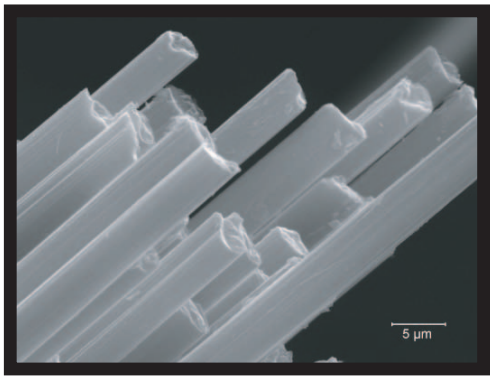

Toray: M60JB–6K—2,450 °C

Figure 2. SEM images of Toray M60JB–6K at different heat treatment temperatures.

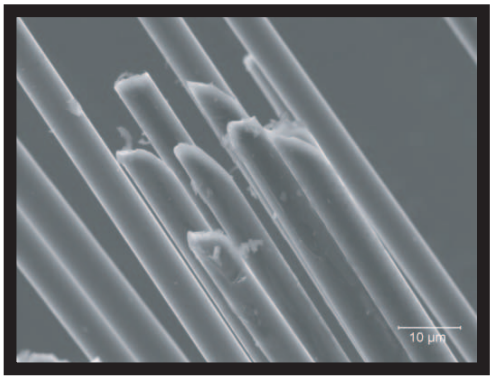

Hexcel: AS4–W–12K—Virgin

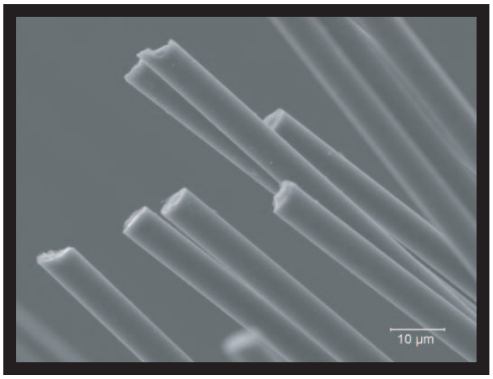

Hexcel: AS4–W–12K—1,700 °C

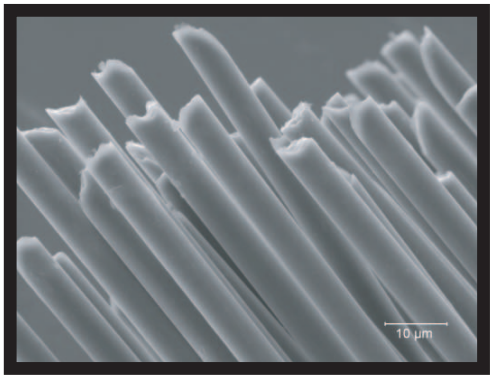

Hexcel: AS4–W–12K—1,850 °C

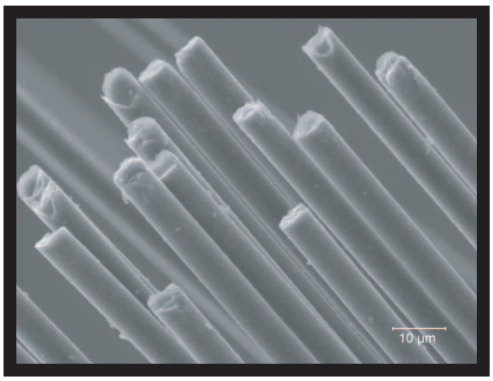

Hexcel: AS4–W–12K—2,450 °C

Figure 3. SEM images of Hexcel AS4–W–12K at different heat treatment temperatures.

The effect of heat treatment on the densities of carbon yarns was measured. As the heat treatment temperatures increased, the densities of the yarns also increased. At 2,450 °C, the densities of the PAN fibers were highly increased (fig. 4). The densities of pitch fibers were gradually increased as the temperature increased. The volume changed more rapidly than the mass changed. The resistivity of PAN fibers decreased with increasing heat treatment temperature. However, the resistivity of some 12k and 6k yarns was not affected as the heat treatment temperature increased from 1,700 °C to 1,850 °C. Figures 5, 6, 7, and 8 show the effect of heat treatment on the resistivity of different types of carbon yarns at different temperatures. The decreasing resistivity with increasing the heat treatment temperature was due to reorder and elongation of carbon backbone and reduction of impurities. Moreover, some pitch fibers behave slightly different than the PAN fibers. NGF CN and XN fibers did not show a large drop in resistivity at 2,450 °C. In addition, XN fibers showed slightly increasing resistivity at 1,850 °C and 2,450 °C.

Planned Future Work

Planned future work is as follows:

- Conduct mechanical property testing such as strength, strain, and surface roughness.
- Determine fiber diameter via laser diffraction and d-spacing with x-ray diffraction.
- Determine chemically active surface areas.
- Conduct interface coating and matrix process trials.
- Perform analysis by SEM.

Publication and Patent Applications

None so far.

Funding Summary

Table 2 presents the fiscal year (FY) 2003 and FY 2004 funding summary for this project.

Table 1. Funding summary.

FY 2003 ($)	FY 2004 ($)
58,200	15,000

Status of Investigation

The initial tasks 1 and 2 were already completed according to the schedule. The analyses to compare the fibers before and after heat treatment were well underway. However, the analyses of these fibers by SEM were delayed due to the Return-to-Flight effort. Otherwise, every thing is working as planned.

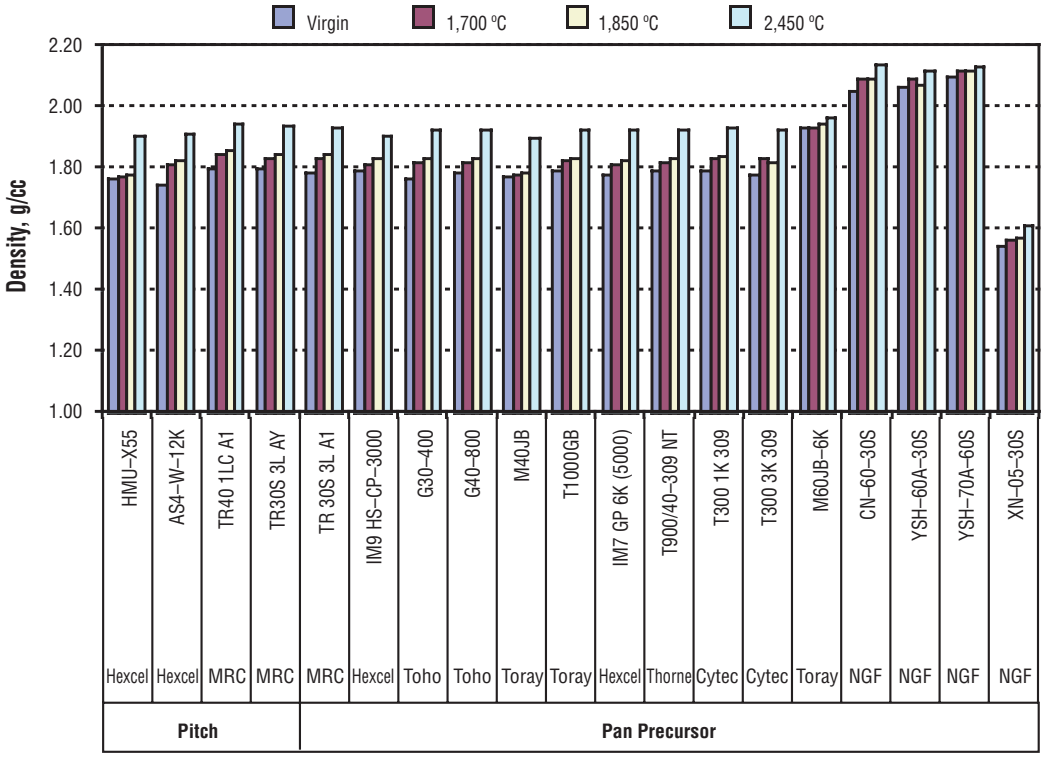

Figure 4. The effect of heat treatment on the densities of carbon yarns.

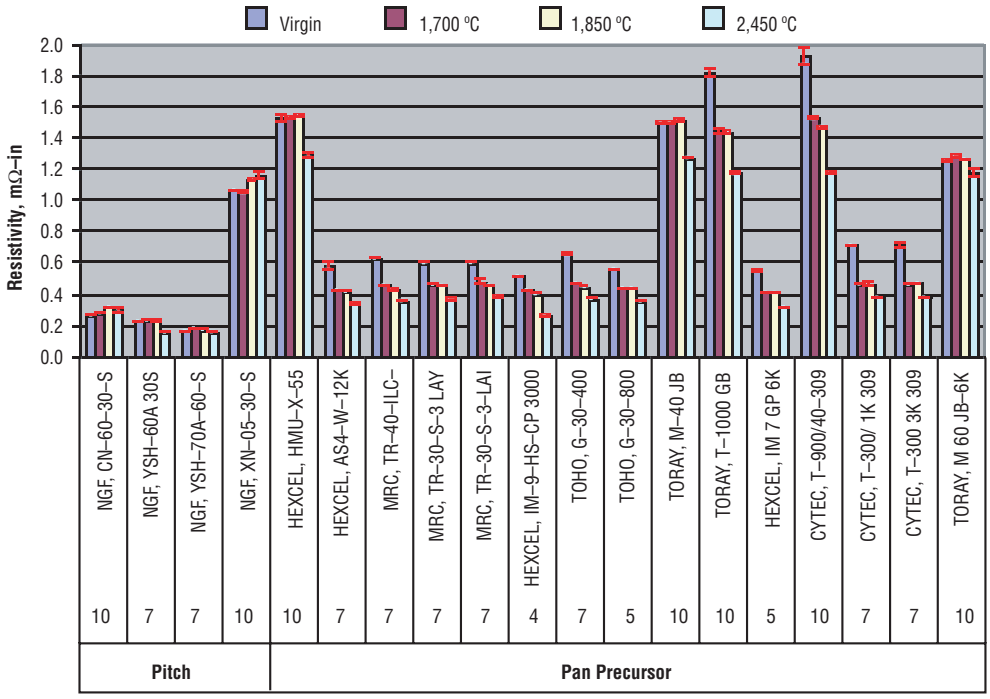

Figure 5. The effect of heat treatment on the resistivity of carbon yarns.

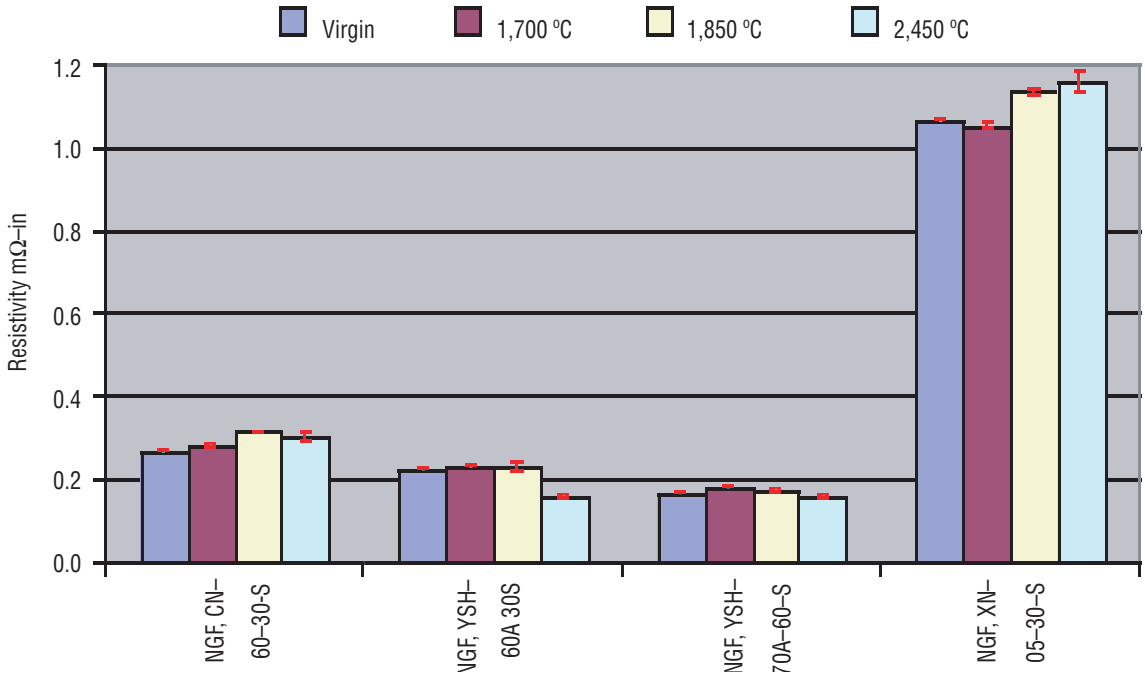

Figure 6. The effect of heat treatment on the resistivity of pitch yarns.

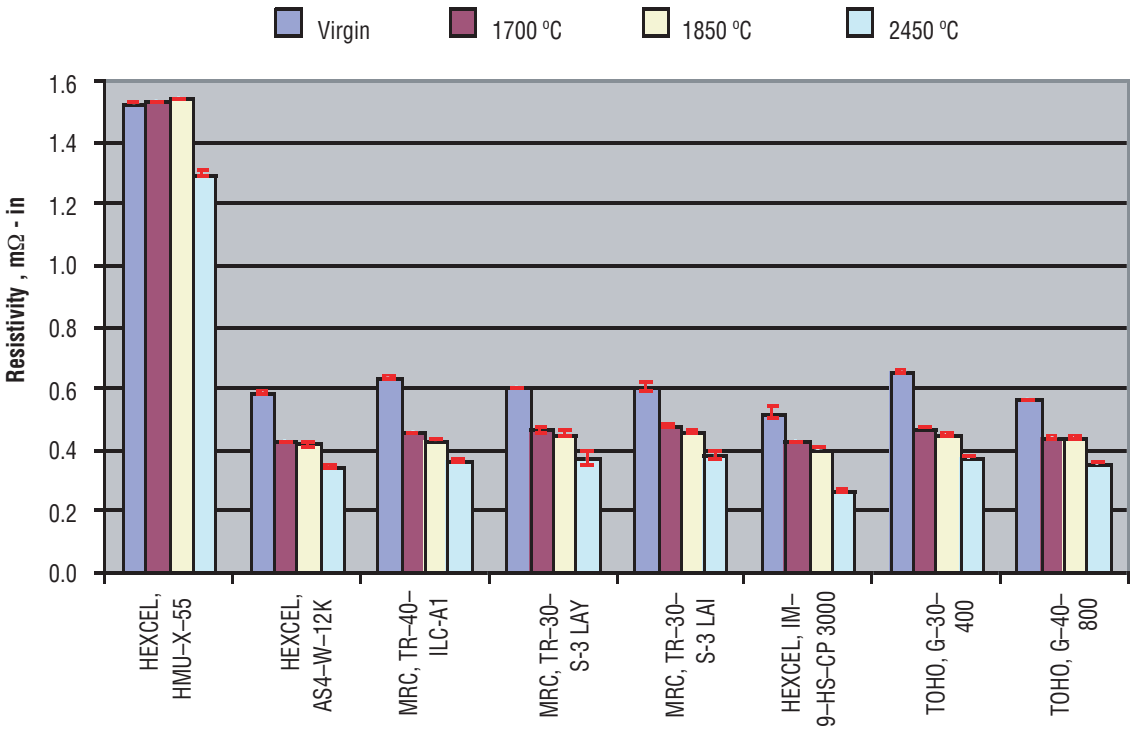

Figure 7. The effect of heat treatment on the resistivity of PAN fibers.

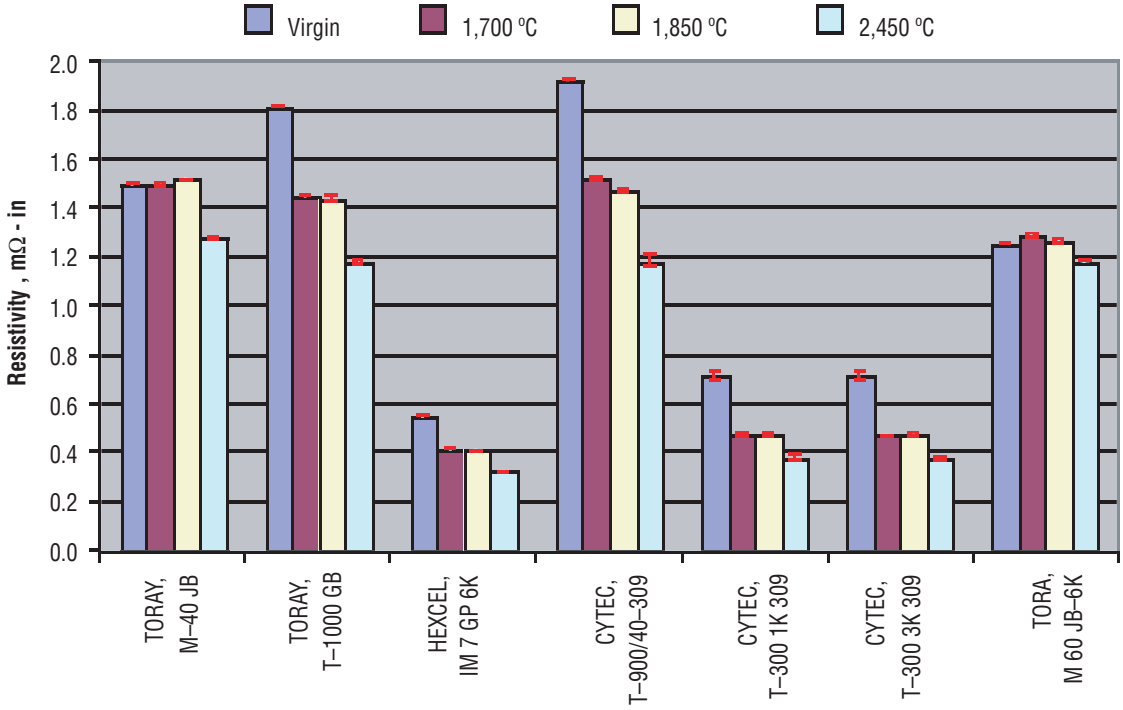

Figure 8. The effect of heat treatment on the resistivity of PAN fibers.

Ultraviolet Radiation and Atomic Oxygen Interaction With Molecular Contamination on External Spacecraft Surfaces

Project Number: **03–26**

Investigators: **Keith C. Albyn/ED31**
Andy Finchum/ED31
Kenneth M. Whitley/ED31

Purpose

Ground testing of materials to simulate on-orbit environmental factors often only addresses one environmental factor rather than the synergy between several environmental factors. This Center Director's Discretionary Fund (CDDF) project focuses on the outgassing of materials and how atomic oxygen and ultraviolet radiation, as individual environmental effects and in combination, enhance or degrade the deposition of molecular contaminants, as quantified by outgassing measurements. Materials currently used for the construction of spacecraft and some pure chemical compounds will be examined to determine the synergistic effects of several environmental factors on the deposition of molecular species.

Background

Contamination sensitive spacecraft, such as the *International Space Station* (*ISS*), have rigorous requirements limiting the amount of molecular contamination that can accrue on the vacuum exposed surfaces of the spacecraft. Environmental factors, such as atomic oxygen and ultraviolet radiation, may alter the rate at which molecular contaminants deposit on a surface producing deposition rates that are not dependant on the temperature of the surface. Measurement techniques, such as the ASTM Method E–1595, are used to screen materials to ensure that materials with low outgassing rates are selected for construction of the spacecraft.

Erosion has been demonstrated where hydrocarbon materials are exposed to atomic oxygen, providing a mechanism to remove some molecular contaminants from surfaces.

Also, atomic oxygen chemically converts some materials such as silicones into silicates, promoting the adherence of some materials to surfaces. Ultraviolet radiation will break chemical bonds in some molecular species while promoting the formation of bonds (cross-linking) in other molecular species. Limited data exists that quantifies the interaction of atomic oxygen or ultraviolet radiation with certain chemical species while the synergy between these environmental factors and specific molecular materials is poorly understood.

Approach

An existing vacuum chamber (fig. 1) with both an atomic oxygen source and a source of vacuum ultraviolet radiation, a deuterium lamp (fig. 2), will be modified and used to measure the rate of deposition of molecular species on the surface of two temperature-controlled quartz crystal microbalances (TQCMs) (fig. 3). The deposition of outgassed molecular species will be measured at several sample and deposition surface temperatures to obtain a baseline matrix of deposition rates. Additional deposition measurements will then be made while atomic oxygen and ultraviolet radiation, individually and in combination, interact with the species depositing on the TQCMs.

To provide supplementary information on the molecular structure of the deposited material(s), witness plates will be placed in the plane of the deposition surfaces, TQCMs, as passive collectors that can be removed from the vacuum chamber for spectroscopic analysis.

Accomplishments

An extensive evaluation of the existing vacuum chamber hardware has resulted in the following:

- Fabrication of new fixturing to accommodate a second TQCM and to fix the geometry between the source of the molecular species being deposited and the deposition surface.
- New fixturing also defines the geometry between the atomic oxygen source, the vacuum ultraviolet radiation source, and the deposition surface.
- Materials currently being used in the construction of spacecraft have been obtained and baseline deposition measurements are being made in an auxiliary outgassing measurement facility.
- A method for calibration of the TQCMs has been developed in support of the planned measurements.

An extensive evaluation of the existing atomic oxygen source identified performance problems with this system. In-house repair efforts and consultation with several external users of

Figure 1. The original Photodeposition Facility prior to modification of the internal hardware.

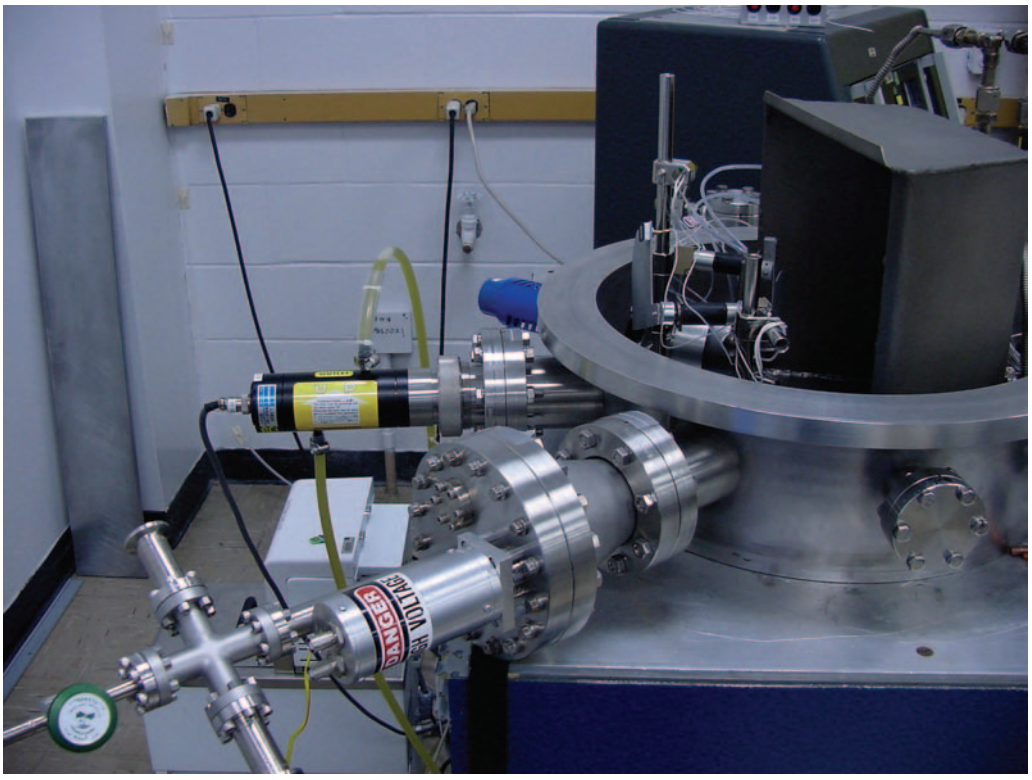

Figure 2. The ultraviolet lamp (the black cylinder with the yellow label) mounted just behind the atomic oxygen source (foreground). The original fixturing can be seen inside the base of the vacuum chamber.

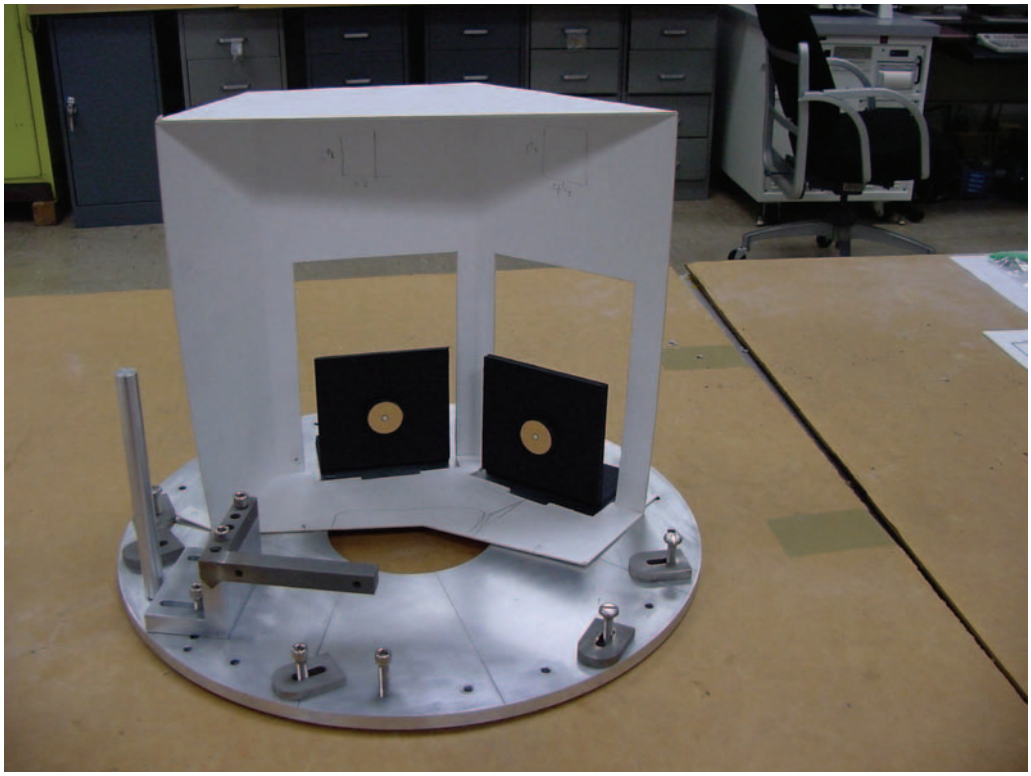

Figure 3. Fixturing with a cardboard mockup of the hardware currently being fabricated. The two copper disks represent the TQCMs that will be used to measure the deposition rate of the molecular contaminants. An effusion cell containing the sample material will be suspended from the horizontal arm at the left side of the picture.

similar equipment revealed that the existing atomic oxygen source will not produce adequate fluxes of atomic oxygen and was possibly producing soft x-rays. This source has been removed from the vacuum system and the decision to retain atomic oxygen as a test parameter is under review by the investigators. Development of an alternative atomic oxygen source is an option under consideration that will be explored in parallel with the continued build up of the existing hardware.

Planned Future Work

Construction of the new fixturing is competing for fabrication support with hardware needed in support of the current Return-to-Flight effort. Fixturing is being received sporadically, delaying the modification of the existing vacuum chamber. Baseline measurements will continue in auxiliary systems, completing the preliminary outgassing measurements in parallel with the chamber modifications. Investigation of the synergy between the molecular deposition process and ultraviolet radiation will begin once the chamber modifications are complete.

Funding Summary

Table 1 presents the funding for fiscal year (FY) 2003 and FY 2004. The FY 2004 allocation is being used to complete the fixturing (labor and materials) for the facility.

Table 1. Project funding summary.

	FY 2003 ($)	FY 2004 ($)
Allocation	24,000	9,000
Expenditures		
Photodeposition Facility (samples and new hardware)	14,500	N/A
Facility fabrication fixturing	9,500	9,000

Status of the Investigation

The preliminary outgassing measurements on two materials, an epoxy and a Teflon, are being made in an auxiliary facility. The data generated is being used to support the *ISS* Program and is being archived in the Space Environmental Effects Database for use by other programs. A draft technical memorandum on the TQCM calibration technique has been written and is currently under internal review.

Fabrication of the new vacuum chamber fixturing is nearing completion and the remaining components are in work as scheduling allows.

Novel Approach to Fabricating Sample Containment Assemblies

Project Number **03–28**

Investigators: **Glenn Williams/ED34**
Ken Cooper/ED34
Mike Fiske/MRC

Purpose

Over the course of the next decade, NASA has planned the deployment of the Materials Science Research Rack (MSRR), a multiexperiment facility for the *International Space Station* (*ISS*). The MSRR is designed to accommodate NASA's current and evolving cadre of peer-reviewed science investigations. The facility will provide the apparatus for satisfying near-term and long-range Materials Science Discipline goals and objectives to be accomplished in the microgravity environment of the United States (U.S.) Laboratory on the *ISS*. The rack will consist of multiple experiments, dedicated to various aspects of materials processing. In some configurations, the rack may support a single furnace system with modular, replaceable furnace modules. To date, no requirements for geometrical commonality have been imposed on these furnace systems. Therefore, each of these configurations will require the development of unique Sample Containment Assemblies (SCA).

Laser Engineered Net Shaping (LENS) is a unique manufacturing process recently developed at Sandia National Laboratories. The process uses additive fabrication techniques to deposit metal powders and thus form a fully dense three-dimensional object directly from computer-generated drawings; therefore, no tooling or fixtures are required. The Marshall Space Flight Center (MSFC) has 1 of only 10 of these LENS systems available in the world, and this paper discusses a Center Director's Discretionary Fund (CDDF) project to successfully demonstrate that hermetic (nonporous) sample containment assemblies can be fabricated using LENS at a substantial time or cost savings over other manufacturing techniques, including chemical vapor deposition (CVD) and vacuum plasma spray (VPS).

Background

An SCA is used to contain and support microgravity sample ampoule/crucibles during the crystal growth or solidification process. These ampoule/crucibles are typically hermetically sealed tubes made of quartz, alumina, boron nitride, or other similar materials. Because these materials are subject to breakage and other high-temperature failures, reliable safe containment of the experimental science sample materials is not assured by the use of ampoule/crucibles made of these materials. Typical crystal growth/solidification materials of interest include GaAs, HgCdTe, CdZnTe, PbSnTe, Pb-based alloys, Al-based alloys, Si, etc. Many of these materials have high-vapor pressures of known toxic materials (e.g., vapor in GaAs) and many are known to be carcinogenic. Because the MSRR will be installed in the manned environment of the *ISS*, assurance of safe containment of these hazardous chemicals is required by *ISS* flight rules. To meet this requirement, the ampoule/crucibles are typically sealed into a uniquely designed metal cartridge to preclude crew exposure to sample materials.

The use of a metal cartridge, and in some cases even the ampoule/crucible, is unique to the microgravity environment. In terrestrial crystal growth practices, the use of toxic gas monitors, chemical exhaust cabinets, and equipment isolation is more routinely used to protect personnel. Therefore, while the development of microgravity-based furnaces requires modifications of well-established terrestrial technologies, the SCA fabrication problem is a relatively new technical requirement imposed by the safety concerns and flight rules for microgravity experimentation. The following three principal requirements for acceptable SCA performance have been identified:

1) The ability of the SCA to contain the pressure associated with the sudden rupture of an ampoule/crucible during performance of a crystal growth/solidification experiment. Implicit in this requirement is also the requirement to contain the pressures associated with processing an SCA containing an undetected fractured ampoule/crucible.
2) Assessment of the probability of ampoule/crucible failure or fracture through an approved ampoule/crucible qualification and test plan.
3) Determination that the selected SCA cartridge material would exhibit sufficient chemical passivity in the event of its high-temperature exposure of the sample chemicals such that it will maintain absolute containment, and not permit chemical breach of the safety level of containment required of a qualified SCA.

In many cases, a refractory metal such as molybdenum, tungsten, niobium, or tantalum has been identified as a suitable cartridge material for containment of sample material at temperature, based on a lack of chemical reactivity of these materials. However, the typical length/diameter aspect ratios of these cartridges (between 22:1 and 32:1) do not lend themselves to easy fabrication using conventional methods. A rolled and welded tube with a welded end cap is difficult to qualify for space flight applications. Advanced techniques have been utilized, such as CVD. While a CVD process yields a hermetic tube of required material and has actually been used in space flight applications, it is typically a very time-consuming and expensive process.

VPS tubes have also been evaluated with mixed results. While the VPS process is relatively fast and inexpensive, difficulties in achieving a hermetic structure have thus far precluded its use as a space flight cartridge material.

Cost and schedule can often be drivers for SCA development because the development programs for most SCAs are typically started relatively late compared to the development of an associated furnace module. As an example, the current cost for fabricating SCAs range typically from $1,000–$1,500 for an extruded Inconel cartridge with a welded end cap. For a CVD tungsten cartridge the cost increases to $5,000–$6,000 each. For a VPS tungsten cartridge, the cost is only $500–$1000 and VPS is very fast compared to CVD (1 day versus 5 days). However, as mentioned, it is historically difficult to obtain VPS cartridges that are hermetic.

LENS is a unique manufacturing process recently developed at Sandia National Laboratories. The process uses additive fabrication techniques to deposit steel powders and thus form a fully dense three-dimensional object directly from computer-generated drawings; therefore, no tooling or fixtures are required. MSFC has 1 of only 10 of these LENS systems available in the world, thus providing a unique advantage in accomplishing the goals of this proposal. The objective of this project was to successfully demonstrate that hermetic (nonporous) sample containment assemblies of refractory metals (such as tungsten and niobium) could be fabricated using LENS at MSFC with relative cost and schedule benefits as compared to the CVD and VPS processes.

Approach

Initial trials were conducted on an Optomec LENS 750 machine at MSFC (550-W max laser) using materials already known to the process. Stainless steel 316 (SS316) was initially used to verify the ability to meet the required configuration. We then advanced through Inconel 718 to evaluate any required modifications to the experimental setup. SS316 and Inconel 718 samples were processed at MSFC. SCAs were laser deposited of a standard geometry: 1/2-in diameter cylinder with 0.03-in wall thickness. A goal was to also have a closed spherical end on the tube by the end of the project. The length of the tubes required for porosity testing were determined and established during the experiment. It should be noted that the current system setup at MSFC will allow for the fabrication of a maximum 10-in length, whereas the end-use cartridges for the *ISS* will need to be 16–22-in long. The deposition of such thin-walled structures introduced a new set of operational challenges; therefore, a process to determine deposition parameters for even known materials was established. As sample tubes were successfully deposited, they were then leak tested to confirm hermeticity and also sectioned and evaluated metallographically.

Accomplishments

For statistical purposes, it was determined to make multiple tubes using identical processing parameters for characterization of leak rate. Eleven tubes of SS316 between 6- and 10-in long were successfully produced at MSFC. Six Inconel 718 tubes of similar length were produced at MSFC.

Selected samples were sectioned both axially and radially to evaluate microstructure, and the remainder were used to evaluate hermeticity by welding a plug on one end and attaching the other to a helium (He) detector. A vacuum was pulled on the inside of the tube and He was free-flowed around the tube outer diameter (OD) while monitoring the He detector. Table 1 identifies the final parameters selected for the processing of all tube samples under this effort.

Table 1. Processing parameters used for LENS SCA development.

Parameter	Measurement	
Material	MSFC SS316	MSFC Inconel 718
Laser amperage (A)	42	45
Laser power (W)	265	290
Oxygen level (ppm)	60	55
Feed rate (ipm)	15	40
Feeder speed (rpm)	9	6
Mass flow (rpm)	5	5
Layer thickness (in)	0.01	0.01

From a manufacturing standpoint, it took only about 1 h to build a 6-in long SS316 sample on the LENS machine at MSFC. The processing time for a 6-in long Inconel sample was about 4 h. Some additional time is allocated for finishing and testing of the samples, but these results confirm the validity of this process for rapid fabrication of sample cartridge tubes.

The results obtained from He leak testing of the MSFC SS316 samples indicated an average leak rate of 1.2×10^{-8} standard cubic centimeters per second (SCCS) of He. The average leak rate for the MSFC Inconel 718 tubes was 6.5×10^{-8} SCCS of He. No single tube of any material had a leak rate higher than 4×10^{-7} SCCS He. These results are excellent in that they confirm the ability of this process to form a hermetically sound structure before any possible postfabrication operations (e.g., hot isostatic pressing), and without any fine-tuning of selected processing parameters for this effort. In the past, hermeticity was traditionally defined by NASA safety personnel as having a leak rate of less than 1×10^{-6} SCCS He. Because of the long manned durations aboard the *ISS*, a sample cartridge containing a toxic material must now meet a leak rate of less than 1×10^{-9} SCCS of He. However, this leak-rate requirement may be lower for nontoxic samples. Since the viability of the LENS process can be improved for this application with successful postfabrication processing, the authors are comfortable that even the tighter leak-rate requirement can eventually be met.

Planned Future Work

With adaptations, the LENS process appears to be a viable, low-cost, quick alternative to CVD or VPS production of refractory metal high-aspect ratio cartridge tubes for microgravity materials processing. Some adaptations being evaluated for future LENS sample processing include the following:

- Increasing the laser power for a more thorough weld through the previously deposited layers. The laser in the MSFC LENS system has been retuned to provide an approximate 100-W higher output. While this is not expected to support tungsten processing, improvements are hoped for in terms of reducing porosity in the melt pool.
- The translation axes (X, Y, and Z) of the build stage will be reencoded for a continuous tube forming motion, essentially transitioning from the previous technique of depositing successive two-dimensional circles, and instead forming with a continuous helix motion. It is anticipated that this will reduce the effects of pauses between layers.
- Reduction of oxygen content in the build envelope, which is expected to reduce the effects of oxidation during the welding process.
- Continuation of software development to allow a hemispherical, closed-end cap to be deposited on the top of a tube.

Future efforts will focus on incorporation of the aforementioned adaptations and on the deposition of higher temperature refractory materials, specifically tungsten and niobium, using systems with higher laser power capabilities. These materials, if successfully LENS deposited, will allow NASA to begin qualification testing of LENS SCAs for possible future experiment processing aboard the *ISS*.

Publications and Patent Applications

None yet.

Funding Summary

Table 2 presents the funding summary for fiscal year (FY) 2003 and FY 2004.

Table 2. Funding summary.

	Received ($)	Spent ($)	Notes
FY 2003	35,000	33,598.89	
FY 2004	0	1,163.18	Rollover from FY 2003
Anticipate $35,000 second year funding to continue into tungsten development.			

Status of Investigation

We are currently in the process of reprogramming motion controllers for continuous deposition motion. First samples were invalidated by the new sample ampoule cartridge assembly (SACA) flight specifications. The next steps will be redepositing and reevaluation of steel and Inconel samples at new operating parameters to try and meet the updated flight specifications. Then we will purchase tungsten and/or niobium powder for high temperature development.


Flight Projects
Directorate
(b) 334 Hz
(c) 500 Hz
NASA MSFC
Center Director's
Discretionary Fund
FY 2003
Annual Report

Web-Based Request-Oriented Scheduling Engine

Project Number: **02–16**

Investigators: **John Jaap/FD42**
Elizabeth Davis/FD42
Lea Richardson/FD42

Purpose

The purpose of this Center Director's Discretionary Fund (CDDF) research is to develop the enabling technologies that will allow new approaches to planning and scheduling space activities. This technology will have three components: A modeling schema, a scheduling engine, and a system architecture. The modeling schema must be able to represent all scheduling requirements so that an automatic scheduling engine can produce a satisfactory schedule. The scheduling engine must be able to correctly schedule all the information in the models. The architecture must allow multiple remote users to simultaneously build a single timeline.

A robust implementation of a Web-based request-oriented scheduling engine (ROSE) based system would support multiple simultaneous users, each formulating models (defining scheduling requirements), submitting these models via the Internet to a single scheduling engine operating on a single timeline, and immediately viewing the resulting timeline. ROSE is significantly different from the engines currently in use. Current engines support essentially one person at a time with a predefined set of requirements from many tasks, working in either a batch scheduling mode or an interactive-/manual-scheduling mode.

Background

The Ground Systems Department of the Flight Project Directorate at the Marshall Space Flight Center (MSFC) has more than 30 years of experience in payload activity planning and scheduling as follows: Beginning with Skylab, 16 Spacelab missions, and continuing with the *International Space Station* (*ISS*). Planning for manned space missions has always been labor intensive. During Skylab, it was done with charts that were hand-drawn on paper; now it is done manually with the aid of computer-based timeline editors. Several automatic schedulers have been written, but none have been truly successful. The objective of this research is to define a scheduling engine that enables the migration to planning and scheduling paradigms that have the use of an automatic scheduler as their central tenant.

The current state of the art in modeling methodologies and scheduling engines results in a linear paradigm with knowledge contributed by task experts, vehicle experts, and scheduling engine experts. This paradigm requires significant effort and flow time and is depicted in figure 1. With sufficient software innovations, a modeling methodology could be devised such that the vehicle experts could enter the system and hardware constraints independently of the task knowledge. The task experts could then enter their requirements directly into the scheduling engine. A scheduling engine could be built that understands the requirements as presented by the task experts and eliminates the need for scheduling experts. This paradigm is depicted in figure 2.

The anticipated results of the ROSE research are a modeling methodology and a scheduling engine that will allow the new paradigm to be implemented.

Approach

Poor modeling is the downfall of automatic scheduling. If all the requirements are not included in the model, then the scheduler has little chance of producing a satisfactory schedule. The modeling schema must have an available representation for all the constraints and be friendly enough to allow the user to enter all of them without excessive labor. The scheduling systems currently used in NASA's manned space flight program cannot capture many of the constraints that describe the operation sequences required to operate the Shuttle or the *ISS*, especially those required by the science payloads. This failure of the modeling schema has begotten the scheduling cadre who digest all the requirements, build the best models allowed by the current schema, make notes containing the remainder of the requirements, and then generate the timeline using a timeline editor.

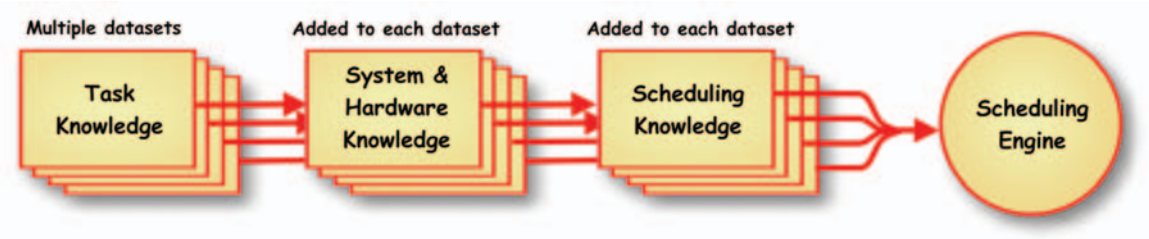

Figure 1. Current scheduling paradigm.

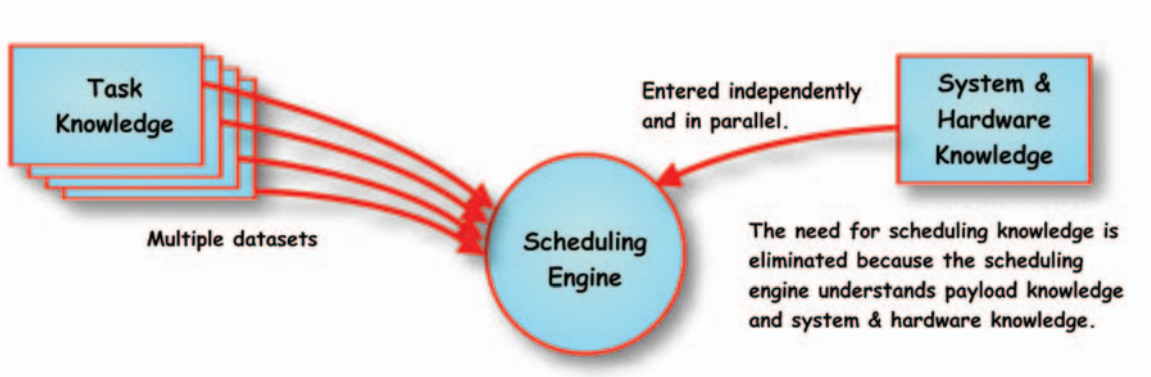

Figure 2. A future scheduling paradigm.

Evaluate Past and Present Systems

The team will evaluate past and present planning and scheduling systems. As both developers and users, the investigators of ROSE have first-hand knowledge of the scheduling system used for most Spacelab missions. The investigators have been in direct contact with the designers and users of the system used for the *ISS*. The team will evaluate the system to be used by the European Space Agency for their *ISS* module and the system used by the Jet Propulsion Libratory (JPL) for many of their space missions.

Design and Prototype of a New System

The first task of the ROSE research is to define and prototype a maximally expressive modeling schema that can easily capture all the requirements and constraints. The second task of the ROSE research is to define and demonstrate a scheduling engine that can schedule the maximally expressive models automatically.

Accomplishments

Evaluations

One team member visited Deutschen Zentrum für Luft- und Raumfahrt (DLR) in Germany. A day was devoted to meetings where DLR explained and demonstrated their planning and scheduling tools (entitled Plato and Pinta) to be used for scheduling the activities of the Columbus module of the *ISS*. The ROSE team obtained and installed Plato and Pinta at MSFC.

Two team members visited JPL's planning and scheduling team for a 1-day meeting to review their scheduling methodology and to solicit comments about the design of our new scheduling algorithm. A copy of their scheduling software (ASPEN), including source code, was obtained and reviewed. The Consolidated Planning System (CPS), developed by the Johnson Space Center (JSC), is used by JSC to schedule Shuttle tasks and by MSFC and JSC to schedule *ISS* tasks. CPS is locally installed and was reviewed by the team. Analyzing these tools has affected the ROSE modeling schema and the scheduling algorithm. In particular, a conversation with Dr. Martin Wickler at DLR was instrumental in the design of our scheduling algorithm.

Web Environment

The Web server environment to support the ROSE research was purchased and set up in March and April of 2002. The topology is shown in figure 3. Two server-class computers were purchased and installed. Each computer consists of dual Pentium-III-S processors running at 1.26 GHz, two 18-Gb SCSI disk drives, and a DVD drive. One has a CD writer and one has a tape drive. Both machines are running the Windows 2000 server. One machine is running the Internet Information Services Web server software and the other is running Microsoft's Sequel Server 2000 software. Development software was purchased for all three team members.

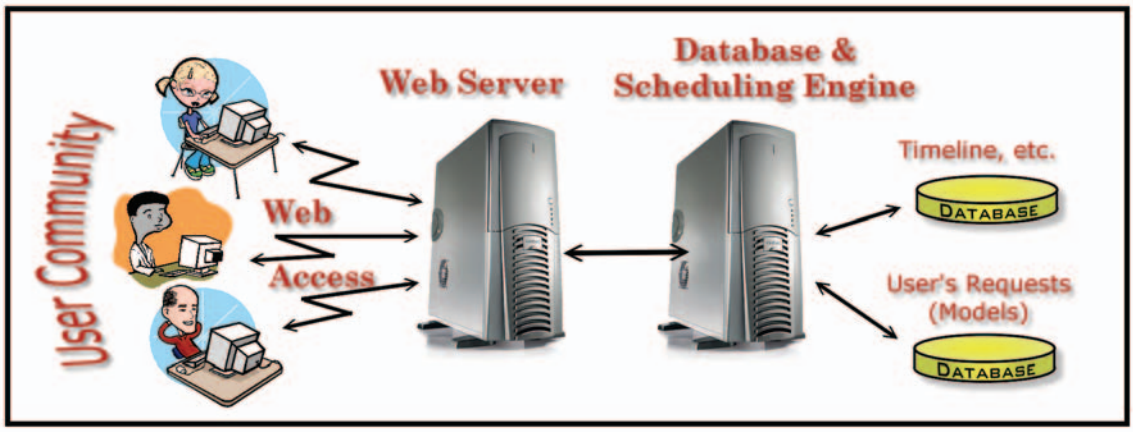

Figure 3. ROSE hardware topology.

Web Environment

The Web server environment to support the ROSE research was purchased and set up in March and April of 2002. The topology is shown in figure 3. Two server-class computers were purchased and installed. Each computer consists of dual Pentium-III-S processors running at 1.26 GHz, two 18-Gb SCSI disk drives, and a DVD drive. One has a CD writer and one has a tape drive. Both machines are running the Windows 2000 server. One machine is running the Internet Information Services Web server software and the other is running Microsoft's Sequel Server 2000 software. Development software was purchased for all three team members.

Modeling Schema

A modeling schema for representing all the requirements of tasks to be scheduled was designed and implemented. The schema is a synergy of technological advances and domain-specific innovations. Some of the key features are as follows:

- Decomposition of the problem into salient components: Operations are decomposed into activities that define resource requirements and sequences that define relationships between activities. Sequences can also contain other sequences, repeated activities and sequences, and optional activities and sequences.
- Graphical paradigms: Simple graphical paradigms such as outlines and networks are used to build and depict the models. Modeling itself is done using techniques such as drag and drop.
- Modeling equipment modes: Equipment mode models define implicit resource requirements. This is the mechanism that separates the task models from the hardware/system models.
- Intuitive and rich expression of the relationships between components: The schema employs common-sense representations of temporal relationships using everyday concepts like sequential, during, and overlap. Innovative enhancements to represent the continuance of resource usage between tasks, the interruption of tasks, minimal percent coverage, and temporal relationships to outside tasks have been added to the modeling schema.
- Public services: The schema also introduces the concept of public services; models that are scheduled at the request of another model.

The term maximally expressive has been applied to this schema (See published papers in a later paragraph.).

Scheduling Engine

A scheduling algorithm was designed, partially implemented, and demonstrated. The new scheduling algorithm is named Scheduling Algorithm for Temporal Relation Networks (SATRN). SATRN is an incremental scheduling engine that schedules a request (adding one or more tasks to the timeline) and then waits for the next request. SATRN converts the temporal relations of a sequence to time bounds on the sequence entities (embedded sequences or activities). As each entity is scheduled, the bounds on not-scheduled entities are shrunk. Recursion is used to process embedded sequences. An activity's requirements are checked by a depth-first search. Variable activity durations are utilized to stay within the time bounds. When an entity cannot be asserted (scheduled but not committed to the timeline), already asserted entities are adjusted to free up resources or smart backtracking and reordering is used to unshrink the bounds on the hard-to-schedule entity. Backtracking is also used to explore alternate requirements.

End-to-End Demonstration

An end-to-end demonstration of ROSE was presented to the Flight Projects Directorate management in October of 2003. This demonstration included using the Web-based access to build/edit a model (create a scheduling request), submit it to the remote scheduling engine, and display the results.

Spinoff

The ROSE modeling schema is an evolutionary extension of the modeling schema currently used to collect planning and scheduling requirements for *ISS* payloads. In February 2002, some of the modeling enhancements developed for ROSE were implemented in the current *ISS* software.

Planned Future Work

Work on the partially implemented scheduling algorithm is continuing and a paper describing the algorithm will be written. The ROSE prototype has been retitled Nexus and features are being added to improve the demonstration. Figure 4 shows a screen shot from the demonstration.

Demonstration Booth at SpaceOps 2004

Nexus will be demonstrated in the Ground Systems Department's booth at the 8th International Conference on Space Operations in Montréal, Canada, May 17–20, 2004. This demonstration will be remotely connected to a host computer at MSFC.

Future Applications

Nexus is well suited for use at a lunar base. The astronauts could use it to schedule their daily activities while controllers on Earth could remotely access the base to schedule essential crew tasks and to schedule unattended tasks. The salient features of Nexus that make it suitable for remote usage are as follows:

- Support for virtually simultaneous building of a single timeline by multiple local/remote users.
- The user-friendly interface, maximally expressive modeling, and the immediate feedback significantly reduce the time required to learn how to model and schedule.
- Separating tasks modeling from hardware and system modeling allows Earth-based controllers and lunar-based astronauts each to contribute their unique knowledge.

These same features also make Nexus well suited for use on a trans-Mars vehicle and on a Mars base.

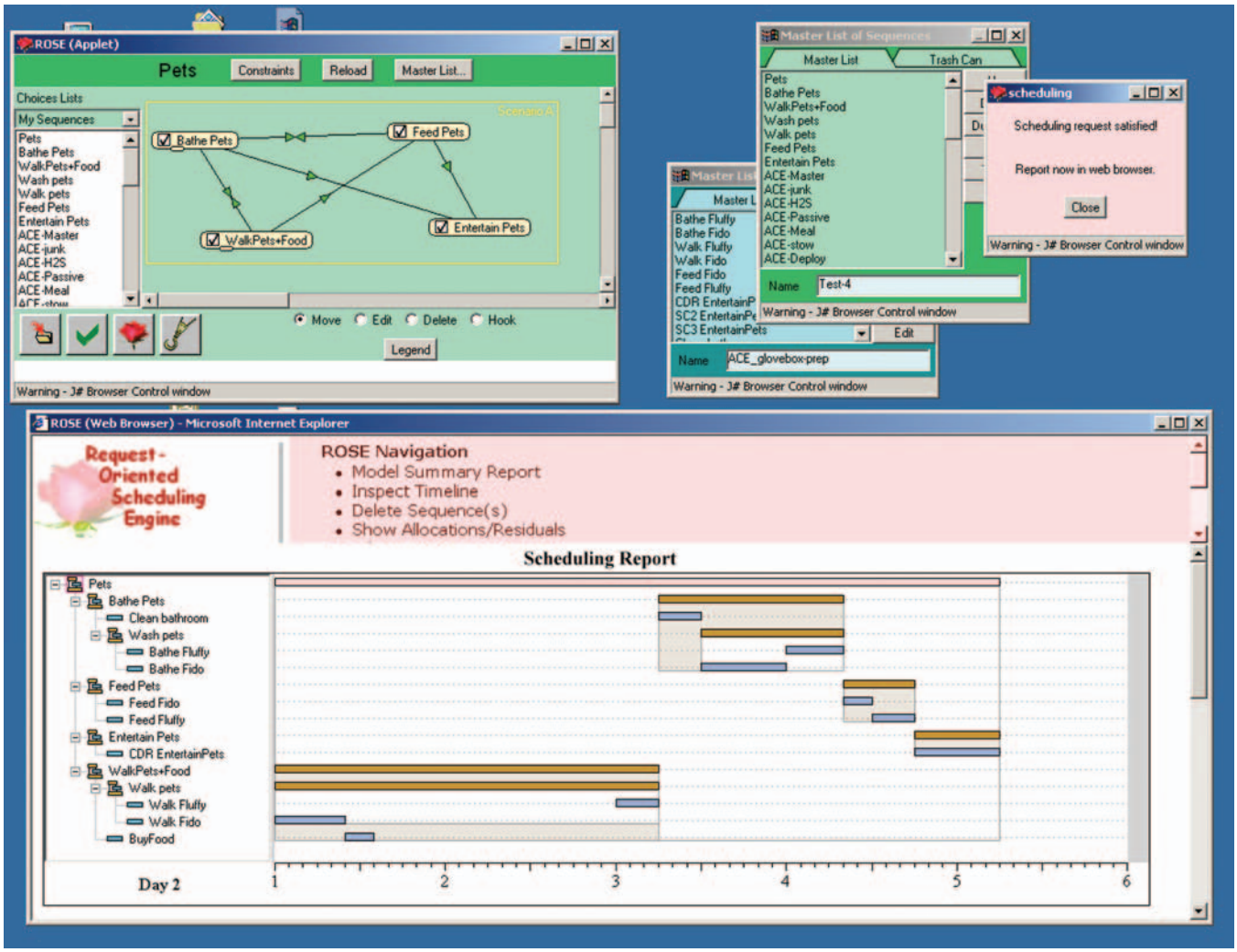

Figure 4. Screen capture from the Nexus (ROSE) demonstration.

Publications and Patent Applications

Significant publications about ROSE are as follows:

- A paper entitled "Modeling Complex Operations Sequences" was presented to the ISOMA 2002, 8th International Symposium on Manufacturing and Applications, June 9–13, 2002. Dr. John M. Usher, Mississippi State University and John Jaap coauthored this paper. The following is an abstract of this paper.

  ### Abstract

  This paper presents a modeling tool that is a part of the ROSE system being designed at NASA for the scheduling of payload space activities on board the *ISS*. The resident modeler provides a robust method for easily representing complex sequences of activities for use in planning and scheduling activities. Although directed toward space activity scheduling, the paper addresses other application areas for this technology.

- A paper entitled "Maximally Expressive Modeling of Operations Tasks" was presented to the 2003 IEEE Aerospace Conference, March 8–15, 2003. Members of the research team coauthored this paper. The following is an abstract of this paper.

  ### Abstract

  Planning and scheduling systems organize tasks into a timeline or schedule. The tasks are defined within the scheduling system in logical containers called models. The dictionary might define a model of this type as a system of things and relations satisfying a set of rules that, when applied to the things and relations, produce certainty about the tasks that are being modeled. One challenging domain for a planning and scheduling system is the operation of on-board experiment activities for the *ISS*. In these experiments, the equipment used is among the most complex hardware ever developed, the information sought is at the cutting edge of scientific endeavor, and the procedures are intricate and exacting. Scheduling is

made more difficult by a scarcity of *ISS* resources. The models to be fed into the scheduler must describe both the complexity of the experiments and procedures (to ensure a valid schedule) and the flexibilities of the procedures and the equipment (to effectively utilize available resources). Clearly, scheduling *ISS* experiment operations calls for a maximally expressive modeling schema.

- A paper entitled "An Enabling Technology for New Planning and Scheduling Paradigms" will be presented to the 8th International Conference on Space Operations, May 17–21, 2004. John Jaap, Elizabeth Davis, and Patrick Meyer coauthored this paper. The following is an abstract of this paper.

  Abstract
  The Flight Projects Directorate at NASA MSFC is developing a new planning and scheduling environment and a new scheduling algorithm to enable a paradigm shift in planning and scheduling concepts. The current paradigm starts by collecting the requirements, called task models, from the scientists and technologists for the tasks that are to be scheduled. Next, a cadre with knowledge of vehicle and hardware systems modifies these models to encompass and be compatible with the hardware model. Finally, the models are modified to be compatible with the scheduling engine. A future paradigm would provide a scheduling engine that accepts separate science models and hardware models. The modeling schema would have the capability to represent all the requirements without resorting to notes. Furthermore, the scheduling engine would not require that the models be modified to account for the capabilities (limitations) of the scheduling engine.

- A paper entitled "Maximally Expressive Modeling" has been submitted to the 4th International Workshop on Planning and Scheduling for Space, June 23–25, 2004. Members of the research team coauthored this paper.

- A presentation describing a ROSE-based operations concept for *ISS* operations was presented to the Payloads Operations Concept Architecture Assessment Study team, chartered by Headquarters to evaluate the current operations processes for *ISS* payloads.

ROSE was presented to the MSFC center staff in August 2003. The papers and selected presentations are online at http://nexus.msfc.nasa.gov/publications.

Funding Summary

Table 1 identifies the funding summary for fiscal year (FY) 2002 and FY 2003.

Table 1. Funding summary for FY 2002 and FY 2003.

	Funding ($)
Requested	10,000
Expended	9,000
Not used	1,000

Status of Investigation

This CDDF project is complete.

Wireless Services in the Space Flight Operations Services Grid Prototype

Project Number: 02–17

Investigator: Robert Bradford/FD40

Introduction

This Center Director's Discretionary Fund (CDDF) project was initially defined as a study of the effectiveness of applying wireless technology to Marshall Space Flight Center (MSFC) test area activities using existing Payload Operations integration Center (POIC) based services like the Telescience Resource Kit (TReK) and the Internet Voice Distribution System (IVoDS) to reduce test area setup and operational costs. The wireless aspect was twofold: To implement wireless local area network (LAN) technology up to 11 Mb and to demonstrate the feasibility of using TReK and IVoDS over wireless technologies in the test area itself. The initial project focus was changed due to the fast wireless technology evolution and the installation of wireless technologies in the test area during the latter half of the first year of the CDDF project. This change is embodied in the development and ongoing implementation of a Space Flight Operations Services Grid (SOSG) prototype to no longer attempt to present test area telemetry and video to wireless devices like handheld computers, personal digital assistants (PDAs), and cell phones but present payload science telemetry and video (in this case) to *International Space Station* (*ISS*) principal investigators (PIs). This change is using wireless technologies listed above in the larger study of applying Grid technologies to spaceflight operations at remote end user and control center operational locations. This study is in the form of a collaborative effort between MSFC's Flight Projects Directorate (FPD), Ground Systems Department, Johnson Space Center's (JSC's) Mission Operations Directorate (MOD), Operations Research and Strategic Development Branch, and Ames Research Center's (ARC's) NASA Advanced Supercomputing (NAS) Division Grid Team to apply Grid technologies to specific end-user services (telemetry, commanding, voice, and video) used by the POIC to conduct space flight science operations. Also included are new services like data mining and new collaborative tools. This effort is being led by MSFC. An initial non-Grid enabled prototype is being developed that is scheduled to be ready around July 2004 with a final Grid enabled prototype scheduled for March 2005. Once the space flight operational services that are not in support of actual space flight operations are in place, wireless technologies will be used to display telemetry, provide commanding, and be able to converse with centralized operational facilities personnel. Enabling telemetry, voice, and video to wireless devices is a goal of the SOSG. Most of the CDDF project resources were expended in fiscal year (FY) 2003 to acquire platforms and software to enable the distribution of services to wireless devices. Acquisition of a 1-year wireless service in support of the SOSG will be made in the last quarter of FY 2004 in support of the initial July 2004 SOSG prototype.

The following is a description of the SOSG, the services to be provided, and Grid technologies to be used and/or developed. With the exception of this section, this report is the SOSG paper to be presented at SpaceOps 2004 in May 2004.

It is strongly noted that the services described in this report are being developed as a demonstration of Grid technologies and the services are not to actually support mission operations.

Background

NASA organizationally supports many types of space-based operations using many types of applications from five different locations. These five locations are JSC for Shuttle and *ISS* vehicle operations, Kennedy Space Center (KSC) for launch operations and MSFC *ISS* payload operations all in support of manned flight, Jet Propulsion Laboratory (JPL) for deep space projects, and Goddard Space Flight Center (GSFC) for free-flying satellites. These delineations evolved early in NASA's creation and still exist today. Because of early technologies and operational concepts, most services in support of NASA missions were developed in a stovepipe fashion specifically for an individual mission. Networks were nonexistent. Communications were provided by point-to-point circuits at very low speeds. Personal computers were nonexistent. Computing was expensive and primitive. Data storage was cumbersome and also expensive. Since NASA's support of space flight mission operations, computing technology, and concepts, communications in the form of networking and data storage and archiving have evolved to the point where application of advanced concepts to space flight operations and other nonflight operations activities is necessary. NASA has implemented information technologies such as client/server, Web, and higher bandwidth circuitry but at the same time has become a follower in technology use and implementation. NASA's networks are still virtually point-to-point circuits of moderate speeds. NASA has not been the leader of technology provisioning that it used to be; instead, it seems to shy away from advanced technologies.

Approach

Statement of Problem

Over the years, NASA has developed many types of technologies and conducted various types of science resulting in numerous variations of operations, data, and applications.

For example, operations range from deep space projects managed by JPL, Saturn and Shuttle operations managed from JSC and KSC, *ISS* science operations managed from MSFC, and numerous low-Earth-orbit satellites managed from GSFC that are varied and intrinsically different but require many of the same types of services to fulfill their missions. Also, large data sets (databases) of Shuttle flight data, solar system projects, and Earth observing data exist that, because of their varied and sometimes outdated technologies, are not and have not been fully examined for additional information and knowledge. Many of the applications/systems supporting operational services such as voice, video, telemetry, and commanding are outdated and obsolete. The vast amounts of data are located in various formats, at various locations, and range over many years. The ability to conduct unified space operations, access disparate data sets, and to develop systems and services that can provide operational services does not currently exist in any useful form. In addition, adding new services to existing operations is generally expensive and, with the current budget constraints, are not feasible on any broad level of implementation.

The Space Flight User-Based Services are those services required to conduct space flight operations. Network Services are crucial to any type of remedy and are evolving adequately to support any technology currently in development and will be briefly discussed. Grid services are those Grid services that will be used to overcome, through middleware software, some or all the problems that currently exist. The following discussions are presented to provide a better understanding of each of these service.

Space Flight User-Based Services: These services enable Space and Ground operations to occur. The existing services are voice, video, telemetry management, and command management. The importance of each of these, with the exception of telemetry and command management, depends on the mission being supported. Manned flight is much more dependent on voice communications than is free-flying satellite operations. These four base services are currently provided by many disparate systems and applications. For NASA to support the new Mars Initiative, new services must be integrated into the mix of services. New services include Web-based measurement delivery and video distribution, high-performance processing (i.e., access to supercomputing services), data mining, visualization, collaborative tools for development, operations, and subsequent science and discipline-specific application sharing. These services do not interact well, if at all. Replacement of services is not currently considered feasible on a wide basis such as making services like command management available to some current and all future projects and programs from a single source.

Network Services: Networks have evolved over the last decade to the point that effective throughput has enabled Grid technologies to emerge and evolve. Once network technology evolved beyond the T1 (1.544 Mbps), Grid type technologies were possible, although initially limited. With the emergence of Dense Wave Division Multiplexing (DWDM), data transfer rates are very adequate to support space flight operations. Figure 1 depicts the network connectivity to be in support of the SOSG.

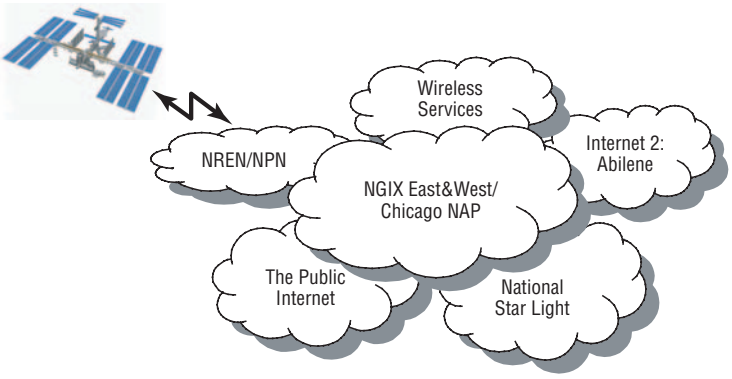

Figure 1. Existing network connectivity in support of the SOSG.

Grid Services: Grid services will provide the middleware services required to deliver current and new services to the user. In this case, the user can be a flight controller at JSC, an *ISS* payload PI or a flight/payload vehicle engineer. Grid technologies embody the services that bring together disparate applications, services, data, and operations. Some core grid services include resource location, security both machine-to-machine and user, high-speed file transfer, Brokering Service, Naturalization Service, Execution Service, Event Monitoring Service, and Information Service.

In the Grid model depicted in figure 2 the three components are comprised of: Resources that are services listed in table 1, the Network as depicted in figure 1, and the development of the Grid middleware required to enable Grid services along with ancillary services like portal and portlet development. A portlet is a server component that controls a small, user-configured window in a pane on the user's Web browser.[1] Several Grid services specific to the implementation of the SOSG are required. They are systems performance and measurement, profile database and virtual organization manager, network services, streaming management service stream binding service, and an SOSG application launcher. Figure 3 presents the Grid model in greater detail.

Hypothesis

Given the evolution in network technology and current state of Grid technologies, a Grid implementation of the services previously described, embodied in an SOSG prototype, will demonstrate the feasibility of applying Grid technology to space flight operations. Further, that Grid technologies will:

- Enable collaboration between scientists, engineering, and operations that will enhance their respective disciplines in ways not visualized today.
- Provide new services to many projects/programs/disciplines that are not feasible when applied to an individual requirement.

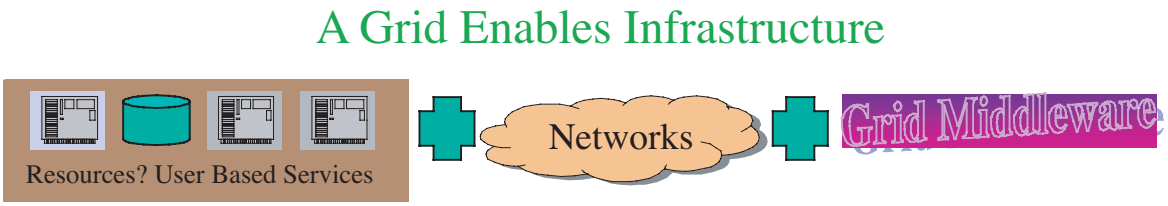

Figure 2. The Grid model.

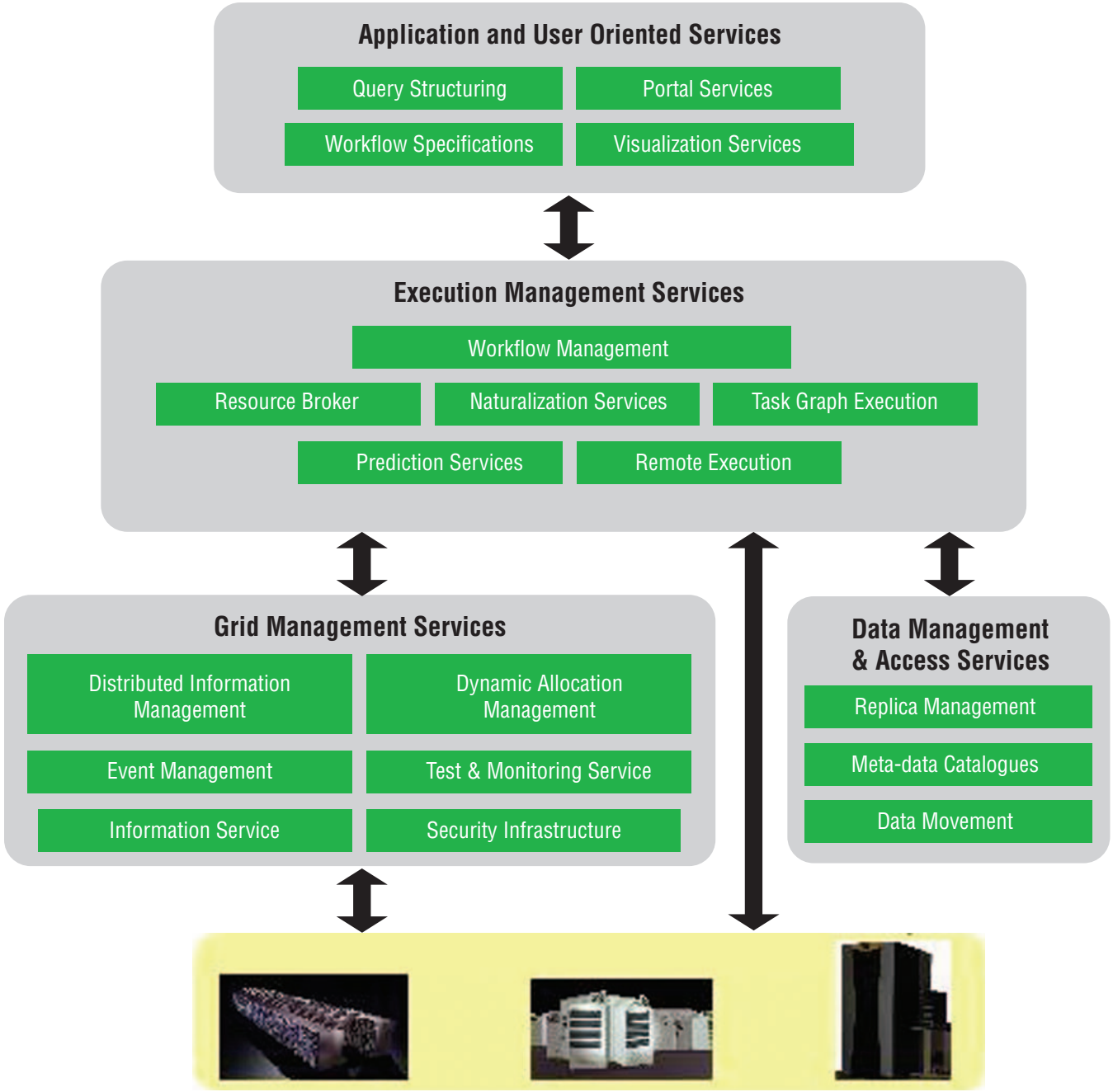

Figure 3. The Grid model in greater detail.

Table 1. Services list,

User Based Service	Base System/Status	Definition
Data/telemetry management	TReK/operational	Provide TReK telemetry management services
Experiment/system CMD management	TReK/operational	Provide TReK command management services
ISS DL video distribution	GViDS/in development	Provide varying bandwidth rates to all virtual organizations (Vos), sense native network and adjust rate
Web measure delivery with wireless services	TReK/EZStream/ operational	Provide individual measurements over the Web and to wireless devices
High-performance processing	ARC/information power grid (IPG)/operational	Access massively parallel and other processing cycles in real and near real-time
Data mining	University of Alabama in Huntsville (UAH) data mining/ operational	Analyze and combine new and archived data to find new information and knowledge
High-volume network storage	UAH NW storage/ operational	Use massive storage capabilities thru the Web securely
Mission voice	IVoDS/operational	Access the mission voice loops provided by IVoDS
Collaborative Internet voice	CVoDS/in development	Upgrade to IVoDS to provide application sharing, IM, video teleconferencing, and mission voice
Video auditorium	Video auditorium/in testing	A new approach to video teleconferencing still in development
Application sharing (example)	Caution and warning/ currently being Web enabled	Ability for a user to plug in discipline specific applications under the Grid services umbrella
System performance and measurement	TBD	For the prototype and beyond measure network and application performance
Networks connectivity	NREN/Abilene/ operational	All network connectivity from the prototype to the users
Network service	TBD	

- Generate new information and knowledge from the disparate data located throughout the Agency.

It is anticipated that by applying Grid technologies to NASA systems, applications, and data, Grid technologies will make current systems/applications supporting space flight activities more efficient, reduce development costs for future space flight system replacements and upgrades, and enable interdiscipline science collaboration creating new information and knowledge with significant cost savings. In addition, collaboration (more effective communications) between various NASA organizations, programs, and projects will occur.

Solution

Begin the Solution by Creating a Grid Prototype for Demonstration Purposes: This prototype will consist of all the end-user services listed in table 1, Grid enable them where feasible based on Grid technologies; and, where Grid technologies are not feasible, base the end-user services implementation on Web-based technologies. This will be accomplished through a collaborative effort between several NASA centers, academia, and industry.

The premise associated with a prototype is that the services supporting *ISS* payload operations are operational at the POIC located at MSFC, Huntsville, AL. These services will be either

replicated or provide streams from the operational systems (video and telemetry) for the prototype in a quasi-operational mode. However, there are no operational services supporting any mission related activities with this prototype. New services that are currently not provided by the POIC are being generated by other systems currently under development. These systems are depicted by other than operational status. Table 1 identifies the service, followed by the service/application system provider/status, and a brief description of the service. As shown, most services are ready for Grid enabling.

Use Case Description: What follows is a visionary description of a remote PI using the SOSG to conduct science from his/her experiments that are running on the *ISS*.

A PI has an experiment that has been accepted for flight on the *ISS*. The first thing this PI does is to register using the SOSG registration portlet. At this point, the PI has created an account within the SOSG environment. After registration, the PI's portal environment will be set such that the PI now has access to the following services:

- Registration Service Portlet.
- New Service Request Portlet.
- Certificate Request Service Portlet.
- Information Service Portlet.

Each of these will be presented in individual portlets from within the overall SOSG portal.

After initial registration set up, the PI will need to request an SOSG user certificate via the request certificate portlet. This certificate will be an X.509 certificate and will be issued by the NASA IPG's Certificate authority. This certificate will allow the PI to have single sign-on access to all accessable resources and applications while using the SOSG services. After receiving the certificate, the PI will now be able to construct the portal interface to provide access to the applications needed to conduct his science.

Let's assume this PI has been authorized to use a telemetry processing service such as TReK and has an allocation on the High-Performance Computers (HPC) at the NASA Advanced Supercomputer Center. The PI will use the portal customization screen to organize applications. From a pulldown menu, the PI selects TReK and HPC. By doing this, several additional portlets are added in addition to the two selected. This is due to dependencies that are prearranged. By selecting HPC, a portlet for access to the IPG resource broker is available, as well as a portlet for the IPG execution manager. In addition, data mining tools are provided. By selecting TReK, additional portlets will be available. The PI can then place the portlets in a configuration that is acceptable, then save the state so that he can now log out and log back in and his environment will be reestablished, this is called the PI's Grid Context.[1]

To begin using these applications, the PI would use TReK as normal, except he would be using the interfaces provided by the portal. Let's assume that he is monitoring a few parameters for off-nominal conditions, and that this condition is met. The PI can then take these parameters and drag them from the TReK portlet into the job creation window where a Grid job is created based on some preconfigured data the PI added, such as the code set to be run, the input parameters, etc. After dragging the data to the job creation window, the PI can now launch a data-mining job to locate any previous results that shared similar conditions. He can also fire off a simulation that uses these off-nominal parameters to predict possible evolutions of the experiment if the *ISS* environment is not corrected, etc. It is desirable that the previous actions be scriptable so that the PI does not need to be monitoring the portal. In addition to the core applications that the PI uses, he also has the ability to display various environmental data in graphical form within his portal. For example, he can have a portlet that represents the power production of the *ISS* solar panels, the current job load of the NAS computation grid, live video of his experiment on the *ISS*, and a list of other associates that are currently working on experiment data.

Let's assume that after the data mining and simulation are completed some interesting results are produced. The PI is now able to use chatting and video services to collaborate with his associates within his virtual organization (VO) on the results. A VO is a group of like-minded predetermined participants (e.g., a specific science discipline).

Finally, after all the collaboration and excitement is completed, the PI is preparing to exit the portal when he is prompted to enter some metadata about the data and results that were just collected and analyzed. Upon completion, all the data products that were created, the recipe for creating them, and the metadata the PI entered is stored into the SOSG data archives so that others within the VO can search it, and, in the future, this data will be available for other science and public use.

The Space Flight Operations Services Grid Architecture: Figure 4 shows a conceptual diagram that represents the services-based model that will be used to support the SOSG prototype. Through various mechanisms, (e.g., portals, user written applications, command line programs, etc.), a user will have access to various capabilities instantiated as Grid Web services. Through these services, users will have a consistent access to various resources as well as capabilities that can easily be reused or stitched together to form larger complex applications that bring to bear multiple capabilities for a particular purpose.

The overall architecture for the SOSG consists of two elements: A portal architecture for presentation, administration, and access to SOSG services; and a services architecture for creation of, and access to, SOSG services. These are described in more detail below.

The Space Flight Operations Services Grid Portal: The vision for the SOSG portal is for it to be the single interface that brings together all the SOSG applications for the benefit

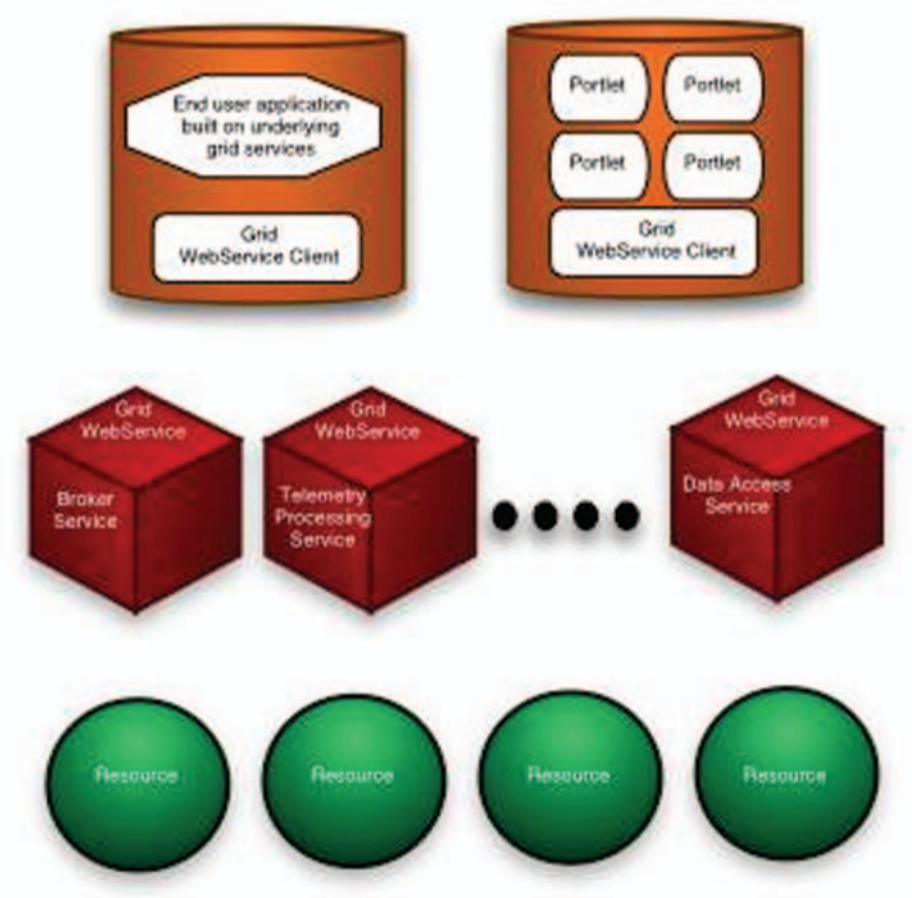

Figure 4. The SOSG services-based architecture concept diagram.

of the users of the four VOs that the SOSG will be supporting. It is the vision that this portal will be a captured portal where users are able to access all tools and services needed to conduct science research setup based on the user's profile. The portal provides this access in a secure controlled fashion. For this to be true, all applications and/or services must be Grid enabled Web services.

The SOSG portal effort we will be adopting is the Global Grid Forum (GGF) recommended portal architecture, which is based on the idea that the portal server is the container for user-facing Grid service clients that are designed according to the portlet model specified in the JAVA standards document, JSR168 Portlet Specification: http://jcp.org/aboutJava/communityprocess/review/jsr168/.

Space Flight Operations Services Grid Services Architecture: One of the goals of the SOSG is to eventually provide a consistent interface to several applications that are part of the NASA MSFC POIC. A consistent and standard interface will allow for general reuse of common software, easier access to multiple services, and the ability to easily link several services together to create a new more intelligent or capable service.

To accomplish this, the SOSG team has decided to adopt the standards from the W3C and GGF as the guiding standards for the construction of SOSG services. For the SOSG, there will be two types of services; (1) Basic SOSG Grid Service (BGS) and (2) Enhanced SOSG Grid Service (EGS). In short, the BGS will primarily be a Web service based on the W3C standards, but will incorporate a GSI-Enables WS_SECURITY library that supports Grid authentication and authorization. An EGC will be a fully compliant Open Grid Services Architecture (OGSA) Grid Service. The reason to have the basic option is to provide an alternative for those applications that do not require the OGSA extensions such as statefullness, stateful interactions, transient instances, lifetime management, etc.[2] Figure 5 represents a layered architecture for both the SOSG BGS and EGS.

This architecture relies on the following enabling technologies to accomplish the objectives:

- **Grid Infrastructure Toolkits**
  The Globus Toolkit® is a set of fundamental technologies needed to build computational and data grids; persistent environments that enable software applications to integrate instruments, displays, computational, and information resources that are managed by diverse organizations in widespread locations. The toolkit consists of a set of core services that can be used independently or together to develop useful Grid applications and programming tools. These include services for job management, data movement, resource information, and security.[3]

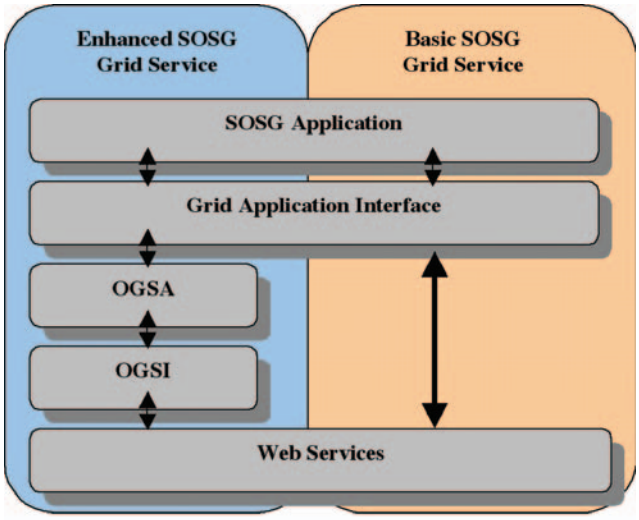

Figure 5. SOSG layered approach to Grid services.

- **Web Services**
  The advent of Extensible Markup Language (XML) makes it easier for systems in different environments to exchange information. The universality of XML makes it a very attractive way to communicate information between programs. Programmers can use different operating systems, programming languages, etc., and have their software communicate with each other in an interoperable manner. Moreover, XML, XML namespaces, and XML schemas provide useful mechanisms to deal with structured extensibility in a distributed environment.

  Similar programmatic interfaces to the ones available since the early days of the Web via HTML forms, programs are now accessible by exchanging XML data through an interface, e.g., by using SOAP Version 1.2, the XML-based messaging framework produced by the XML Protocol Working Group.

  The power of Web services, in addition to their great interoperability and extensibility thanks to the use of XML,[4,5] is that they can then be combined in a loosely coupled way in order to achieve complex operations. Programs providing simple services can interact with each other in order to deliver sophisticated added-value services (http://www.w3.org/2002/ws/Activity).

- **Open Grid Services Architecture**
  The OGSA integrates key Grid technologies (including the Globus Toolkit®) with Web services mechanisms to create a distributed system framework based on the OGSI.[6] A Grid service instance is a potentially transient service that conforms to a set of conventions, expressed as Web Service Definition Language (WSDL) interfaces, extensions, and behaviors, for such purposes as lifetime management, discovery of characteristics, and notification. Grid services provide for the controlled management of the distributed and often long-lived state that is commonly required in sophisticated distributed applications. OGSI also introduces standard factory and registration interfaces for creating and discovering Grid services. It should be noted that OGSI and Web services standards are being combined into a new set of standards, the WS-Notification and the WS-Resource Framework that was announced in January 2004.

- **Security**
  Security for these services through Grid technology has and is being designed into the technology. This is unlike the Internet/Web technologies that were developed without security in mind. Grid security is maintained on several levels. Grid enabling services provides for local security policy management (without affecting local security), and provides strong encryption and authentication for access and networking. Grid security is a significant focus of the Grid standards development effort of the Global Grid Forum.[7]

Space Flight Operations Services Grid User Base: Once the Prototype User-Based services are created and Grid/Web enabled, four virtual organizations will be initiated with the objective that users identified with each VO will use and assess the services. The four VOs are as follows:

- Payload Control Center Operations (PCCO).
- Payload Science Operations (PSO).
- Flight Control Center Operations (FCCO).
- Educational Outreach (EO).

For each VO, a user base will be selected from the following:

- The POIC for PCCO.
- For the PSO, several university based PIs who either are flying or have flown experiments on *ISS*.
- For the FCCO, the JSC Mission Control Center.
- For the EO, a select set of schools already organized under one of several NASA sponsored educational programs will be recruited.

Specific services will be assigned for each VO, as indicated in table 2. These services are required for each VO to function. Although collaboration is not a VO, the user-based services to be provided by the SOSG will enable significant collaboration between disparate NASA user communities.

Once the user-based services are Grid enabled, the Grid services identified in SOSG Portal paragraphs are functional and the VOs are organized for parallel use by the four VOs. A written questionnaire with a follow up interview process will be initiated to determine usefulness, technical and cost feasibility, and other applicability factors for each user-based service. With this user-generated data, the insight of our hands-on implementation of the SOSG prototype, and an appropriate peer review, a set of recommendations will be made concerning the efficacy of the application of Grid technologies to space operations and possibly NASA ground activities.

Table 2. Virtual organization predominate service summary.

	Service	PCCO	PCO	FCCO	EO
1	Data/telemetry management	X	X	X	
2	Experiment/system CMD managment	X			
3	*ISS* DL video distribution	X	X	X	X
4	Web measure delivery	X	X	X	X
5	High performance processing	X	X	X	
6	Data mining	X	X	X	
7	High volume network storage	X	X	X	X
8	Mission voice	X	X	X	
9	Collaborative Internet voice		X		
10	Video auditorium	X	X	X	X
11	Application sharing		X		X
12	System performance and measurement	X		X	
13	Networks connectivity	X	X	X	X

Accomplishments

By fall 2004, provide a demonstration of wireless telemetry and video service to handheld computers, PDAs, and/or cell phones.

Planned Future Work

If wireless and Grid services are considered feasible, then we will move to acquire funding to apply them to various programs and functions.

Publications and Patent Applications

"Spaceflight Operations Services Grid Prototype," The 55th International Astronautical Congress, Vancouver, Canada, October 2004.

"Spaceflight Operations Services Grid Prototype," SpaceOps, May 2004.

No patents are anticipated.

Funding Summary

Hardware/Software $39,235.

Status of Investigation

Prototype wireless services are scheduled to be operational by July 2004 within the SOSG Prototype development effort.

References

[1] Gannon, D.: "Grid Portals: A Scientist's Access Point for Grid Services (DRAFT)," M.P.G. Fox, B. Plale, G. von Laszewski, et al. (eds.), *Global Grid Forum Standards Document*, 2003.

[2] Parastatidis, S. "Web and Grid Services: Architectures and Technologies," http://savas.parastatidis.name.

[3] The Globus Project, The Globus Alliance. http://www.globus.org.

[4] Fallside, D,: "XML Schema Part 0: Primer," World Wide Web Consortium Draft, September, 2000. http://archive.dstc.edu.au/mpeg7-ddl/latest_primer.html

[5] Hoheisel, A.; and Der, U. "An XML-Based Framework for Loosely Coupled Applications on Grid Environments," *Lecture Notes on Computer Science*, in preparation, 2003.

[6] Tuecke, S.; Czajkowski, K.; Foster, I.; et al.: "Open Grid Services Infrastructure Version 1.0," The Global Grid Forum, June 27, 2003.

[7] Foster, I.; Kesselman, C.; Tsudik, G.; and Tuecke, S.: "A Security Architecture for Computational Grids," presented at 5th ACM Conference on Computer and Communications Security, 1998.

Process Gas Decontamination Using a Metallic, Ultrashort Channel-Length Monolithic Catalyst Substrate

Project Number: 02–18

Investigators: Jay L. Perry/FD21
J.D. Tatara/QUALIS

Purpose

The purpose of this Center Director's Discretionary Fund (CDDF) project is to demonstrate the integration of a thermal catalytic reactor that uses an ultrashort channel-length monolithic (USCM) catalyst substrate with a recuperative heat exchanger to characterize its performance under variable process conditions, namely process air flow. Primary project objectives are the following:

- Evaluate resource requirements under varying process flow conditions.
- Evaluate process performance on a variety of contaminants under varying process flow conditions.
- Evaluate the USCM's economics when incorporated in niche applications.
- Provide data necessary to serve as a basis for process scale-up.

Secondary objectives to be addressed as a matter of course during the project's conduct are the following:

- Demonstrate the physical integration of the USCM with an *International Space Station* (*ISS*) Trace Contaminant Control Subassembly (TCCS) flight-like recuperative heat exchanger.
- Determine the duration of the thermal transient experienced by the integrated test article/heat exchanger assembly at varying process airflow rate conditions and electrical power inputs.
- Determine the lag between the time electrical power is applied to the test article and the time that oxidation reaction light off occurs.
- Characterize the test article's steady-state electrical power requirements under low-, moderate-, and high-process airflow conditions.

Background

Contaminated process gases, whether in a crewed spacecraft cabin atmosphere, the working volume of a microgravity science or ground-based laboratory experiment facility, or the exhaust from an automobile, are pervasive problems that can have effects on human health, performance, and well-being. The need for highly effective, economical decontamination processes spans a wide range of terrestrial and space flight applications. Typically, gas decontamination processes rely upon adsorption and absorption processes with most industrial-packed bed adsorption processes using activated carbon. Once saturated, the carbon is either dumped or regenerated. In either case, the dumped carbon and concentrated waste streams constitute a hazardous waste that must be handled safely with minimal environmental impact. Thermal catalytic systems are moving to the forefront of cleaner gas decontamination processes. By tailoring the reactor and catalyst design, more complete contaminant destruction is achieved, leading to reduced waste handling, process downtime, and maintenance.

Trade assessments of candidate gas decontamination technologies have demonstrated that a unique reactor design based upon an USCM substrate provides the solution for improving process economics and performance of thermal catalytic oxidation processes. The USCM substrate may expand the use of thermal catalytic oxidation to a wider range of space flight and terrestrial applications. The basic USCM technology, developed by Precision Combustion, Inc. (PCI) of North Haven, CT and adapted to space flight applications under NASA Marshall Space Flight Center (MSFC) guidance, uses a series of short-channel-length, high-cell-density monoliths to provide a high catalytic conversion efficiency while minimizing boundary layer buildup and reactor size.

Technology Description and Applications

The USCM thermal catalytic reactor technology developed by PCI is based upon an innovative reactor design approach that effectively employs the use of a static mixer as the catalyst substrate. Coating catalysts on a static mixer has been the focus of several notable projects outside of NASA; however, none of these efforts have specifically addressed nonindustrial applications. The USCM thermal catalytic reactor technology addresses the unique requirements of portable gas and process exhaust conditioning for the automotive industry. Many of these requirements apply to space transportation.

The USCM thermal catalytic oxidizer (fig. 1) is composed of structured substrate consisting of a series of high-cell-density, ultrashort-channel-length metal monoliths. The catalyst is applied to the substrate via a specialized coating process that resists spalling. The reactor design will improve both process economics and performance since the series of ultrashort-channel monoliths provide a significant reduction in boundary layer buildup that occurs in conventional monolithic substrates. Figure 2 illustrates a comparison of the boundary layer buildup of the USCM-based reactor with that of a conventional ceramic monolith. Table 1 compares performance characteristics to

conventional monolithic and pellet substrates. As can be seen, the USCM technology provides a significantly improved mass transfer performance, and thermal mass is also reduced. This may lead to smaller, less power-intensive reactors for an expanded suite of space flight applications.[1,2]

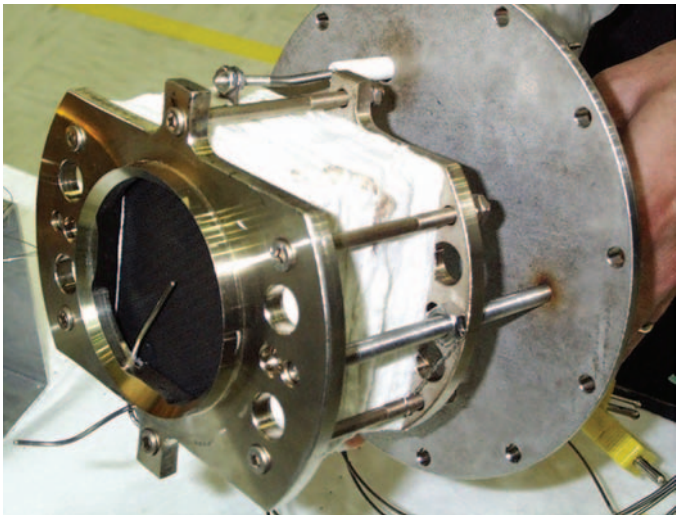

Figure 1. Prototype USCM reactor.

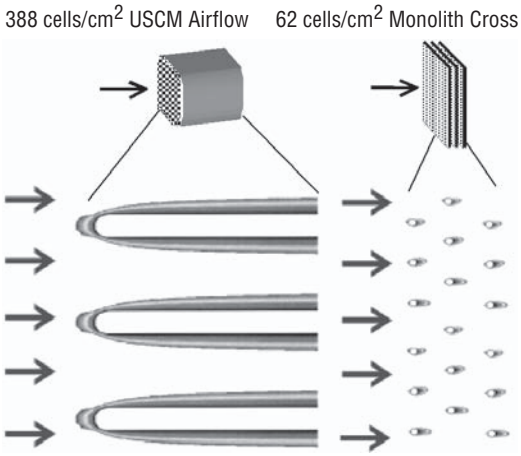

Figure 2. Comparison of boundary layer buildup in monolithic substrates.

Table 1. Catalyst substrate physical properties.

Property	Substrate		
	USCM	Pellet	Monolith
Cell density (cpsc)	388	n/a	62
Void fraction	0.62	0.4	0.65
Surface area (cm^2/cm^3)	62	11	19
Mass transfer coefficient. (cm/s)†	68	19	6.7
Heat transfer coefficient. (W/m^2K)†	640	120	51

†350 °C air at 3.1 m/s: Mass transfer based on propylene diffusion in air.

Potential space flight applications include cabin air quality control and payload process gas purification. Adsorption processes that rely upon expendable resources dominate both applications. While adsorption is a proven process for cleaning process gases, the expendable materials used possess high operating costs associated with ground processing and Earth-to-orbit transportation. Eliminating or reducing the reliance upon adsorption in these applications will lead to improved operating costs and operational flexibility.

In order to fully understand the benefits of a USCM substrate, it is necessary to integrate it with a highly efficient recuperative heat exchanger and operate the integrated assembly under a range of electrical power and process airflow conditions that bound the potential space flight applications. This project will allow the USCM's performance characteristics under a variety of process flow and contaminant loading conditions to be observed and evaluated against the performance of present and future gas purification processes.

Approach

A small-scale thermal catalytic reactor based upon the USCM substrate was integrated into a test stand that provides varying process gas flow and contaminant loading conditions. The experiment is based upon a fractional factorial design that allows for the use of robust design techniques during future scale-up. Data were collected on electrical power input, thermal transient duration, and pressure drop at the varying process flow conditions. Chemical contaminants representative of the various niche applications for the technology were injected into the process gas stream. Contaminant oxidation efficiency was monitored based upon the carbon dioxide concentration difference between the reactor inlet and outlet. Data were analyzed for comparison of the USCM-based system to existing technologies in use by NASA for gas decontamination onboard the *ISS* as well as for a design basis for future applications in payload gas purification and spacecraft cabin air quality control for future crewed space exploration initiatives.

Accomplishments

During this 2-year project, all proposed tasks were completed. The first year was the development and implementation of the detailed project plan, test stand setup and checkout, experimental run definition, and test article integration and checkout. Early experimental runs began during the first year and extended through the first half of the second year of the project. All of the experimental runs were completed by January 2003. At the conclusion of the test runs, some additional runs were conducted to gather duplicate data where needed. In March 2003, the test article entered a period of endurance testing. The endurance testing was designed to demonstrate the long-term performance. At the official conclusion of the project, on September 30, 2003, the test article had accumulated approximately 6 months of continuous operation. Although the project support expired at that time, it was decided to continue the endurance testing because the full cost of operations was found to be an extremely minor

component of the overall test facility operational overhead. As of March 1, 2004, approximately 11 months of continuous operations have been accumulated. Test article performance has remained steady throughout the endurance testing. Specific details concerning the project's accomplishments are summarized by the following discussion.

Test Stand Setup

The USCM catalytic reactor test article shown by figure 1 was integrated into the existing regenerative life support equipment (RLSE) test stand thermal catalytic oxidizer (TCO) assembly. Figure 3 shows the TCO assembly before the USCM catalytic reactor was installed. The USCM catalytic reactor assembly was inserted inside the large opening and then bolted into place. The USCM catalytic reactor test article is comprised of a catalyst/heater element assembly, a support structure, an interface adapter, and an end-plate adapter containing instrumentation feed throughs. Electrical wiring and instrumentation wiring are also a part of the assembly. Instrumentation is in the form of thermocouples mounted at the inlet and outlet of the catalyst/heater element subassembly. Figure 4 shows the TCO assembly containing the USCM catalytic reactor installed in the test stand.

Experimental Run Challenge Selection

A review of the potential niche applications for the USCM catalytic reactor defined the test runs necessary to characterize its performance and best meet the project objectives. An injection system was built with the capability to introduce both liquid and gaseous chemical challenges into the process gas stream just upstream of the USCM catalytic reactor. Table 2 summarizes the chemical challenges selected. The injection rate used was designed to produce a minimum 100 ± 10-ppm_v concentration at the TCO assembly inlet.

Figure 3. RLSE test stand TCO with catalyst bed removed.

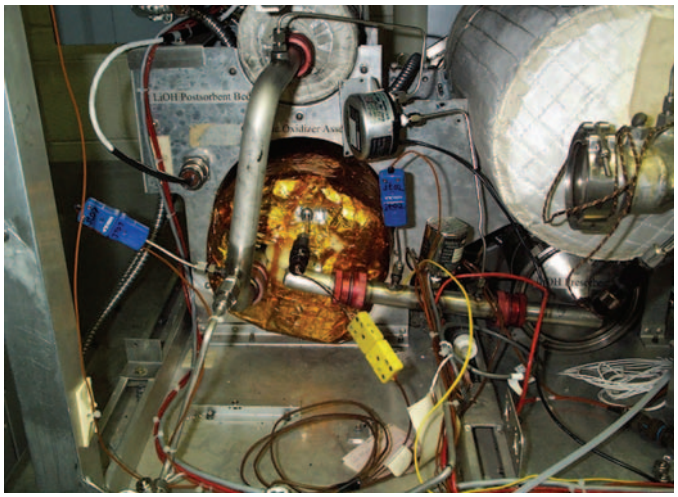

Figure 4. TCO assembly containing the USCM catalytic reactor installed in test stand.

Table 2. USCM catalytic reactor contaminant challenge.

Compound	Molecular Weight (g/mole)	Inlet Concentration (mg/m^3)	Injection Rate (mg/h)
Light alcohol*	60.09**	246**	1,451***
Butanol	74.12	303	1,788
Acetone	58.08	238	1,404
Toluene	92.15	377	2,224
Methane	16.04	66	389
2-ethoxyethanol	90.12	369	2,177
Octafluoropropane	188.02	769	4,537
Sulfur hexafluoride	146.05	597	3,522

*Methanol, ethanol, or isopropanol
**As isopropanol
***At maximum USCM reactor flow condition of 5.9 m^3/h

Experimental Results

Experimental runs covered five process-airflow and four power-supply conditions. All contaminant oxidation challenge runs and thermal transient runs were completed by January 2003. A total of 20 experimental runs were conducted for each challenge chemical listed in table 2. In addition, 20 experimental runs were conducted to investigate the thermal transient duration at the 20 process airflow and power supply conditions. Test run data were reduced and subjected to engineering analysis.

A composite evaluation of reactor performance found that nonmethane volatile organic compound (VOC) oxidation reaction light off occurs at a reactor process temperature of approximately 150 °C. Figure 5 illustrates the composite oxidation efficiency for nonmethane VOC. Also, the best minimum operating temperature was found to be 300 °C for nonmethane VOCs. Methane oxidation performance, shown by figure 6, requires a temperature closer to 400 °C and, as such, will typically drive the specification of process conditions. Figure 7 shows the reactor temperature response. Based upon the temperature response and observed nonmethane VOC oxidation performance, the minimum reactor power condition is 110 W at the flow conditions investigated. This condition will result in a methane oxidation efficiency of 15–20-percent efficiency. Increasing the power input to the reactor is required to improve the methane oxidation efficiency. Therefore, depending upon the application, a trade will be required between nonmethane VOC and methane oxidation performance to determine the optimum reactor operating condition. The observed oxidation performance is comparable to pellet-based catalytic reactors presently in use on board the *ISS*.[3] Figure 8 shows the pressure drop of the reactor integrated with the TCO heat exchanger assembly. Observed oxidation performance indicates the 5.1-m^3/h (3-cfm) flow-rate condition is the maximum flow for achieving the best performance. In this case, for the desired reactor temperature range, the pressure drop ranges between 1 kPa (4.1-in H_2O) and 1.2 kPa (4.7-in H_2O). Compared to similar equipment presently on board the *ISS*, the test article's pressure drop of 1 kPa (4-in H_2O) at 4.6 m^3/h (2.7 cfm) is 9 percent lower.[4] The observed oxidation, temperature response, and pressure drop performance indicate that the USCM-based reactor is suitable for retrofit into existing *ISS* systems as well as for use in identified niche applications.

Endurance Testing

Characterization of the USCM reactor's durability was demonstrated during the last 7 months of the project. During this time, approximately 6 months of cumulative continuous operation was achieved. Methane was injected periodically at a rate sufficient to provide 65 ± 7 mg/m^3 (100 ± 10 ppm_v) at the TCO assembly inlet. Carbon dioxide concentration at the thermal catalytic oxidizer assembly exhaust was monitored during the methane injection periods to determine oxidation performance. The project plan called for the durability characterization to continue for a minimum of 8 weeks and as long as 6 months; however, evaluation found that continuing to operate the test article beyond the project end date was an insignificant part of the overall test facility overhead. For this reason, the endurance testing has continued and is still being performed as of March 1, 2004. Approximately 11 months of continuous operation have

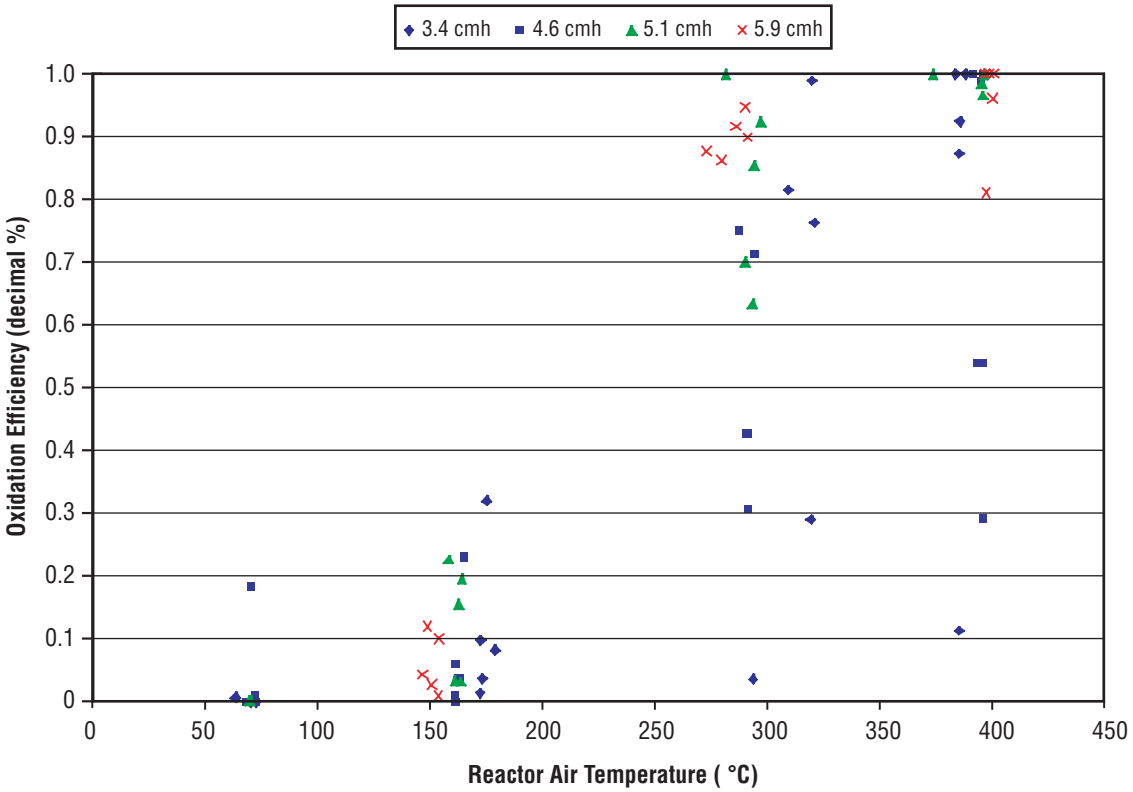

Figure 5. Nonmethane VOC oxidation efficiency.

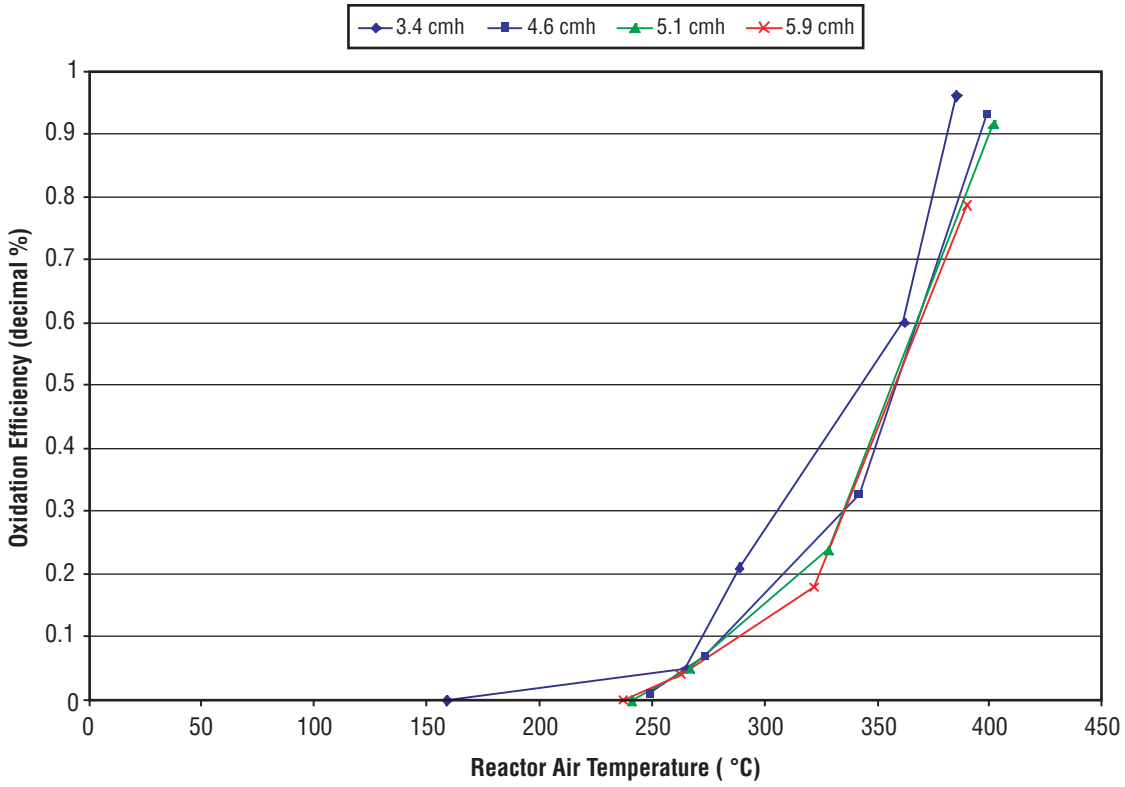

Figure 6. Methane oxidation efficiency.

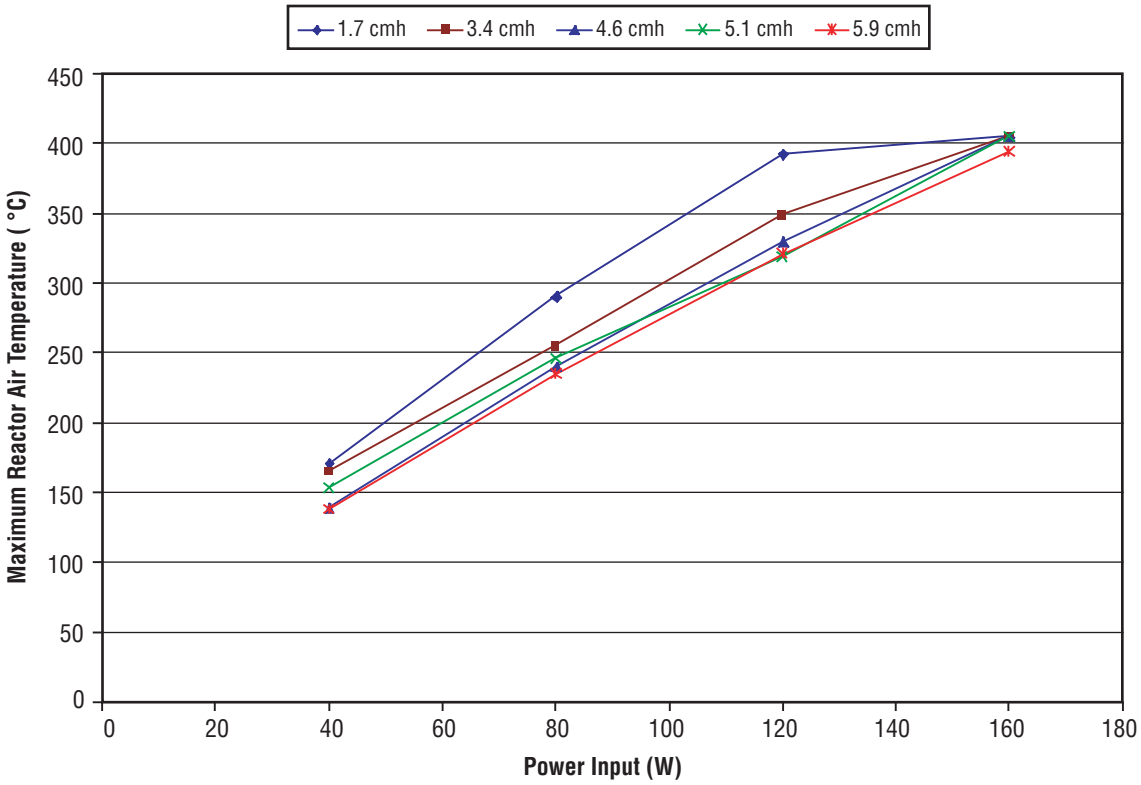

Figure 7. Reactor temperature response.

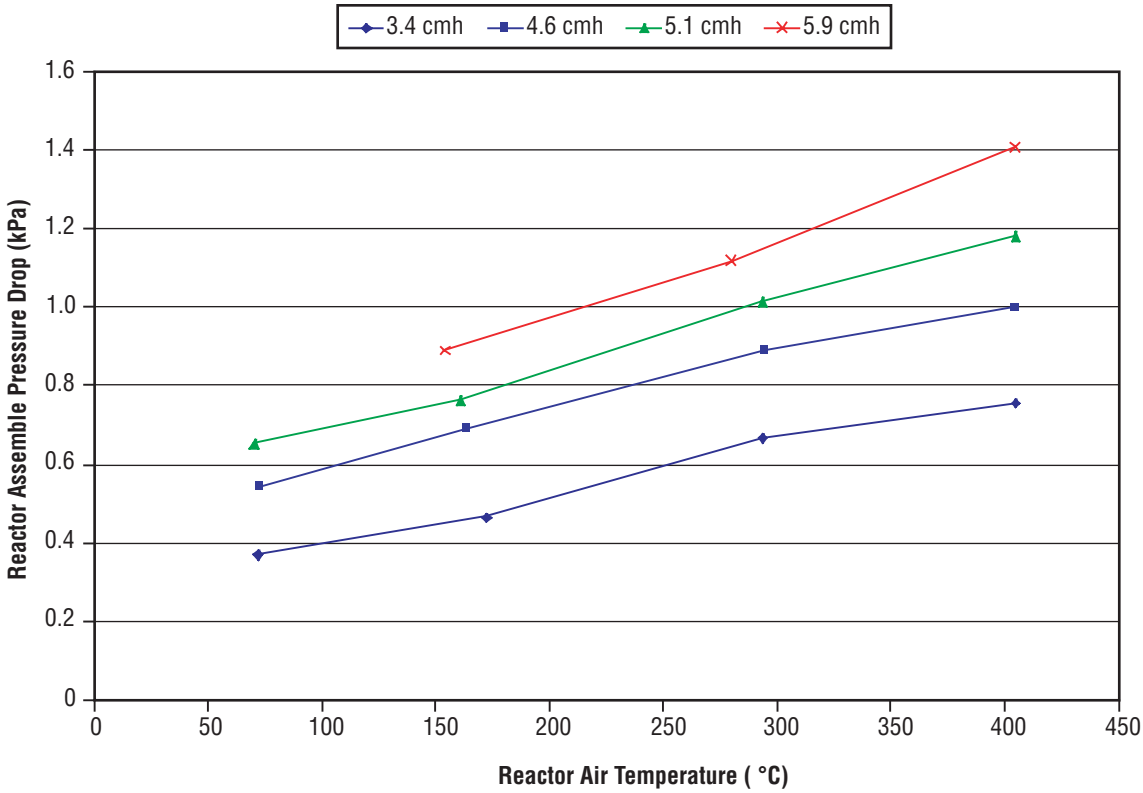

Figure 8. Reactor pressure-drop response.

been accumulated. The endurance testing will continue until at least 2 years of cumulative continuous operation has been achieved or as long as the facility overhead can accommodate the continued testing. The 2-year goal will equal the endurance testing of thermal catalytic oxidation equipment presently deployed on board the *ISS*. The objective of endurance testing is to understand the long-term operational characteristics of the USCM reactor assembly.

Future Work

Endurance testing will continue as long as test facility overhead can accommodate it or until 2 years of cumulative continuous operations are achieved. The detailed final report will be completed and submitted for publication as a NASA Technical Memorandum under the NASA formal publication series.

Publications and Patent Applications

The USCM technology is protected under the United States (U.S.) Patent number 6,328,936. Detailed results of this effort will be published as a NASA Technical Memorandum as well as future technical conference proceedings.

Funding Summary

Table 3 summarizes the fiscal year (FY) 2003 and FY 2004 resource for the project in full time equivalents (FTEs) and in dollars. All available funding was used as planned with an end-of-project under-run of approximately $1,000.

Table 3. Project resource summary.

ITEM		FY 2002	FY 2003	TOTAL
(FTEs)	Contract labor*	3.4	1.6	5
	Civil service labor*	6	2.5	8.5
($)	Contract labor cost	36,808	29,500	66,308
	Materials and equipment	13,592	0	13,592
	Total	50,400	29,500	79,900

*Labor units are person-months.

Status of Investigation

All proposed tasks have been completed and a detailed report is in preparation for publication as a NASA Technical Memorandum.

References

[1] Carter, R.N.; Bianchi, J.F.; Pfefferle, W.C.; et al.: "Unique Metal Monolith Catalytic Reactor for Destruction of Airborne Trace Contaminants," *SAE 972432*, Society of Automotive Engineers, Warrendale, PA, pp. 1–3, July 1997.

[2] Roychoudhury, S.; Muench, G.; Bianchi, J.F.; et al.: "Development and Performance of Microlith™ Light-Off Preconverters for LEV/ULEV," *SAE 971023*, Society of Automotive Engineers, Warrendale, PA, pp. 56–57, February 1997.

[3] Wright, J.D.; Chen, B.; and Wang, C.M.: "Trace Contaminant Oxidation Catalyst Poisoning Investigation," *NAS8–38250–15*, TDA Research, Inc., Wheat Ridge, CO, pp 16–20, March 1996.

[4] Tatara, J.: "TCCS Life Testing Status Through Week 33," Ion Corp, Huntsville, AL, June 1993.

Multiphase Fluid System Design for Microgravity Environments

Project Number: 02–19

Investigators: D. Layne Carter/FD21
Donald W. Holder, Jr./FD21

Purpose

NASA's Office of Biological and Physical Research (OBPR) Enterprise sponsors basic and applied research in the area of fluid physics, taking advantage of low-gravity environments to create unique test conditions not possible on Earth. The knowledge gained from this research advances the fundamental knowledge of fluid-phase phenomena. Within this field, multiphase fluids exhibit particularly unique phenomena that are important design drivers for spacecraft systems, such as those for environmental control and life support, thermal control, propellant management, and microgravity science fluid loops. Unfortunately, the link between multiphase fluid basic research and applied system design practices for low-flow spacecraft fluid systems is not strong within NASA.

The Flight Project Directorate's Environmental Control and Life Support (ECLS) Group strategically plans to position itself, within the next 5 years, as the Agency's premier engineering organization for the design of spacecraft multiphase fluid systems. Such a position will allow the ECLS Group to better align itself with, and provide needed support to, Marshall Space Flight Center's (MSFC's) roles in space transportation and microgravity sciences, while expanding its customer base beyond the *International Space Station (ISS)*. This research activity represents an investment towards that goal.

Background

The dynamics of two-phase (gas and liquid) fluid flow in microgravity present significant design challenges for spacecraft systems. In the absence of gravity, surface tension and capillary forces play a significant role in low-flow, two-phase fluid dynamics. The effects of these forces are not well characterized in the microgravity environment. Since current state-of-the-art understanding of two-phase behavior in microgravity is limited to the simplest of physical geometries and flow conditions, personnel in the MSFC ECLS Group (FD21) have had to conduct experiments to support the design of life support hardware for the Node 3 ECLS System (ECLSS). These efforts have focused primarily on fluid flow through packed beds and mechanical restrictions, common features of many ECLS technologies. A key example is the Volatile Removal Assembly Flight Experiment (VRAFE) flown on STS–96, which was needed to demonstrate acceptable performance of a packed-bed catalytic oxidation reactor operating in a microgravity two-phase environment. ECLS also developed a complementary experiment conducted on the NASA KC–135 Microgravity Plane to characterize the distribution and transport of gas and liquid through a nonoperating packed bed. An unexpected finding from the STS–96 experiment was that the performance of a membrane phase separator was detrimentally impacted by the absence of gravity. The root cause for the performance decline was traced to an alteration of the membrane's surface properties by foreign contamination to an extent that was masked by gravitational influences during preflight and postflight ground testing.

The current experience base with two-phase fluid flow indicates that gas collects in flow regions where there is insufficient liquid flow to either push out the gas or provide the necessary pressure drop to move the gas. In this environment, the gas volume increases until a steady state condition is achieved in which additional gas is swept away by the liquid flow. However, the ability to accurately model and predict this phenomenon in microgravity does not currently exist.

The accumulation and release of gas in fluid systems can impact fluid system performance. For example, when designing a heating section, the potential for gas to accumulate in that section must be considered. Instrumentation sensitive to gas must be designed to prevent gas accumulation. In fluid systems where gas is not desired, hardware must be designed to catch, accumulate, and release gas in a manner that it can be accommodated downstream. Furthermore, the tendency for gas accumulation to affect pressure drop must be considered in fluid systems where pressure variances may affect system performance.

These issues have a broad range of applications to the design of ECLSS hardware on *ISS* and future manned exploration missions. All three *ISS* assemblies currently being developed by MSFC—the Urine Processor Assembly, Water Processor Assembly, and Oxygen Generator Assembly—have had to address design issues related to two-phase flow in microgravity environments. Detection and measurement of two-phase flow in microgravity are also of interest to the NASA team working on orbital cryogenic fluid management (CFM) technology. Science payloads and facilities being developed for the *ISS* will also have fluid loops with two-phase conditions present.

Approach

The initial task in this Center Director's Discretionary Fund (CDDF) research project was to identify physical differences between gas and liquid phases that could be used to separate the two phases. The key physical parameters that led to development concepts included density and surface tension. The primary objective for the initial year of this development effort was to identify, manufacture, and test concepts for the

accumulation and controlled release of free gas in two-phase microgravity systems.

The coalescer designs have met the following key requirements specified in the initial proposal:

- Accumulate and release free gas such that it can be detected by existing optical gas sensor technologies (minimum bubble size of 3 mm).
- Accumulate and release free gas at a reduced frequency.
- Minimize pressure drops under single- and two-phase conditions.
- Must function in a microgravity environment.
- Require no power.
- Design must support the use of materials compatible with fluids typical of ECLS systems and cryogenic fluids.
- Materials must not introduce chemicals into the process fluid.

The first concept is mechanical filtration through hydrophilic filters. A hydrophilic filter will preferentially allow the liquid phase to pass through the available pores. The gas phase will pass through only when the pressure drop across the filter exceeds the bubble point for the particular filter's material and micron rating. In ideal circumstances, gas will accumulate on the filter until a sufficient area of the flow path is blocked, leading to an increase in pressure drop exceeding the bubble point. At this time, gas intrusion through the filter will occur. Once gas intrusion is initiated, the majority of the gas volume will pass through the filter, thus achieving the goal of coalescing and controlling the release of the gas. Once this volume of gas goes through the filter, the filter surface rewets and prevents passage of the gas until it accumulates again.

To evaluate various filters as coalescers, multiple filters were acquired representing a range of hydrophilic materials and micron ratings. A summary of the filter materials and micron ratings are provided in table 1. The filters were flat, circular filters, approximately 50 mm in diameter. The liquid velocity was set to provide a face velocity on the filter of 0.02 in/s and 0.1 in/s, with the volumetric flow rate of gas set at one percent of the liquid flow rate. The test schematic is provided in figure 1, and a photograph of the test setup is provided in figure 2. Clear tubing was used around the filter housing and at the filter effluent to support a visual assessment of the two-phase flow exiting the filter. A video of the test proceedings was also conducted.

Table 1. Summary of filter testing.

Material	Micron Rating	Flow Rate (ml/min)	Comments
Millipore polypropylene	1.2	146	Continuous release of fine bubbles
	10	146	Continuous release of fine bubbles
	80	146	Continuous release of fine bubbles
Millipore nylon net	11	146	Continuous release of fine bubbles
	60	146	Effective coalescer, though some degradation with time
	100	146	Controlled release of ~5–10 ml with some stray bubbles
	180	146	Limiting coalescing, but mostly continuous release of fine bubbles
Millipore durapore membrane	0.65	146	Membrane ruptured at 5 psi delta P
	8	146	Membrane ruptured at 4 psi delta P
Gelman SS metal screen	Unknown	146	Continuous release of fine bubbles
TWP metal screen	55	146	Continuous release of fine bubbles
	279	146	Continuous release of fine bubbles
	105	146	Continuous release of fine bubbles
	178	146	Limited coalescing, too many stray bubbles to be effective
	10	146	Continuous release of fine bubbles
	2	146	Continuous release of fine bubbles
Millipore nitrocellulose	0.8	146	Filter ruptured as pressure increased
	3	146	Filter ruptured as pressure increased
	5	146	Filter ruptured as pressure increased
	8	146	Filter ruptured as pressure increased
Osmonics polycarbonate	20	146	Limited coalescing
	10	146	Continuous release of fine bubbles
	1	146	Continuous release of fine bubbles

continued

Table 1. Summary of filter testing. (continued)

Material	Micron Rating	Flow Rate (ml/min)	Comments
Osmonics magna nylon	1.2	146	Continuous release of fine bubbles
	10	146	Limited coalescing, but also minor release of fine bubbles
	20	146	Continuous release of fine bubbles with limited coalescing
Miami aquaculture polyester mesh	300	146	No gas retention due to large pore size
	200	146	Continuous release of fine bubbles
	150	146	Continuous release of fine bubbles
	41	146	Limited coalescing, though release of fine bubbles and small bubbles was fairly frequent
Pall Supor 8000	0.8	146	Filter ruptured as pressure increased
Millipore polypropylene	1.2	29	Limited coalescing, continuous release of fine bubbles and small bubbles released every 2–4 min
	10	29	Continuous release of fine bubbles with limited coalescing
	80	29	Continuous release of bubbles with limited coalescing
Millipore nylon net	11	29	Continuous release of fine bubbles
	60	29	Effective coalescer, but several small stray bubbles periodically released
	100	29	Effective coalescer, but several small stray bubbles periodically released
	180	29	Effective coalescer, but several small stray bubbles periodically released
Millipore durapore membrane	0.65	29	Filter ruptured as pressure increased
	5	29	Continuous release of fine bubbles
Gelman SS metal screen	Unknown	29	Limited coalescing, but continuous release of fine bubbles
TWP metal screen	55	29	Fairly constant release of fine bubbles
	279	29	Fairly constant release of fine bubbles
	105	29	Fairly constant release of fine bubbles
	178	29	Fairly constant release of fine bubbles
	10	29	Fairly constant release of fine bubbles
	2	29	Fairly constant release of fine bubbles
Millipore nitrocellulose	0.8	29	Filter ruptured as pressure increased
	3	29	Filter ruptured as pressure increased
	5	29	Filter ruptured as pressure increased
	8	29	Filter ruptured as pressure increased
Osmonics polycarbonate	20	29	Effective coalescer at lower flow rate, infrequent release of stray bubbles
	10	29	Limited coalescer, frequent release of large stray bubbles
	1	29	Limited coalescer, frequent release of large stray bubbles
Osmonics magna nylon	1.2	29	Continuous release of fine bubbles
	10	29	Continuous release of fine bubbles
	20	29	Continuous release of fine bubbles
Miami aquaculture polyester mesh	300	29	Continuous release of fine bubbles
	200	29	Continuous release of fine bubbles
	150	29	Limited coalescing, but continuous release of fine bubbles
	41	29	Limited coalescing, but continuous release of fine bubbles
Pall Supor 8000	0.8	29	Filter ruptured as pressure increased
Coorstek ceramic	51	29	Continuous release of fine bubbles
	100	29	Continuous release of fine bubbles
	14	29	Continuous release of bubbles in center, large bubbles around edges
	1.7	29	Continuous release of fine bubbles
	1.7	29	Continuous release of fine bubbles, excessive pressure drop
	4	29	Continuous release of fine bubbles, excessive pressure drop
	100	29	Limited coalescing, but continuous release of fine bubbles
	51	29	Continuous release of fine bubbles

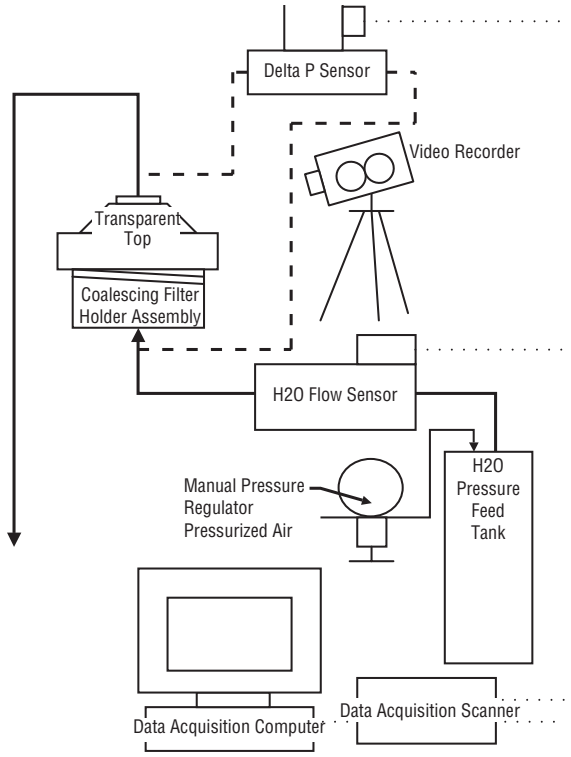

Figure 1. Test schematic for mechanical filter.

Depending on the filter material and micron rating, multiple scenarios occurred related to coalescence of the gas. In several instances, gas was unable to pass through the filter resulting in a high pressure drop and damage to the filter. This typically occurs because the filter's pore size is too small, thus requiring an excessively high bubble point for gas intrusion. In the other extreme, the filter's bubble point is too low and a continuous stream of fine bubbles is released. Several filters were also unable to effectively rewet after gas intrusion initially occurred, thus allowing gas to continually pass through the filter.

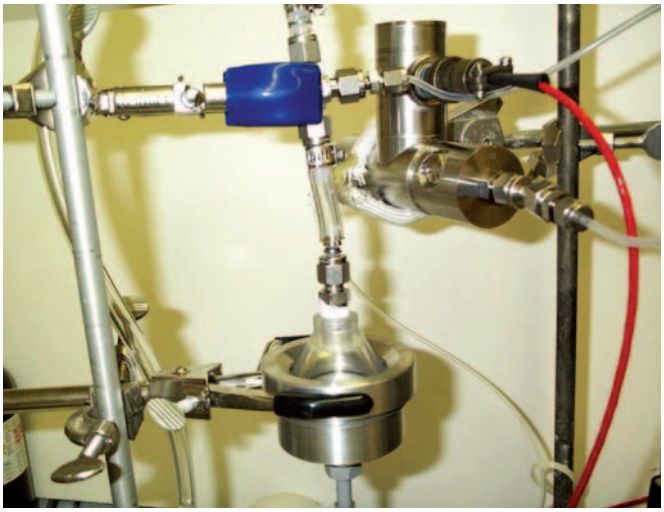

Figure 2. Test rig (showing filter housing and ΔP sensor).

Accomplishments

The filter testing identified several filter materials as potential candidate coalescers, including the Millipore nylon and the Osmonics polycarbonate. The nylon mesh filter from Millipore provided the best performance and will be further evaluated over a range of flow rates and micron ratings. This filter material was evaluated in the microgravity testing planned for 2003.

The second concept developed in the first year of this effort is illustrated in figure 3. Hamilton Sundstrand and MSFC personnel jointly developed the concept for this device. Relative to mechanical filtration, this coalescer allows for accumulation of a greater volume of free gas before release. The two-phase fluid flow is introduced to the external section of the housing. The liquid phase initially flows through the first-stage hydrophilic filter at the effluent of the housing. As gas accumulates in this section and blocks off the filter, liquid flow will begin

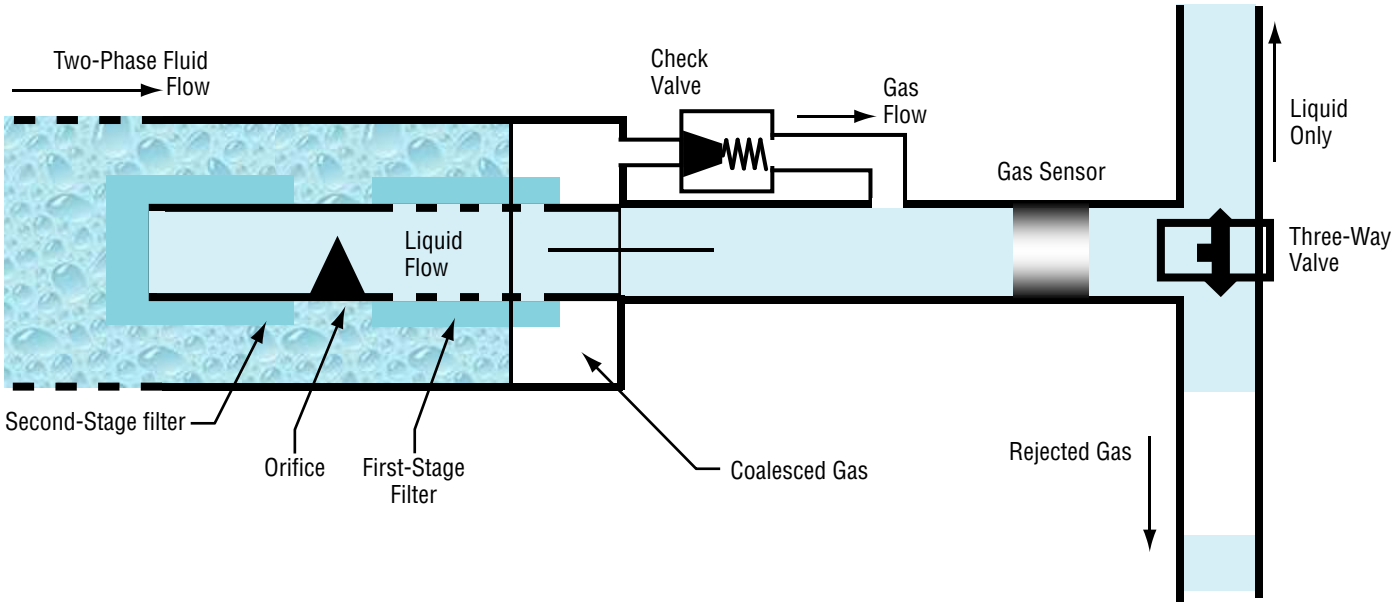

Figure 3. Mechanical coalescer concept.

in the second-stage filter. When the gas phase also blocks off this section of the filter, the pressure drop between the influent and effluent of the housing will increase sufficiently to open the check valve at the housing effluent and subsequently release the accumulated gas. To minimize the pressure drop in this device, the check valve is specified to open at 0.75 psid and reseat at 0.25 psid. The orifice in the standpipe will ensure there is sufficient pressure drop through this flow path to keep the check valve open until liquid flow is reinitiated through the first-stage hydrophilic filter.

The concept for the mechanical coalescer was provided to the ECLS test team. The lead mechanical engineer produced design drawings for the concept and oversaw manufacturing. Due to the tight design requirements for the check valve pressure drop, this item was designed and built on-site by the ECLS test team. A photograph of the completed coalescer, without hydrophilic filters installed, is provided in figure 4.

Figure 4. Mechanical coalecer (without hydrophilic filters).

Planned Future Work

Due to delays in the procurement of the hydrophilic filters, testing of the mechanical coalescer will be conducted in the second year of this research effort. The test rig built for the mechanical filter evaluation will be used for the mechanical coalescer. The coalescer will be evaluated over a range of flow rates and gas/liquid ratios to assess its effectiveness.

Another concept that will be pursued in the second year of this effort is a vortex concept illustrated in figure 5. The two-phase fluid flow is introduced tangentially to the cylinder so that the higher density liquid phase is pushed toward the outer edge while the gas phase collects in the middle of the cylinder. As the gas volume increases, it will eventually grow into the liquid flow path and exit the cylinder. Further studies will be required to determine the optimal geometry and dimensions for the chamber. Since this concept will only function in the absence of gravity, evaluating its performance will be done on the NASA Microgravity Plane.

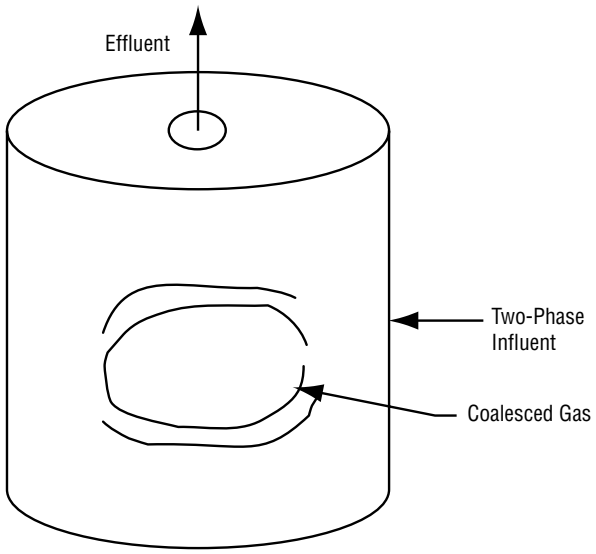

Figure 5. Vortex separator.

The most successful concepts identified during the ground tests were tested on the NASA Microgravity Plane in 2003. Based on the results of the first year of research, the Millipore Nylon filter and the mechanical coalescer developed by Hamilton Sundstrand will be tested in 2004. If sufficient development effort is made prior to the microgravity flight, the vortex separator concept will also be evaluated. In this test phase, various two-phase mixtures will be introduced to the coalescer to assess its performance in microgravity. This effort will be conducted through a grant with the Center for the Commercial Development of Space Power at Texas A&M University. This group has extensive experience conducting experiments on the NASA Microgravity Plane, including a previous experiment with FD21 in which two-phase fluid flow through packed media was successfully characterized (Contract #NCC8–177) and the effect of two-phase flow in the conductivity sensor proposed for use on the *ISS* Water Processor was characterized.

The testing to be conducted in this task will utilize the same test rig employed for the previous experiments with Texas A&M. This test rig has been built by Texas A&M for two-phase fluid-flow experiments and would provide the physical interfaces required to evaluate the performance of the coalescer concepts. MSFC will provide the coalescer concepts for use in the experiment while Texas A&M will integrate the test stand, work with MSFC to develop the test procedures, and coordinate with the KC–135 program regarding schedule and submittal of the safety package. This approach will avoid the cost of having to build a new test rig at MSFC. Because of the advantages of utilizing Texas A&M's expertise and hardware, FD21 will not work the KC–135 effort through MSFC. This approach has been followed in FD21's previous KC–135 efforts.

Publications and Patent Applications

Hamilton Sundstrand and MSFC personnel jointly developed the concept for the mechanical coalescer device pictured in figure 3. As a result of this CDDF effort, a patent will be submitted for this technology titled "The Mechanical Coalescer."

Funding Summary

Table 1 presents the proposed funding for fiscal year (FY) 2002 and FY 2003 for this project. In FY 2002, approximately $90,000 was expended for the tasks defined in the initial proposal. A total of $71,000 is requested for FY 2003. An additional 0.1 FTE ($11,000) is proposed above that initially requested for contractor personnel at the ECLS Test Facility, to support the assembly and delivery of hardware required for the microgravity testing.

Table 1. Project funding summary.

Funding Element	FY 2002		FY 2003	
	(FTEs)	($)	(FTEs)	($)
Civil Service			0.2	
MSFC support contractor			0.1	11,000
Center for Space Power				40,000
NASA Microgravity Plane				20,000
Total		~90,000		71,000

Status of Investigation

Status of Investigation: The end product for this effort is a conceptual design for a coalescer that can be used in two-phase fluid systems for the accumulation and controlled release of gas, and a methodology to predict its performance. This design and methodology will be the result of research and analysis of two-phase fluid dynamics and testing of development hardware in normal Earth gravity and in microgravity. The data generated will be documented in a final report.

Following our work in FY 2002, we were unable to make any significant progress on this task in FY 2003. During FY 2002, MSFC FD21 completed initial assessments of various mechanical coalescer concepts, primarily mechanical filtration. This effort was continued in FY 2003 with a concept developed by Hamilton Sundstrand personnel. However, the development item was not able to successfully coalesce gas, potentially because the development item could not adequately reflect the physics of the development concept with the limited budget available. Further research on this effort was not pursued due to higher priorities related to the Node 3 ECLS flight hardware program. However, a grant was established with the Center for Space Power at the Texas A&M University for further testing on the NASA Microgravity Plane. Personnel from MSFC FD21 and the Center for Space Power identified an additional coalescing concept utilizing a passive vortex that also has potential for microgravity applications. This concept and the best-performing mechanical filters are now being assessed for an experiment on the NASA Microgravity Plane in September 2004.


Science
Directorate
(b) 334 Hz
(c) 500 Hz
NASA MSFC
Center Director's
Discretionary Fund
FY 2003
Annual Report

The Development of Multilayer Hard X-Ray Optics

Project Number: 02–20

Investigators: **Brian D. Ramsey/SD50**
R.F. Elsner/SD50
S.L. O'Dell/SD50
A. Shapiro/SD72
R. C. Sisk/SD22

Purpose

The purpose of this Center Director's Discretionary Fund (CDDF) project is to develop a system to deposit reflectivity-enhancing multilayer coatings on the interior cylindrical surface of electroform nickel-replicated x-ray mirrors.

Background

With the Compton Observatory discovery of titanium (Ti)-44 nuclear lines in the spectrum of supernova remnant Cas-A and the information they contain for stellar evolution, the search for these lines has become an important component of future hard x-ray missions. However, hard x-ray optics, currently fabricated at the Marshall Space Flight Center (MSFC) and used in our HERO balloon program, are limited in their ability to resolve the Ti x-ray lines. MSFC optics are coated with iridium, the most x-ray reflective element; however, even this becomes absorbing around the energies of these lines, rendering the optics inefficient for this important study.

The best solution to increasing mirror reflectivity in this energy region is to apply multilayer coatings. These are alternating layers of high-optical-contrast materials that can give useful reflectivity at much higher energies than pure iridium. The difficulty with this task is that the multilayers are extremely thin (down to 3 nm), must be highly uniform and precisely controlled in thickness, and must be applied to the inside of the mirror shell, which is a highly curved surface. This representsa significant technical challenge, which this project will address.

Approach

Our approach is to design a thin-film coating/vacuum system to deposit multilayer coatings on in-house-fabricated replicated x-ray optics. Precise control of hundreds of layers of sputtered films in the 1–100-nm range will be done through automated control of the target translation rate while rotating and translating individual mirror shells to ensure uniformity. Film characteristics will be determined by several parameters such as initial vacuum pressure, plasma-gas pressure, sputtering rate, sputtering geometry, and optic temperature. Test flats will be coated to optimize these parameters in preparation for coating the shallow-graze-angle replicated optics. Test optics will then be coated to quantify and control uniformity with single deposited materials. After that, test multilayer coatings will be applied and evaluated. Figure 1 is a picture of the current multilayer coating system.

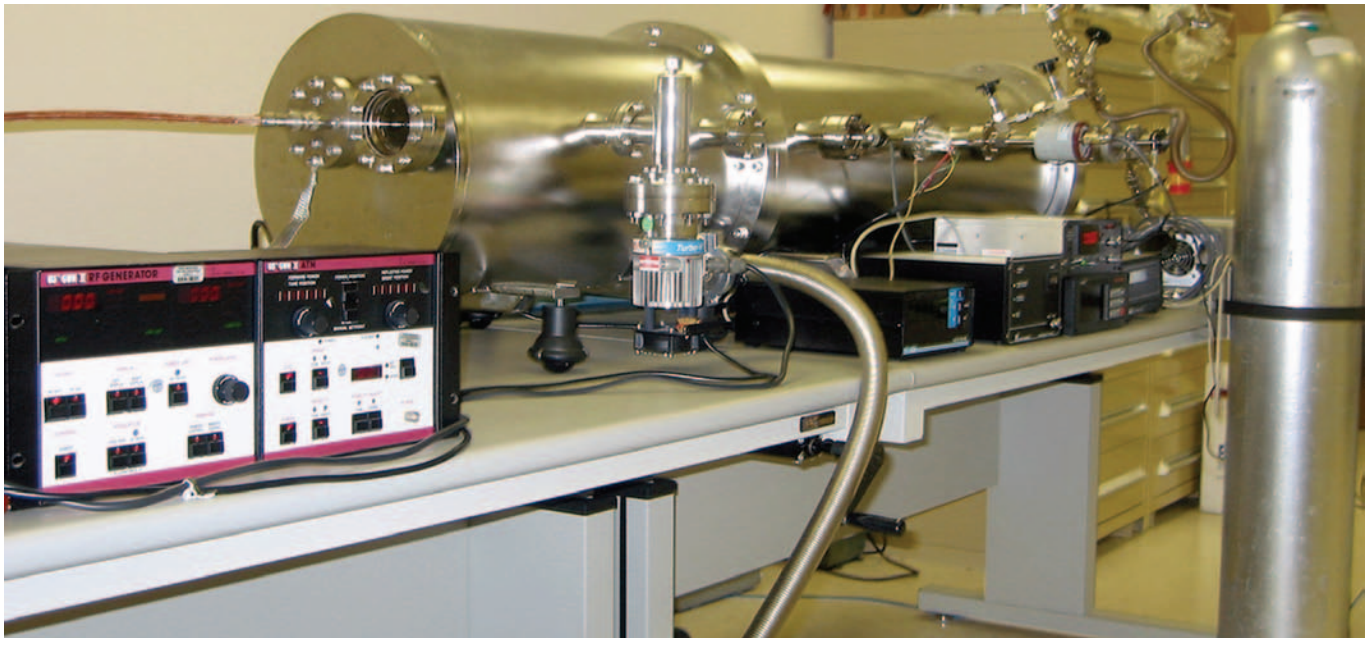

Figure 1. Multilayer coating system.

Accomplishments

Assembly of the large vacuum chamber and replicated optic motion control has been completed. Software for controlling optic motion during deposition and monitoring of vacuum pressure has been developed. The radio frequency (RF) sputtering system has been built with the capability to accept a large range of target materials and geometries. The entire chamber, with all attached hardware, has been helium leak checked and routinely demonstrates acceptable overnight pump downs. Test coatings of various materials have been performed to obtain optimum coating conditions. Both tungsten and silicon, a candidate multilayer pair of materials, can be coated with near bulk density (95 percent) and with surface roughness equivalent to the underlying substrate. Test shells with single element coatings have been evaluated for uniformity.

Planned Future Work

Planned future work includes uniformity control via computer and then the test coating of multilayers on representative optics. After that, work will begin coating HERO balloon program outer-shell hard-x-ray optics with multilayers to enable the resolution of the Ti lines.

Publications and Patent Applications

There are none at this time.

Funding Summary

Table 1 identifies the funding for fiscal year (FY) 2002 and FY 2003.

Table 1. Funding summary.

	FY 2002 ($)	FY 2003 ($)
Allocated	37,000	12,500
Obligated	37,000	12,500

Status of Investigation

The assembly of the coating/vacuum system, translating/rotating system is complete. Initial sputter coatings on test flats have been accomplished varying parameters such as target geometry, target material, RF power, and plasma-gas pressure to obtain near-bulk density in candidate materials.

In Situ Studies of Structural Transformations in Undercooled Liquids via Beam-Line Electrostatic Levitation

Project Number: 02–21

Investigator: **Dr. Jan Rogers/SD46**
Dr. Michael B. Robinson/SD46
Dr. Kenneth Kelton/Washington University, St. Louis
Mr. Thomas Rathz/University of Alabama in Huntsville

Purpose

The purpose of this project is to provide research capabilities and data to help meet NASA's requirements for advanced materials. The tool developed under this Center Director's Discretionary Fund (CDDF) yields detailed information on the structural transformations in undercooled liquids and high-temperature materials. This information is needed to develop and characterize new materials.

Background

The electrostatic levitator (ESL) provides an ideal platform for stabilizing, melting, and undercooling a wide range of materials while in the direct path of the 125-keV x-ray beam of the advance photon source (APS) at the Argonne National Laboratory. It provides for a quiescent melt and the heating is decoupled from sample positioning. The proposed efforts utilize the Marshall Space Flight Center (MSFC) refined electrostatic levitating technique, adapted to the APS beam-line, in order to study the structure and transformation of high-temperature, highly reactive, undercooled liquids of technologically important materials.

Approach

The research plan involves the integration of the Beam-Line Electrostatic Leviation (BESL) unit with the x-ray beam-line source at the Argonne National Laboratory. The procedures used in the MSFC ESL unit are employed to levitate and melt samples in the BESL. After the sample is fully molten, controlled cooling will begin. The sample will be cooled and held at the desired temperature. The beam-line shutter will then be opened and the undercooled liquid sample will be exposed to the x-ray beam line. Measurements of the x-ray diffraction pattern will be generated. Analysis involves the interpretation of the x-ray diffraction patterns. Since the sampling rate is high and measurements will be taken over a wide range of undercooling temperatures, the x-ray pattern analysis will be accomplished at MSFC and Washington University with guidance from the APS team. In addition, the microstructures of selected samples will be fully analyzed using standard metallographic techniques.

Accomplishments

During fiscal year (FY) 2003, the BESL unit was deployed at the APS of the Argonne National Laboratory. The results are the first-ever data from an ESL on an x-ray beam line. The project involves collaboration with Dr. Ken Kelton of Washington University at St. Louis. MSFC provided the BESL equipment, operations/science team, and support for the travel and labor from Dr. Kelton's group. Dr. Kelton provided access to the APS facility and 2 weeks of time for BESL integration and data collection on the beam line. Time on the beam line is valued at approximately $350/hr. The BESL was deployed at the APS during March 2002. The facility is operated on a 24-h per day 7-day per week basis. The BESL system was used to process 93 different samples of metals, alloys, elements, quasicrystal forming alloys, and bulk metallic glasses for a total of 612 melt cycles. Approximately 4,000 x-ray diffraction patterns were generated during the processing of materials over a wide temperature range (300–1,900 °C). Experiments included evaluation of a new imaging system that produced x-ray diffraction patterns at speeds up to 5,000 times faster than image plate technology. Analysis of the data will provide insight into the phase transformation processes in a wide range of materials and information needed to evaluate the use of the BESL technique for use in the rapid determination of phase behavior in high-temperature materials.

Planned Future Work

Prototype instrument development and operations were successfully completed. Data analysis and preparation of publications will continue in collaboration with Dr. Kelton's research team.

Publications

Kelton, K.F.; Lee, G,W.; Gangopadhyay, A.K.; et al.: First X-Ray Scattering Studies on Electrostatically Levitated Metallic Liquids: Demonstrated Influence of Local Icosahedral Order on the Nucleation Barrier," *Physical Review Letters*, Vol 90, No. 19, p. 195,504, May 16, 2003.

This paper was selected by the Editor of *Science* as the Highlight of Recent Literature for Physics in the May 30, 2003 issue and will also be featured in the cover article of *Physic Today* in the July 2003 issue. This paper provides new insight into the structural transformations in undercooled liquids. For many years, it has been shown that many metallic liquids could be undercooled, but the physics of undercooling has not been understood. Undercooling occurs when the metallic melts remain liquid while the temperature is decreased far below their equilibrium melting temperature prior to crystallization. Use of the BESL at the APS of Argonne National Laboratory provided the first-ever data to validate a 50-year old hypothesis about the nature of undercooling. Additional papers are under preparation.

Funding Summary

Table 1 identifies the funding associated with this project.

Table 1. Funding summary.

	FY 2002 ($)	FY 2003 ($)
Allocated	37,000	12,500
Obligated	37,000	12,500

Status of Investigation

This investigation has been successfully completed. The BESL prototype was developed and implemented. The data produced by the prototype has resulted in significant publications. As a result of the CDDF research and the resultant article published in *Physical Review Letters* in May 2002, a workshop on BESL technology and science was organized. A joint NASA/DOE Ames Laboratory Materials Science Workshop on BESL was held on February 26–27, 2004 at the APS of Argonne National Laboratory. Twenty scientists and engineers drawn from the containerless solidification, x-ray scattering, and high-temperature intermetallics communities (including two members of the National Academy of Engineering) participated in a workshop sponsored by NASA and Ames Laboratory. The workshop was organized and led by Dr. Ken Kelton, Washington University in St. Louis; Dr. Alan Goldman, Ames Laboratory and Iowa State University; and Dr. Jan Rogers, MSFC/SD46. Results from experiments using the prototype BESL unit, possible applications, scattering data/analysis, and x-ray optics were presented. Working sessions identified the anticipated scientific results, including applications for high-temperature materials to support NASA's exploration and technical modifications needed to optimize performance. A document summarizing the results of the workshop is under preparation. Proposals are being prepared to obtain support for the development of an advanced BESL, optimized for high-temperature materials studies.

Rapid Prototyping of Propulsion Components With Nanocrystalline Microstructure

Project Number: 03–29

Investigators: **Dr. Sridhar Gorti/SD46**
Dr. Subhayu Sen/BAE SYS
Dr. Adrian Catalina/BAE SYS

Purpose

The long-term goal of this Center Director's Discretionary Fund (CDDF) project is to develop a rapid prototyping process to fabricate composite materials of precise thickness and functional characteristics for high-temperature propulsion applications. To achieve this long-term goal objective, we propose to develop a vacuum deposition process for generating a nanocrystalline structure and to characterize the nanocrystalline structure to quantify the relation between the structure and processing variables. The proposed research will focus specifically on intermetallic compounds such as gamma-titanium aluminum (γ-TiAl) deposited as thin films on silicon substrates. The purpose of this investigation is to identify specific processing variable(s) that enable precise control of deposition of thin films that exhibit increased ductility, superplasticity, thermal protection, etc.

Background

Gamma-TiAl-based alloys are regarded as potential candidates to replace nickel (Ni)-based superalloys currently used in thermal protection systems and engine components. However, there is a limitation in the forming methods that can be used with TiAl alloys because of their brittleness. Attempts to improve ductility of the alloys by chemical modifications or microstructural control have shown limited success.[1,2] Very brittle ceramics, in general, have been shown to exhibit a fair degree of ductility at room temperature if they have a nanocrystalline structure.[3] A critical grain size, below which ceramic and intermetallic materials can become ductile, has been theoretically predicted.[4,5] To date, state-of-the-art deposition technologies have not been successful in developing a high-temperature material with nanocrystalline microstructure. Controlling the crystalline structure at the nanoscale level has great potential in the development of material with high specific strength at elevated temperatures.

We proposed that the state-of-the-art could be advanced with the development of a vacuum deposition process capable of not only high-deposition rates, but also control of the grain size at the nanoscale level.

Approach

This investigation makes use of a technique called Vacuum Arc Vapor Deposition (VAVD) by which high-temperature alloys can be fabricated with a nanocrystalline microstructure. The VAVD process was developed as part of a NASA funded project and the hardware is currently housed at The University of Alabama in Huntsville (UAH). The process was initially developed as a method for vapor deposition of thin metallic and ceramic films. In brief, a high-energy heat source is used in the VAVD process to melt a wide variety of materials including ceramics and can attain deposition rates as high as 3.5 μm per min. A constant flow of argon gas is introduced over the molten substrate that disperses ionized metal atoms into a cloud formed within the deposition chamber. The high-energy metal atoms may interact with the gaseous cloud to form metal complexes that subsequently deposit onto a substrate/target. The chemical/physical state of the thin-film deposit is a manifestation of not only interactions of metal ions within the gaseous cloud, but also nucleation and growth of grains composed of metal-ion complexes formed on the substrate. Process variables such as, current density, argon flow rate, metal-ion composition of the target, substrate temperature, etc., all combine to control the chemical/physical state of the deposited thin film.

In this work, the chemical/physical state of the deposited thin film is characterized at the nanoscale level using primarily atomic force microscopy/scanning tunneling microscopy (AFM/STM). Other characterization techniques, such as x-ray scattering, scanning and/or tunneling electron microscopy, and chemical-etching methods are also used. Such characterizations answer fundamental questions related to formation of nanocrystals, grain growth and migration, and its effect on mechanical properties. The obtained results will then be analyzed using a mathematical model based on a Monte Carlo simulation[6] to predict microstructure evolution at the nanoscale. A validated numerical method will serve as a high-resolution real-time microscope to predict microstructure development as a function of processing parameters. The developed mathematical model based on Monte Carlo simulation will thus enable the prediction microstructural evolution as a function of processing parameters.

Accomplishments

At the end of the first year of the 2-year investigation, the following has been accomplished:

- Numerous TiAl alloy thin-film samples on silicon substrates have been prepared by the VAVD technique.
- Modification to the present VAVD process had been implemented to determine the chemical composition of TiAl complexes from atomic absorption spectrum of the metal-ion components produced within the deposition chamber. As shown in figure 1, the various peaks of the obtained spectra can be readily assigned to the presence of Ti or Al. The unassigned peaks may well represent either contaminants within the chamber or complexes of TiAl formed within the diffuse cloud.

Characterization of the TiAl alloy thin films had been performed at the nanoscale using AFM. Typical AFM images obtained from various TiAl thin films are shown in figures 2–4. In figure 2(a), an image obtained by AFM of the surface of a TiAl thin film deposited on a silicon wafer obtained is shown. Readily observable is the presence of highly organized crystals that are possibly comprised of TiAl complexes. In figure 2(b), a graph measuring the thickness/height (~15 nm) of the formed crystals with linear dimension on the order of ~100 nm is also shown. In figure 3(a), an image obtained by AFM of the surface of a TiAl thin film deposited on a silicon wafer obtained is shown. In the image, highly ordered crystals comprised of TiAl, the composition of which has yet to be determined, are observed. While the height of the observed structures is also ~15 nm, the linear dimension of these structures is ~500 nm. Shown in figure 3(b), is a higher resolution image of the highly ordered structures that exhibits further ordering within the crystals. In figure 4(a), an image obtained by AFM of the surface of a TiAl thin film deposited on a silicon wafer obtained is shown. In the image, the TiAl substrate does not exhibit higher order structures but rather appears amorphous in nature. In figure 4(b), a graph measuring the thickness/height (~5–10 nm) of possibly crystalline spherulites with linear dimension on the order of ~10 nm is also shown. In all cases shown, the chemical make-up of the deposited film has yet to be determined.

Compositional analysis using electron microprobe is shown in figure 5. While the microprobe analyses can determine elements present within thin films, the method is incapable of determining either the physical (crystalline, amorphous, etc) or the chemical (complexes) state of the thin films.

A mathematical model based on Monte Carlo simulation[6] to predict microstructural evolution as a function of processing parameters has been developed. In brief, the model describes the mechanisms involved in the nucleation and subsequent growth of grains formed upon a given substrate. Based upon the energetics of the system, particulars of the nucleated grains, such as grain size and surface roughness, are predicted.

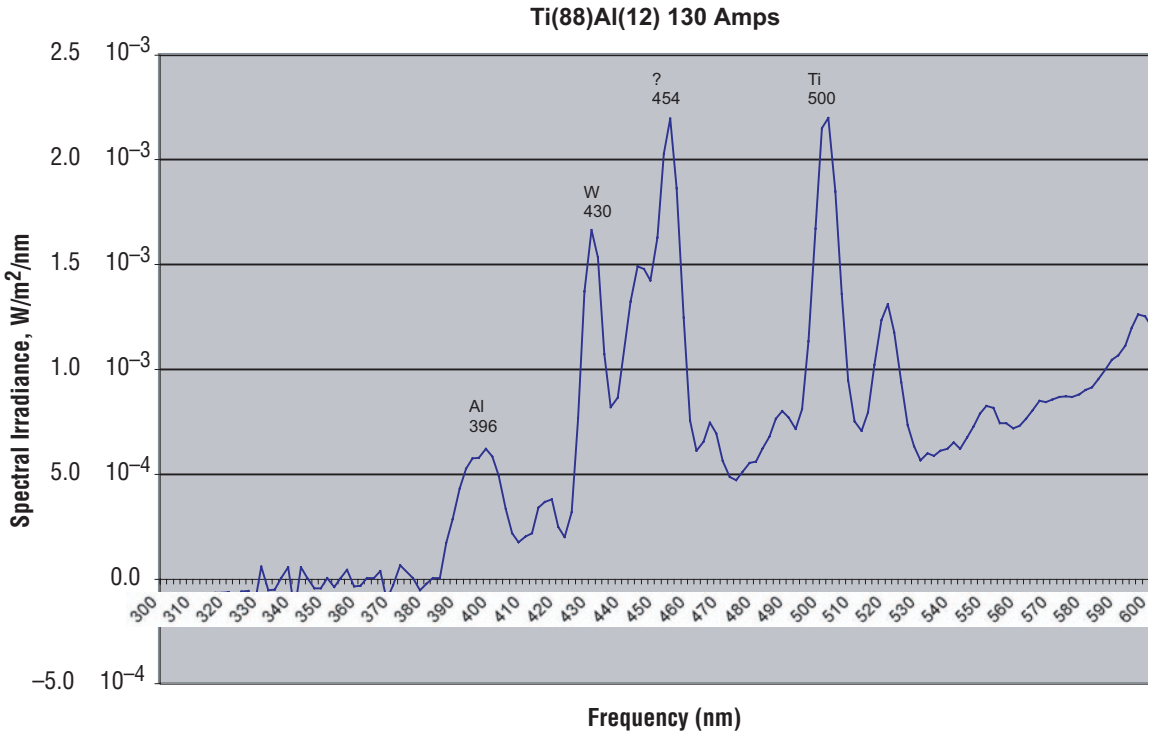

Figure 1. An atomic absorption spectrum of the metal ion components produced within the deposition chamber of the Vacuum Arc Vapor Deposition chamber is presented.

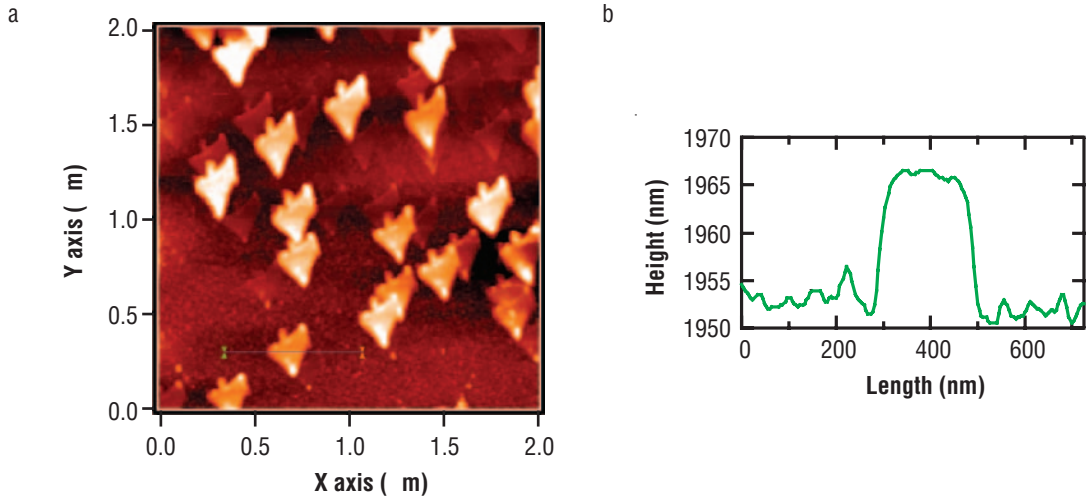

Figure 2. In (a), an image obtained by AFM of the surface of a TiAl thin film deposited on a silicon wafer is shown. In (b), a graph measuring the thickness/height (~15 nm) of the formed crystals with linear dimension on the order of ~100 nm is also shown.

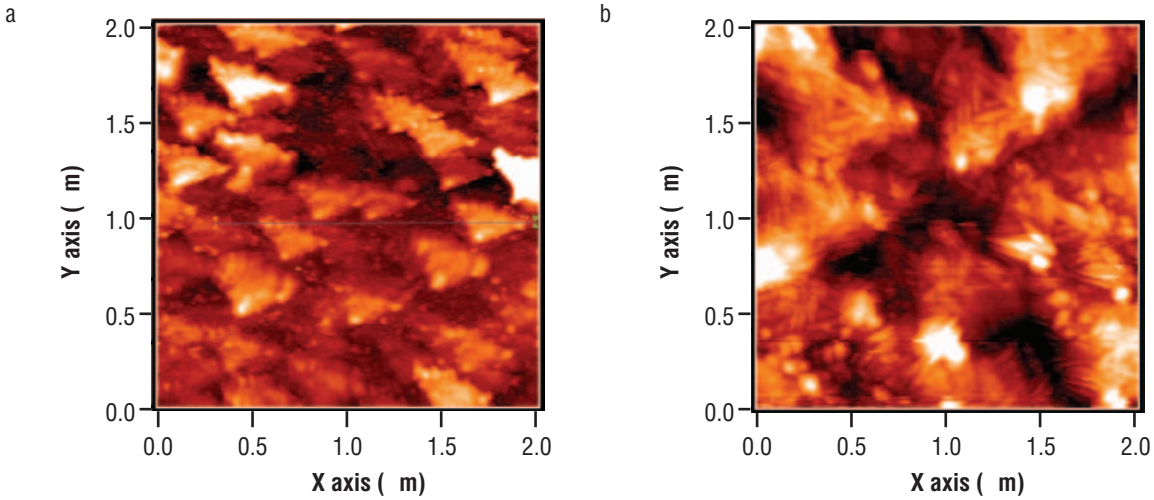

Figure 3. In (a), an image obtained by AFM of the surface of a TiAl thin film deposited on a silicon wafer is shown. Shown in (b), is a higher resolution image of the highly ordered structures that exhibits further ordering within the "crystals."

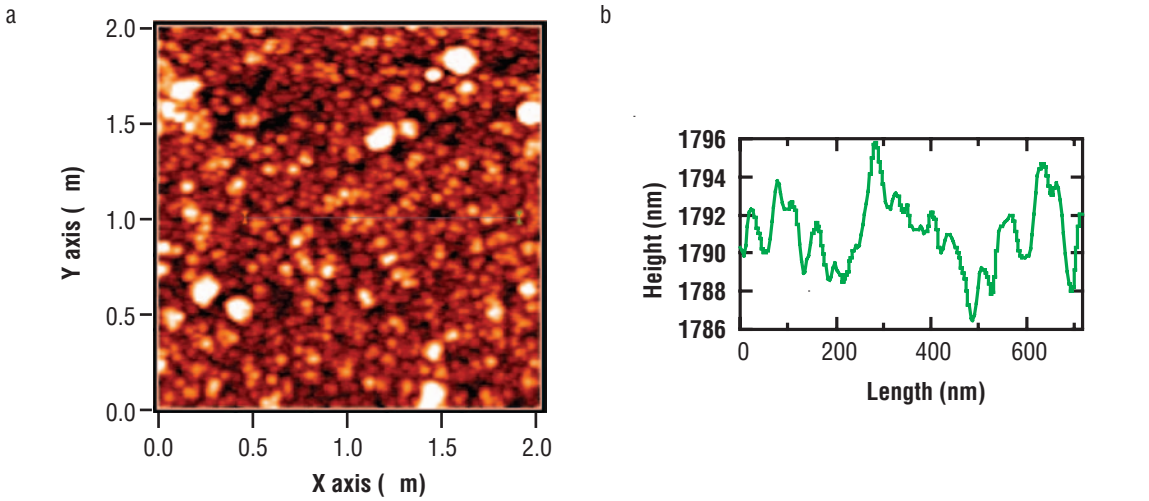

Figure 4. In (a), an image obtained by AFM of the surface of a TiAl thin film deposited on a silicon wafer is shown. In (b), a graph measuring the thickness/height (~5–10 nm) of possibly crystalline spherulites with linear dimension on the order of ~10 nm is also shown.

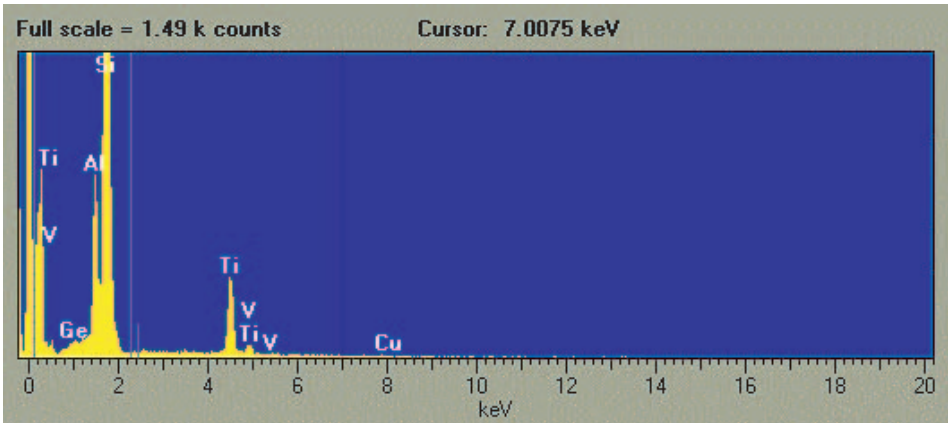

Figure 5. Spectrum obtained upon an electron microprobe analysis is shown.

Planned Future Work

While considerable progress in the development of a rapid prototyping process to fabricate composite materials has been made, it is duly considered that precise control of processing parameters must be determined experimentally and theoretically prior to implementation. Based upon our immediate experiences of the deposition processes, work planned for the determination of the control variables are as follows:

- Modification of sample preparation at all stages of the deposition process to ensure the deposition of the exact physical state of TiAl complexes.
- Determine the chemical composition of TiAl complexes from atomic absorption spectrum of the metal-ion components produced within the deposition chamber.
- Characterization of the TiAl alloy thin films had been performed at the nanoscale using AFM and STM.
- Compositional analysis of deposited TiAl thin films using electron microprobe, x-ray, and chemical etchants.
- Determination of a causal relationship between ductility, etc., and the nanocrystalline structure of TiAl deposited thin films.

Further development of mathematical models to predict micrstructural evolution as a function of processing parameters has been developed.

Publications and Patent Applications

None submitted. Several planned.

Funding Summary

Year 1 funding at the level of $56,218 has been completed.

Table 1 identifies the anticipated funding for year two of the project.

Table 1. Anticipated funding for year two of the project.

Purpose	Funding ($)
Target raw materials: Al, Ti, and alloys	5,000
Substrate raw materials: Teflon, foam, and glass	1,000
Fabrication and installation of second VAVD gun (heat source)	10,000
Microprobe analysis	5,000
Contracted effort (UAH technician)	10,000
Contracted effort (BAE)	18,000
Total Funding	**49,000**

Status of Investigation

Anticipated to continue in second year.

References

[1] Kim, Y.-W.; and Dimiduk, D.M.: "Designing Gamma TiAl Alloys: Fundamentals, Strategy and Production," M.V. Nathal, R. Darolia, C.T. Liu, et al. (eds.), *Structural Intermetallics*, TMS, Warrendale, PA, pp. 531–543, 1997.

[2] Imayev, V.M.; Salishchev, G.A.; Imayev, R.M.; et al.: "An Approach to Ductility Improvement of TiAl and Ti3Al Titanium Aluminides Based on Microstructure Control," M.V. Nathal, R. Darolia, C.T. Liu, et al. (eds.), *Structural Intermetallics*,TMS, Warrendale, PA, pp. 505–514, 1997.

[3] Karch, J.; Birringer, R.; and Gleiter, H.: "Ceramics Ductile at Low Temperature," *Nature*, Vol. 330, pp. 556–558, 1987.

[4] Schulson, E.M.: "Comments on The Brittle to Ductile Transition of Long-Range Ordered Alloys," *Res. Mech. Lett*. Vol. 1, pp. 549–554, 1981.

[5] Chan, K.S.: "Theoretical Analysis of Grain Size Effects on Tensile Ductility," *Scr. Metall.*, Vol. 24, pp. 1725–1730, 1990.

[6] "Monte Carlo mathematical Simulation Model."

Performance Verification of Cadmium Zinc Telluride Crystal Growth Techniques for Large-Scale Gamma-Ray Imagers

Project Number: **03–30**

Investigators: **Jerry Fishman/SD50**
(B. Alan Harmon/SD50 original principal investigator)
Ching-Hua Su/SD46
Sandor Lehoczky/SD46
Robert B. Wilson/SD50
Arnold Burger/Fisk University, Nashville, TN

Purpose

Our goal is to obtain large, high-quality cadmium zinc telluride (CZT) ingots that can be made into high resolution gamma-ray detectors. Growth techniques will be investigated for producing CZT crystals with reduced charge trapping, twinning, tellurium precipitates, and other common nonuniformities that degrade the performance of CZT for gamma-ray detectors. At the same time, we want to minimize unusable material that greatly increases the cost of commercially available CZT.

The strategy is to use modified Bridgman techniques or vapor transport growth in a systematic program to optimize growth parameters. It is expected that the correlation between these characterized material properties and the parameters of their growth processes will be unambiguously established. From this correlation, the optimum growth parameters will be determined and standard procedures will be established for high-yield production of detectors. The ultimate goal is to produce higher yield, larger volume CZT detectors that can be used in various high-energy astrophysics applications.

Background

The room-temperature semiconductor, CZT, has become a detector of choice for many applications in high-energy astrophysics because of its high density, high atomic number and superior energy resolution. In this investigation, CZT growth techniques will be examined for application to large-scale arrays for gamma-ray astronomy and, in particular, for the Energetic X-Ray Imaging Survey Telescope (EXIST) mission. Various advanced crystal growth techniques will be used to improve CZT gamma-ray detectors via improved growth recipes, testing of crystal furnace temperature profiles in a multizone furnace, quality control during growth, and examination of electrical contact preparation for the transformation of CZT crystals into gamma-ray detectors. The ultimate goal is to produce thicker, more uniform detectors in the 20–700-keV energy range for future NASA missions such as EXIST, a Beyond Einstein mission.

Current research in CZT sponsored by NASA focuses on the development of the geometry, readout, and compensation techniques to deal with the peculiar charge trapping and other defects characteristic of commercially available CZT. Here we propose a complementary effort emphasizing the connection of growth recipes, quality control during growth, and posttesting with the performance of a fully functional, large-scale element of a CZT array.

Our approach capitalizes on our expertise in materials processing, coupled with an intensive crystal characterization plan. The emphasis of the research is to determine the effects that can be correlated with growth procedures such as second-phase segregation at the micron and submicron scales, charge mobility, and electric field uniformity. We are also interested in properties affected by the growth geometry, thermal environment, and the growth rate on the compositional homogeneity of CZT crystals.

Accomplishments

CZT crystal ingots have been successfully grown in the Materials Science Laboratory of the Marshall Space Flight Center (MSFC) Science Directorate. Figure 1 shows one of the first ingots of CZT after being sandblasted. This ingot was grown in the multizone furnace in MSFC Bldg. 4481, in the crystal growth laboratory of SD46. Several other ingots have been successfully grown and characterized.

Figure 1. One of the first ingots of CZT after being sand blasted.

Using existing instrumentation in SD46, the composition of an ingot was accurately determined on the surface. These results are shown in figure 2. The zinc composition remained near 20 percent throughout most of the ingot, once stability was established at about 15 mm from the start of growth at the ingot tip.

A slice from an ingot, ~2-mm thick, was made so that a backscattering electron microscopic image along the surface could be obtained. The resulting image is shown in figure 3. Indications are that at this position in the ingot, a nearly perfect single crystal was grown. This was also verified by x-ray diffraction. These early ingots show that eventually, high-quality detectors might be obtained by the multizone furnace growth methods used in SD46.

However, due to impurities (mainly copper), these initial crystals cannot be made into useful detectors. Several additional ingots of CZT have been grown and are in the process of being tested.

Planned Future Work

Further crystal growth and characterization are planned that may lead to successful detector fabrication. Sources of contamination have been identified, so that the higher resistivity material and better detectors can be fabricated. This investigation is planned to be completed in the second quarter of fiscal year (FY) 2004. The results of this investigation will be used in a future Code S SR&T proposal.

Funding Summary

Approved: $60,000.
Disbursed: $60,000.

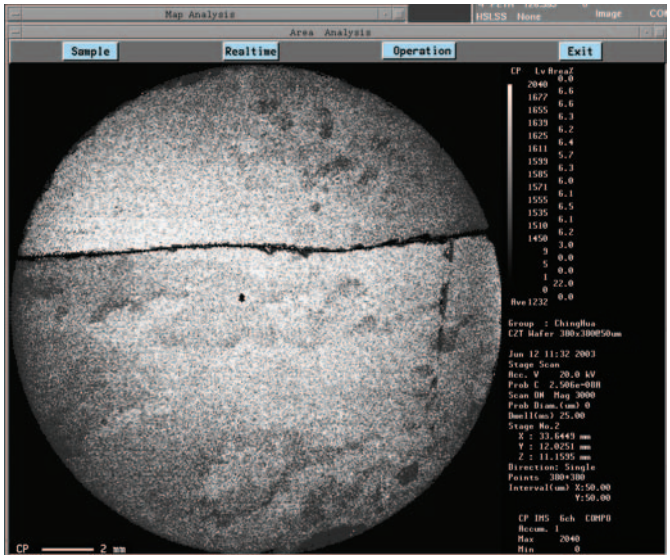

Figure 3. Backscattering electron microscopic image along the surface of an ~2-mm thick ingot slice.

Status of Investigation

This Center Director's Discretionary Fund (CDDF) project (#279–03–30) activity began in December 2002. In January 2003, Dr. Harmon, the original principal investigator (PI), departed NASA and transferred into a position within the Department of Energy in Germantown, Maryland. Dr. G.J. Fishman then succeeded Dr. Harmon as PI for this project.

The PIs initiated a parallel program to develop new scintillation detectors. While these detectors will not have energy resolution as good as CZT, it is believed that they will be more efficient and can be made in larger volumes than CZT. This later property is very important for several types of astrophysical investigations, particularly in the MeV gamma-ray region. The status of the CZT semiconductor detector versus advanced scintillation detectors will be determined during the coming year.

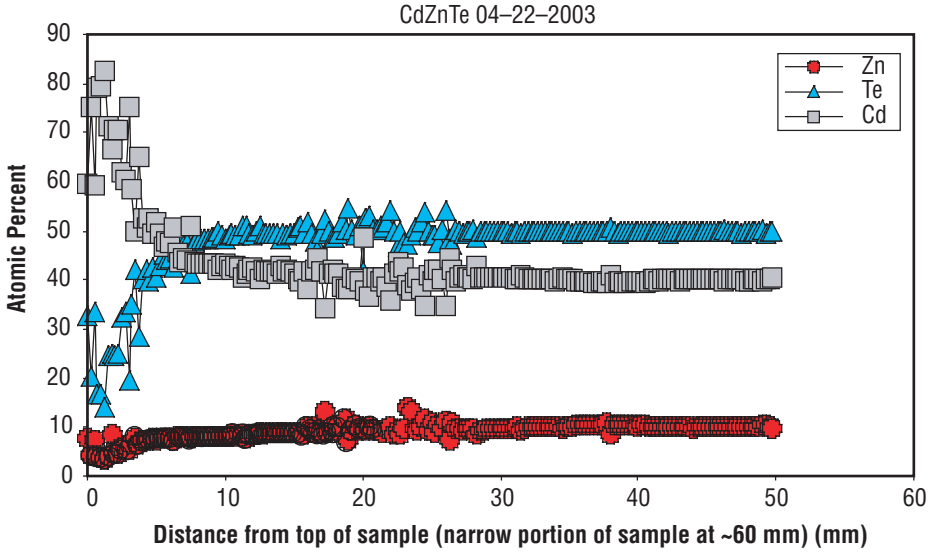

Figure 2. Determination of an ingot composition using existing instrumentation in SD46.

Development of Thin-Disk Laser Architecture for use in Power Beaming Applications and Science Instruments

Project Number: 03–31

Investigators: **W. Scott Smith/SD70**
Andrew S. Keys/SD71
Tim S. Blackwell/UAH

Purpose

The purpose of this Center Director's Discretionary Fund (CDDF) project is to develop, build, and characterize a high-power, high-efficiency solid-state laser based on an innovative thin-disk gain medium architecture and to reconfigure this architecture into a compact and rugged package suitable for use in the space environment. The resulting miniaturized laser will be the first laser source of its kind to be packaged to withstand launch vibration loads and to operate for extended periods of time in a space environment. Applications standing to benefit from this thin-disk laser architecture include long-distance power beaming, interferometry, space propulsion, and free-space optical communication.

This current investigation has an immediate goal of producing a compact thin-disk laser prototype capable of delivering 500 W of output power and an advanced goal of delivering 2 kW of output power at up to 50 percent optical efficiency. Beyond the initial prototype, this effort endeavors to provide an enabling technology for a number of potential and proposed missions and mission scenarios at the Agency level. The Marshall Space Flight Center (MSFC) will directly benefit by having developed the first directed energy device even remotely suited to alternative propulsion activities.

Background

Numerous studies regarding the potential use of a laser-power transmission system have been developed, and the need for such systems has been identified. Until the recent MSFC/Dryden Flight Research Center (DFRC) beamed power flight demonstration (NASA MSFC Press Release 03–180), practical tests in beamed energy had not been conducted, as the existing laser technology was deemed inadequate in power levels and beam quality for this purpose. Pulsed lasers have been developed that are in the kilowatt range and have been proposed for power beaming support of high altitude, beam-powered aircraft and satellites. These lasers are yet impractical for power transmission due to undesirable effects on the power receiving materials (such as ringing and poor power conversion efficiencies). The thin-disk laser architecture developed by this current effort will provide continuous power and will address issues of improved efficiency and beam quality.

The current world level of development in thin-disk lasers is best exemplified by the production of welding lasers from the Haas Corporation. The Hass laser uses technology developed by the University of Stuttgart, Germany and attains a maximum power output of 4 kW with a beam divergence factor of more than 20 (the beam expands very rapidly, something like a flashlight), following the trend of increased beam divergence that varies with respect to increased output power. This divergence, though not critical for near-field welding applications, is detrimental to long-distance space-based laser-power transmission applications. With high divergence, the beam energy quickly dissipates as it traverses long distances, rendering it useless for most proposed space applications. Also, as the power level of 4 kW is adequate for welding, no commercial efforts are being undertaken to increase output power levels and resulting beam quality. These commercially available systems are of such poor beam quality that they are of no use in power beaming or other proposed NASA applications.

To correct this deficiency in high-power laser sources for space application, the thin-disk laser architecture is being adapted for use in space systems. This architecture shows promise for better beam performance in the kilowatt power range than either diode-pumped or lamp-pumped-rod laser configurations. The output wavelength of a thin-disk laser using Yb:YAG is 1.03 microns, a wavelength that is useful for power transmission and also suitable for interferometer missions such as NASA's Laser Interferometer Space Antenna (LISA) mission. Additionally, the physics of the thin-disk resonator cavity inherently demonstrate stabilities exceeding 10^{-14}, well within the stability region for formation flying and other precision space measurement applications employing interferometry-based measurements.

The thin-disk laser technology development for space-based applications is currently regarded to be at a technology readiness level (TRL) 3. The culmination of this prototyping effort will advance the state-of-the-art to at least TRL 4.

Approach

The laser design is based on technology developed at the University of Stuttgart, Institut fur Strahlwerkzeuge (Institute for Laser Research (IFSW)) in Germany. IFSW's small-volume, large-area thin-disk gain medium design shows considerable promise for high-efficiency, compact, and lightweight laser packages; exhibiting the same qualities and power levels of

much larger laser systems. Key to the high-efficiency of the thin-disk laser is the ability of the pump cavity to repeatedly reflect the pump beam off of the thin-disk amplification medium. This elegant pump cavity design allows a high level of energy transfer from the pump to the active gain medium, in turn allowing high lasing efficiencies. See figure 1 for a graphical rendering of the pump cavity.

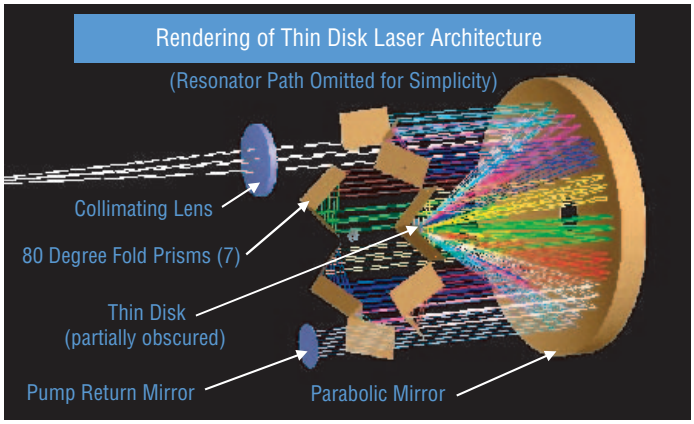

Figure 1. Rendering of pump cavity, illustrating the multiple pass of the pump beam onto the thin-disk gain medium.

Once a complete laser prototype is constructed and characterized, the thin-disk laser technology will be the basis for further proposed efforts to develop systems of increased output power through power scaling techniques. This technology development effort directly benefits small satellite systems and remote power users by reducing the amount of fuel necessary to be carried on the satellite or to remote locations, providing the vehicle a virtually unlimited operating life without fuel limitations.

To prove out the concept of laser-sourced power beaming, MSFC and DFRC have teamed together to perform a series of demonstrations aimed at characterizing beamed power for flight vehicles. The completed thin-disk laser would provide a small, compact, high-power, high-efficiency source for use in the continuance and improvement of the joint MSFC/DFRC solar- and beam-powered aircraft program.

As designed, the laser is modular in nature. A single laser module is constructed using up to four 250-W diode pump arrays, one homogenizer unit, one pump module, and an optical resonator module, resulting in an output of up to ~500 W (accounting for a 50-percent efficiency factor). Two of these 500-W units may be combined to create a 1-kW unit. The power-scalability feature of this architecture lends itself to further long-range goals of combining multiple 1-kW units to deliver even higher powers. Conceptual designs provide a roadmap for attaining up to 150 kW of output power through the staged combination of these basic thin-disk laser units.

Accomplishments

The parabolic mirrors required by the laser pump cavity have been designed and fabricated by the optics shop of MSFC's SD70, as shown in figure 2. Materials used include both metal (Ni:Al) and low expansion Zerodur glass. A high reflectivity coating designed to be highly reflective at a wavelength of 940 nm at ~10 degree angle-of-incidence has been applied to the Zerodur parabola pump-cavity mirror.

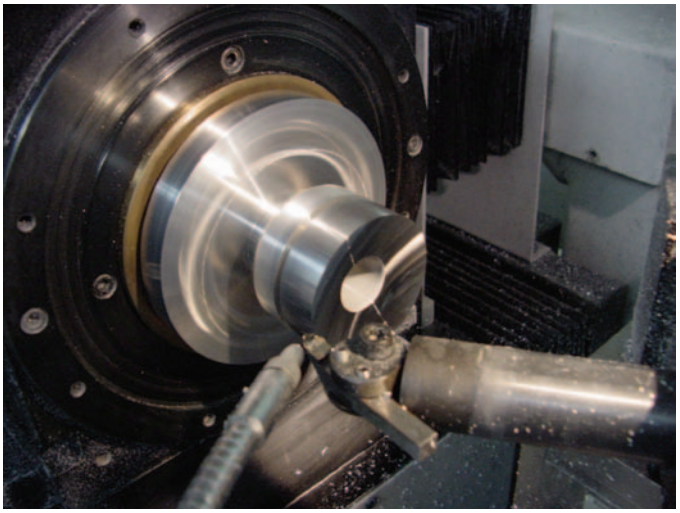

Figure 2. The pump cavity's parabolic mirror is diamond-turned using a Ni:Al blank.

To bring the laser prototype from design to reality, a new Laser Development Laboratory has been established within the National Space Science and Technology Center (NSSTC). All design, test, assembly, characterization, and operation activities of the thin-disk laser and the supporting pump lasers are being conducted here. The facility includes an optical spectrum analyzer, which has recently been calibrated and is now incorporated into the optical test setup for the pump diodes. Additionally, the chillers required to operate the pump cavity diodes and the gain cavity have been assembled within the laser facility and have been tested for proper operation. Two of the 250-W diode arrays to be used as the laser pump source (Yb(10 percent):KYW) have been verified in the laboratory to properly operate at the expected wavelength of 930 nm. Seven of the 250-W diode arrays to be used as the laser pump source (Yb(10 percent):YAG) have been verified in the laboratory to properly operate at the expected wavelength of 940 nm. These two wavelengths may be simultaneously used to pump the laser through a wavelength-mixing strategy. Additional tests performed on the laser diodes include verification of diode laser beam parameters—required for the uniform homogenization of the pump energy prior to its projection into the pump cavity.

Commercial, off-the-shelf (COTS) turning mirrors have been acquired that are adequate to supply the function of the pump-beam fold prisms within the pump cavity.

Designs for the pump diode mounts for these and higher energy systems are on going. The mounts must provide coolant to the diode laser units while also providing the ability to align the lasers to each other and to the specially made glass director used to couple the output of several diode laser units into the conditioning homogenizer.

Planned Future Work

After the laser has been built and tested, this technology will be proposed for further funding to produce high-power sources capable of providing on-orbit propulsion and planetary exploration power. Further development of the laser systems will have dual goals: To reach higher output powers with high efficiency and high beam quality through the staging of modular laser units and to customize individual units for specific space environment applications.

The resulting prototype laser will also be made available to MSFC and DFRC to facilitate the continuance of their solar and beam powered aircraft activities.

Publications and Patent Applications

Patent applications will be filed regarding novel aspects and applications of the laser as they are discovered.

Funding Summary

Fiscal year 2003: $67,000
Fiscal year 2004: $0

Status of Investigation

The investigation has completed the first year of a 2-year effort. Refer to the accomplishments section for a description of first-year activities.

Quantitative Flow Cytometry for Evaluation of Biological Effects of Simulated Microgravity and Radiation

Project Number: **03–32**

Investigators: **Robert Richmond/SD46**
Angela Cruz/NRC

Purpose

The immediate aim of this Center Director's Discretionary Fund (CDDF) project is to develop a method to quantify absolute fluorescence values using the flow cytometer as a method to compare the effects of simulated microgravity and radiation on cells in ground-based experiments. Flow cytometry employs the use of lasers to quantify fluorescence intensity data that provide information about cell populations. Molecules of equivalent soluble fluorochrome (MESF) units may be used for obtaining estimates of the degree of expression of cellular antigens when immunostained with the corresponding fluorochromes. The long-term aim is to be able to adapt this method for utility in assessing risks of radiation-induced damage to astronauts; a recognized high-priority NASA-specific problem in regards to exploration.

Background

Detecting initial responses of cells to environmental conditions such as radiation or microgravity may yield increments and/or decrements of expression of proteins, whose significance relates to the quantitative aspects of observed change.

Radiosensitivity has been shown to be linked to the insulin-like transforming growth factor I (TGF–I) receptor in ataxia-telangiectasia (A–T) cells.[1] Ionizing radiation has revealed susceptible cleavage points in cytokeratin 18.[2] A commercially available antibody, M30, recognizes a cytokeratin 18 neoepitope unmasked by caspase-3 mediated cleavage, which has the ability to show response to radiation.[3] Other cellular markers seen to exhibit response to radiation include γ–H2AX[4] and alpha2beta1 integrin.[5]

Approach

A–T is a radiation-sensitive syndrome expressed in the homozygous state as cutaneous, neurological, and immunological abnormalities predisposing to ionizing radiation-induced cell death, carcinomas, lymphomas, and leukemia.[6] Individuals who are heterozygous carriers were, in turn, observed to have an excess of breast cancer incidence, associated with up to 5 percent of all breast cancers.[7] Dr. Mike Swift's pedigree study of more than 5,000 A–T family members reported the relative risk for breast cancer of A–T heterozygotes to be 1.7–8.4 fold that of noncarriers, at 95 percent confidence levels.[8] The WH612/3 breast cells included in our study were obtained from a 41-year old woman who elected to undergo the surgical procedure of prophylactic mastectomy due to being identified through pedigree analysis as an obligate A–T heterozygote.[9] Thus, these cell isolates are expected to represent an accelerated model in studying the early progression towards breast cancer following radiation.

Cells are retrieved from nitrogen storage and plated onto two 100-mm tissue culture dishes to late log growth (= pass 6). Cells are then trypsinized and plated onto twelve 25-cm tissue culture flasks (= pass 7). These flasks are divided into 4 groups of triplicate flasks to be irradiated at midlog phase at 30, 60, and 90 rads using the Shepherd external beam Cs-137 irradiator on-site at the United States (U.S.) Army Missile Command on the Redstone Arsenal, with one group kept as an unirradiated control. Irradiated and unirradiated cells are replated onto 75-cm flasks and allowed to grow to late log phase (= pass 8), after which they are trypsinized and fixed for immunostaining with antibodies to radiation-responsive markers and subsequent quantitative flow cytometric analysis.

Accomplishments

Typically, cells undergo apoptosis in the hours immediately after irradiation. In the case of our experiments, cells are not harvested immediately after irradiation. Instead, they are passaged and allowed to proliferate prior to analysis; this approach is selected because these surviving cells are the ones that may go on to become cancer cells. It should be noted that early effects of radiation are not detected using our method; instead, persisting effects are detected that may figure more prominently in cancer risk assessment. We have consistently found no difference in cell cycles among the various radiation doses used (fig. 1), but we did find radiation-induced effects on marker expression in the same cells. Most radiation-dose effects revealed from preliminary colorimetric immunostaining results were confirmed using flow cytometry. In addition, they were able to be quantified using the quantitative flow cytometry approach.

Prior to the irradiation experiments, control experiments for quantitative flow cytometry have been performed regarding antibody incubation times and temperatures (fig. 2), presence or absence of primary blocking antibodies, and specific antigen-antibody compatibilities with ethanol or paraformaldehyde fixation (fig. 3). Preliminary results show differences in marker expression using this method at the radiation doses used. With paraformaldehyde fixation, levels of phospho-keratin 18 in unirradiated controls are lower than in irradiated cells (fig, 4), while with ethanol fixation, levels of its caspase-3

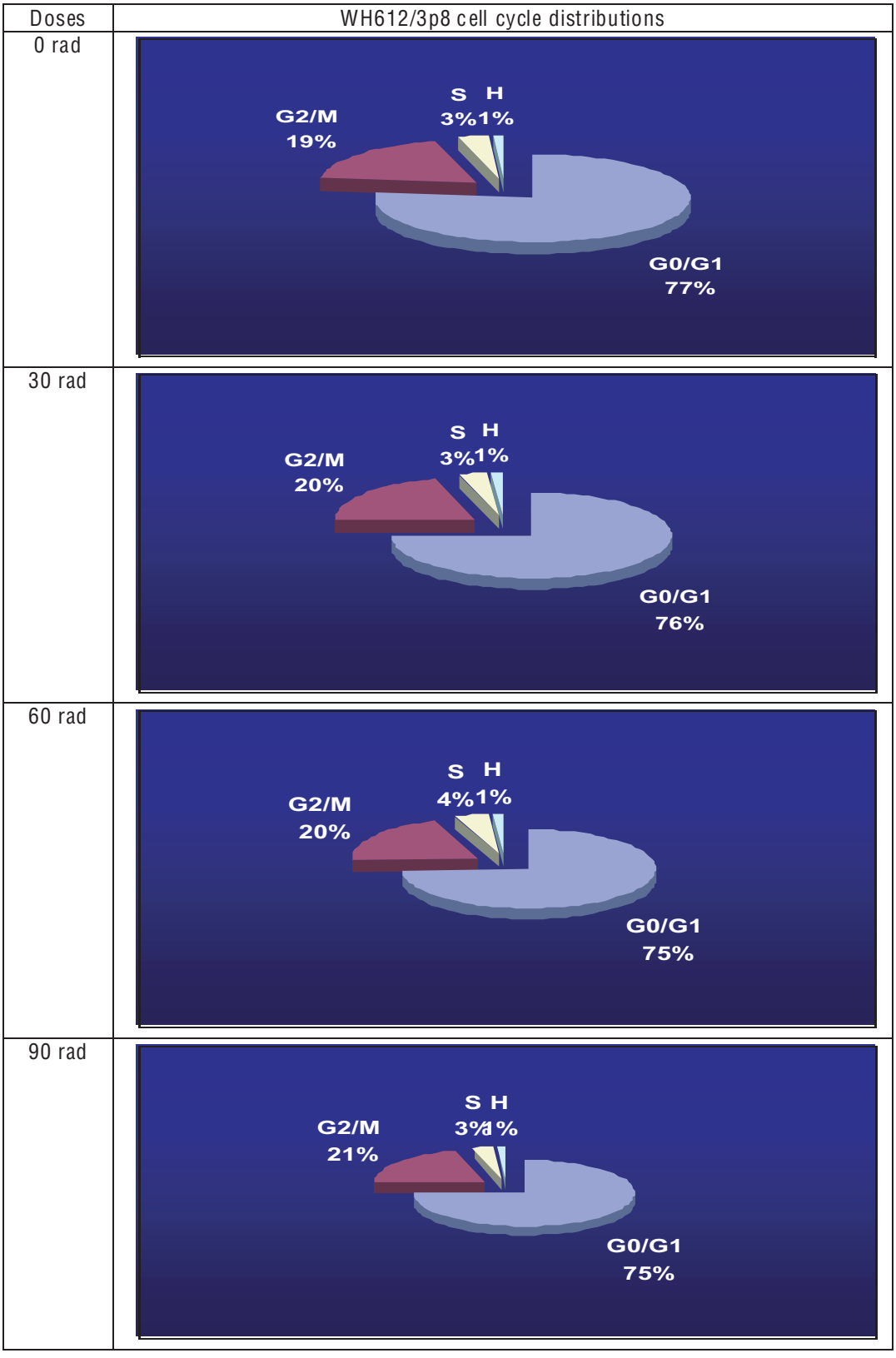

Figure 1. Cell-cycle distribution in percent of total WH612/3p8 cells irradiated at various doses. Cells were stained with propidium iodide and analyzed on the Becton Dickinson FACSCalibur flow cytometer. No significant differences in cell-cycle distribution are seen. Cell-cycle phases: G0/G1=diploid cell phase; G2/M=tetraploid cell phase; S=intermediate phase between diploid and tetraploid; H=ploidy greater than tetraploid.

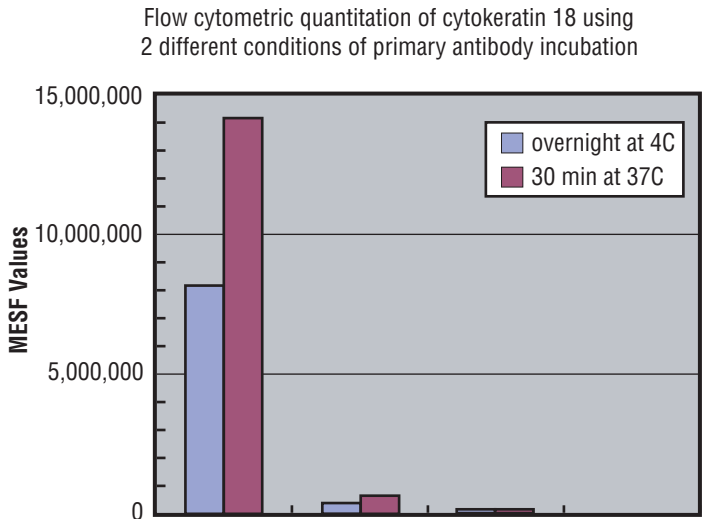

Figure 2. Comparison of marker detection between 2 sets of conditions regarding primary antibody incubation time and temperature (overnight at 4 °C and 30 min at 37 °C). MESF values=molecules of equivalent soluble fluorochrome units based on analysis of fluorescein isothiocyanate (FITC) bead standards; ck18=cytokeratin 18 primary antibody; IgG=mouse immunoglobulin G primary antibody; no prim=no primary antibody used; and no aby=no primary nor secondary antibodies used. Choice of conditions depends on specific experimental parameters and reagents.

WHp8	0 rad	30 rad	60 rad	90 rad
FITC signals with ethanol fixation	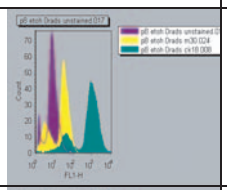	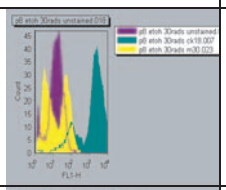	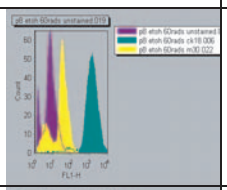	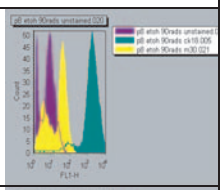
FITC signals with paraformaldehyde fixation	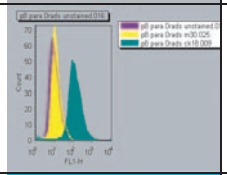	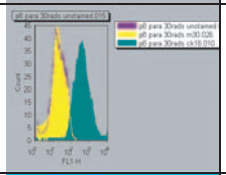	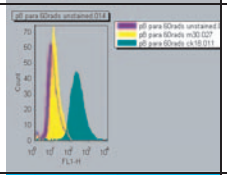	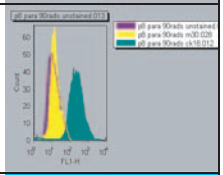
PI signal with ethanol fixation	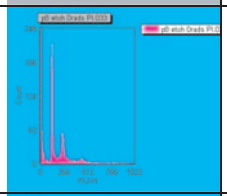	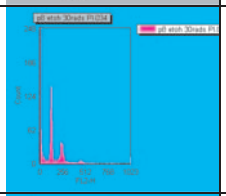	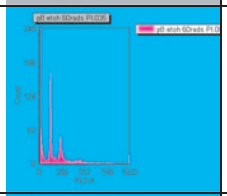	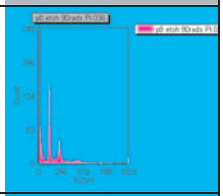
PI signal with paraformaldehyde fixation	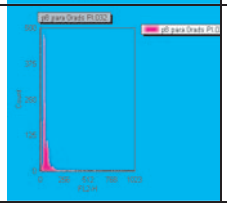	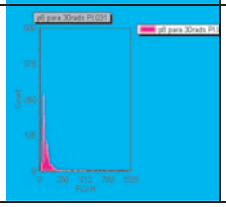	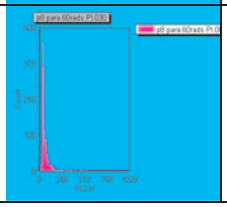	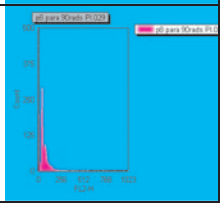

Figure 3. Effect of ethanol and paraformaldehyde fixation on cellular marker detection. With ethanol, fluorescence peak signals are shifted to the right (higher fluorescence intensities) and greater peak discrimination is displayed (bimodal fluorescence peaks). This finding led to a routine comparison between ethanol and paraformaldehyde fixation for specific antibodies. Laser excitation of FITC at 488-nm results in peak fluorescence emission at 530 nm, while propidium iodide (PI) excitation at 488-nm results in 630-nm peak emission.

cleavage product M30 are inversely correlated to radiation dose (fig. 5). Radiation-induced phosphorylation of keratin 18 seemed to protect against its cleavage into M30 fragments (fig. 6). Also with ethanol fixation, levels of IGF–IR were seen to be higher in unirradiated controls than in irradiated cells (fig. 7), while levels of phospho-histone H2AX were inversely correlated with radiation dose (fig. 8). Radiation was seen to lower levels of phosphorylated H2AX linearly (fig. 9). There was no discernible trend with alpha2beta1 integrin levels and radiation dose, either in paraformaldehyde- or ethanol-treated cells, although there was increased detection with paraformaldehyde fixation compared to ethanol fixation. All experiments were run parallel with individual controls for cell permeabilization: such as Tween-20 for phospho-keratin 18, M30, and IGF–IR; Triton X–100 for H2AX; and no permeabilization for alpha2 beta1 integrin. Cellular roles of M30 and H2AX are described below.

WH612/3p8	0 rad	30 rad	60 rad	90 rad
FITC Signals	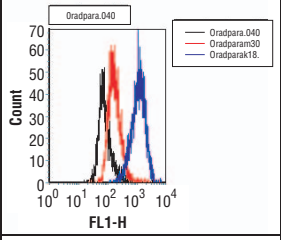	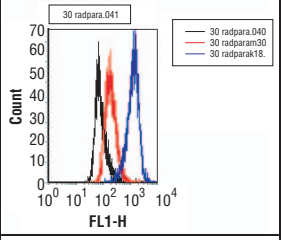	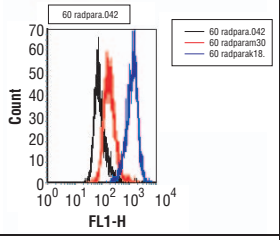	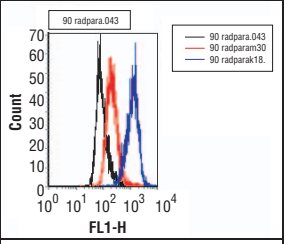
Phospho-k18 (MESF)	183,375.8	246,745.4	251,394.8	233,486
No antibody (MESF)	6,526.4	4,632.2	6,009.8	6,698.6

Figure 4. MESF quantification of phospho-k18 (blue peaks) and controls for absence of antibody (black peaks) at various radiation doses. Levels of phospho-k 18 are higher in irradiated cells (30, 60, and 90 rads) than in unirradiated cells (0 rad).

WH612/3p8	0 rad	30 rads	60 rads	90 rads
FITC Signals	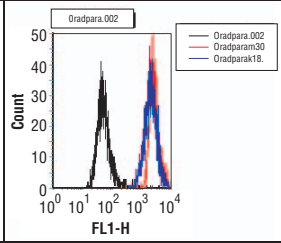	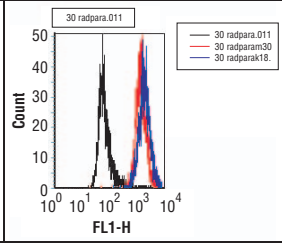	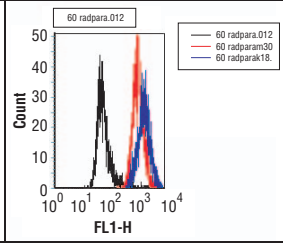	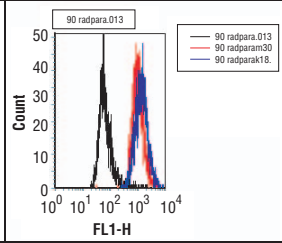
M30 (MESF)	408,957.8	231,247.4	163,917.2	138,431.6
No antibody (MESF)	327.2	2,738	499.2	2,049.2

Figure 5. MESF quantification of M30 (red peaks) and controls for absence of antibody (black peaks) at various radiation doses. Levels of M30 exhibit an inverse proportionality to radiation dose.

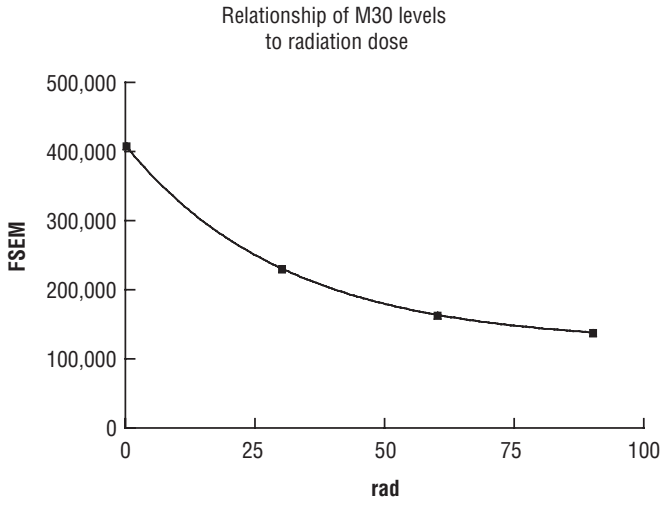

Figure 6. M30 levels decreased with increasing radiation dose, halving at increments of 21.42 rads in this experiment.

Two markers stand out from these preliminary experiments as having potential radiation biodosimetric values: H2AX and M30. Caspase-mediate cleavage of cellular contents occurs early in apoptosis, before annexin V reactivity or positive DNA nick end labelling. Cytokeratin 18 is cleaved by caspase-3, resulting in disassembly of the cytoskeleton and allowing later apoptotic events to proceed. It would therefore be of interest to study caspase-3 activation in these cells in response to radiation dose. Double-strand breaks (DSBs) are generally accepted to be the most biologically significant lesion by which ionizing radiation causes cancer and hereditary disease. When DSBs occur, ATM rapidly phosphorylates the histone H2AX causing it to form foci around the DSBs.[10] The H2AX foci formation around the DSBs serves to recruit DNA repair factors to the site, among them the DNA protein kinases (DNA PKcs). H2AX has been assayed quantitatively[11] and is cited as a sensitive biological dosimeter;[12] however, flow cytometric assays of H2AX have never before been correlated with MESF values, and this correlation may become key to establishing future dose-response models to radiation.

Graphical correlation was attempted between the levels of the two markers (fig. 10); as such, correlations may have future value in determining orders of crosstalk signaling involved.

	0 rad	30 rads	60 rads	90 rads
WH612/3p8 FITC Signals	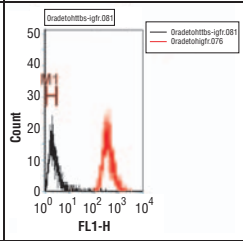	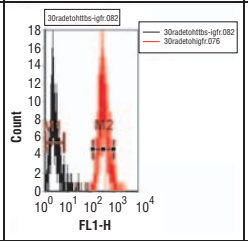	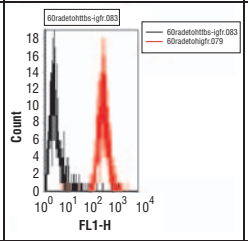	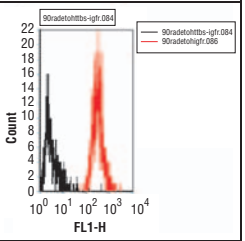
IGF–IR (MESF)	1,242,953	837,248	897,003	1,038,528
No antibody (MESF)	3,823	3,823	3,823	3,823

Figure 7. MESF quantification of insulin-like growth factor I receptor (red peaks) and controls for absence of antibody (black peaks) at various radiation doses. Levels of IGF–IR are higher in unirradiated cells (0 rad) than in irradiated cells (30, 60, and 90 rads).

WH612/3p8	0 rad	30 rads	60 rads	90 rads
FITC signals	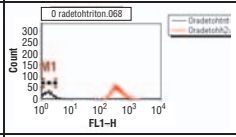	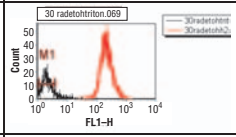	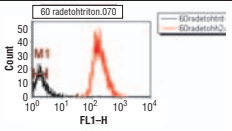	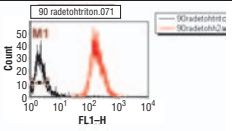
H2AX (MESF)	812,088	667,418	551,053	412,673
No antibody (MESF)	3,823	3,823	678	3,823

Figure 8. MESF quantification of H2AX (red peaks) and controls for absence of antibody (black peaks) at various radiation doses. Levels of H2AX are inversely proportional to radiation dose.

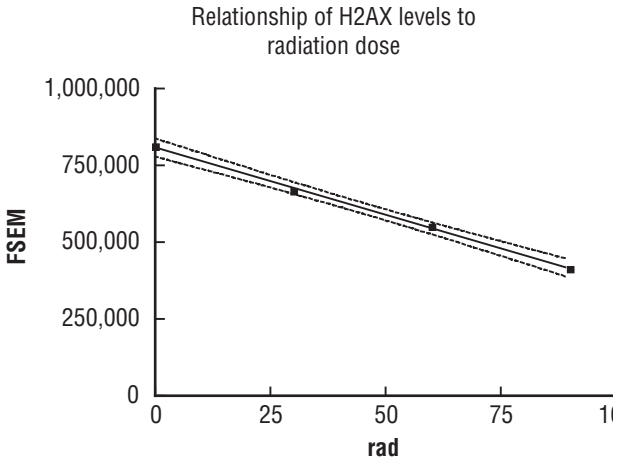

Figure 9. H2AX levels decreased with increasing radiation dose, at the rate of –4,382 MESF units/rad in this experiment.

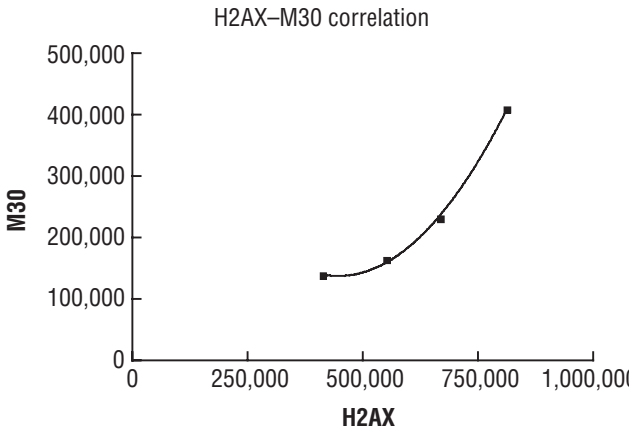

Figure 10. M30 levels rise with H2AX levels in this experiment.

Currently, there are no reports directly linking these two markers; however, it is known that caspase-3 proteolytic activity activates a DSB-generating endonuclease, the DNA Fragmentation Factor 40 (DFF40) or Caspase-activated DNase (CAD).[13] Caspase-3, in turn, can be activated by gamma radiation and may exhibit a dose-dependent response. Therefore, one of the earliest biodosimetric responses of these cells to the radiation doses used may be caspase-3 activation, and downstream effects may depend upon the effect of radiation on interposited signals in the cascade, such as the ataxia telangiectasia mutated (ATM) protein for H2AX and the death effector domain containing DNA binding protein (DEDD) for M30.[14] It will be worthwhile to see if caspase-3 displays a radiation dose-response like its downstream effectors H2AX and M30. Radiogenic damage adds to background deficit of damage such that post-irradiation apoptosis may lead to a pass-8 population reduced in background levels of spontaneous apoptosis, thus reflecting an observed dose-dependent decrease in apoptosis-related markers of M30 and H2AX. A study on the isoendpoints from different sublethal radiation sources on the levels of these markers should also be of immediate interest.

In summary, these postirradiative cells do not experience a change in cell cycle, may exhibit a lesser degree of cytoskeletal turnover, and may incur additional mutations causing subsequent inability to respond to adverse environmental agents. However, these changes do not affect their proliferative capacity and thus they may constitute the very early cell population predisposed to carcinogenic transformation.

Planned Future Work

There is a need to continue the value generated during year one for marker-based radiation risk assessment. Second year experiments are planned towards a consideration of the binding capacities of the target antibodies to determine biodosimetric value. Year two should provide the basis for continued study on the preparation of beads coated with fluorescent-tagged antibodies, where streptavidin may have particular application. In principle, biotin can then be added in quantities suited for calibration before the fluorescent-tagged antibody of interest is added. This approach may be modified in order to accommodate new developments in flow cytometry quantification. The resource requirement for second year activity is outlined in table 1.

Table 1. Resource requirements for the second year activity.

Year Two Resource Requirements				
	Organization	**FTEs (%)**	**Requested Funding ($)**	**Notes**
Personnel				
R. Richmond	MSFC	10	Civil Service	
A. Cruz	NRC	25	16,000	With overhead
Technologist		50	16,000	With overhead
Personnel Total		**85**	**32,000**	
Supplies				
Maintenance of flow cytometer			8,000	
Tissue culture supplies and immunostaining reagents			15,000	
Flow cytometer calibration materials			25,000	
Supplies Total			48,000	
Total Requested Funding			**80,000**	

Publications and Patent Applications

Richmond, R.; Cruz, A.; and Bors, K.: 'Biodosimetry as a New Paradigm for Determination of Radiation Risks and Risk-Mitigation in Astronauts Exposed to Space Radiation," Report submitted to the 75th Aerospace Medical Association (AsMA) Annual Scientific Meeting to be held at the Convention Center in Anchorage, AK, May 6, 2004.

Cruz, A.; Bors, K.; Jansen, H.; and, Richmond, R.: "Radiation Dose-Effects on Cell Cycle, Apoptosis, and Marker Expression of Ataxia Telangiectasia-Heterozygous Human Breast Epithelial Cells," Poster presented at the 5th annual UAH Biological Science Retreat at Guntersville State Park in Guntersville, AL, October 11, 2003.

Cruz, A.: "Three-Dimensional Breast Organoid Formation and Tumor Marker Expression in Microgravity Conditions," Presented at National Research Council Associateship Programs Staff Visit at NASA MSFC, Huntsville, AL, June 6, 2003.

Funding Summary

Table 2 presents the funding summary for this project.

Table 2. Funding summary.

Funding Item	Requested Funding ($)
Year one total request	50,000
Year one expenses	47,115
Personnel	
Coinvestigator (A. Cruz)	14,000
Technologists (K. Bors and H. Jansen)	19,000
Personnel Total	**33,000**
Supplies	
Flow cytometry	714.00
Tissue culture	4,866.14
Assay reagents	2,575.85
Laboratory	2,510.06
Computer	620.64
Office	2,828.31
Supplies Total	**11,286.69**

Status of Investigation

While on schedule with regards to tests for biological effects of radiation, parallel development of ground-based microgravity culture model needed to test for biological effects of simulated microgravity expectedly takes longer. Laboratory personnel support will be arranged for the second year.

Bibliography

[1] Peretz, S.; Jensen, R.; Baserga, R.; and Glazer, P.M.: "ATM-Dependent Expression of the Insulin-Like Growth Factor-I Receptor in a Pathway Regulating Radiation Response," *Proc. Natl. Acad. Sci.*, Vol. 98, No. 4, pp. 1,676–1,681, February 13, 2001.

[2] Prasad, S,; Soldatenkov, V.A.; Srinivasarao, G,; and Dritschilo, A.: "Identification of Keratins 18, 19, and Heat-Shock Protein 90 Beta as Candidate Substrates of Proteolysis During Ionizing Radiation-Induced Apoptosis of Estrogen-Receptor Negative Breast Tumor Cells," *Int. J. Oncol.*, Vol. 13, No. 4, pp. 757–764, October 1998.

[3] Mirzaie-Joniani, H.; Eriksson, D.; Sheikholvaezin, A.; et al.: "Apoptosis Induced by Low-Dose and Low-Dose-Rate Radiation," *Cancer*, Vol. 94, No. 4, pp. 1,210–1,214, February 15, 2002.

[4] MacPhail, S.H.; Banath, J.P.; Yu, T.Y.; et al.: "Expression of Phosphorylated Histone H2AX in Cultured Cell Lines Following Exposure to X-Rays," *Int. J. Radiat. Biol.* Vol. 79, No. 5, pp. 351–358, May 2003.

[5] Carnevali, S.; Mio, T.; Adachi, Y.; et al.: "Gamma Radiation Inhibits Fibroblast-Mediated Collagen Gel Retraction," *Tissue Cell*, Vol. 35, No. 6, pp. 459–469, December 2003.

[6] Hopper, J.L.; and Carlin, J.B.: "Familial Aggregation of a Disease Consequent Upon Correlation Between Relatives in a Risk Factor Measured on a Continuous Scale." *Am. J. Epidemiol.*, Vol. 136, pp. 1,138–1,147, 1992.

[7] Athma, P.; Rappaport, R.; and Swift, M.: "Molecular Genotyping Shows That Ataxia-Telangiectasia Heterozygotes are Predisposed to Breast Cancer," *Cancer Genet. Cytogenet*, Vol. 92, No. 2, pp.130–134, December 1996.

[8] Nagasawa, H.; Cremesti, A.; Kolesnick, R.; et al.: "Involvement of Membrane Signaling in the Bystander Effect in Irradiated Cells." *Cancer Res.*, Vol. 62, No. 9, pp. 2,531–2,534, May 1, 2002.

[9] Kraemer, K.: "Progressive Degenerative Diseases Associated With Defective DNA Repair: 'Xeroderma Pigmentosum and Ataxia Telangiectasia.' In: DNA Repair Processes," W. Nichols; and D. Murphy, (eds.), *Symposia Specialists*, Miami, pp. 37–71, 1977.

[10] Burma, S.; Chen, B.P.; Murphy, M.; et al. "Phosphorylates Histone H2AX in Response to DNA Double-Strand Breaks," *J. Biol. Chem.*, Vol, 276, No. 45, pp. 42,462–42,467, November 9, 2001, and . *Epub.*, Sep 24, 2001.

[11] MacPhail, S.H.; Banath, J.P.; Yu, T.Y.; et al.: "Expression of Phosphorylated Histone H2AX in Cultured Cell Lines Following Exposure to X-Rays." *Int. J. Radiat. Biol.*, Vol. 79, No. 5, pp. 351–358, May 2003.

[12] Pilch, D.R.; Sedelnikova, O.A.; Redon, C.; et al.: 'Characteristics of Gamma-H2AX Foci at DNA Double-Strand Breaks Sites," *Biochem. Cell Biol.*, Vol. 81, No. 3, pp. 123–129, June 2003.

[13] Widlak, P.: "The DFF40/CAD Endonuclease and Its Role in Apoptosis," *Acta. Biochim. Pol.*, Vol. 47, No. 4, pp. 1,037–1,044, 2000.

[14] Lee, J.C.; Schickling, O.; Stegh, A.H.; et al.: "DEDD Regulates Regradation of Intermediate Filaments During Apoptosis," *J. Cell. Biol.*, Vol. 158, No. 6, pp. 1,051–1,066, September 2002.


Space Transportation Directorate
(a) 155 Hz
(b) 334 Hz
(c) 500 Hz
p_{max} [MPa]: 0.5 0.8 1.3 2.0 3.2 5.0 7.9 12.6 19.9 31.5 50.0
NASA MSFC
Center Director's Discretionary Fund
FY 2003
Annual Report

Altitude Compensating Nozzle Design Technology

Project Number: 00–29

Investigators: Joseph Ruf/TD64
David McDaniels/TD63

Purpose

The goal for this Center Director's Discretionary Fund (CDDF) project was to develop the tools and databases to enable rapid trade studies of altitude compensating nozzles (ACN) for future launch systems. This goal required both a broad scope looking at a wide range of possible ACN concepts and a focused scope to look deep into the details of the nature of a specific ACN. To address the broad scope, this CDDF created performance databases for a set of four different ACN configurations all designed for the same launch mission. The focused scope of this CDDF developed design tools and created key performance databases for the aerospike nozzle configuration. Specific objectives of this CDDF were:

- Develop in-house aerodynamic design capability for aerospike nozzles and gain experience testing them.
- Develop nozzle databases for computational fluid dynamics (CFD) verification,.
- Obtain thrust vector control (TVC) performance for an annual aerospike.
- Acquire a performance database for a variety of ACN concepts.

Background

A rocket engine produces high-pressure combustion products. The rocket engine's nozzle expands this high-pressure gas supersonically to significantly increase thrust. If the nozzle expands the gas to a pressure equal to ambient pressure, it is said to be optimally expanded. This is the condition of maximum efficiency and is the design point for the nozzle. If the nozzle expands the gas to a pressure below ambient pressure (overexpanded) or to a pressure above ambient pressure (underexpanded) the thrust produced will be less than optimum. An ACN has design features that recover some of the thrust normally lost during off design operations. These design features might include variable geometry, multiple expansion surfaces, multiple throats, or unrestricted plumes allowing ambient pressure to dictate effective exit area. The most common ACN configurations discussed are the dual bell, expansion deflection, dual expander, mechanically translating nozzle extension, and aerospike.

In the 1960s, quite a bit of development was done for aerospike nozzles. Test data and theory indicate that aerospike nozzles offer significant potential gain in rocket performance relative to standard bell nozzles. This additional performance could be used to launch larger payloads or it could be used to increase the launch system's robustness while maintaining its current performance. Unfortunately, the development of aerospike nozzles stopped in the 1970s. Many of the tools and most of the detailed knowledge required to design aerospikes have been lost to time.

Because aerospike nozzles expand the gases externally, their design and testing is more complicated than a traditional bell nozzle. While the basic performance features of aerospike nozzles are understood, many of the important configuration dependent details are not understood. It is these less well-understood details that can have a significant impact on the performance advantage of an aerospike over a bell nozzle. The same argument applies to other ACN concepts as well. These details must be understood and quantified so that reliable ACN performance data are available for launch vehicle trade studies.

The best approach for understanding all of the significant details is to go through the whole process of designing, testing, and performing posttest analysis of an aerospike nozzle. It is through this end-to-end effort that a much more thorough understanding of aerospike nozzle performance characteristics will be obtained. Much of this knowledge developed for aerospikes would apply directly to other ACN concepts.

One of the key requirements for developing a launch vehicle system is an accurately defined TVC effectiveness map. An aerospike TVC response, like thrust, varies with altitude. Limited historical data for annular nozzles indicate that a TVC can vary by as much as a factor of 10 and at times the effective thrust vector can be opposite to that intended.

Another complicating factor is that the flow over the launch vehicle can affect the aerospike nozzle's performance. Also, from a launch vehicle system standpoint, the best aerospike will probably not be the highest performance nozzle. The evaluation of aerospike nozzles (or any ACN) for potential launch vehicles requires an integrated effort to develop the optimum nozzle for the entire system.

Approach

This CDDF acquired nozzle performance and tool validation datasets on a set of ACNs all designed for the same launch vehicle. Figure 1 is an image of the common design point ACN cold-flow test hardware. This set of nozzles produced nozzle performance data that enabled direct comparison between baseline bell nozzles and common ACN concepts. This was the

Figure 1. Cold-flow test hardware for the common design point altitude compensating nozzles.

broad aspect of this CDDF; to determine the performance of multiple ACN configurations.

The focused aspect of this CDDF was concentrated on the annular aerospike nozzle configuration. One of the major products of this CDDF was the aerospike design and prediction tool (ADAPT). This tool automatically generates aerodynamic contours of aerospike nozzles and then evaluates nozzle performance over a wide range of independent design variables. The ADAPT generates two-dimensional, annular, and axisymmetric cluster aerospike nozzle configurations. The aerospike nozzle designs can have one of three thruster configurations: Two-dimensional slot-throat, annular-throat, and clustered-bell nozzles. Plumetech, a local small business with extensive experience in nozzle design and analysis codes, produced the ADAPT tool.

The aerodynamic contour of an annular, segmented aerospike nozzle was generated with the ADAPT tool. This set of aerodynamic contours was used to develop a test article for the Marshall Space Flight Center (MSFC) Nozzle Test Facility (NTF). This test article provided validation data for the ADAPT tool and CFD codes. In addition, the test article produced a dataset of the TVC effectiveness for annular aerospikes. The model requirements were developed by TD63 and TD64. The test article mechanical design was done by TD62. TD74 conducted the test in the MSFC NTF. A cross section of the test article is shown in figure 2. Figure 3 shows the annular aerospike in the NTF during model build up.

Pretest CFD predictions of the test article's flow field were made for key test points. The CFD compared well with the experimental data.

An opportunity presented itself midway through the year that could not be turned down. During this CDDF, a related task was cut short that was to produce a dual throat linear (DTL) aerospike cold-flow test article. This hardware and the expected test results were relevant to the CDDF goals; therefore, the hardware design and testing were completed under this CDDF. The dual throat means that there were two rows of thrusters on each side of the aerospike. Figure 4 is a cross section of the mechanical design. Figure 5 is an image of the test hardware. This hardware was designed to enable many configuration parametrics: Multiple sidewall fences, multiple base-bleed flow rates, and different altitude modes (both thrusters flowing or only one thruster flowing).

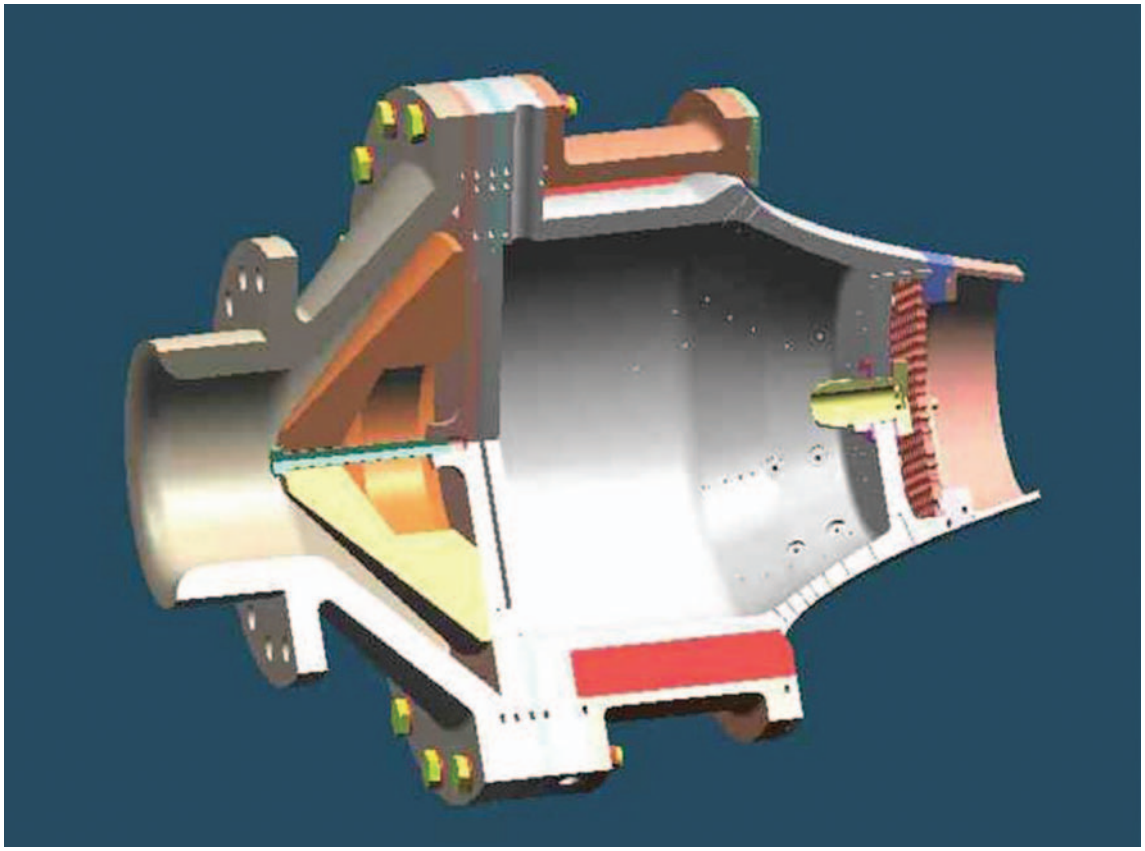

Figure 2. Isometric view of the mechanical design of the annular aerospike nozzle test article.

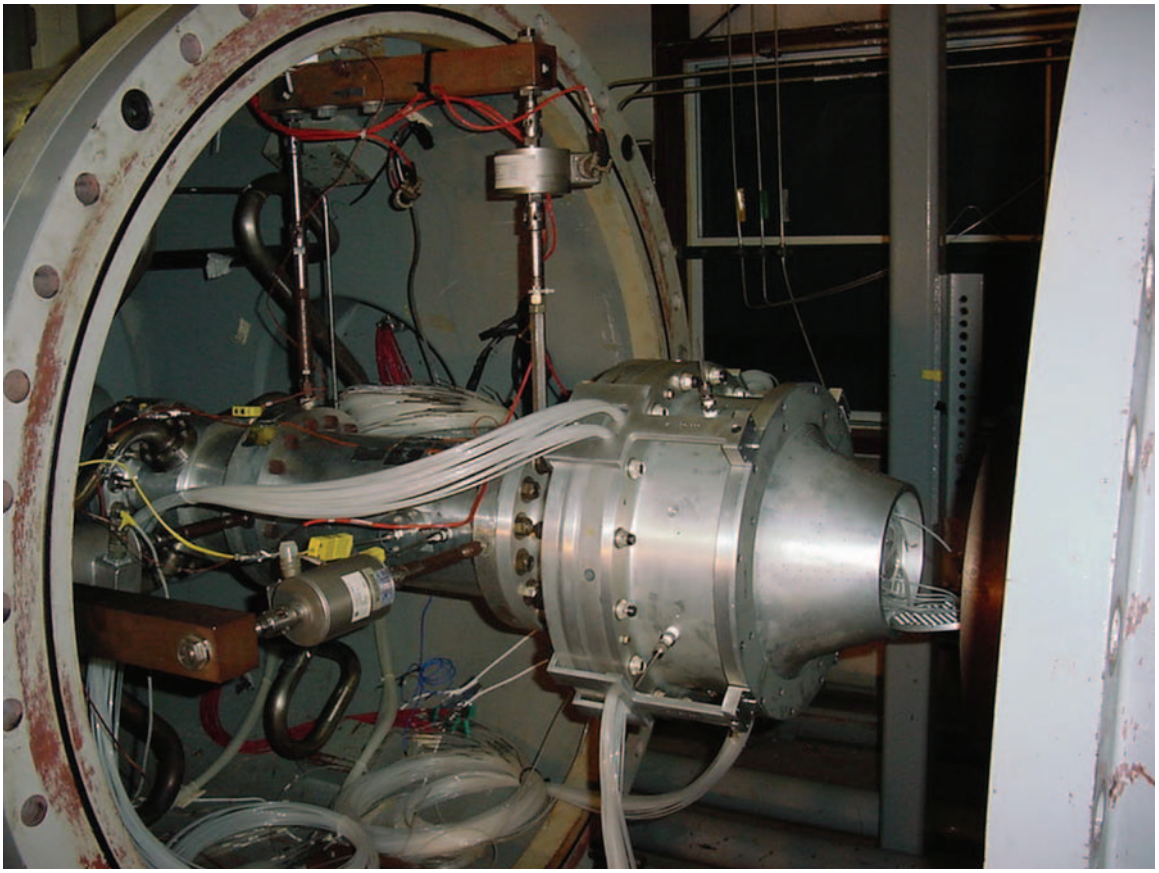

Figure 3. The annular aerospike nozzle test article being installed in the Nozzle Test Facility.

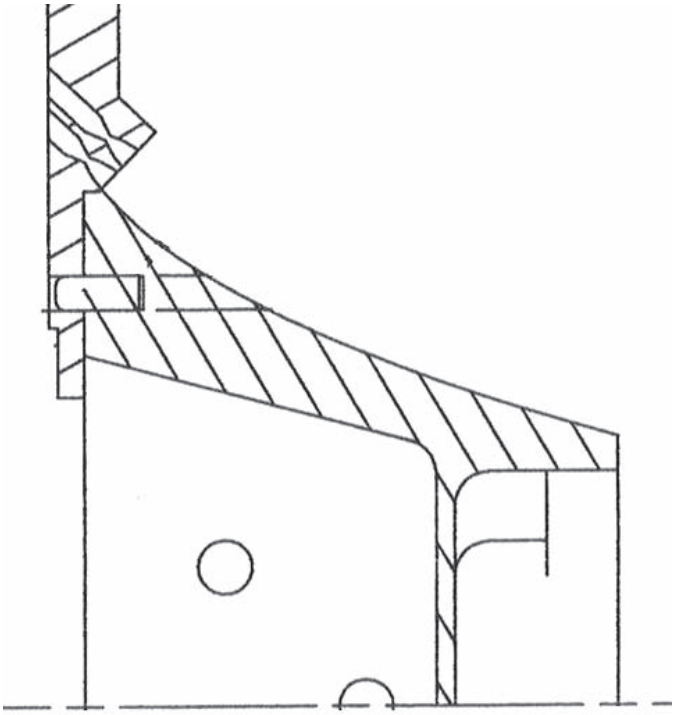

Figure 4. Cross section of the dual-throat linear aerospike.

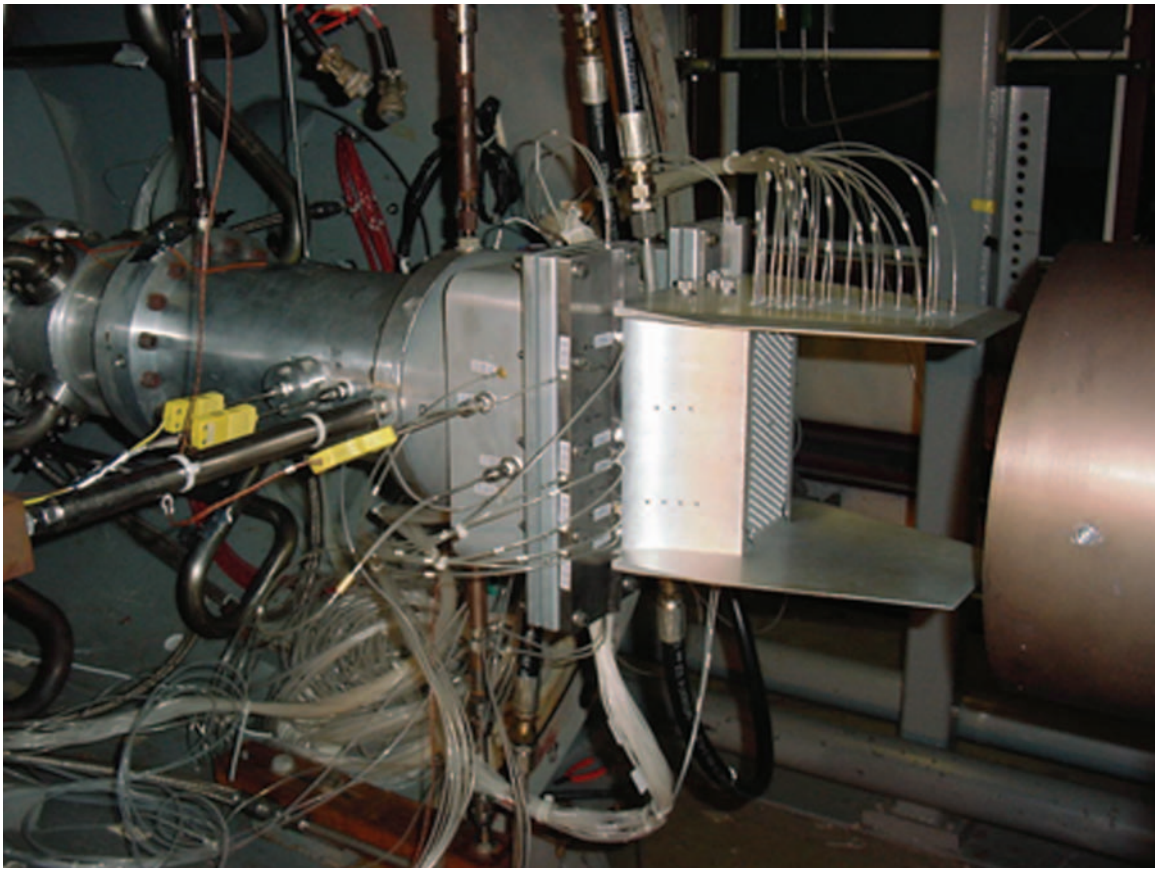

Figure 5. The dual-throat linear aerospike installed in the Nozzle Test Facility.

Pretest CFD was performed on the DTL to benchmark the CFD code and modeling approach.

Accomplishments

All of the six Common Design Point (CDP) nozzles were tested in the NTF. The test data for some of the ACN concepts have been analyzed. Preliminary results were presented in references 1 and 2. Further data reduction and analysis will be conducted as time allows. The test data will be published in NASA Technical Memoranda.

The ADAPT tool was completed. The tool and its documentation were delivered. ADAPT was tested for functionality. The annular aerospike was fabricated and tested. This test article was unique in that it allowed for differential throttling of the chamber pressure to induce TVC. The data analysis and interpretation of the experimental data for the annular aerospike has been completed. This test completed most of its key objectives. One was to provide test data to verify the modeling techniques used for estimating TVC forces produced by differential throttling. Much additional nozzle performance data was obtained. A thorough test report is being written. It will be published as a NASA Technical Memorandum. The test results have already been presented once in preliminary form[3] and will be presented in detail[4] in May 2004.

The DTL mechanical design was completed, fabricated, and tested for axial performance for many configuration parametrics. Several of these were extensively analyzed with pretest CFD. The agreement between the CFD and the experimental data was excellent. The CFD and preliminary experimental results were presented in references 5 and 6. Further data reduction and analysis of the experimental data is required. This will be conducted as time allows. The experimental results will be published as a NASA Technical Memorandum.

Planned Future Work

This task is complete. More thorough documentation of the common design point ACNs, the annular aerospike, and the dual-throat aerospike will be completed as time allows.

Publications and Patent Applications

No patents have been produced. The ADAPT final report[6] was provided by Plumetech to MSFC/TD64. Several papers were published and are listed as References 1 through 5 and 7.

FY 2001 Funding Summary

The summation of this CDDF funding over its 3 years was $235,000.

Status of Investigation

The investigation is complete except for the detailed final test reports that will be completed as time allows.

References:

[1] McDaniels, D.M.; and Ruf , J.H.: “Altitude Compensating Nozzle Concept Comparison Test Status,” JANNAF 38th Combustion Subcommittee Meeting, April 2002.

[2] McDaniels, D.M.; and Ruf, J.H.: “Common Design Point Altitude Compensating Nozzle Test Data Status,” MSFC Fall Fluids Workshop, November 2002.

[3] Ruf, J.H.; and McDaniels, D.M.: “Experimental Results for an Annular Aerospike With Differential Throttling,” 5th International Symposium on Liquid Space Propulsion, October 2003.

[4] Ruf, J.H.; and McDaniels, D.M.: “Experimental Results for an Annular Aerospike Nozzle With Differential Throttling,” JANNAF 52nd Joint Propulsion Meeting, May 2004.

[5] Ruf, J.H.; and McDaniels, D.M.: “Computational and Experimental Results for a Dual Throat Linear Aerospike,” MSFC Fall Fluids Workshop, November 2002.

[6] Smith, S.D.: “ Final Report: Aerospike Design and Performance Tool,” Contract ESI–SUB–002, Prime Contract NAS8–00002, Plumetech, Huntsville, AL., August 6, 2001.

[7] Ruf, J.H.; and McDaniels, D.M.: “Computational and Experimental Results for a Dual Throat Linear Aerospike,”14th Annual Propulsion Engineering Research Center Symposium, December 2002.

Automated Postprocessing

Project Number: 02–25

Investigator: Suzanne Miller Dorney/TD64

Purpose

Computational Fluid Dynamics (CFD) is commonly used in the design phase of major engine components. In cases where an engine component does not operate as designed, CDF is one of the tools used in the failure analysis phase. The heavy reliance on CFD analyses has resulted in large increases in both the number of simulations that need to be run as well as the analysis time to evaluate the results. To meet this increased demand, a series of automated tools has been developed and expanded to aid in the preprocessing and postprocessing phases of a CFD analysis.

Background

Setting up a CFD simulation and analyzing the results is not a trivial process. It is important to realize that the result of a CFD analysis is not a single number. Concisely stated, it is a set of flow values for each grid point used in the simulation. A typical simulation may require a geometric grid consisting of millions of points to accurately model the flow field in, or around, the component being analyzed. Therefore, in order to efficiently and effectively use the results of a CFD simulation, visualization tools are often used to create graphical images of the results. These tools are used in all stages of a CFD simulation, including preprocessing, interim processing, and postprocessing. Each of these stages requires visualization tools that allow one to examine the geometry of the component, as well as the partial or final results of a computational simulation. A careful analysis of the resulting plots and images can enable a trained engineer to better understand the physics of how the fluid flow is interacting with the physical device. Of particular interest are detecting features such as shocks, areas of secondary flow, and vortices in order to determine areas of high stress and/or loss.

The two main objectives of this work were to add to the current visualization capabilities used to analyze CFD results and to advance the state-of-the-art in visualization by investigating possible applications of feature extraction capabilities to automatically interrogate a CFD solution. A third objective was to aid in the ability to efficiently conduct a full parametric CFD study by automating as much of the case setup and analysis of the results as possible.

Approach

The initial approach used to accomplish the objectives of this task was to work closely with the engineers in the Applied Fluid Dynamics Group, TD64, to determine the processes they use to perform the different steps of a CFD simulation. As this process is better understood, the areas that can be automated become clear and the additional visualization capabilities that are needed can be identified. Development of the automated feature extraction utilities was conducted with Mr. Robert Haimes of the Massachusetts Institute of Technology (MIT). Mr. Haimes has considerable knowledge in the development and application of automated feature extraction utilities.[1–4]

Accomplishments

The ability to easily generate and show animations is useful since it is often needed for analysis and presentation purposes. Through the development of the tool Animator, such a capability exists and is used extensively by engineers in TD64. To further add to the usefulness of this tool, its capabilities were extended to work with unstructured data sets as well as the current structured data sets.

Other capabilities were also added to Animator such as the display of separation lines in contour plots; the capability to calculate additional functions for contour plots such as blockage, bulk velocity, and density gradient; and Cp. The ability to generate images referred to as contact sheets was also added. A contact sheet consists of several different views of the same image so that a three-dimensional result can be displayed with more information than a single two-dimensional image. Figure 1 shows an example contact sheet of a turbine.

In the area of automated feature extraction, the ability to visualize secondary flows was implemented. The concept of secondary flow in turbomachinery is not well defined, but commonly referenced. Some attempts at rigorously defining this idea include the following:

- "…component of absolute vorticity in the direction of the relative streamline."[5]
- Secondary flow in broad terms means flow at right angles to the intended primary flow.[6]
- Due to viscous effects, end walls divert primary flow produced by blades and vanes, to give rise to what has come to be called secondary flow.[7]

Of the three definitions listed above, only the second provides a definition that could be made operational. The notion of primary flow is what is required and can be defined. Unfortunately, by the time one gets a CFD solution, the notion of intended is lost.

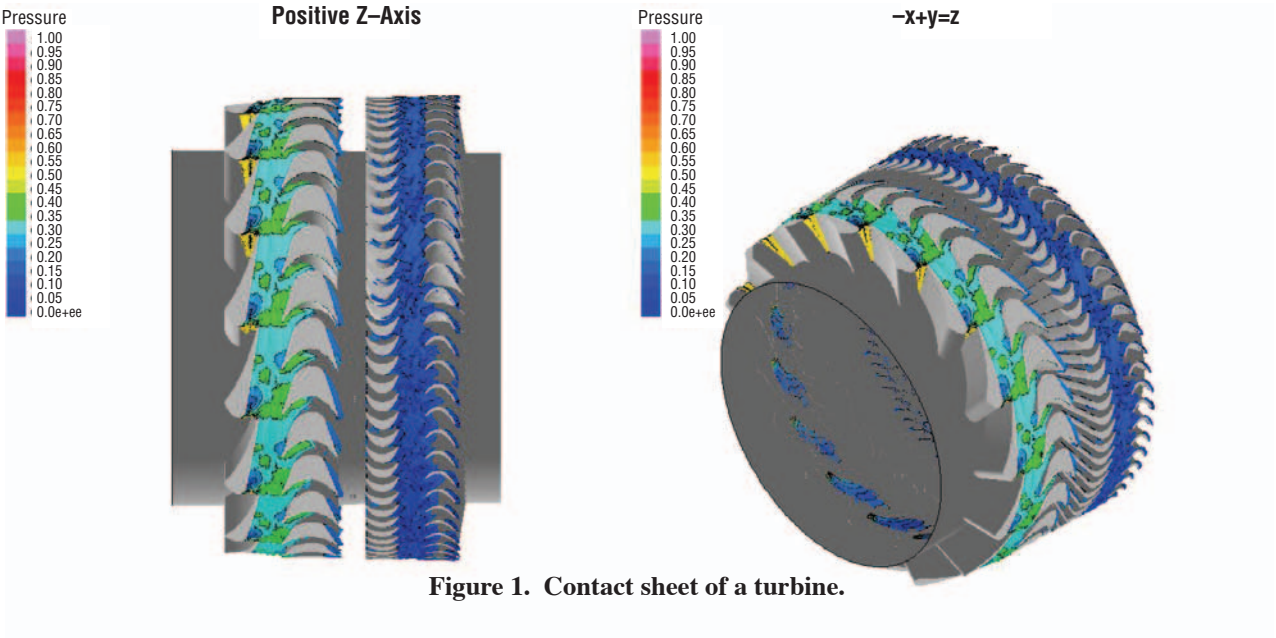

Figure 1. Contact sheet of a turbine.

The desire to view perturbations from the primary flow direction can give insight into the viscous, reverse flow, and vertical effects that deviate from the design. To this end, it is obviously desirable to be able to generate two-dimensional vector plots that display the secondary flow, given a CFD solution. Figure 2 shows an example of a vortex chamber and the resulting secondary flow.

The capability to visualize vortex cores was also implemented. Figure 3 shows the vortex cores within the same vortex chamber shown in figure 2.

A prototype utility was developed as part of a 2002 Center Director's Discretionary Fund (CDDF) project to aid in the management of a parametric study. In a parametric study, a range of geometric and flow conditions are analyzed and compared in order to determine the best design and flow conditions. In such a study, it is not uncommon to run several hundred different cases. This task can quickly become unmanageable and error prone. Prototype tools were developed to directly support an injector parametric study being lead by P. Kevin Tucker, of TD64. In the initial stage of this study, 52 separate simulations were to be conducted. Automated tools were used in setting up and organizing each case, the monitoring of the cases as the computer simulations were running, and the final postprocessing of the results. In 2003, this study was again performed with a different set of flow conditions. It is important to note that this study would not have been redone if it were not for the presence of this set of automated tools. To take advantage of running the multiple cases on remote computers, a new tool was developed, SetUpCases. This new tool can perform the following tasks:

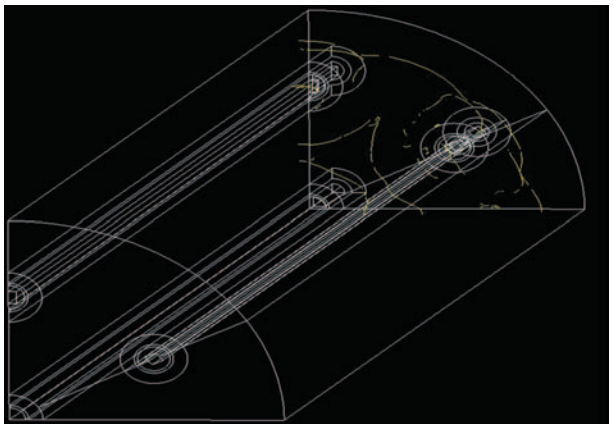

Figure 2. A vortex chamber and the resulting secondary flow.

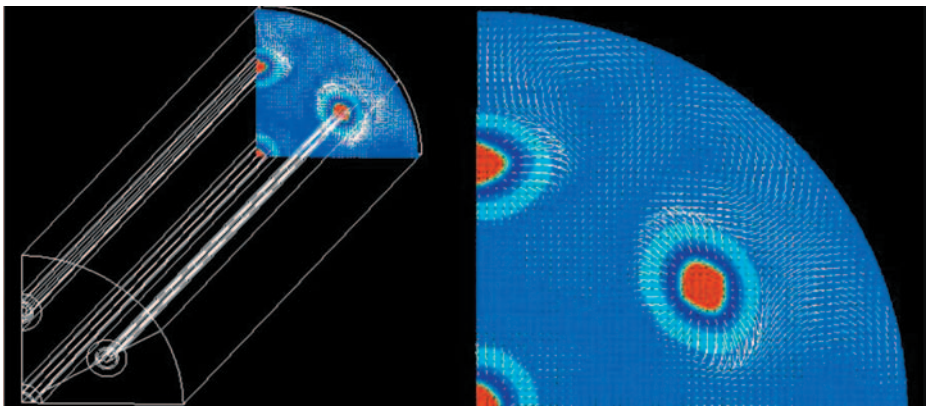

Figure 3. Vortex cores within the same vortex chamber shown in figure 2.

- Create directories on remote computers.
- Transfer the necessary files into the newly created directories.
- Start simulations.

The tool CheckCase, used in the previous task to validate the geometry of each grid against the predefined specifications for each case, was eliminated and its capabilities were added to the postprocessing tool AutoPlot. This was done so that the case-specific assumptions could be removed and a more general tool could be used.

Planned Future Work

Because of the success of the initial automated feature extraction utilities, work will continue with Mr. Robert Haimes of MIT. This work will be funded via a 2004 CDDF. The support work for parametric studies will also continue under the 2004 CDDF.

Publications and Patent Applications

At this time, no patent applications have been made for any of the tools developed under this CDDF. Dr. Suzanne M. Dorney presented a paper at the 39th AIAA/ASME/SAE/ASEE Joint Propulsion Conference in July 2003.[8]

Funding Summary

In addition to the 1/3 full time equivalents (FTEs) funded by this CDDF the amount of $50,000 was given to Mr. Robert Haimes of MIT as a grant to aid in the development and implementation of the automated feature extraction capabilities.

Status of Investigation

All work specified in this CDDF has been completed.

References

[1] Lovely, D.; and Haimes, R.: "Shock Detection From Computational Fluid Dynamics Results," *AIAA Paper No. 99–3285*, Norfolk, VA, June, 1999.

[2] Haimes, R.: "Using Residence Time for the Extraction of Recirculation Regions," *AIAA Paper No. 99–3291*, Norfolk, VA, June, 1999.

[3] Haimes, R.; and Kenwright, D.: "On the Velocity Gradient Tensor and Fluid Feature Extraction," *AIAA Paper No. 99-3288*, Norfolk, VA, June, 1999.

[4] Haimes, R.; and Jordan, K.E.: "A Tractable Approach to Understanding the Results From Large-Scale 3D Transient Simulations," *AIAA Paper No. 2001–0918*, Reno, NV, January. 2001.

[5] Hawthorne, Cambridge University Report, CUED/A-Turbo/TR 63, 1974.

[6] Cumpsty, N.A.C.: *Compressor Aerodynamics*, ISBN 0–582–01364–X, Longman Science and Technology, United Kingdom, p. 316, 1989.

[7] Langston, L.S. "Secondary Flows in Axial Turbines—A Review," *Annals New York Academy of Sciences*, May 2001.

[8] Dorney, S.M.: "CFD Process Pre- and Post-processing Automation in Support of Space Propulsion," *AIAA Paper No.2003–5051*, Huntsville, AL, July 2003.

Liquid Oxygen/Liquid Hydrocarbon Combustion Wave Ignition

Project Number: 02–34

Investigator: Brad Bullard/TD61

Purpose

The goal of this continuing Center Director's Discretionary Fund (CDDF) investigation is to expand the capability of combustion wave ignition (CWI) systems such that they are able to use liquid hydrocarbon fuels. This will allow the igniter in hydrocarbon-fueled, multithruster liquid rocket engines (LREs) to employ the same propellants as the thrust chambers, eliminating the need to carry additional propellants solely for the ignition system.

Background

The basic CWI concept, in which a single spark ignites a combustible mixture in a pressurized chamber and simultaneously propagates a detonation wave to multiple thrusters, is relatively simple to implement and requires minimal hardware. This makes the system very cost efficient and reliable when compared to systems in which separate spark initiators are required at each thruster, any of which could fail to light at startup. Reusability is also maximized due to the low part count and relatively benign operating environment since the system operates at pressures substantially below the chamber pressure and is only exposed to combustion gas temperatures for a very brief time before purges activate. Additional benefits of this ignition scheme include restart capability, small system volume, and installation/packaging flexibility. A CWI was successfully demonstrated on the X–33 engine.

Although CWI systems have proven to be a compact, lightweight, and reliable means of igniting multiple thrust chambers, these systems typically require gaseous reactants, which limit their applicability to many engine systems unless additional propellants are stored solely for the igniter. A CWI system capable of operation with the same liquid propellants as the thrust chambers that they support would eliminate the need of carrying additional propellants solely for operating the ignition system. They would also have an ample supply of reactants available should the need arise for relighting the engine. The ability to produce a detonable mixture from the liquid main propellants that is suitable for a CWI system was the focus of this research.

Approach

Originally, this work was intended to be a 4-year effort divided among the Marshall Space Flight Center (MSFC), the Glenn Research Center (GRC), a private hardware development contractor, and a university. The hardware development contractor and the university would work together to develop a demonstration or proof-of-concept system; MSFC would then continue with the development of a flight-like system.

GRC was to be funded through different channels to conduct a parallel investigation utilizing fine mist atomization, while also providing engineering support to this effort. However, several procurement difficulties were encountered while attempting to award the hardware development contract, resulting in the cancellation of this portion of the task. In addition, GRC funding did not come through. These events necessitated significant modifications to the approach.

The university grant was awarded to Pennsylvania State University (PSU). The initial PSU scope of work was for numerical and analytical investigations into the startup and transient operation of a CWI system, plus modeling support to the hardware development contractor as required to help resolve any flow-related issues that they encountered. After loss of the development contract, the funding intended for that effort was rolled into the PSU grant and additional modeling work was commissioned.

Accomplishments

The specific tasks originally given to PSU were as follows:

- Determine the minimum ignition energy required to ignite a liquid oxygen (LOX)/JP–7 rocket thruster.
- Model ignition of the premixed gases in a CWI system and the subsequent evolution into a propagating deflagration, then detonation wave, while considering the effects of cell size, tube diameter, and induction length.
- Model the energy losses in the system during transmission that could result in a failure to deliver the required ignition energy.
- Provide analytical/modeling support to the hardware development effort that was to be conducted in parallel with this work (no longer applicable).

During the fiscal year (FY) 2002 period of performance, the PSU researchers (Drs. Vigor Yang and Jeong-Yeol Choi) were able to generate detailed numerical models of the transient processes involved in a gaseous-oxygen (GOX), gaseous-hydrocarbon CWI system. The models accounted for the detailed chemical kinetic processes and were able to accurately reproduce the familiar smoke-foil patterns characteristic of detonation propagation in a constant-area duct. A numerical image of these phenomena is shown in figure 6 of reference 1, where the cellular structure can be seen in the time-lapse images.

Detonation transmission into the branches of a piping network was also modeled, but the wave consistently degraded into a deflagration for each of the cases modeled. Figures 1–7 show time-lapse images in the form of numerical Schlieren (figs. 1–6) and smoke foil or maximum pressure distribution (fig. 7) plots for an incoming detonation wave passing through a branched intersection. Inset pictures to the left and right of the branch tube in each time slice are enlarged frames near the wave front in the branch and horizontal tubes, respectively. It may be seen that, although the wave continuing through the intersection begins to degrade into a deflagration, it is ultimately able to reform into a detonation downstream of the intersection. However, the reaction zone in the branch tube becomes increasingly detached from the leading shock after encountering the expansion corner and ultimately degenerates into a deflagration.

Video clips of the propagating detonation, as well as that of a standing detonation in a uniform tube with incoming gas approaching the wave at the Chapman-Jouget velocity, were provided as deliverables under the grant.

The FY 2002 CDDF annual report for this task[1] contains more details of the work performed during the FY 2002 period of performance.

During FY 2003, the personnel conducting this work at PSU changed. The new researchers were Dr. Vigor Yang and Fuhua Ma.

In the follow-on (FY 2003) work for this task, the following was requested of PSU:

- Provide additional modeling focus in the region around the tube junctions in order to understand the mechanisms that dictate whether a detonation will survive or degenerate in the branch tube.
- Perform code refinements where possible in order to speed up the computation efficiency.
- Determine the minimum ignition energy required to ignite a LOX/liquid JP–7 thruster at conditions provided by the Contracting Officer's Technical Representative (COTR).
- Provide a report summarizing the current state-of-the-art in modeling techniques and stabilization devices being used in the field of liquid rocket engine combustion instability, as well as the relative strengths and weaknesses of each.

Figure 1. Snapshot prior to arrival at the branch.

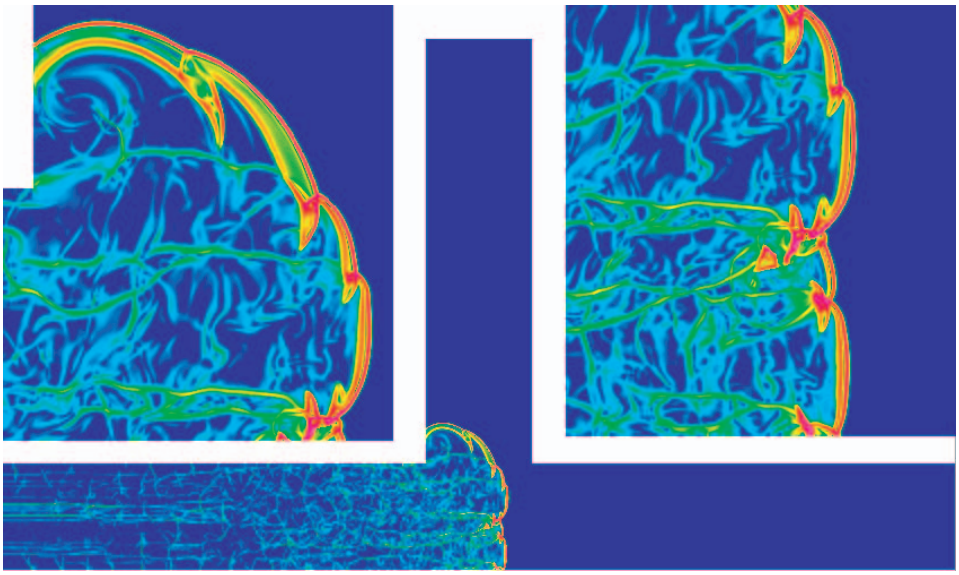

Figure 2. Snapshot immediately after passing the intersection corner.

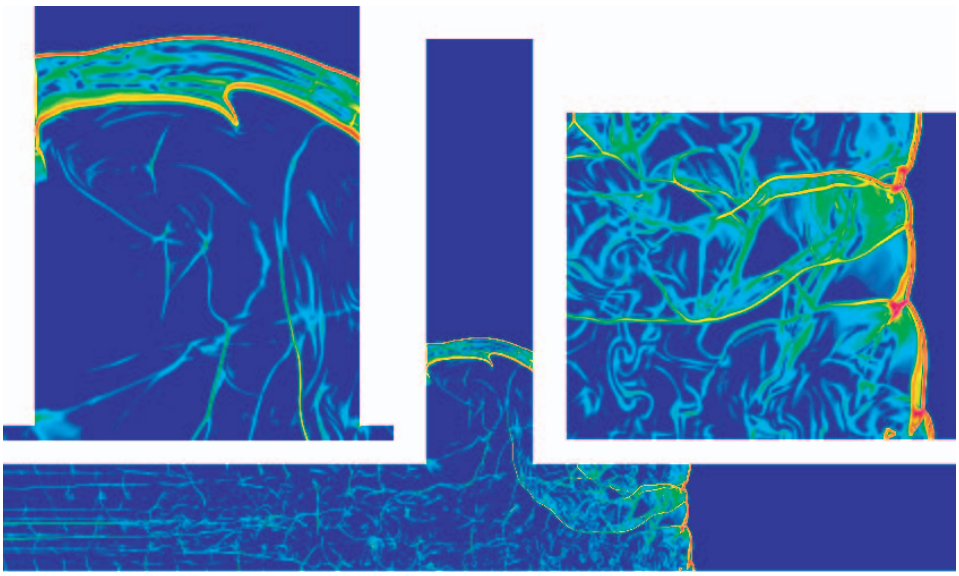

Figure 3. Snapshot after passing the intersection.

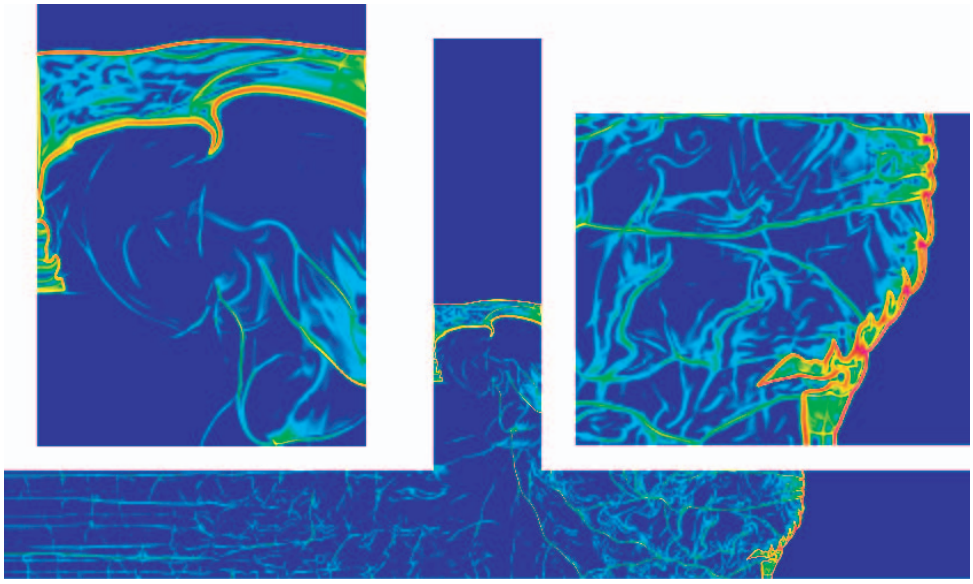

Figure 4. Snapshot of degenerated detonation wave front.

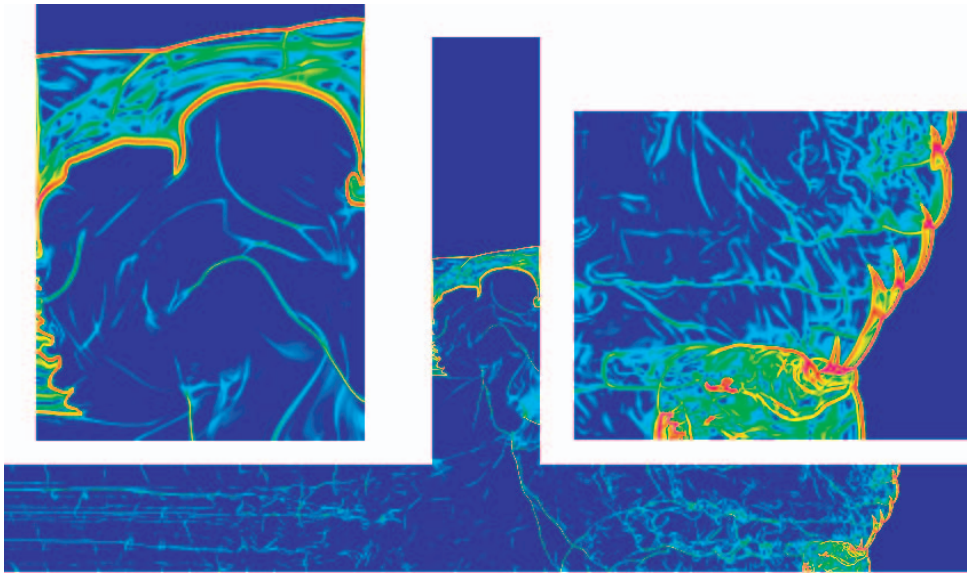

Figure 5. Snapshot of reinitiated detonation wave front.

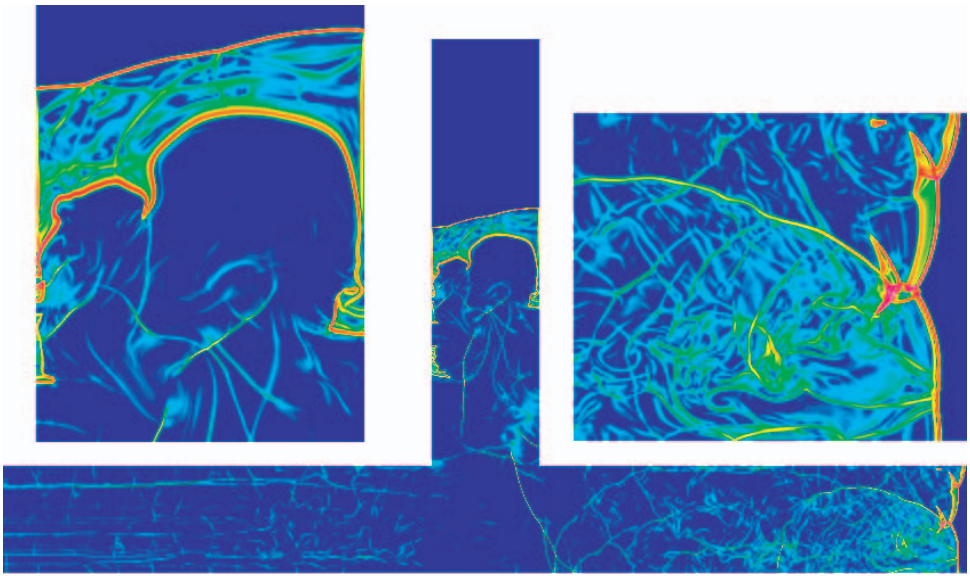

Figure 6. Snapshot of reinitiated detonation wave developing as a regular detonation wave front.

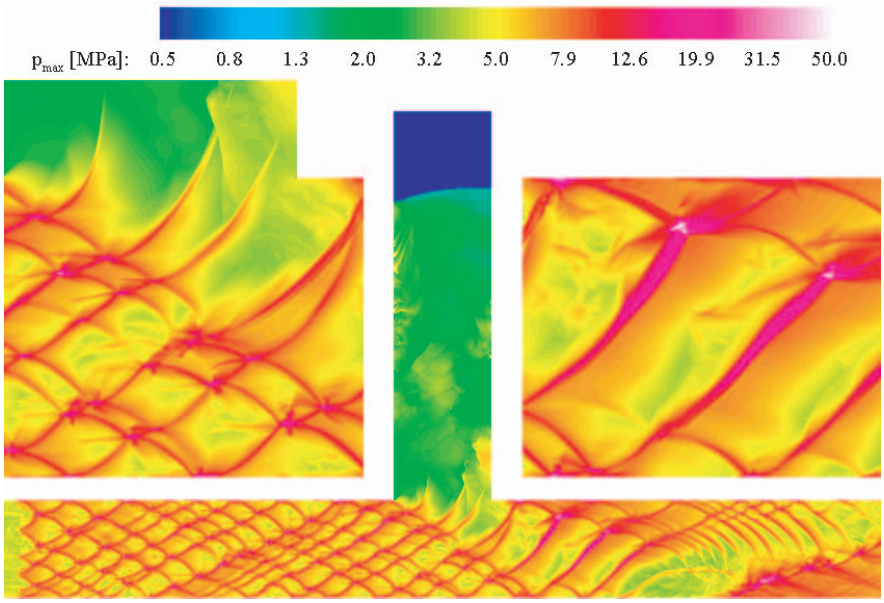

Figure 7. Numerical smoked-foil plot (max pressure) of a two-dimensional detonation in T-shaped flame tube.

Heat loss effects during wave propagation, an issue raised in the initial statement of work, were found to be negligible due to the rapid transit time of the wave.

During the current period of performance, successful transmission of a sustained detonation wave into a branch tube, oriented at a 90-degree angle to the main line, was achieved. It was found that the branch tube diameter plays a significant role in determining whether or not the wave will degenerate upon encountering the expansion corner and propagate into the branch. Branch tube diameters of 0.5 and 1 mm both produced successful transitions through a T junction, whereas the tube diameter modeled in FY 2002 was much larger (on the order of 1 cm or larger). Timelapse images of the propagation through a 1-mm branch are presented in figure 8.

In figure 8, it can be observed that the wave continuing through the intersection sustains itself as a detonation and, in contrast to the work presented earlier, does not exhibit the initial tendency toward a decoupling of the shock and combustion wave. In the perpendicular branch section, the leading shock and reaction zone do begin to decouple when they first encounter the left-hand corner of the tube; but, upon reflection of the shock to the opposite side, the detonation reforms and is sustained.

Two branching scenerios have been investigated to date: Varying branch tube diameter and multiple branches with variable spacing. All have been successful. Propagation through a tube with four branches is shown in figure 9. All calculations begin with an initial condition of P=1 atm and T=300 K and the Chapman-Jouget solution for the propellants used GOX and catalytically decomposed JP–7 is P=33.4 atm and T=3,835 K.

A code refinement was also made early in this reporting period. Extremely small grid sizes (anywhere from 25 nm to 0.1 mm) and time steps (eight from 10–12 s) are required to model the complex detonation propagation process, which can translate into enormous run times for each case. Due to successful parallelization of the analysis code, PSU was able to reduce the turnaround time for their most time-consuming analyses from approximately 1 month to less than a day, greatly increasing the number of model scenarios that can be investigated.

Relative to task 4 in the FY 2003 statement of work, two reports have been received to date detailing progress made on this effort and are available upon request.

Planned Future Work

Due to a late award date for the follow-on work, the current investigation will continue until September 30, 2004. During this time, they will perform the following:

- Continue to investigate the factors influencing detonation passage through an intersection, increasing branch diameter until the critical breakdown diameter is reached.
- Define the minimum ignition energy required to light a LOX/JP–7 thruster based on rocket chamber conditions provided by the MSFC COTR.

Publications and Patent Applications

Work accomplished on this CDDF was presented in AIAA 2003–5207, as well as at the 14th Annual Pennsylvania State University Propulsion Engineering Research Center Symposium in 2002.

No patents have been applied for under this CDDF.

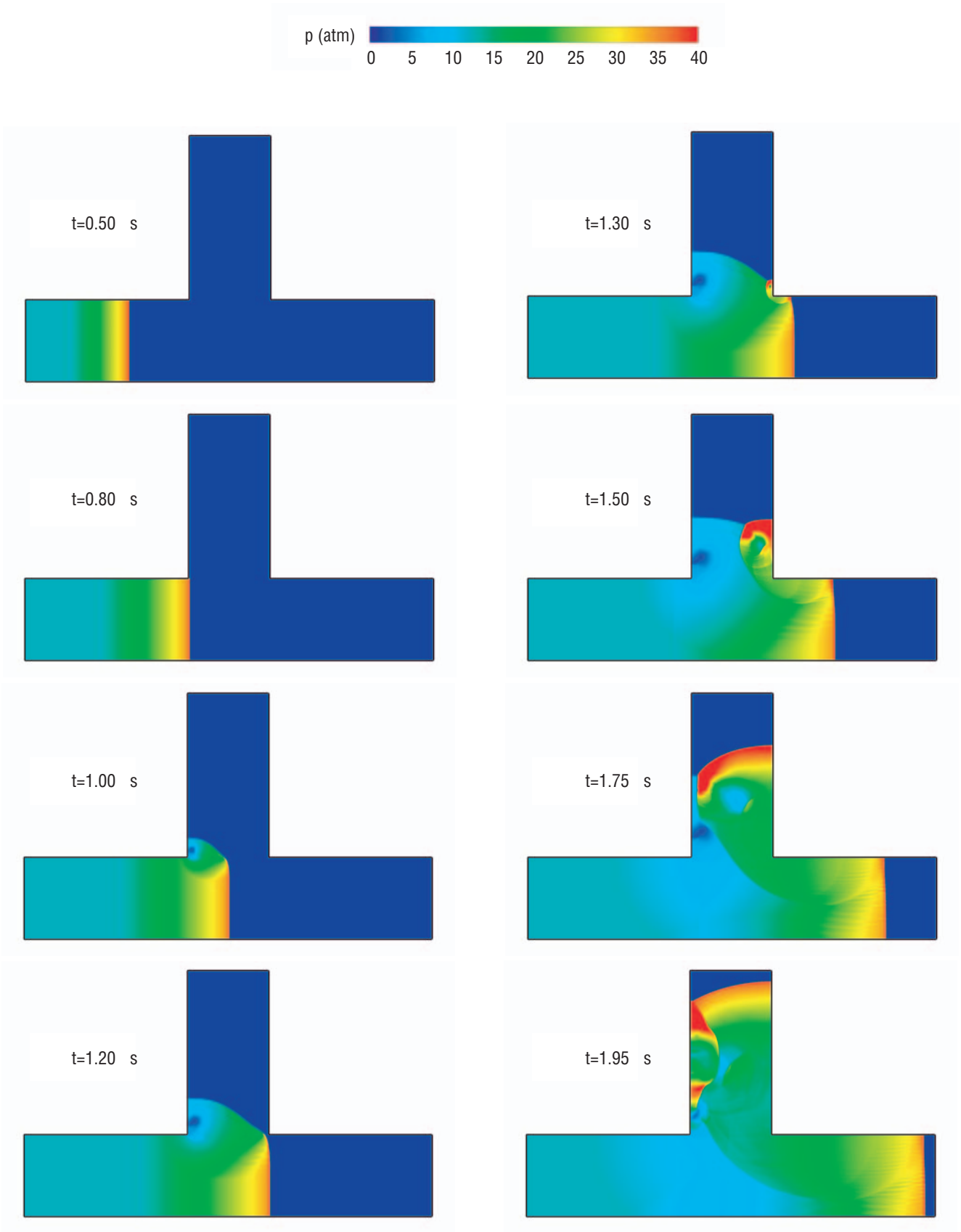

Figure 8. Time evolution of pressure field, single branch tube with width of 1 mm.

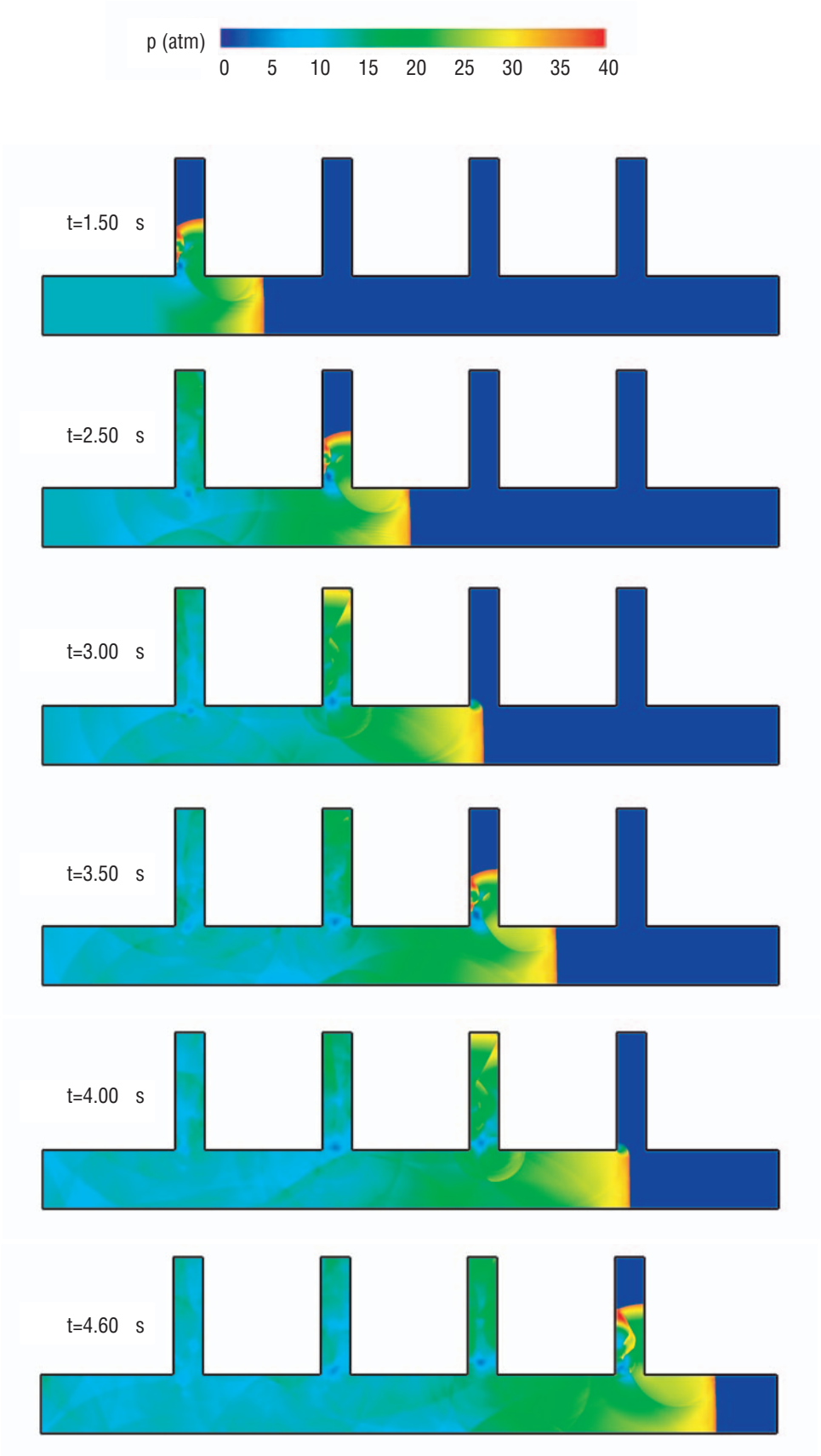

Figure 9. Time evolution of pressure field, four branch tubes.

Funding Summary

Table 1 identifies the funding for this project.

Table 1. Funding summary.

Expenditure	Amount ($)	Comments
Total CDDF allocation	225,000	Total funding allocated
Analysis support grant	–5,000	PSU grant for FY 2002
Analysis support grant	–150,000	PSU grant for FY 2003
Development contract	00	Never awarded
Total remaining funds	00	

Status of Investigation

The PSU research is due to conclude on September 30, 2004.

Reference

[1] "LOX / Liquid Hydrocarbon Combustion Wave Ignition," *CDDF Annual Report for Task 279–02–34*, 2002.

Development of a Fundamental Database on High-Pressure Flames Using a Lab-Scale Combuster

Project Number: **03–01**

Investigators: **John A. Blevins/TD40**
Christopher I. Morris/TD40

Background

The next generation of space launch vehicles will require unprecedented levels of liquid rocket engines' reliability and reusability in order to make significant improvements in both cost and safety. However, there remains a lack of detailed understanding of the high-pressure combustion environment characteristic of liquid rocket combustion chambers and preburners.

Purpose

The high-pressure liquid rocket combustion environment consists of a broad range of phenomena occurring over a wide range of length scales. An understanding of these phenomena is critical to accurate prediction of mixing lengths, energy release, wall and injector-plate heat transfer, and other parameters of decisive engineering importance in rocket engine design. A full-scale rocket engine consists of many injector elements, each of which produces a complex turbulent diffusion flame. The flow field is strongly influenced by supercritical effects at the high pressures characteristic of booster-class liquid rocket engines. Accurate understanding of the evaporation and combustion of oxidizer (or fuel) droplets and ligaments under supercritical conditions is of key importance to modeling these flames.

Approach

The research work discussed in this interim report has encompassed a review and initial application of advanced optical diagnostics for the harsh combustion environment. At present, the application of the diagnostics is limited to known environments, either noncombusting or with a flat flame burner that proposes to produce known flame conditions of approximately an adiabatic premixed diffusion flame. The primary diagnostic tool employed during the first year study is Raman scattering.

Visible laser Raman scattering thermometry has been demonstrated in a hydrogen/air combustor up to 20 atm.[1,2] In that investigation, the ratio of the intensities of two rotational Stokes Raman hydrogen spectral lines was used to calculate a product gas temperature of 1,889 K from a ϕ=1.34-microtube burner, just above the flame zone. The experimental spectral profile of the Stokes Raman vibrational hydrogen and nitrogen bands were compared to modeled bands at the measured temperature, and qualitative agreement was observed. For these tests, an injection seeded, Q-switched, frequency doubled, Nd:YAG laser operating at approximately 1 J per pulse was used. The maximum energy per pulse was reduced by 90 percent by pulse stretching optics that changed the nominal pulse duration from 8.4 ns to 75 ns. This was done to prevent laser-induced breakdown, while keeping the total energy per pulse high. The spectral intensity from 250 shots was summed in order to get a relatively large signal.

These previous efforts demonstrated that visible laser Raman spectroscopy can be used to determine temperature from the ratio of rotational line intensities if excess hydrogen is available. However, greater confidence could be achieved with a larger number of lines used in the thermometry. Also, the temperature measured was not compared to any independent quantitative model or experimental measurement. The spectral model that was used only incorporated the Q branch of the vibrational transitions and not the S and O branches that also contribute to the overall spectral intensity, albeit to a lesser extent, which would be of greater importance in concentration measurements but were not undertaken. Even with the pulse stretching technique employed and the relatively high pressure, single-shot spectral measurements were not obtained.

Single-shot Raman scattering measurements have been made with visible laser excitation in a liquid oxygen and gaseous hydrogen rocket combustor.[3] In that study, the temperature and species concentration profile downstream from a swirl-coaxial injector in a 429-psig, $(O/F)_{mass}$=1 operating condition was determined. For these tests, a Q-switched, frequency doubled Nd:YAG laser operating at approximately 300 mJ per pulse with 5-ns pulse width was used. The temperature and concentration measurements from the high-pressure combustion chamber were compared with calibrated measurements using a thermocouple in a flat-flame burner to get absolute property values. The authors assumed that the ideal gas law was valid in the flow regime and iteratively solved for temperature and concentration. An uncertainty analysis showed approximately 19-percent uncertainty in the temperature measured. The authors hypothesized that the calibration uncertainty, which made up 75 percent of the total uncertainty, could be reduced by a factor of 2.5 with an increased number of calibration data points.

Ultraviolet (UV) laser Raman scattering measurements have also been conducted on high-pressure oxygen/hydrogen combustion systems using a variable power, narrowband, tunable KrF excimer laser.[4] Use of the UV laser allowed for time-resolved single-pulse measurements with an unfocused beam.

However, photochemical, fluorescence, and stimulated Raman scattering interference was observed because of the relatively high-energy photons in this region of the spectrum and the high chamber pressure. The presence and relative concentrations of major species downstream of a swirl injector were determined for chamber pressures up to 35 atm. Absolute concentration measurements were not undertaken because calibration data was not gathered.

Experimental Setup

For spontaneous Raman scattering experiments, a frequency doubled, vertically polarized, Q-switched Nd:YAG laser is used. The laser exits the laser port and is focused by a 300-mm focusing lens to the probe volume. A beam stop collects the laser light behind the focal point of the beam. Collection optics are placed perpendicular to the laser light. A 250-mm lens collimates the Raman signal from the probe volume. The line of collimated light is then rotated 90° by a series of two mirrors. The line then passes through a focusing lens, which focuses the light into the entrance slit of a spectrometer. A Princeton Instruments PI-Max charge-coupled device (CCD) camera images the signal. A Winspc/32 program controls the camera and the spectrometer and is used to acquire the spectroscopic data. A diagram of the experimental setup is shown in figure 1.

When using spontaneous Raman scattering spectroscopy, the spectroscopic data acquisition setup must be chosen carefully. The Raman signal is much smaller than other scattering signals, such as Mie scattering and Rayleigh scattering. Both of these extraneous signals occur at the frequency of the laser and can be filtered using the proper optical components. A Schott glass filter can be used in some instances and is often desirable due to its cost efficiency. However, for this application, it is necessary to be able to observe rotational Raman lines that are very close to the laser wavelength. The Schott glass filter does not allow sufficient transmittance at these wavelengths. In order for the holographic notch filter to be used optimally, the light must be collimated and s-polarized upon entering the filter. The scattered light is already polarized but must be collimated using a collecting lens at the focal point away from the probe volume. A holographic notch filter centered at the laser wavelength in this configuration provides rejection of the Rayleigh and Mie scattering but sufficient transmittance at the wavelengths of the Raman rotational lines.

The experimental system is configured such that the CCD camera is only active when the laser is pulsed. This allows the signal to be collected only when the scattering is occurring, reducing extraneous light collection that could overpower the Raman signal. To further improve signal-to-noise ratio, several Raman signals can be integrated over multiple laser pulses.

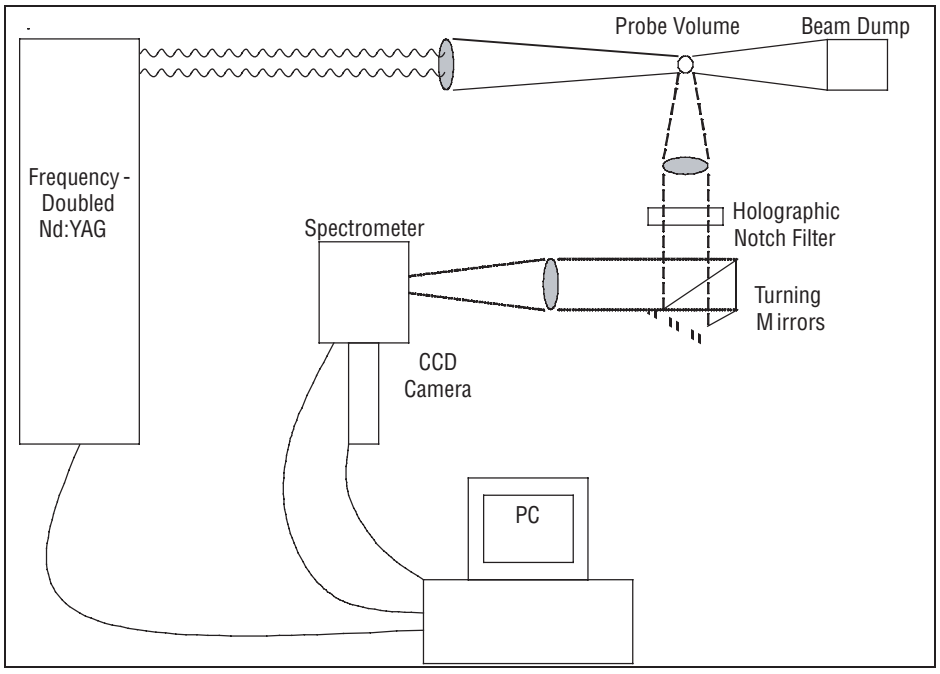

Figure 1. Raman spectroscopy experimental setup.

Accomplishments

During the year-one effort, Raman spectroscopy measurements were taken of known environments ranging from water vapor in air, fully nitrogen environment, and using a flat flame. All of the testing to date has occurred at atmospheric pressure, with the intent to increase pressure. At the time of this reporting, diagnostics research is focusing on repeatability and consistent laser-pulse energy for shot-to-shot repeatability before increased pressure testing is performed.

Also, a pressure vessel has been designed, fabricated, and tested for known environment optical access combustion testing for pressures up to 250 psi. A picture of the pressure vessel test article is shown in figure 2.

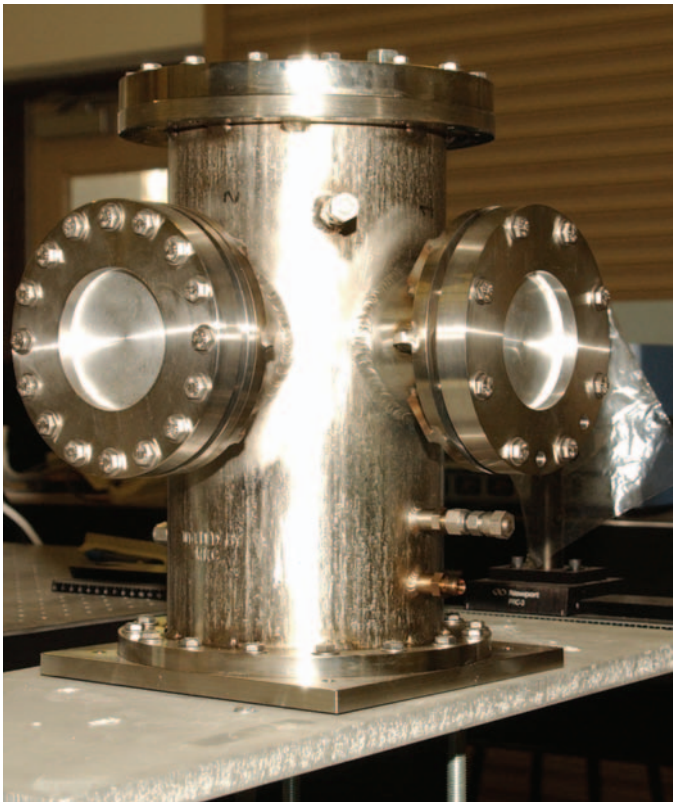

Figure 2. Pressure vessel for elevated pressure diagnostics.

Planned Future Work

Once successful known environment testing is complete at atmospheric pressure, diagnostic tests will be conducted using the pressure vessel with known environments including nitrogen and adiabatic combustion diffusion flames of hydrogen/air and hydrogen and oxygen. Additionally, the product of this effort is scheduled to be applied to numerous other efforts including a Marshall Space Flight Center (MSFC) CDDF project on combustion scaling.

Publications and Patents

No open literature publications of the work were achieved in the initial year of effort. The investigators are submitting an abstract for the American Institute of Aeronautics and Astronautics Aerospace Sciences Meeting to be held in January 2005.

Funding Summary

During the first year effort, $90,000 was awarded for the project effort. Only $40,000 was spent as shown in table 1. The remaining balance is being spent with the year-two award to purchase a high-speed camera ($70,000) to improve diagnostics capabilities toward the goals of better time-resolved measurements.

Table 1. Expenditures for year 1.

Description	Costs ($)
Raw materials (e.g., steel)	5,000
Optical diagnostics	15,000
Collaborative Penn State University assistance	20,000

Status of Investigation

The investigation focused on diagnostics in the combustion environment and is working toward being applied in a recently awarded CDDF project on combustion scaling. As the present effort works to achieve successful spatial resolution of temperature and species in a combustion environment during the final year effort, the newly awarded CDDF will design hardware to accommodate optical diagnostics refined in this effort.

References

[1] Kojima, J.; and Nguyen, Q.-V.: "Spontaneous Raman Scattering Diagnostics for High-Pressure Gaseous Flames," *AIAA 2002–3041*, 22nd AIAA Aerodynamic Measurement Technology and Ground Test Conference, St. Louis, MO, June 24–26, 2002.

[2] Kojima, J.; and Nguyen, Q.-V.: "Laser Pulse-Stretching With Multiple Optical Ring Cavities," *Applied Optics*, Vol. 41, No. 30, pp. 6,360–6,370, October 20, 2002.

[3] Yeralan, S.; Pal, S.; and Santoro, R.: "Experimental Study of Major Species and Temperature Profiles of Liquid Oxygen/Gaseous Hydrogen Rocket Combustion," *Journal of Propulsion and Power*, Vol. 17, No. 4, pp. 788–793, July–August 2001.

PHANTOM: Unified Flow Analysis for Turbines and Pumps

Project Number: 03–02

Investigator: Daniel J. Dorney/TD64

Purpose

The goal of this Center Director's Discretionary Fund (CDDF) project was to extend the three-dimensional unsteady perfect-gas flow analysis tool, CORSAIR, to incompressible flows using the Generalized Equation Set (GES). The new code, which is called PHANTOM, is capable of solving flows ranging from incompressible to hypersonic speeds (i.e., be applicable to both turbine and pump flow fields).

Background

Turbomachinery devices are in use around the world in an almost uncountable number of applications. The working media employed in these diverse applications incorporate nearly every fluid known to man. There are turbomachinery implementations that deal with gases, liquids, cryogenics, slurries, multiphase and multicomponent fluids, supercritical fluids, and more. There is perhaps no other class of engineering devices for which the diversity of fluids is so great.

Despite this diversity of working fluids, the primary emphasis of Computational Fluid Dynamics (CFD) applications in turbomachinery has traditionally been restricted to perfect gases, with a secondary emphasis on incompressible fluids. The primary reasons are that the field of CFD has been driven by aerospace applications in which perfect gases are the dominant fluid and because the initial emphasis in turbomachinery was on high technology, perfect-gas applications such as aircraft gas turbines, where the nontrivial development costs of code development can be more easily amortized.

Although incompressible fluid codes have also been developed, they have been largely independent of compressible flow codes and have used algorithms that are completely different from compressible algorithms. As a consequence, the simulation of both a perfect gas and an incompressible fluid through a given turbomachine has typically required two completely different codes. This separation of codes and algorithms by specific fluid type is an issue of particular importance in turbomachinery where, as noted above, a broad spectrum of fluids is the rule not the exception.

The turbomachinery applications in liquid propellant rocket engines are a classic example of the global fluid diversity seen in the broader turbomachinery field. The turbomachinery in rocket engines typically pump or expand liquids, supercritical fluids, cryogenic fluids, hot combustion gases, and multiphase fluids, all in a single engine. This is a major contrast to aircraft engines where the working fluid is nearly always limited to air or vitiated air. In addition to a broad variety of fluids, the rocket engine also involves more types of turbomachinery (centrifugal, axial, impellers, etc.) than do aircraft engines that are often limited to axial machines. This breadth of turbomachinery types dictates that the CFD codes for rocket turbomachinery be more general and more flexible, and again argues for a broad fluid capability in a single code, rather than requiring a different code for each fluid.

The purpose of this project is to implement a common algorithm for solving the equations of motion for a general fluid independent of its property characteristics into an existing code. The code, called PHANTOM, uses a common flow solver for the conservation relations while relegating the fluid properties to subroutines specialized for the fluid of interest.

Approach

The approach taken to accomplish the objectives for this task was to work closely with Dr. Charles Merkle (formerly of the University of Tennessee Space Institute but now at Purdue University), who has pioneered the use of the GES, and Dr. Douglas Sondak (of Boston University) who is codeveloper of both CORSAIR and PHANTOM. The core of the CORSAIR code was retained, while the GES was implemented in place of the perfect-gas flow equations. Fluid property routines were generated using equations provided by Dr. Joseph Oefelein of Sandia Laboratories and by fitting surfaces to data from the National Institute of Standards (NIST).

Accomplishments

The GES was successfully implemented into PHANTOM. The code was validated using incompressible, subsonic, transonic, and supersonic test cases (using both liquids and gases). The code has also been applied to several relevant problems, two of which are outlined below.

1. Space Shuttle main Engine (SSME) Low-Pressure Oxidizer Turbopump (LPOTP) First Stage Nozzle Redesign: The SSME LPOTP was recently the subject of an in-depth investigation because cracks were discovered on the first stage vanes. Computational simulations (using CORSAIR) were used to determine that vortex shedding was the probable cause of the cracks, and experimental data was used to pinpoint the shedding frequency at approximately 36 kHz. The two-dimensional version of PHANTOM was used to further investigate the turbine flow field using both the original nozzle and a redesigned nozzle. The operating fluid in the turbine is liquid oxygen. The nozzle

vortex shedding frequency predicted using PHANTOM was 37 kHz, which is very close to the experimentally deduced value of 36 kHz. Figure 1 shows instantaneous pressure and velocity contours from the PHANTOM simulation. Simulations were also performed for the turbine stage containing a redesigned nozzle. Dr. Man Mohan Rai, at NASA Ames Research Center, designed the nozzle using optimization techniques. The redesigned vane was successful in reducing the amplitude and frequency (moving it away from a natural frequency of the nozzle structure), but did increase the unsteadiness on the rotor blades. The effects of the increased unsteadiness on the rotor are currently being assessed.

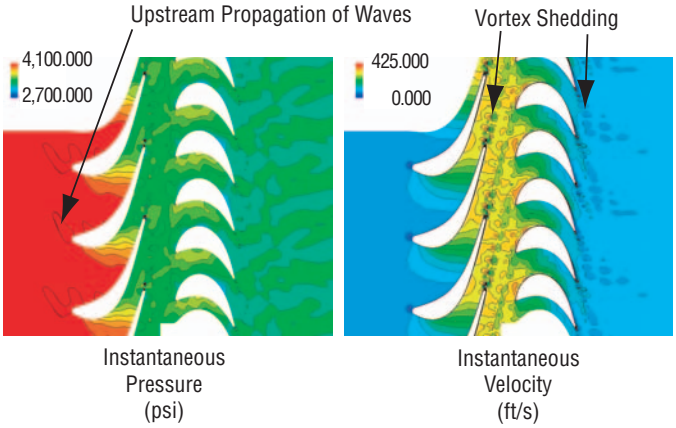

Figure 1. Instantaneous pressure and velocity contours from the PHANTOM simulation.

2. Deep Throttling Turbopump Stage: The geometry of interest is a pump stage consisting of a high-head impeller and a vane-island diffuser (fig. 2). The goal of these simulations was to validate PHANTOM for deep throttling pumps, and to study new diffuser airfoil designs. The impeller contains 6 main blades and 6 splitter blades, while the diffuser contains 13 airfoils. The pump was tested in water at a temperature of 550 °R. At the design flow rate of 1,210 gpm, the inlet pressure is 115 psig, and the impeller rotates at 6,322 RPM. In addition to a design-flow simulation, five off-design simulations (four low flow, one high flow) were performed. Figure 3 shows instantaneous and time-averaged pressure contours at the design flow rate. In an effort to better understand the interaction between the impeller blades and diffuser airfoil, unsteady pressure traces were recorded near the trailing edge of impeller blades and near the leading edge of the diffuser vanes. Figures 4 and 5 show the pressure traces and the corresponding Fourier decompositions. These two figures indicate that the diffuser airfoils experience a significant amount of unsteadiness at the impeller wake passing frequency, while the impeller blades exhibit a smaller amount of unsteadiness at both the diffuser passing frequency and its first harmonic. In addition, an inspection of figures 4 and 5 reveals that, during some portion of the impeller rotation, the throat for the diffuser moves from inside the diffuser passage to the region between the impeller trailing edge and the diffuser leading edge. Finally, figure 6 contains a comparison between the predicted and experimental static head coefficients for the impeller and diffuser over the wide range of flow conditions. In general, very good agreement is observed between the predictions and data.

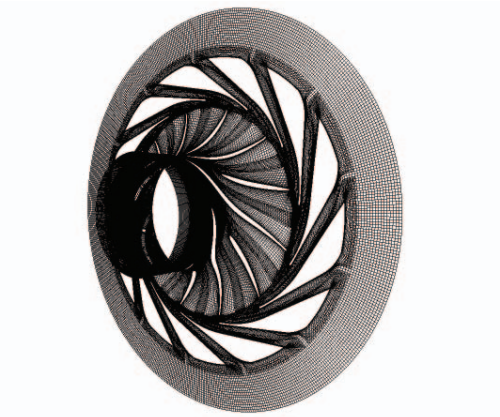

Figure 2. Pump stage consisting of a high-head impeller and a vane-island diffuser.

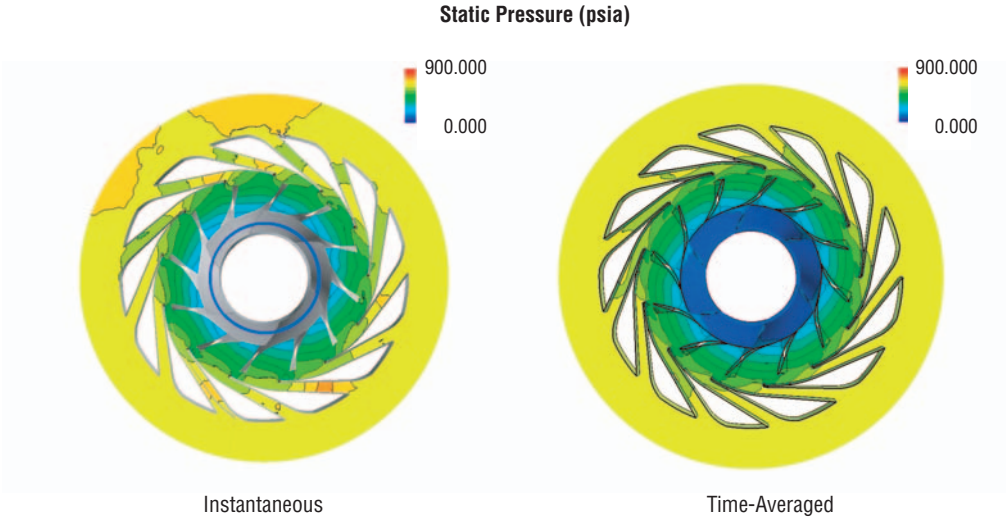

Figure 3. Instantaneous and time-averaged pressure contours at the design flow rate.

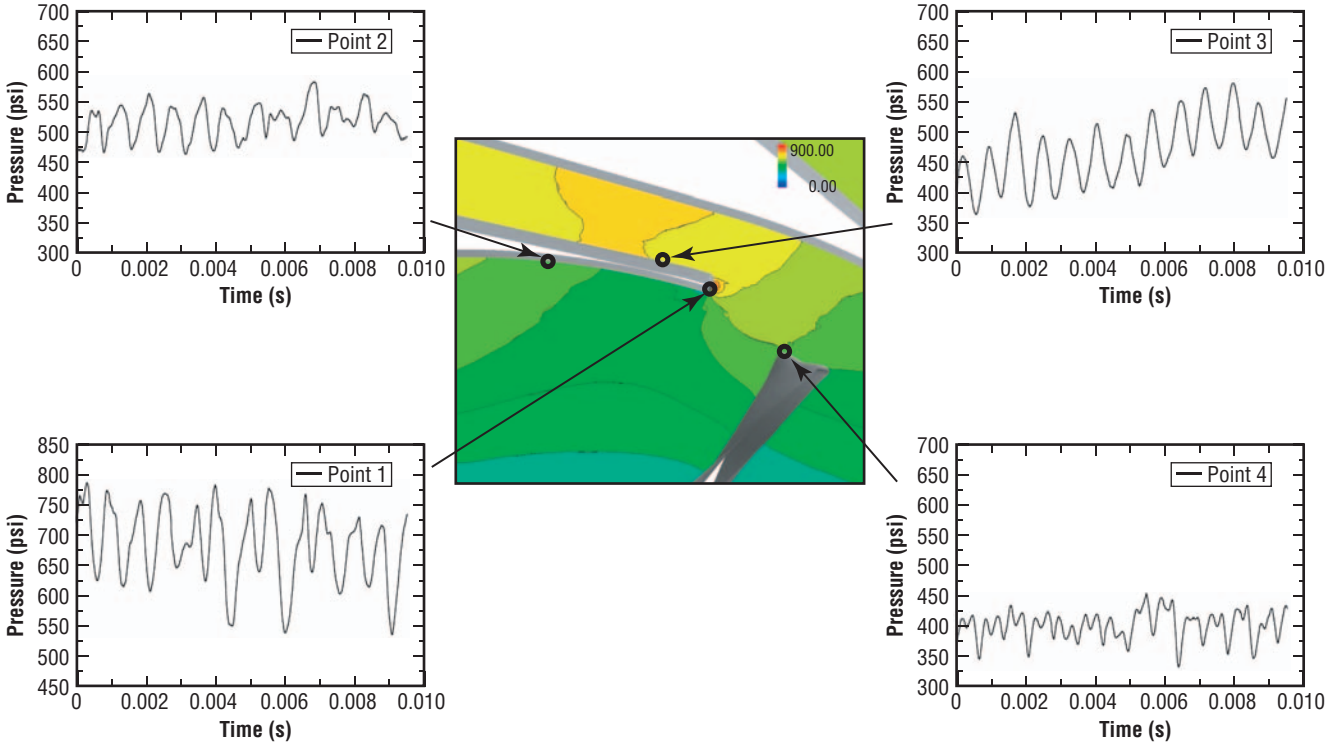

Figure 4. Unsteady pressure traces at midheight near the impeller trailing edge and the diffuser leading edge.

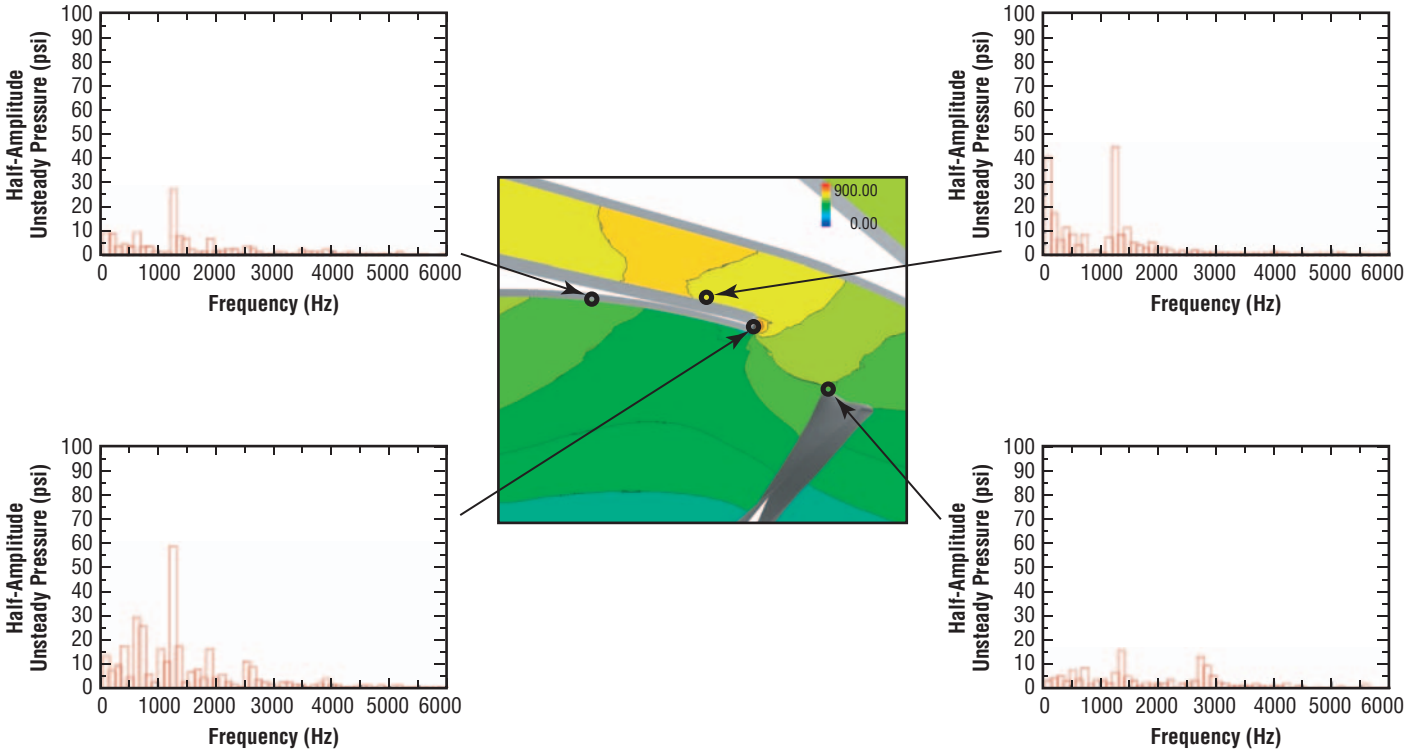

Figure 5. Fourier decomposition of the unsteady pressure traces.

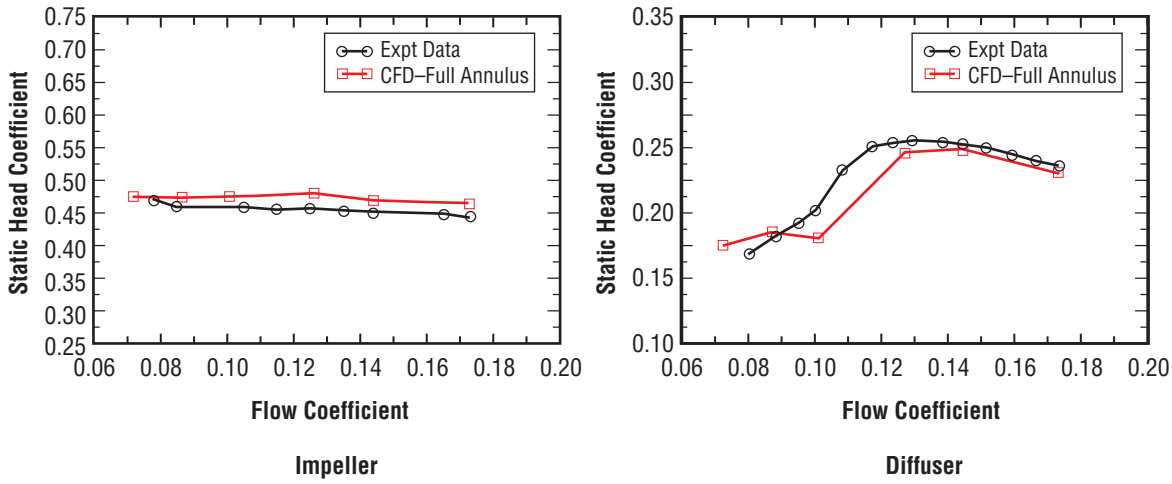

Figure 6. Static head coefficients for the impeller and diffuser.

Planned Future Work

Based on the success of the current project, work on PHANTOM will continue. In addition to implementing a cavitation model, the speed and accuracy of the real-fluid routines will be improved. This work will be funded via a fiscal year 2004 CDDF.

Publications and Patent Applications

Dorney, D.J.; and Sondak, D.L.: "Application of the PHANTOM Anaylsis to Deep Throttling Turbopumps," JANNAF 27th Airbreathing Propulsion Subcommittee Meeting, Colorado Springs, CO, December 1–5, 2003.

Sondak, D.L.; and Dorney, D.J.: "General Equation Set Solver for Compressible and Incompressible Turbomachinery Flows," *AIAA 2003–4420*, 39th AIAA/ASME/SAE/ASEE Joint Propulsion Conference and Exhibit, Huntsville, AL, July 20–23, 2003.

Merkle, C.L.; Venkateswaran, S.; Dorney, D.J.; and Sondak, D.L.: "A Generalized Fluid Formulation for Turbomachinery Computations," *AIAA 2003–3999*, 33rd AIAA Fluid Dynamics Conference and Exhibit, Orlando, FL, June 23–26, 2003.

Funding Summary

In addition to the ¼ full time equivalents funded by this CDDF, a $30,000 grant was given to Dr. Douglas Sondak of Boston University to assist in the development of PHANTOM and a $20,000 grant was given to Dr. Charles Merkle of UTSI/Purdue University to assist in the implementation of the GES.

Status of Investigation

All work specified in this CDDF has been completed.

High-Energy Fuels and Catalysts

Project Number: 03–03

Investigator: Rudy Gostowski/TD40

Purpose

This research had two distinct goals:

1. Develop high-energy fuels that would be hypergolic with high-concentration hydrogen peroxide (HTP) oxidant in a bipropellant engine.

2. Produce monopropellant catalysts that are tolerant of the high temperatures present during decomposition.

Background

Hypergolic fuels eliminate the requirement for ignition devices permitting simple, reliable, compact, and low-mass propulsion systems. If this property is combined with high-energy density, the resulting fuel will provide performance that facilitates a versatile range of applications. Lower toxicity fuels, hypergolic with an equally benign oxidizer such as HTP, will lower the cost associated with ground handling, improve mission turnaround time, and reduce toxic exposure risk for the flight and ground crews. HTP has been known for some time but recent advances in the propellant's stability, in compatible materials, and with improved fuels like those described here make a real breakthrough in its application imminent. Fuels hypergolic with HTP are also likely to react similarly with other traditional oxidizers such as nitrogen tetroxide (N_2O_4) and inhibited red fuming nitric acid (IRFNA), allowing implementation in some existing systems.

Monopropellant systems are even simpler than hypergolic bipropellant engines. Certain new lower toxicity high-energy-density monopropellants (HTP, DMAZ, and HEHN/HAN) may offer advantages over the hypergolics while approaching their performance. A challenge to implementation is the high temperature generated when the propellant decomposes on a catalyst surface. To facilitate the use of these propellants, thermally robust catalysts are required that have the appropriate chemical reactivity and surface-area to volume ratio.

Approach

The plan to reach our goals included the following five steps:

1. Evaluate selected fuels expected to be hypergolic with HTP for ignition delay.
2. Synthesize new fuels coupling a high-energy moiety with one expected to be hypergolic.
3. Test putative fuels for ignition delay and other physical properties.
4. Prepare heat tolerant catalysts.
5. Characterize the catalysts and evaluate their activity with low-toxicity high-energy-density monopropellants.

Hypergolic ignition delay was measured by dropping the oxidizer into an optical quartz cuvette containing the potential fuel. A pump-activated syringe that yielded a highly reproducible volume was used to produce the oxidizer drop. A trigger signal from the syringe pump activated a high-speed camera that captured the event. The moment of contact between the oxidizer drop and the fuel was taken as the beginning of the ignition delay. Times until intervening events, for example decomposition of HTP, were also recorded. The delay interval ended at the flash of ignition.

Combining an energetic moiety with one expected to be hypergolic produced new fuels. Energetic moieties included those with significant angle strain. Groups of atoms expected to make a fuel hypergolic included amines and alkylboranes.

Catalysts were prepared by wetness impregnation of a support material with a compound of an active metal. The compound was subsequently converted to the metallic form by temperature-programmed reduction.

Accomplishments

Various fuels were tested to evaluate the effects of substituent groups (amines, azide, and boranes), ring strain, and vapor pressure on ignition delay. The results of this testing is found in table 1. As expected, increased vapor pressure appears to reduce ignition delay but is not sufficient alone to account for hypergolic behavior. Pentane, having a high vapor pressure, would not ignite even with the addition of an initiator. Likewise, cyclopropane, which has a significantly higher vapor pressure than the tertiary amines tested, had a much longer ignition delay. For the compounds tested, ring strain did not appear to enhance tendency for hypergolicity. This testing was conducted in collaboration with Dr. John Blevins (TD40). For this purpose, Wendy Eccles, a graduate student in chemistry at Vanderbilt University, synthesized two of the fuels tested. These materials were (dispiro[2.0.2.1]hept-7-ylmethyl)amine and bicyclopropylidenylboronate. Professor Piotr Kazinsky supervised her work.

Table 1. Ignition delay testing with 98 percent HTP.

		No Initiator		Cobalt (II) 2-ethylhexylhexanoate Initiator (10 v/v %)	
Fuel	Vapor Pressure (mmHg)	HTP Decomposition (ms)	Ignition (ms)	HTP Decomposition (ms)	Ignition (ms)
Nonane	10	No decomposition	No ignition		No ignition
Octane	11	No decomposition	No ignition		No ignition
Pentane	434	No decomposition	No ignition		No ignition
N, N-Dimethylhexylamine	4	No decomposition	No ignition	6.1	12.7
N, N-Dimethylbutylamine	46	No decomposition	No ignition	5.2	9.8
2-Azido-N, N-dimethylethanamine (DMAZ)*	11	No decomposition	No ignition	6.8	12
Cyclopropylamine	241	No decomposition	No ignition	7	16
(Dispiro[2.0.2.1]hept-7-ylmethyl) amine		No decomposition	No ignition		No ignition
Bicyclopropylidenylboronate		No decomposition	No ignition		No ignition

*Boeing proprietary information. Data is not for general distribution

Catalysts were prepared using dihydrogen hexachloroiridate (IV) and 25–30-mesh alumina. This material will be compared to Shell 405 and S–405 catalyst obtained from Aerojet Corporation.

Planned Future Work

Catalysts will be evaluated using differential scanning calorimetry (DSC). In this experiment, the temperature is ramped and the heat flow observed. Monopropellant will be contained in a high-pressure capsule and the onset of decomposition temperature recorded. The experiment will then be repeated after adding a catalyst to the capsule. Lowering of the onset temperature will indicate the catalyst's effectiveness.

New catalysts will be prepared using other iridium-containing compounds, other active metals, and other substrates to arrive at a heat-tolerant and effective catalyst.

Publications

Blevins, J.A.; Gostowski, R.; and Chianese, S.: "An Experimental Investigation of Hypergolic Ignition Delay of Hydrogen Peroxide With Fuel Mixtures," *AIAA 2004–1335*, 42nd AIAA Aerospace Sciences Meeting and Exhibit, Reno, NV, January 2004,

Funding Summary

- $150,000/year.
- 2.5 full time equivalents/year.

Status of Investigation

Further activity in development of a high-energy hypergolic fuel will consist of monitoring research in the area. CDDF funding for fiscal year 2004 will facilitate continuation of the catalyst development effort.

Pulsed Electromagnetic Thrusters for High-Power Space Propulsion

Project Number: 03–06

Investigators: **Thomas E. Markusic/TD40**
Richard H. Eskridge/TD40
Adam K. Martin/TD40

Purpose

The purpose of this Center Director's Discretionary Fund (CDDF) project is to develop two high-power pulsed electromagnetic accelerator concepts that show promise for application in nuclear electric propulsion (NEP). The thrusters differ in the manner by which the accelerating field is coupled to the propellant—direct coupled (with electrodes) versus inductively coupled (without electrodes). Preliminary analysis shows that both concepts can theoretically meet the formidable performance requirements ($I_{sp} > 4{,}000$ s, $h_t > 60$ percent) for a viable high-power propulsion system. The aim of this project is to construct prototype thrusters and experimentally demonstrate the predicted performance.

Background

Fast, large Δv missions will require high jet-power, high specific-impulse thrusters. These thrusters must also have high thrust efficiency so that the savings in propellant are not cancelled by increases in powerplant mass and other overhead. No single electric propulsion system is best suited for all missions. For example, ion thrusters may work best for large Δv, long-duration missions; however, if short trip times are required, their characteristically low thrust density may preclude their use altogether. Hall thrusters have attractive performance at intermediate specific impulse levels (~ 2,000 s), but fundamental physical limitations prevent them from achieving the high specific impulse levels required for some missions. magnetoplasmadynamic (MPD) thrusters have high thrust density and may have high efficiencies ($h_t \sim 60$ percent), but only within a certain specific impulse range ($I_{sp} = 4{,}000$–$5{,}000$ s and $I_{sp} > 12{,}000$ s). In short, every type of electric propulsion device has a parameter space within which it performs best.

It is our contention that pulsed electromagnetic thrusters may have unique capabilities to satisfy the propulsion needs for missions that require high specific impulse, high thrust efficiency, and high thrust density. Pulsed-plasma acceleration may be done directly, as in a pulsed-plasma thruster (PPT), or indirectly (i.e., inductively) in a plasmoid thruster. Both methods have potential advantages, and we are investigating both concepts through the CDDF program. Although these two concepts are different in implementation, they draw on the same fundamental technology, and can share the equipment and capabilities of the Propulsion Research Center's (PRC's) pulsed-power laboratory. The two parallel efforts are described below under the headings: Gallium Electromagnetic (GEM) Thruster, and Plasmoid Thruster Experiment (PTX).

Approach

Gallium Electromagnetic Thruster

The GEM thruster uses a two-stage acceleration scheme, and liquid-metal propellant, to circumvent some of the deficiencies that have plagued earlier thruster designs. High-energy PPTs have already been experimentally shown to be capable of accelerating current sheets to speeds greater than 150 km/s (corresponding to a specific impulse above 15,000 s). Another study demonstrated high-energy PPT operation at greater than 60-percent thrust efficiency. These experiments prove that there are no fundamental physical limitations that will prevent us from attaining our stated design goals. Our approach is unique for its use of a liquid propellant in a PPT and electrode geometry. It is proposed that use of a molten metal propellant and a two-stage acceleration scheme provides potential benefits that may be exploited to overcome many of the negative issues associated with PPTs, such as propellant utilization inefficiency and mechanical reliability. The GEM thruster project aims to provide the high performance observed in earlier PPTs, but with design enhancements that eliminate all moving parts and high-current electrical switches and dramatically improve system reliability.

Plasmoid Thruster Experiment

A plasmoid is magnetized plasma with a closed magnetic field-line structure. The thruster works by repetitively forming plasmoids and accelerating them to high velocity with magnetic pressure. The potential advantages of this concept are as follows:

- The entire process is inductive, so there are no electrodes.
- The closed magnetic field-line structure of the plasmoid provides some degree of confinement so that the energy required to heat the plasma to a sufficiently conducting state is not lost to the walls.
- The plasmoid is not magnetically attached to the accelerating field, which should readily facilitate detachment of the plasmoid from the thruster.

A schematic of the experiment is shown in figure 1. The plasmoid is formed inside of a glass tube (that serves as the vacuum wall) that sits inside of a conical theta-pinch coil, with cone angle of 17.58°. The propellant (e.g., hydrogen) is puffed into the tube. Then, a bias magnetic field is generated and the gas is preionized, freezing in the magnetic field. The field in the coil is then quickly reversed. The reversed (or compression) field reconnects with the bias field to make the plasmoid. The compression heats and fully ionizes the plasma. The magnetic pressure of the reversed field pushes on the plasmoid and accelerates it out of the thruster. A single capacitor bank (560 nF, 35 kV) that performs all three functions of preionization, bias-field loading, and field reversal drives the coil. The device, as constructed now, allows us to run only in a single-shot mode, although some of the components have been designed to allow rep-rated operation, which would be necessary for an actual thruster. Understanding the fundamental formation and acceleration mechanisms is most easily done using single-shot operation, which allows detailed study of the individual plasmoid.

The objectives of this work are as follows:

- Determine if and how the concept works.
- Determine how to maximize the thruster's efficiency.
- Identify the component technologies that will need development in order to make the concept work.

Accomplishments

Gallium Electromagnetic Thruster

Work completed in the first year of this effort has demonstrated the feasibility of an electromagnetically pumped liquid-metal feed system and a liquid-metal-fed plasma injector. Several versions of the pump have been developed. Gallium propellant flow in tubes, consistent with the flow rates required for high-power electric propulsion, has been demonstrated. The success of this effort has stimulated interest in this feed system for the bismuth Hall thruster (Busek, Inc.) and the lithium MPD thruster (NASA Jet Propulsion Laboratory). The feed system has been coupled with a prototype first stage, and plasma production has been demonstrated. Design and fabrication of the high-energy second stage has been completed.

Plasmoid Thruster Experiment

The apparatus was built during fiscal year (FY) 2003, and some initial measurements have been made that were reported at the 2003 Joint Propulsion Conference. The principle diagnostics used were a high-speed framing camera and external magnetic field probes. Initial studies focused on the preionization and formation process.

It was found that preionization and bias-field loading, occurs along the inside surface of the coil, at the coil mouth. Measurements of the flux excluded by the plasma (fig. 2) demonstrate

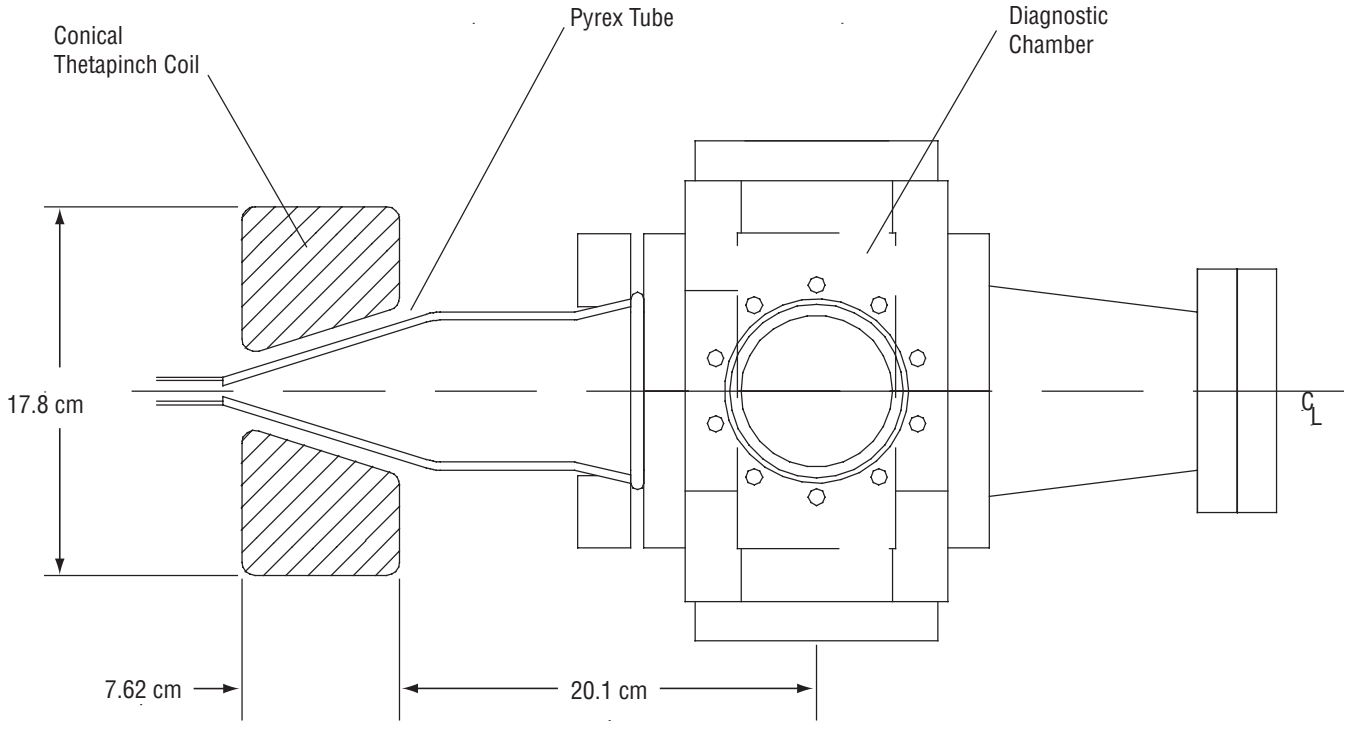

Figure 1. Plan view of PTX device.

that this occurs during the second half cycle. Compression and reconnection occurs during the third half-cycle. This means that plasmoid formation begins on the second half-cycle, and the resulting plasmoid is expelled on the third half-cycle. In this case, the propellant used was a mixture of hydrogen (H_2) and helium (He) (6 percent H_2 in He). The ionization characteristics of this mixture are likely dominated by the H_2. Subsequent measurements taken with pure H_2 show the same behavior. With argon, the process is advanced one half-cycle, so that the plasmoid is likely expelled on the second half-cycle. Velocities as high as 20 km/s were measured for a plasmoid propagating into a static back-fill of gas (fig. 3—pictures taken with Cordin 220B framing camera). By using a puff valve to load the propellant into the thruster, higher velocities should be easily achievable; numerical simulations predict velocities of up to 100 km/s.

Presently, we are using a single capacitor bank to drive the coil. However, independent preionization may be required for efficient operation of the device, so that the formation of the plasmoid begins on the first half-cycle of operation, so as to minimize resistive losses in the coil. Also, for efficient operation, there must be strong coupling between the plasma and the external driving circuit. This means that the bias field may have to be produced independently of the reversed field so that the current waveform in the theta-pinch coil can be a critically damped discharge.

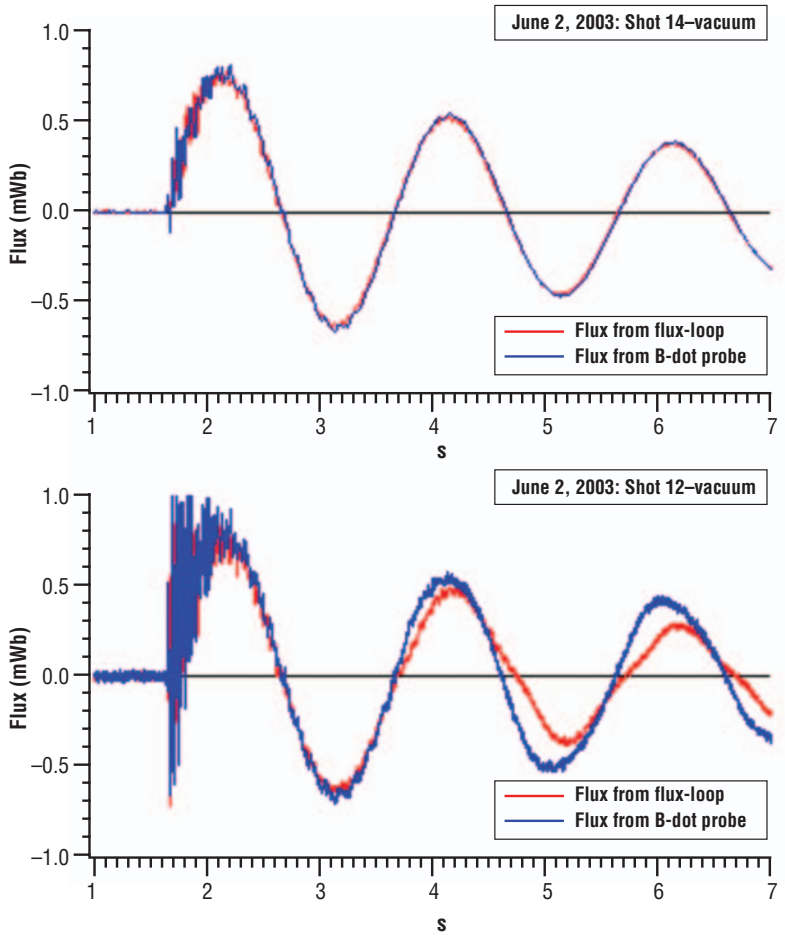

Figure 2. Excluded flux measurement shows the presence of a conducting plasma beginning on the third half-cycle.

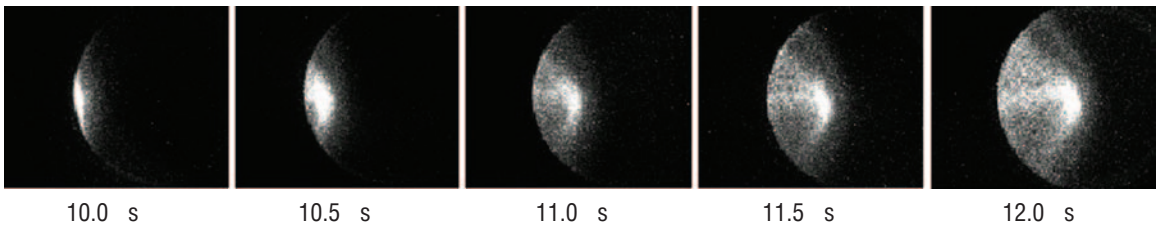

Figure 3. Side view of a plasmoid moving down stream in the PTX device. Conditions: 6-percent H_2 in He, 95-mTorr back-fill pressure. The theta-pinch coil current is 53.5 kA.

Planned Future Work

Gallium Electromagnetic Thruster

Our development plan for the GEM thruster consists of the following three phases:

1. Design and test breadboard devices that make up the major components of the GEM thruster,
2. Design and test a repetitively pulsed GEM thruster at 100-kW input power,
3. Design and test the final GEM thruster configuration at 500-kW input power.

We hope to complete major tasks 1 and 2 using CDDF funds. The results from this work will form the basis of an NRA proposal (Prometheus high-power in-space propulsion), from which we will acquire funding for task 3.

Plasmoid Thruster Experiment

The development plan for the plasmoid thruster is as follows:

- Make use of additional diagnostics (Quantities to be measured are in parenthesis.):
  - Internal magnetic field probes (plasmoid shape, and magnetic field structure).
  - Interferometry (plasma density).
  - Quadruple Langmuir probe (plasma density, electron temperature, and flow velocity).
- Measure the velocity, mass, and impulse bit.
- Replace existing vacuum chamber with a larger chamber for improved diagnostic access.
- Install a different coil (8.58° cone angle), to study effects of thruster geometry on performance.
- Analyze data and compare with theoretical models, including a one-dimensional circuit model of the device, as well as a two-dimensional time-dependent, single fluid MHD code (MOQUI).

These tasks will be performed using fiscal year (FY) 2004 CDDF funds. The results will serve as the basis for two NRA proposals (Prometheus In-Space Propulsion: High-Power and Critical Issues).

Publications and Patent Applications

Gallium Electromagnetic Thruster

Markusic, T.E.; and Thio, Y.C.F.: "Design of a High-Energy, Two-Stage Pulsed Plasma Thruster," *AIAA–2002–4125 Proceedings*, 38th Joint Propulsion Conference, Indianapolis, IN, July 7–10, 2002.

NASA Tech. Briefs, July 2003.

"Liquid-metal-fed pulsed plasma thruster," Invention disclosure accepted by NASA, September 2003.

Plasmoid Thruster Experiment

Koelfgen, S.; Hawk, C.W.; Eskridge, R.H.; et al.: "A Plasmoid Thruster for Space Propulsion," *AIAA–2003–4992*, 39th AIAA Joint Propulsion Conference, Huntsville, AL, July 20–23, 2003.

Funding Summary

Table 1 identifies the FY 2003 and FY 2004 funding summary for this project.

Table 1. Funding summary.

	FY 2003	FY 2004
Personnel (full time equivalents)	6	6
Experiment ($)	165,000	120,000

Status of Investigation

Gallium Electromagnetic Thruster

We have constructed a prototype feed system (fig. 4), first-stage plasma injector (fig. 5), and high-energy second-stage accelerator (fig. 6). The feed system has been extensively tested and will

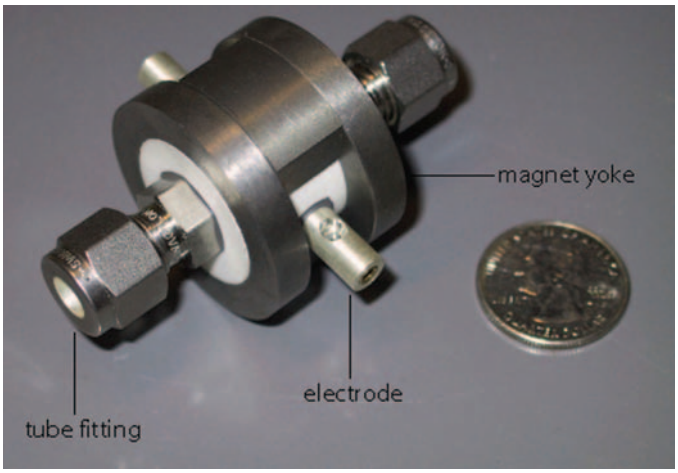

Figure 4. Electromagnetic propellant pump developed for the GEM thruster.

Figure 5. First-stage plasma injector developed for the GEM thruster.

require no further development. The first stage plasma injector has been constructed and tested. Consistent, repetitive pulsing has not been demonstrated. We are presently developing techniques to stop propellant flooding of the interelectrode gap. The second-stage accelerator has been completely constructed and awaits completion of the first-stage injector before full system integration and testing can begin. We have carried out numerical simulations (fig. 7) using the MACH code to predict the performance of the complete GEM thruster and have produced results consistent with expectations.

Figure 6. PI with the second stage of the GEM thruster.

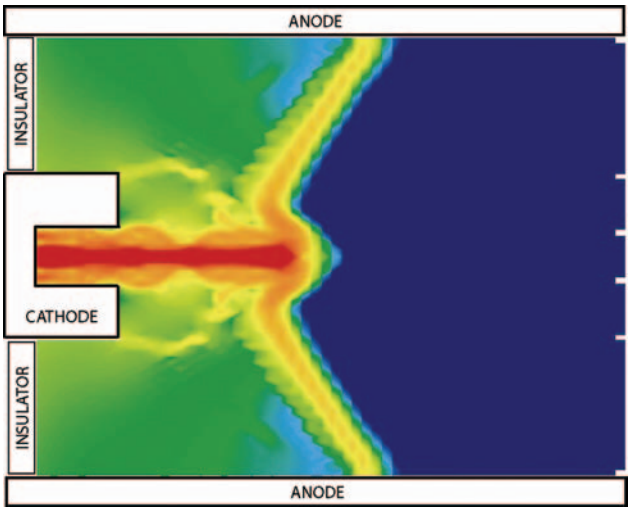

Figure 7. MACH simulations showing current density contours in GEM thruster.

Plasmoid Thruster Experiment

Since the beginning of FY 2004, we have tested a ringing Blumlein circuit for independent preionization of the plasma (fig. 8). This was made from three layers of copper foil, separated by layers of dielectric (Kapton tape), and switched with a spark-gap switch. This did provide independent control of the preionization; however, the dielectric was prone to breakdown due to over voltage. Continued work on improving this component is now being carried out. We also tested a fast gas-puff valve for propellant delivery. A Parker Pneumotronics Series 25 valve was modified by removing the dead volume on the outlet side and driving it by a fast pulser circuit (300 V). The opening time of this valve was found to be in the range of 100–300 μs, and it is capable of delivering up to 1 mg of propellant, with a plenum pressure of 25 psig. Performance measurements are now being conducted with the addition of an internal array of magnetic-field probes, a Langmuir probe, and a HeNe interferometer system.

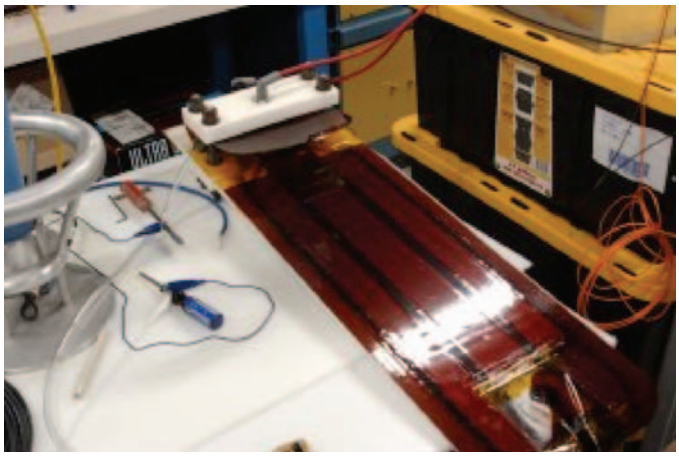

Figure 8. Ringing Blumlein preionizer: C=4.3 nF, V_{Charge}=35 kV. This produces a peak current of 3.3 kA, at a freqency of 5 Mhz.

Enhancement of Generalized Fluid System Simulation Program for Design and Analysis of Propulsion Systems

Project Number: **03–07**

Investigators: **Dr. Alok K. Majumdar/ED25**
Eric Stewart/ED25
Dr. Mehmet Sozen, Embry-Riddle Aeronautical University

Purpose

It is highly desirable to have a computational tool that will perform system level simulation of the entire rocket propulsion system to facilitate new engine design. Such a computational tool will significantly reduce the number of iterative cycles during the design process and reduce the number of tests, resulting in a significant economic savings. Marshall Space Flight Center (MSFC) has developed a general-purpose computer code, Generalized Fluid System Simulation Program (GFSSP) to perform network flow analysis of propulsion systems. The purpose of the present investigation is to enhance GFSSP's capability to model chemical reaction and conjugate heat transfer. These additional capabilities will allow GFSSP to model an entire rocket propulsion system with more fidelity and help design an optimization study.

Background

The GFSSP is a computer program developed at NASA MSFC for analyzing steady-state and transient-flow rates, pressures, temperatures, and concentrations in a complex flow network. The code can handle compressible and incompressible flows as well as phase-change and mixture thermodynamics. The program, which was developed out of need for an easy to use system level simulation tool for complex flow networks, has been used in many NASA programs including Space Shuttle Main Engine (SSME) High-Pressure Oxidizer Turbopump Secondary Flow Circuits, Axial-Thrust Balance of the Fastrac Engine Turbopump, Pressurized Propellant Feed System for the Propulsion Test Article at Stennis Space Center, and *International Space Station*'s Environmental Control and Life Support System. GFSSP's modular code structure allows enhancements to be added to its solver. It was felt that the added capability to model solid to fluid heat transfer (also known as conjugate heat transfer) and chemical reaction will allow GFSSP to model the entire propulsion system from propellant tanks to thruster by a single model that can provide transient solution of thermal and flow parameters during an entire period ranging from chill down to engine shutoff.

Approach

The approach chosen for this investigation is to extend the finite volume procedure of GFSSP to include conjugate heat transfer and chemical reactions. Conjugate heat transfer modeling required the inclusion of solid-node and ambient-node, solid-to-solid, solid-to-fluid, and solid-to-ambient conductors (fig. 1). An additional conservation equation of energy for solid nodes was solved to calculate the temperature of the solid nodes. The convective and radiation heat transfer between solid and fluid nodes constitute the coupling of energy conservation equations for solid and fluid nodes.

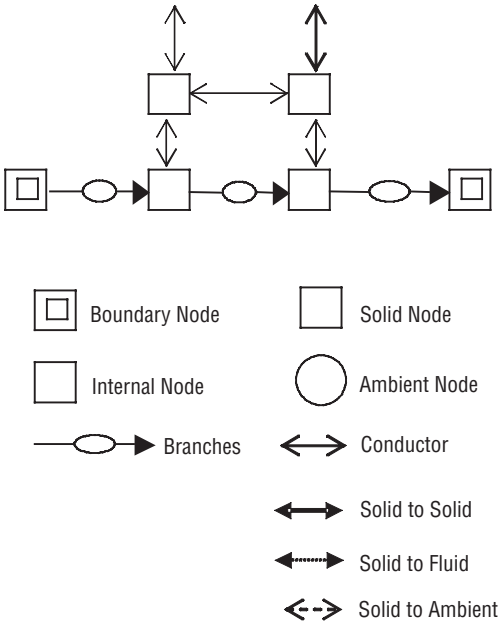

Figure 1. Schematic of conjugate heat transfer model in GFSSP.

The current investigation considers the problem of combustion of liquid hydrogen (LH_2) with liquid oxygen (LOX) in a combustor with the assumption of H_2O, H_2, O_2, OH, H, and O constituting the products of combustion. The schematic diagram of the problem is depicted in figure 2.

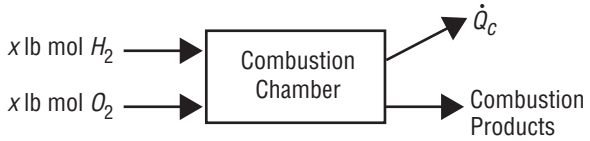

Figure 2. Schematic diagram of the combustion chamber.

Using a chemical equilibrium assumption for the steady-flow case by applying the first and second laws of thermodynamics solves this problem. For given inlet conditions and exit pressure, the resulting equations, which turn out to be coupled, non-linear, algebraic equations, are solved simultaneously. The following three cases are considered for all possible types of environments:

- Stoichiometric case.
- Fuel-rich case.
- Oxygen-rich case.

Accomplishments

Conjugate Heat Transfer Calculation

A benchmark problem of heat conduction with convection was considered for the verification of the model. A 2-in metal rod connects a hot and cold wall as shown in figure 3. There is a simultaneous convective heat-transfer from the wall to ambient with a specified heat transfer coefficient. The calculated temperature distribution was compared with the analytical solution.

The GFSSP model of the problem is shown in figure 4. Nodes 11, 12, 13, and 14 are fluid nodes. Nodes 1 and 10 are ambient nodes representing cold and hot walls respectively. Nodes 2 to 9 are solid nodes. Temperature in the fluid node was kept nearly constant at 70 ˚F by maintaining a large mass flow. The heat-transfer coefficient was maintained constant and was independent of flow rate. The solution compares well with the solution obtained by SINDA/G, a general-purpose computer program for thermal network analysis.

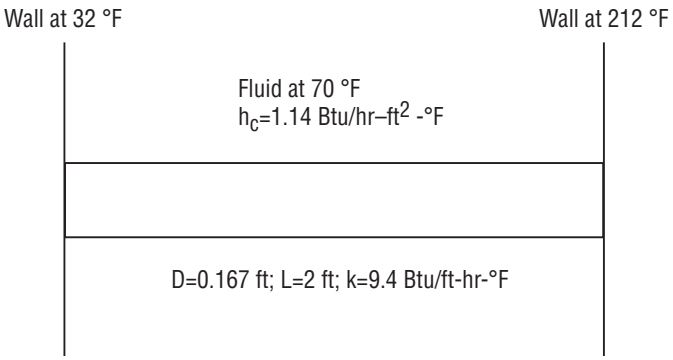

Figure 3. A benchmark problem of heat conduction with convection.

Chemical reaction

The chemical reaction between hydrogen and oxygen for stoichiometric mixture can be expressed by the following equation,

$$2H_2 + O_2 \rightarrow (2a - 2d)H_2O + (2 - 2a - b + d)H_2 + (1 - a - c)O_2 + (2d)OH + (2b)H + (2c)O\,. \quad (1)$$

The four-step chemical reaction yields four chemical equilibrium equations derived from the second law of thermodynamics. When they are combined with the energy conservation equation derived from the first law of thermodynamics, the system of equations provides the mathematical closure of five equations and five unknowns. The five unknowns are the number of moles (a, b, c, and d) and temperature of the product. Five equations are solved simultaneously by a Newton-Raphson method. A typical calculation example is shown in figure 5.

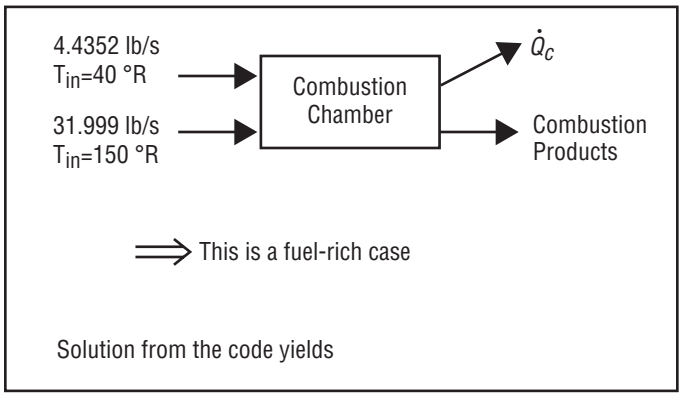

Figure 5. A sample combustion problem and its solution.

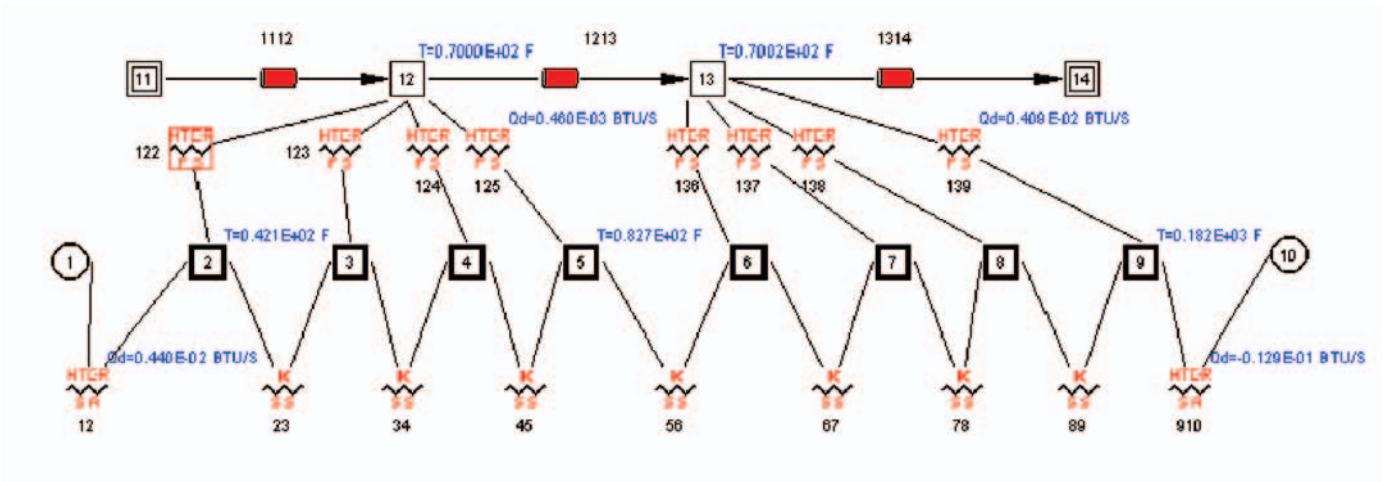

Figure 4. GFSSP Model of the steady-state and transient conduction-convection problem.

Audio-Visual Training CD

An audio-visual training CD containing a training course for GFSSP has been developed and distributed among GFSSP users across the agency and NASA's industrial partners.

Planned Future Work

The future work will focus on design optimization. The ability to perform multiple calculations will be introduced in the code. The chemical reaction capability will also be extended to model combustion of RP–1 and oxygen.

Publications and Patent Applications

Sozen, M.; and Majumdar, A.: "A Novel Approach for Modeling Chemical Reactions in Generalized Fluid System Simulation Program," *Paper No. AIAA 2003–4467*, 39th AIAA/ASME/SAE/ASEE Joint Propulsion Conference, Huntsville, AL, July 20–23, 2003.

A patent application for GFSSP Version 2.01 has been approved. The application for the extension of GFSSP patent application to include additional capabilities is in progress.

Funding Summary

This project received $25,000 in fiscal year 2003. The funding has been used to prepare a training CD ($10,000) and for a research grant ($15,000) to Embry-Riddle Aeronautical University. The received funding has been fully costed.

Status of Investigation

Significant progress has been made to extend GFSSP's capability to handle conjugate heat transfer and chemical reaction.

A 2004 release is planned for a beta version of the code with the capability of conjugate heat transfer. The Users Manual for the code is in the process of being upgraded to reflect the new capabilities of the code. A technical paper is being prepared for presentation in the Thermal Fluid Analysis Workshop to be held in August 2004.

New Detector Configuration for Experimental Characterization of High-Density Nonneutral Plasma in the High-Performance Antiproton Trap

Project Number: 03–08

Investigators: **J. Boise Pearson/TD40**
Glen A. Robertson/TD40

Purpose

This work is a 2-year effort, proposed and awarded as a 2003 Center Director's Discretionary Fund (CDDF) research project. This document is a report on progress to date. The CDDF has been approved for continuation in the 2004 CDDF cycle.

It should be noted that this 2003 CDDF award was not made until April 2003, and funding was not available for use until well into May 2003. Despite the slow start, a significant amount of progress has been made in the research effort.

Background

The objective of this work is to develop a new, higher resolution density detector and more robust electrode structure with improved alignment tolerances to experimentally characterize the density profile and fundamental plasma frequencies of the nonneutral plasma stored in a high performance antiproton trap (HiPAT).

The density profile is determined destructively by extracting the plasma from HiPAT onto a particle detector. The goal is to develop the experimental apparatus and techniques necessary to generate consistent, repeatable density measurements of the trapped plasma, at much better resolution than is currently possible.

The fundamental plasma frequencies are determined nondestructively, by transmitting radio frequency (RF) signals through the plasma as plasma waves. Frequency response characteristics of the transmitted signal identify the fundamental plasma frequencies. These results will be correlated to the density measurements and used as a nondestructive means to determine density and particle count in the trap.

Approach

The plan to accomplish this research effort was broken up into the following four distinct areas:

1) Redesign, manufacture, and installation of a new electrodes and particle detection system.
2) Experimentally determining the density profile of the plasma.
3) Experimentally determining the fundamental plasma frequencies and correlating them to the density data.
4) Investigations in shaping the magnetic field using superconductors for particle extraction and detection.

Accomplishments

New Electrodes and Particle Detection System

There are several hollow cylindrical electrode structures within this experiment. The electrodes in the trap are the critical ones that are the focus of this research. In order to ensure that the new electrode design would function properly, it was used to make a replacement for one of the external beam-line electrodes called an einzel lens. This einzel lens was designed, manufactured, and delivered over the past few months. It has just recently been assembled, and is ready to be bench tested under vacuum and at high voltage. Several flaws in the design have already been identified and will not be present in the trap electrode design. This new electrode structure is the key element of this research effort. Besides the details of the new electrodes themselves, the necessary hardware to install the new electrode structure has been designed, manufactured, and procured.

The particle detection system has been designed, installed, and checked out. It has been tested and appears to be functioning properly. It allows the microchannel plate (MCP) to be masked by a plate with a small aperture. The aperture can be positioned at any radius in the beam pipe. There is a choice of a 3- and a 0.6-mm aperture. This allows a detailed radial survey of particles at the MCP.

Experimental Density Profile

The new detection system has been used to create a preliminary density profile that roughly matches behavior predicted by our in-house code, TRAPEX. However, effective use of the new detector relies on the new electrode structure, which has not been completed yet. The new electrode structure will help eliminate plasma instabilities that currently prevent a repeatable density profile measurement.

Fundamental Plasma Frequencies and Correlation to Density

Research continues in the experimental detection of RF signals from the plasma. Several plasma modes have been identified, but limitations imposed by the current electrode structure make it difficult to identify other key frequencies. The current electrode design incorporates significant improvements that will lead to more stable plasmas and sensitive RF capabilities.

Magnetic Field Shaping Using Superconductors

To start this effort, the literature has been searched and a lab established (from available equipment) to begin investigating large-crystal-growth yttrium barium copper oxide (YBCO) superconductors to determine if a superconducting permanent magnet system could be built and tested for this activity.

To date, a commercially purchased seeded melt-growth single crystal YBCO (~1-in diameter) superconductor was tested in liquid nitrogen and subjected to a 2.5 T ms pulsed magnetic field. The peak measured trapped field was about 1,000 gauss. Under steady state, using rare-earth permanent magnets (~0.5 T) a peak-trapped field of 300 gauss was measured. In both cases, the ratio to applied and trapped was about 50:2 and 50:3 respectively. The steady-state case was better, as has been noted in the literature.

At this writing, large-grain (~1 cm) YBCO superconductors, up to 2-in diameter, have been fabricated in the lab. Field trapping experiment with the rare-earth permanent magnets have shown some sites with fields to 300 gauss on these samples. No pulsing tests have been conducted. Attempts to do seeded melt growth have been done with limited results using in-house produced seed crystals. Commercially produce seed crystals have been ordered for comparison.

Planned Future Work

At the completion of this work, we should have the plasma diagnostics and information necessary to more fully understand the nonneutral plasma in HiPAT. With this information, we will understand the conditions in the trap well enough to aggressively pursue increased storage times, in anticipation of filling the trap with antiprotons at the Fermi National Accelerator Laboratory.

Funding Summary

A breakdown of equipment and support cost estimates for fiscal year (FY) 2003 and FY 2004 is presented in table 1. The budget estimate for FY 2004 has changed slightly from the original proposal, primarily reflecting improved estimates for the cost of the new bore electrode structure.

Status of Investigation

At 5 months into the effort, progress is roughly on track with schedule, accounting for slippage from the late start. All of the procurement for the first year is complete, with all first-year hardware delivered.

The schedule remains the same as in the original proposal, with two exceptions. The first is the obvious slip in start date due to the delay in the award and funding of the 2003 CDDF projects. The second is that the bore electrodes manufacture and installation will be extended one quarter to allow time to eliminate the design flaws found with the einzel lens manufacture.

Table 1. Project funding summary.

Funding Element	FY 2003 ($)	FY 2004 ($)
Electrode materials/high-vacuum bore materials	47,000	N/A
Super conductor (SC) materials/software/magnet hardware	5,000	N/A
Bore electrode hardware/ diagnostic equip	NA	48,000
SC materials/fabrication hardware/magnet supplies	NA	7,000
Contracted technician time	35,000	35,.000
Funding Total	87,000	90,000

Nozzle Side-Load Technology

Project Number: 03–09

Investigators: Joseph Ruf/TD64
David McDaniels/TD63

This Center Director's Discretionary Fund (CDDF) project was submitted as a 2-year task in the fall of 2002. The Columbia Incident required the attention of the principle investigators and use of the experimental facilities during fiscal year (FY) 2003. Some Computational Fluid Dynamics (CFD) analysis did start and the progress on it is reported here. This proposal was resubmitted for a FY 2004 restart.

Purpose

The ultimate goal is to be able to accurately estimate the start and shutdown transient nozzle side loads for a full-scale engine. This will require several years of concerted effort and significant resources to develop the tools and databases. The goal of this CDDF project is to take the first important steps toward understanding and quantifying nozzle side loads for start and shutdown transients.

The objectives of this CDDF are as follows:

- Experimentally quantify nozzle side-load magnitude for multiple nozzle contour types during simulated engine start and shutdown transients.
- Develop an approach to analytically quantify nozzle side-load magnitudes for simulated engine start and shutdown transients using CFD solutions as the basis for defining the nozzle transient fluid dynamics.

Background

Nozzle side loads are lateral forces induced by asymmetric pressure distribution in a nozzle. The most severe nozzle side loads occur during the engine start and shutdown transients as the plume fills and then empties from the nozzle. Two common engine failure modes due to side loads are nozzle-wall high-cycle fatigue and over loading the engine actuators. Almost all liquid rocket engines have, at one time or another, had issues due to nozzle side loads. The J2S had excessive side loads such that an entire engine was ripped from its gimbal structure. The Space Shuttle Main Engine (SSME) had the side-load induced steer-horn fatigue cracks. More recently, the European Vulcain engine and Japanese LE–7A engine also had problems due to nozzle side loads. The Japanese LE–7A nozzle side loads were severe enough to fail the engine actuators and cause the regenerative cooling tubes to rupture.[1] As a result, the LE–7A is currently flying with a truncated nozzle, significantly reducing system performance, while the Japanese completely redesigned the nozzle.

As a result of their side-load issues on Vulcain, the Europeans created a very thorough experimental and analytical program (Flow Separation Control Working Group) in 1993 to understand the nozzle-flow physics that induce side loads.[2,3] This effort started with extensive testing of subscale cold-flow articles to determine the effect of nozzle contour type on the side loads generated. They then proceeded to subscale hot-fire tests to determine the cold-to-hot scaling effects. Complementary analytical efforts were used to interpret test results and matched experimental nozzle side loads to within a few percent.[4]

In the last 3 years, the Japanese had to go through a similar effort first to understand the fluid physics in their LE–7A nozzle and then to devise a fix. Their effort included subscale nozzle hot-fire tests with hundreds of start and shutdown cycles.[5]

The European and Japanese efforts have produced much valuable insight into the fluid physics behind nozzle side loads and into the relative magnitude of side loads for different nozzle contours. They have shared some of their knowledge in open literature, but not the critical elements. One thing their work has proven is that the experimental technique first proposed by Dumnov[6] for measuring nozzle side loads is a highly accurate and reliable approach.

In the United States (U.S.), there has not been a significant effort to advance our understanding of the nozzle side-load phenomena since the 1982 SSME steer-horn investigation. The recently gained knowledge and experience base that now exists in Europe and Japan does not exist here. Particularly, the U.S. does not have experimental data quantifying the nozzle side-load magnitude during start and shutdown transients for different nozzle contours. Furthermore, the U.S. does not currently have an experimental facility able to acquire such data.

It should be noted that both the European and Japanese side-load investigations were started due to unexpected nozzle side loads during full-scale engine testing. It would be prudent for us to begin developing a similar knowledge base and capability given that the next generation of rocket engines is currently in design.

Approach

This CDDF project employs an integrated experimental and analytical approach. The analytical work was begun in FY 2003. However, due to the Columbia Incident, the experimental work was delayed 1 year. The CDDF is a 2-year task, with cold-flow testing occurring late in the first year and into the second year. A task summary is as follows:

- First-year tasks:
  - Research existing test data and empirical and analytical methods.
  - National Transonic Facility (NTF) test to map its nozzle pressure ratio (NPR) ramp-rate control fidelity.
  - Develop quasi-transient CFD approach for separated nozzle flows.
  - Continue developing a full three-dimensional time-accurate CFD approach for separated nozzle flows.
  - Design test hardware and develop testing plans.
  - Initiate purchase of test hardware.

- Second-year tasks:
  - Conduct nozzle side-load tests.
  - Develop side-load prediction method based on quasi-transient CFD.
  - Continue developing three-dimensional time-accurate CFD for separated nozzle flows.
  - Document data and analysis and make future recommendations.

The experimental effort will measure nozzle side loads with the strain tube method first proposed by Dumnov[6] and implemented by the Germans[7] and others. This approach, illustrated in figure 1,[7] is a relatively simple approach enabling accurate measurements of the side loads during nozzle flow transients. The strain gauges measure the deflection of the tube, which can then be interpreted as an aerodynamic induced force. This experimental setup will require designing and building the strain tube and stiffening the nozzle support structure in the NTF. In addition to the aerodynamic induced side loads, nozzle-wall static-pressure measurements will be made. Different nozzle contour types (e.g., truncated ideal, Rao, a scaled SSME, etc.,) will be tested to determine their side loads. A conscious effort will be made to scale the truncated-ideal test article so that this side-load test data is consistent with the RS84 nozzle design.

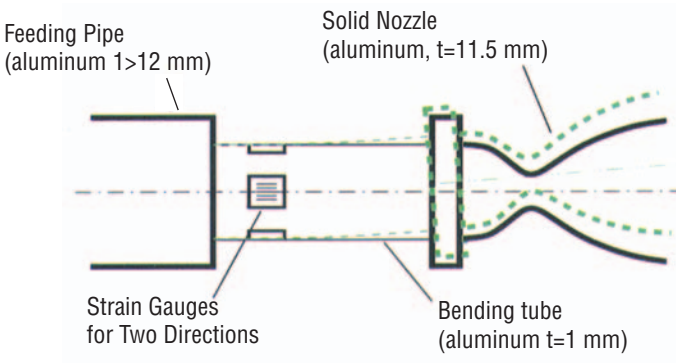

Figure 1. Strain tube method for measuring nozzle side loads. [7]

The analytical effort will consist of two parallel CFD analyses. The first will be a near-term approach similar to that of the Germans[8] and Japanese[9] approach. This near-term approach begins with an effort to build the capability to model a nozzle start and shutdown transient with quasi-transient CFD analysis. In this approach, the start and shutdown transients are solved in time sequentially with a large number of steady-state solutions at small increments of NPR. This analysis will be used to define the nozzle internal fluid physics at each point in time through the nozzle transients. With the wall pressure defined, different empirical approaches will be applied to see which ones best matches the nozzle side load obtained in the experiments. The second, or the long-term approach, will develop a full three-dimensional time-accurate CFD model for nozzle start transient. This effort will build on a previously successful two-dimensional analysis.[10] This fully time-accurate three-dimensional model, if successful, will allow for direct simulation of nozzle flow and subsequent side loads, eliminating the need for empiricism.

Accomplishments

The aforementioned long-term CFD approach began in 2003. Based on a previously successful axisymemtric analysis[10] in which a structured-grid methodology was used, a new unstructured-grid computational methodology is being developed to enhance the computational accuracy and efficiency, and the parallel computing efficiency. This computational methodology is based on a multidimensional, finite-volume, viscous, chemically reacting, unstructured-grid, and pressure-based computational fluid dynamics formulation. A series of two-dimensional planar and axisymmetric analyses simulating the standard-throat SSME thrust chamber assembly during start-up transients were performed. These were followed by full three-dimensional analyses. Currently, the two-dimensional planar and axisymmetric analyses have been completed, while the three-dimensional analyses are in progress. The accomplishments of these efforts are described below.

Two-Dimensional Planar and Axisymmetric Analyses

The objective of this study is to identify and isolate the side-load physics through simplified two-dimensional geometries. The side-load physics captured in the low aspect-ratio, two-dimensional planar nozzle include the Coanda effect, afterburning-to-detonation, and lip Lambda shock oscillation; while those found in the high aspect-ratio, axisymmetric nozzle include the afterburning-to-detonation, transition from free-shock-oscillation to restricted shock oscillation and Lambda shock oscillation at the lip. The results show that the valve sequence, combustion, nozzle area ratio, and ramping rate are important drivers of the nozzle side forces.

Three-Dimensional Analyses

The objective of this study is to identify the three-dimensional side-load physics and to compute the aerodynamic side loads. Figure 2 shows the layout of the computational grid. Currently, the computation has progressed to 1.725 s, out of a 5-s startup transient. During this time period, the sources of side load were found to come from the afterburning-to-detonation and transition from free-shock-oscillation to restricted-shock-oscillation processes. It is expected that the lip Lambda shock oscillation will occur at about 3 s into the start transient. Figure 3 shows the computed aerodynamic side forces from 0 to ~ 1.725 s.

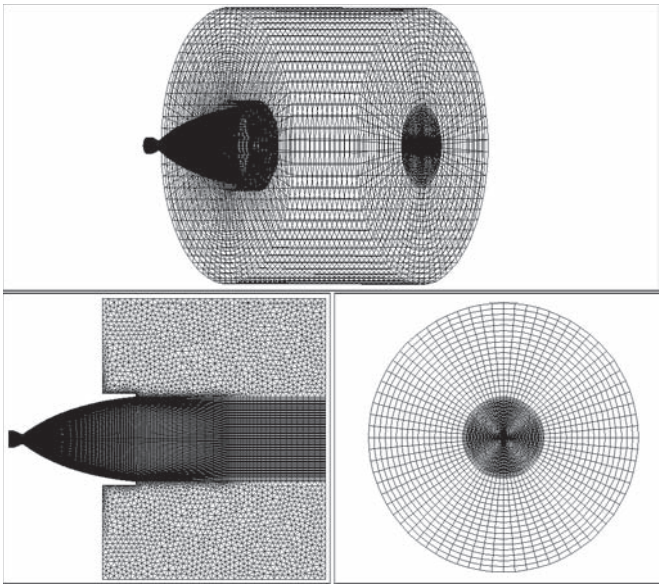

Figure 2. Layout of the computational grid. Upper figure: An overall view. Lower left figure: A cross-sectional cut through the nozzle axis. Lower right figure: The exit plane.

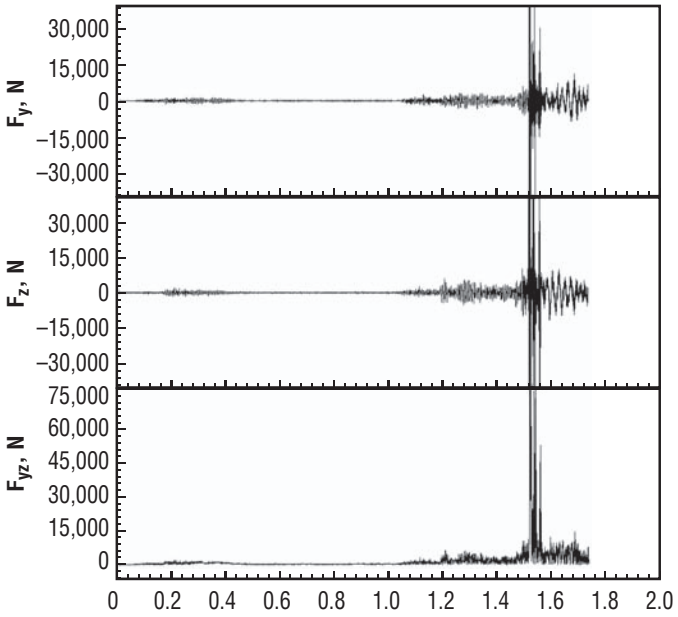

Figure 3. Computed side forces for the SSME nozzle from 0 to ~ 1.725 s.

Planned Future Work

This task was submitted for restart and awarded in fiscal year (FY) 2004.

Publications and Patent Applications

The following three conference papers have been accepted for presentation in the upcoming 40th AIAA/ASME/SAE/ASEE Joint Propulsion Conference and Exhibit, Fort Lauderdale, FL, July 11–14, 2004:

Wang, T.-S.: "Unstructured-Grid Analysis of Performance and Heat Transfer in Liquid Rocket Engines," *AIAA Paper 2004–4016*, 2004.

Wang, T.-S.: "Transient 2–D Analysis of Side Load in Liquid Rocket Engine Nozzles," *AIAA Paper 2004–3680*, 2004.

Wang, T.-S.: "Transient 3–D Analysis of Side Load in Liquid Rocket Engine Nozzles," *AIAA Paper 2004–3681*, 2004.

No patents were produced.

FY03 Funding Summary

The majority of the work on this CDDF project was suspended in deference to the critical support required for the Columbia investigation. With concurrence of center management, $200,000 of the FY 2003 funding was used to support another propulsion technology development activity. An amount of $75,000 was spent on work toward the full three-dimensional CFD transient analysis of start and shutdown loads.

Status of Investigation

Progress was made on some of the analytical half of this CDDF project. The experimental work was delayed 1 year due to the Columbia incident and the CDDF was restarted in FY 2004.

References

[1] Wantabe, Y.; Sakazume, N.; and Tsuboi, M.: "LE–7A Engine Nozzle Problems During the Transient Operations," *AIAA 2002–3841*, July 2002.

[2] Ostlund, J.; et al.: "Side Load Phenomena in Highly Overexpanded Rocket Nozzles," *AIAA 2001–3684*, July 2001.

[3] Terhardt, J.; and Hagemann, G.: "Flow Separation and Side-Load Behavior of Truncated Ideal Rocket Nozzles," *AIAA 2001–3686*, July 2001.

[4] Hagemann, G.: "The Calorimeter Nozzle Programme," *Presentation Charts*, *AIAA2002–3998*, July 2002.

[5] Tomita, T.; et al.: "Sub-Scale Nozzle Combustion Tests of the LE–7A Engine for Clarification of Large Side Load (1) – Formation of RSS Structure Due to Combustion Condition," *AIAA2002–3842*, July 2002.

[6] Dumnov, G.E.: " Unsteady Side Loads Acting on the Nozzle with Developed Separation Zone," *AIAA 96–3220*, July 1996.

[7] Frey, M.; et al.: "Subscale Nozzle Testing at the P6.2 Test Stand," *AIAA 200–3777*, July 2000.

[8] Gross, A.; and Weiland, C.: " Investigation of Shock Patterns and Separation Behavior of Several Subscale Nozzles," *AIAA 2000–3293*, July 2000.

[9] Takahashi, M.; et al.: "Transient Flow Simulation of a Compressed Truncated Perfect Nozzle," *AIAA 2001–3681*, July 2001.

[10] Wang, T.S.: "Numerical Study of the Transient Nozzle Flow Separation of Liquid Rocket Engines," *Computational Fluid Dynamics Journal,* Vol. 1, No. 3, pp. 319–318, October 1992.

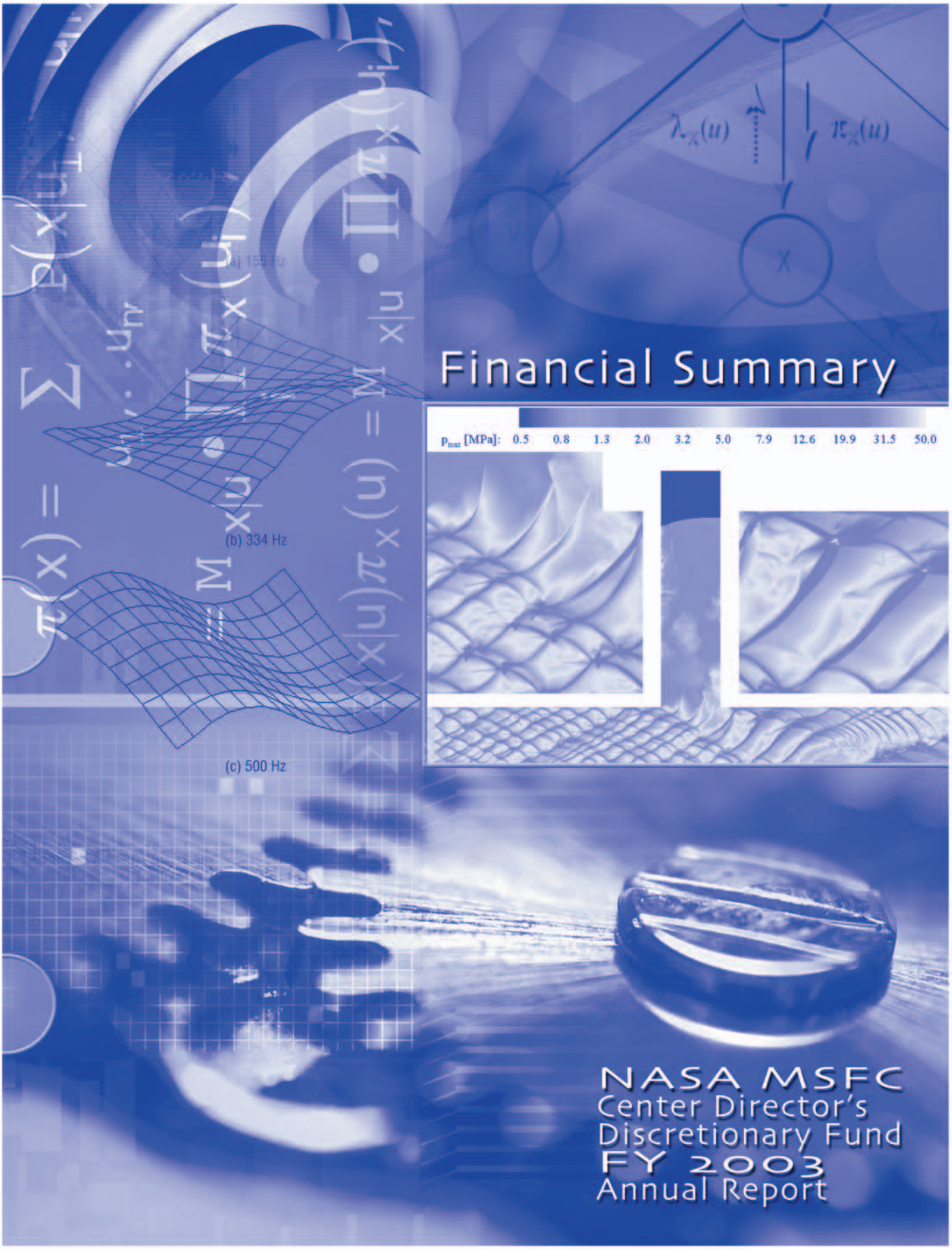
Financial Summary
(a) 155 Hz
(b) 334 Hz
(c) 500 Hz
p_max [MPa]: 0.5 0.8 1.3 2.0 3.2 5.0 7.9 12.6 19.9 31.5 50.0
NASA MSFC
Center Director's
Discretionary Fund
FY 2003
Annual Report

Financial Summary Funding Level ($)

		FY 2002	FY 2003	TOTAL
00–29	Altitude Compensating Nozzle Design Technology	0	15,000	15,000
02–01	Embedded Acoustic Emission Sensors Annual Report	15,500	16,000	31,500
02–02	Vision System Development for Miniature Robotics	23,903	22,882	46,785
02–03	Flight Critical Hardware Voting Development	27,847	10,000	37,847
02–04	Soft Computing for Propulsion Control	30,000	0	30,000
02–05	Architecture for a Fault-Tolerant Smart Servomotor Controller	25,000	23,000	48,000
02–08	Adaptive Structures Applications in Microgravity Vibration Control and Isolation	44,000	36,000	80,000
02–09	Evolutionary Structures Analysis and Testing	23,000	10,000	33.000
02–10	Optimization of a Time-Domain Parameter Estimation Procedure Using a Genetic Algorithm	20,000	0	20,000
02–12	Fiber Placement Module for Processing of Thin Films and Adhesives Into Composite Structures	20,000	24,000	44,000
02–16	Web-Based Request-Oriented Scheduling Engine	7,000	3,000	10,000
02–17	Wireless Services in the Space Flight Operations Services Grid Prototype	39,300	0	39,300
02–18	Process Gas Decontamination Using a Metallic, Ultrashort Channel-Length Monolithic Catalyst Substrate	50,400	30,500	80,900
02–19	Multiphase Fluid System Design for Microgravity Environments	90,000	60,000	150,000
02–20	The Development of Multilayer Hard X-Ray Optics	37,000	12,500	49,500
02–21	In Situ Studies of Structural Transformations in Undercooled Liquids via Beam-Line Electrostatic Levitation	37,000	75,000	112,000
02–25	Automated Postprocessing	50,000	50,000	100,000
02–34	Liquid Oxygen/Liquid Hydrocarbon Combustion Wave Ignition	225,000	0	225,000
03–01	Development of a Fundamental Database on High-Pressure Flames Using a Lab-Scale Combuster		97,000	97,000
03–02	PHANTOM: Unified Flow Analysis for Turbines and Pumps		50,000	50,000
03–03	High-Energy Fuels and Catalysts		150,000	150,000

03–06	Pulsed Electromagnetic Thrusters for High-Power Space Propulsion		176,000	176,000
03–07	Enhancement of Generalized Fluid System Simulation Program for Design and Analysis of Propulsion Systems		25,000	25,000
03–08	New Detector Configuration for Experimental Characterization of High-Density Nonneutral Plasma in the High-Performance Antiproton Trap		87,000	87,000
03–09	Nozzle Side Load Technology		275,000	275,000
03–11	Advanced Sensor Concepts for General Avionics Applications		30,000	30,000
03–13	Torque Limits in Composites		40,000	40,000
03–14	High-Strength and Compatible Aluminum Alloy for Hydrogen Peroxide Fuel Tanks		35,000	35,000
03–15	Rotational Vacuum-Assisted Resin Transfer Molding		40,000	40,000
03–16	Low-Power High-Voltage Power Supply With Fast Rise Time		25,000	25,000
03–17	Coupled-Resonator-Enhanced Sensor Technologies		37,500	37.000
03–18	Space Environmental Effects on Ablative Laser Propulsion Using Multilayer Material Systems		7,000	7,000
03–19	Hardware Evolution of Configurable Closed-Loop Controllers		26,000	26,000
03–20	Orbital Global Positioning System Health Management		23,000	23,000
03–21	Structural Test of a Silicon-Carbon Fiber/Silicon-Carbon Matrix Membrane		40,000	40,000
03–22	Deployable Structures Utilizing Spiral-Wrapped Engineered Fibers		25,000	25,000
03–23	Cryogenic Fracture Toughness Evaluation of Cast Aluminum-Beryllium Alloys for Structural Applications		40,000	40,000
03–24	Modular Avionics Redundancy and Testability Architecture		23,200	23,200
03–25	Characterization and Selection of Carbon Fibers Fabricated in Ceramic Matrix Composites for Propulsion and Third Generation Thrust Applications		58,200	58,200
03–26	Ultraviolet Radiation and Atomic Oxygen Interaction With Molecular Contamination on External Spacecraft Surfaces		24,000	24,000
03–28	Novel Approach to Fabricating Sample Contaminant Assemblies		35,000	35,000
03–29	Rapid Prototyping of Propulsion Components With Nanocrystalline Microstructure		56,218	56,218
03–30	Performance Verification of Cadmium Zinc Telluride Crystal Growth Techniques for Large-Scale Gamma-Ray Imagers		60,000	60,000
03–31	Development of Thin-Disk Laser Architecture for use in Power Beaming Applications and Science Instruments		67,000	67,000
03–32	Quantity Flow Cytometry for Evaluation of Biological Effects of Simulated Microgravity and Radiation		50,000	50,000
	Totals	**764,950**	**1,990,000**	**2,754,950**

Fiscal Year 2004 Project Funding
($)

Engineering Directorate		FY 2004
03–11	Advanced Sensor Concepts for General Avionics Applications Dean Alhorn/ED17	20,000
03–12	Thin-Film Composite Structures Mike Tinker/ED20	25,000
03–13	Torque Limits in Composites Frank Thomas/ED23	0
03–15	Rotational Vacuum-Assisted Resin Transfer Molding Bruce Hulcher/ED34	20,000
03–17	Coupled-Resonator-Enhanced Sensor Technologies Dr. David D. Smith/SD46	43,100
03–18	Space Environmental Effects on Ablative Laser Propulsion Using Multilayer Material Systems Mary Nehls/ED35	5,000
03–19	Hardware Evolution of Configurable Closed-Loop Controllers David A. Gwaltney/ED17	23,000
03–20	Orbital Global Positioning System Health Management Ken Schrock/ED18	0
03–23	Cryogenic Fracture Toughness Evaluation of Cast Aluminum-Beryllium Alloys for Structural Applications Wayne R. Gamwell/ED33	20,000
03–24	Modular Avionics Redundancy and Testability Architecture Kosta Varnavas/ED13	32,600
03–25	Characterization and Selection of Carbon Fibers Fabricated in Ceramic Matrix Composites for Propulsion and Third Generation Thrust Applications Diep Vo Trinh/ED34	15,000
03–26	Ultraviolet Radiation and Atomic Oxygen Interaction With Molecular Contamination on External Spacecraft Surfaces Keith C. Albyn/ED31	9,000
03–27	Investigation to Compare Ground-Simulation Space Environment David T. Hoppe/ED31	15,000
03–28	Novel Approach to Fabricating Sample Contaminant Assemblies Glenn Williams/ED34	35,000
04–01	Redundant Serial Interface Microcontroller Lisa D. Coe/ED13	14,000
04–02	Development of Advance Composite Cryogenic Tanks, Lines, and Ducts Tom Delay/ED34	131,000

04–03	Using Software Complexity in Flight Software Defect Analysis and Prevention Will Crisp/ED14	40,000
04–04	Evaluation, Development, and Test of Metal Foams Binayak Panda/ED33	45,000
04–05	Oriented Nanofiber Ceramic Reinforced Raj K. Kaul/ED34	60,000
04–06	Development of Embedded Packaging Assemblies Michael W. Selby/ED16	64,000
04–07	Polymer Thin-Film Sensors Michael D. Watson/ED12	0
04–08	Coupled Electromagnetic Oscillators David D. Smith/SD46 and Alvin Eric Cantrell/ED18	44,000
04–09	Miniature Inspection System Technologies Jeri M. Briscoe/ED12	44,100
	Subtotal	**704,800**

Flight Projects Directorate

04–10	Development of a Design Tool for Rigorous Simulation of Adsorption Processes for Spacecraft Life Support Jim Knox/FD21	40,524
04–11	Design/Development of Low Gravity Liquid Handling Donald A. Reiss/SD46	50,123
04–12	Application of Off-the-Shelf Environmental Monitoring Hardware to Crewed Spacecraft Cabin Air Quality Analysis Jay L. Perry/FD21	113,137
	Subtotal	**203,784**

Science Directorate

01-05	Application of Nanotube Heat Pipes Michael D. Watson/ED12	129,000
03–30	Performance Verification of Cadmium Zinc Telluride Crystal Growth Techniques for Large-Scale Gamma-Ray Imagers Jerry Fishman/SD50	15,000
03–31	Development of Thin-Disk Laser Architecture for Use in Power Beaming Applications and Science Instruments W. Scott Smith/SD70	0
04–13	Development and Fabrication of a Diamond Turned 0.5-m Diameter Wolter Type-I X-Ray Mandrel and Nickel-Cobalt-Composite Replication Material David L. Lehner/SD73	46,000
04–14	Muscle Atrophy During Long-Term Space Flight Ronald B. Young/SD46	57,000
04–15	Development to Improve Interferometers for Spaceflight Solar Magnetograph Spectral Filters Allen Gary/SD50	35,000

04–16	Storm Airborne Monitor Precipitation Rich Blakeslee/SD60	72,000
04–17	Development of an Imbedded Microvalve for Isolation of Reagents and Targets on a Lab-on-a-Chip Helen J. Cole/SD44	45,000
04–18	Biohydrogen Produced by the Extremophile Spirochaeta Richard Hoover/SD50	63,416
	Subtotal	**342,416**

Transportation Directorate

03–01	Development of a Fundamental Database on High-Pressure Flames Using a Lab-Scale Combuster J. Blevins/TD40	30,000
03–02	PHANTOM: Unified Flow Analysis for Turbines and Pumps Daniel J. Dorney/TD64	50,000
03–06	Pulsed Electromagnetic Thrusters for High-Power Space Propulsion Thomas E. Markusic/TD40	120,000
03–08	New Detector Configuration for Experimental Characterization of High-Density Nonneutral Plasma in the High-Performance Antiproton Trap J. Boise Pearson/TD40	90,000
03–09	Nozzle Side-Load Technology Joseph Ruf/TD64	150,000
04–19	Vacuum Plasma Spray Coating for Injector Applications Sandra K. Elam/TD61	90,000
04–20	Catalyst for Ionic high Energy Nontoxic Propellants Rudy Gostowski/TD40	95,000
04–21	Advanced Control and Control Allocation Charles E. Hall/TD54	48,000
04–22	Development of Advanced Feature Extraction Capabilities Suzanne Dorney/TD62	50,000
04–23	High-Power Electric Propulsion: Physics of Inductively Coupled Plasmas Jonathan E. Jones/TD40	131,000
04–24	Solenoid Valve Health Monitoring John K. Laszar/TD62	21,000
04–25	Turbopump Design Technology for Advanced Second Stage Liquid Oxygen/ Liquid Hydrogen Engines Lisa W. Griffin/TD64	90,000
04–26	Similarity and Scale Effect for Liquid Rocket Injectors John Blevins/TD40	84,000
	Subtotal	**1,049,000**
	Total	**2,300.000**